



PHD

The Influence of Ligand Substitution on the Reactivity of Iron- β -diketimate Complexes

Linford-Wood, Thomas George

Award date:
2023

Awarding institution:
University of Bath

[Link to publication](#)

Alternative formats

If you require this document in an alternative format, please contact:
openaccess@bath.ac.uk

Copyright of this thesis rests with the author. Access is subject to the above licence, if given. If no licence is specified above, original content in this thesis is licensed under the terms of the Creative Commons Attribution-NonCommercial 4.0 International (CC BY-NC-ND 4.0) Licence (<https://creativecommons.org/licenses/by-nc-nd/4.0/>). Any third-party copyright material present remains the property of its respective owner(s) and is licensed under its existing terms.

Take down policy

If you consider content within Bath's Research Portal to be in breach of UK law, please contact: openaccess@bath.ac.uk with the details. Your claim will be investigated and, where appropriate, the item will be removed from public view as soon as possible.

The Influence of Ligand Substitution on the Reactivity of Iron- β -diketimate Complexes

Thomas George Linford-Wood

A thesis submitted for the degree of Doctor of Philosophy

University of Bath

Department of Chemistry

April 2023

Copyright notice

Attention is drawn to the fact that copyright of this thesis rests with the author and copyright of any previously published materials included may rest with third parties. A copy of this thesis has been supplied on condition that anyone who consults it understands that they must not copy it or use material from it except as licenced, permitted by law or with the consent of the author or other copyright owners, as applicable.

Use of this thesis

This thesis may be made available for consultation within the University Library and may be photocopied or lent to other libraries for the purposes of consultation.

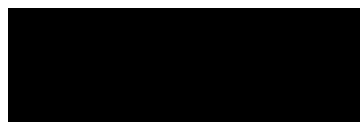
Candidate signature:



Declaration of any previous submission of the work

The material presented here for examination for the award of a higher degree by research has not been incorporated into a submission for another degree.

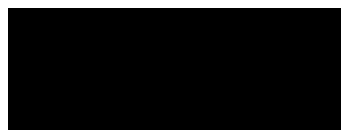
Candidate signature:



Declaration of authorship

I am the author of this thesis, and the work described therein was carried out by myself personally, with exceptions listed below. Hydrogenation experiment of **1a** was conducted by Dr Nathan T. Coles (section **3.4.3**). In the following cases, single crystal XRD data were collected by other parties: (*rac*)-**23** by Dr Samantha L. Lau (University of Bath, UK, section **4.3**), and **39** by Tanner George (Saint Mary's University, Canada, section **5.3**). Solid-state NMR experiments of **poly(34)-poly(36)** were undertaken by Dr Ullrike Werner-Zwanziger (Dalhousie University, Canada, section **5.2.1**). DOSY experiments of **poly(34)-poly(36)** were undertaken by Joe Bedard (Dalhousie University, Canada, section **5.2.1**). MALDI experiments of **poly(34)-poly(36)** were undertaken by Dr Matthew W. Forbes (University of Toronto, Canada, section **5.2.1**). TGA and DSC experiments of **poly(34)-poly(36)** were undertaken by Dr Joe B. Gilroy (Western University, Canada, section **5.2.1**).

Candidate signature:



Contents

0.1	Acknowledgements	5
0.2	Abstract	6
0.3	Associated Publications	7
0.4	Removable Insert and List of Abbreviations	8
1	Spatial Confinement in Iron-β-Diketimate Complexes and its Influence on Reactivity and Catalysis	13
1.1	The β -Diketimate Ligand	14
1.2	Iron β -Diketimates: Reactivity and Catalysis	15
2	Iron-catalysed H/D Exchange of Primary, Secondary and Tertiary Silanes, Tertiary Siloxanes and Pinacolborane	22
2.1	Introduction	23
2.2	H/D Exchange of Primary and Secondary Silanes, Tertiary Siloxanes and Pinacolborane	32
2.2.1	Optimisation	32
2.2.2	Substrate Scope	34
2.2.3	Mechanistic Investigation	36
2.3	H/D Exchange of Tertiary Silanes	51
2.4	Reactivity of (BDK)Fe- κ^2 -9-borabicyclo[3.3.1]nonane Complexes	55
2.5	Hydrophosphination of Allenes	58
2.6	Conclusions and Future Work	60
2.7	Experimental	62
2.7.1	General Considerations	62
2.7.2	General Method for Deuteration of Silanes	62
2.7.3	Substrate Scope Spectroscopic Data	62
2.7.4	Method for Deuterium Labelling of Propylbenzene	67
2.7.5	Method for Hydrogenation of Methylphenyl(silane- d_2)	68
2.7.6	Ligand and Complex Syntheses	68
2.7.7	Reaction Monitoring Method	76
2.7.8	General Method for Hydrophosphination of Allenes	76
2.7.9	Substrate Syntheses	76
2.7.10	Computational Method	81

3	Room Temperature Iron-catalysed Transfer Hydrogenation Using ⁿButanol and Poly(methylhydrosiloxane)	82
3.1	Introduction	83
3.2	Optimisation	90
3.3	Substrate Scope	93
3.4	Mechanistic Investigation	95
3.4.1	Alkene Isomerisation	95
3.4.2	Gas Evolution Experiments	95
3.4.3	Hydrogenation Experiments	97
3.5	Mono-deuteration of Alkenes	98
3.6	Proposed Mechanism	100
3.7	Dehydrocoupling of Poly(methylhydrosiloxane) and Alcohols	101
3.8	Conclusions and Future Work	102
3.9	Experimental	103
3.9.1	General Considerations	103
3.9.2	Optimisation	103
3.9.3	General Method for Hydrogenation of Alkenes	103
3.9.4	Substrate Scope Spectroscopic Data	104
3.9.5	Deuterium Labelling Experiments	109
3.9.6	Deuterium Labelling Spectroscopic Data	109
3.9.7	Gas Evolution Experiments	113
3.9.8	H ₂ Experiments	113
4	2nd Generation Chiral β-Diketiminates: Towards Enantioenriched Main-Group Compounds	115
4.1	Introduction	116
4.2	DFT-Derived Enantioselective Insertion	121
4.3	Optimisation of Unsymmetric (<i>rac</i>)-Iron- β -Diketimate Pre-catalyst	125
4.4	Synthesis of Unsymmetric (<i>R</i>)-Iron- β -Diketimate Pre-catalyst	129
4.5	Conclusions and Future Work	133
4.6	Experimental	135
4.6.1	(<i>rac</i>)-Ligand and Complex Syntheses	135
4.6.2	(<i>R</i>)-Ligand and Complex Syntheses	139
4.6.3	Enantioselective Hydroboration	144
4.6.4	Transfer Hydrogenation	145
4.6.5	Computational Method	146
5	Synthesis of Cage-Dense, PN-Containing Polymers of Varying Electron Density	148
5.1	Introduction	149
5.2	Synthesis and Characterisation of Cage-Dense Polymers	151

5.2.1	Polymer Synthesis and Characterisation	151
5.2.2	Repeat-Unit and End-Group Determination	153
5.3	Mechanism for Polymerisation	153
5.4	Conclusions and Future Work	156
5.5	Experimental	158
5.5.1	General Considerations	158
5.5.2	Chlorophosphine Synthesis	158
5.5.3	Syntheses of PN-Cages	160
5.5.4	Polymer Synthesis	160
5.5.5	General Method for Reaction Monitoring Experiments	163

6 Crystal Data and References **164**

0.1 Acknowledgements

Foremost, my immense gratitude goes to principal investigator Dr Ruth L. Webster. This endeavour could not be accomplished without such infectious scientific curiosity and leading insight. Her combination of measured guidance whilst nurturing a freedom for autonomous research, favours a unique and harmonious supervisory method. I am thankful for all her support. I am also grateful to co-investigator Dr Matthew N. Grayson- consistently available to provide theoretical understanding. Without his intuition, multi-faceted mechanistic exploration could not be achieved. Furthermore, my appreciation extends to co-investigator Dr Saurabh S. Chitnis for mediating research in Canada. His enthusiasm for new discovery makes all laboratory endeavours worthwhile.

My thanks to Dr Adam N. Barrett. To share the PhD experience and friendship has been a delight. I am grateful for all the advice provided, and will continue to provide, throughout the years. I have been fortunate to benefit from outstanding postdoctoral support. Great thanks to Dr Samantha L. Lau and Dr Thomas M. Hood. Because of this infamous partnership and accompanying first-rate synthetic and crystallographic understanding, many of my challenges were circumvented. Any successes described herein are a function of their wealth of expertise. This credit extends to the remainder of the research group and other influential members of the department; Mirela A. Johnson, Charlie L. Cavens, Emily E. Pockock, Dr Danila Gasperini, Dr Nathan T. Coles, Dr Cei B. Provis-Evans, Dr Callum R. Woof, Dr Kyle G. Pearce, Dr Anne-Frédérique Pércharman, Dr Samuel E. Neale and Dr Elliot H. E. Farrar. It was an honour to work with such a knowledgeable, and personable group of scientists. My appreciation to all departmental technical staff, namely Dr Mary F. Mahon, Dr Catherine L. Lyall and Dr John P. Lowe, for supplementing the research. Furthermore, my gratitude to the EPSRC Centre for Doctoral Training in Catalysis for funding the project.

Chapter 5 testifies to the warm welcoming I received in Halifax, Nova Scotia. Thanks to Joe Bedard for graciously sharing the project and facilitating a productive and cohesive partnership. Moreover, the friendship, hospitality and generosity will not be forgotten. This acknowledgement extends to Dylan J. Hale, Erin N. Welsh, Tyler M. Saunders, Matthew J. Margeson, Tyler J. Hannah, Dr Mohsen Shayan, Priscila M. Pukaro and Gustavo S. Dantas. My best wishes for their future endeavours, as it is their influence that made the experience so joyous and is held dearly at heart.

My choice to follow a career in chemistry was influenced by the attentive mentorship of Tim James and Dr Roberto Nolla-Saltiel. I am immensely grateful for all their time surrendered to further my education.

My utmost gratitude to Mum and Dad for their continual support throughout higher- and postgraduate education. I am forever indebted. Finally, thank you Emma L. Daniels, beloved and inspirational fiancée. Here's to the next chapter together.

0.2 Abstract

The β -diketiminato (BDK) ligand has become one of the most ubiquitous scaffolds in organometallic chemistry. This is a function of it being tunable and proficient at stabilising reactive, low-coordinate complexes. With the emerging challenges associated with diminishing precious metal resources, discovering analogous reactivity utilising abundant elements is a desirous objective of chemical research. Hence, many iron-BDK complexes have been developed and ground-breaking examples are highlighted in chapter 1. Ligand modulation leads to altered spatial confinement. In some cases, this facilitates orthogonal reactivity- a recurrent theme throughout the thesis.

Chapter 2 details the first example of iron-catalysed hydrogen/deuterium exchange of silanes with deuterium gas. By variation of ligand environment, near complete deuterium incorporation is observed for primary, secondary, and tertiary silanes, tertiary siloxanes and pinacolborane. An accompanying mechanistic study reveals an iron-deuteride is responsible for isotope exchange. Stoichiometric reactions facilitate isolation of a new class of iron-hydride complexes, with record-breaking downfield ^1H NMR resonances.

Studies into the iron-catalysed transfer hydrogenation (TH) of carbon-carbon double bonds are reported in chapter 3. Using benign TH reagents (n -butanol and poly(methylhydrosiloxane) (PMHS)), a range of allyl arenes, styrenes and aliphatic olefins undergo reduction. By careful selection of deuterium and hydride sources, regioselective transfer hydrodeuteration can be achieved. In the absence of alkene substrate, dehydrocoupling of various alcohols with PMHS is observed, generating high yields of hydrogen gas within 30 minutes.

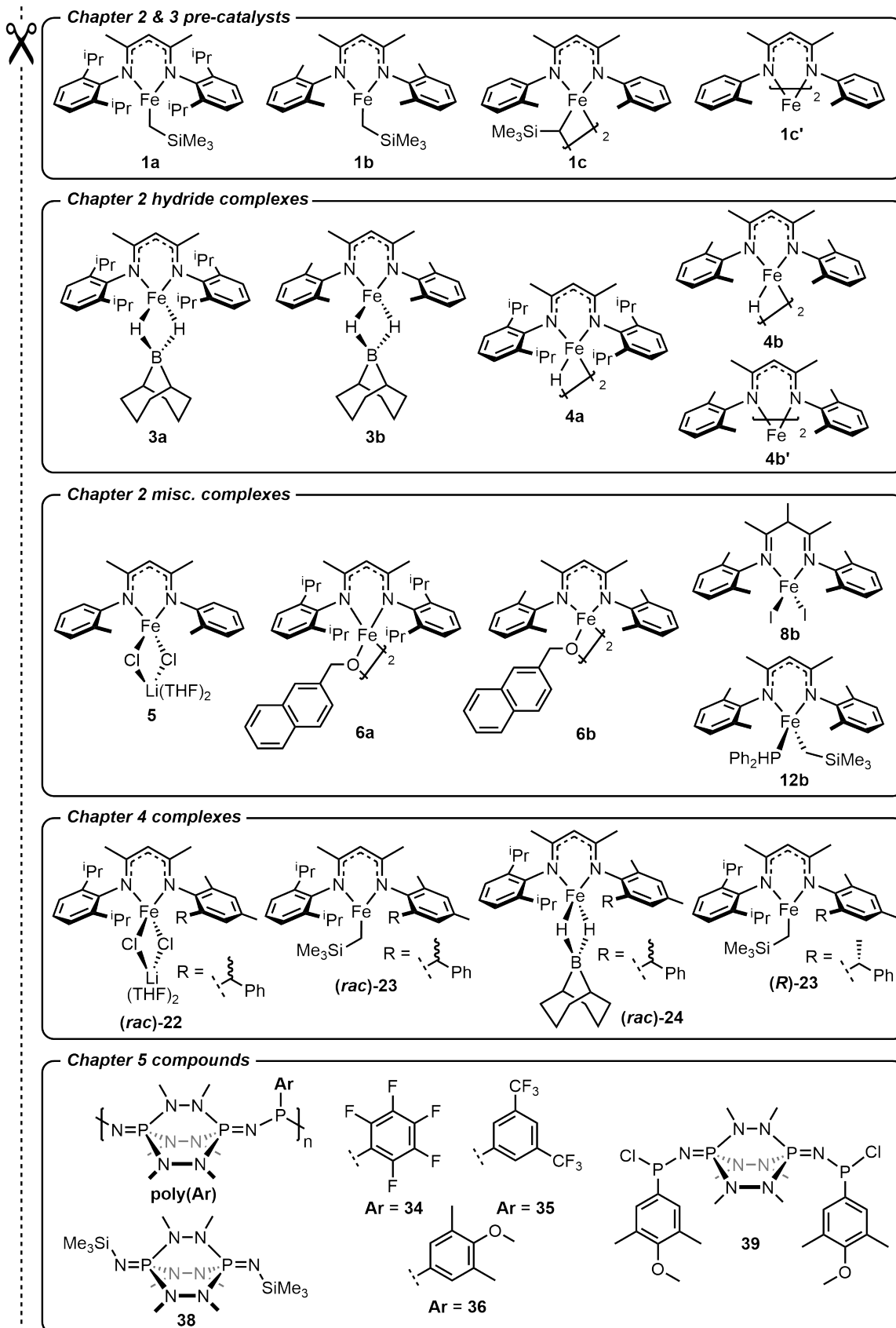
Chapter 4 describes the optimisation of a 2nd generation chiral BDK, derived from *N*-aryl-containing flanking groups. Density functional theory is deployed as a predictive tool, suggesting the corresponding iron(II)-hydride, bearing this ligand, will undergo enantioselective insertion of carbon-carbon double bonds. Pro-ligand optimisation, along with its associated iron complexes, is described, culminating in the first iron-BDK-catalysed asymmetric hydrofunctionalisation.

Polymeric materials featuring cage-dense moieties are rarely reported. This is surprising given they demonstrate excellent thermal properties. The major challenge is finding stable and accessible cage-derived monomers. Chapter 5 details the synthesis and characterisation of an array of phosphazabicyclo[2.2.2]octane polymers, containing (aryl)dichlorophosphine co-monomers. *In situ* reaction monitoring experiments provide insight into the polymerisation mechanism, along with the impact of electron-density on reaction rate.

0.3 Associated Publications

1. T. G. Linford-Wood, M. F. Mahon, M. N. Grayson and R. L. Webster, Iron-Catalyzed H/D Exchange of Primary Silanes, Secondary Silanes, and Tertiary Siloxanes, *ACS Catal.*, 2022, **12**, 5, 2979-2985.
2. C. R. Woof, T. G. Linford-Wood, M. F. Mahon and R. L. Webster, Catalytic Hydrophosphination of Allenes Using an Iron(II) β -Diketiminato Complex, *Synthesis*, 2022, 10.1055/a-1902-5592.
3. T. G. Linford-Wood, N. T. Coles and R. L. Webster, Room temperature iron catalyzed transfer hydrogenation using *n*-butanol and poly(methylhydrosiloxane), *Green Chem.*, 2021, **23**, 2703-2709.
4. J. Bedard, T. G. Linford-Wood, B. C. Thompson, U. Werner-Zwanziger, K. M. Marczenko, R. A. Musgrave and S. S. Chitnis, A Robust, Divalent, Phosphaza-bicyclo[2.2.2]octane Connector Provides Access to Cage-Dense Inorganic Polymers and Networks, *J. Am. Chem. Soc.*, 2023, **145**, 13, 7569-7579.

0.4 Removable Insert and List of Abbreviations



List of Abbreviations

ΔG	Gibbs free energy change
σ -CAM	σ -Complex assisted metathesis
6-31G**	Pople split-valence double- ζ basis set
9-BBN	9-Borabicyclo[3.3.1]nonane
<i>ee</i>	Enantiomeric excess
<i>rac</i>	Racemic
$T_{d, \max}/\%$	Temperature of maximum decomposition rate/percentage weight loss
T_g	Glass transition temperature
T_m	Melting temperature
^oMe	2-Methylphenyl
acac	Acetylacetonate
B3PW91	Exchange-correlation hybrid functional containing local-spin density gradient and exact-exchange terms
BDK	β -Diketiminato
BP86	Generalised gradient approximation density function containing Becke's exchange and Perdew's correlation functionals
cat	Catechol
CC	Cross-coupling
cHATH	Cooperative hydrogen atom transfer hydrogenation
COD	1,5-Cyclooctadiene
CPME	Cyclopentyl methyl ether
cyp	Cyclopentyl

D3BJ(solvent)	Grimme's D3 empirical dispersion correction program with Becke-Johnson damping functions
DBU	1,8-Diazabicyclo[5.4.0]undec-7-ene
Def2-TZVP	Ahlrich's valence triple- ζ polarization basis set
DFT	Density functional theory
DHC	Dehydrocoupling
dipp	2,6-Diisopropylphenyl
DMAP	4-Dimethylaminopyridine
dmp	2,6-Dimethylphenyl
DOSY	Diffusion-ordered spectroscopy
DP	Degree of polymerisation
DSC	Differential scanning calorimetry
DS	Dean-Stark apparatus
EA	Elemental-analysis
FCC	Flash column chromatography
HA	Hydroamination
HDF	Hydrodefluorination
HMDS	Hexamethyldisilazane
HPLC	High-performance liquid chromatography
IEF-PCM(solvent)	Solvent polarizable continuum model approximation using the integral equation formalism variant
KIE	Kinetic isotope effect
KS	Kohn-Sham
M_w	Average polymer molecular weight
MALDI-TOF	Matrix-assisted laser desorption/ionisation-time of flight spectrometry
mes	2,4,6-Mesityl
MOTM	Man on the Moon apparatus
MPV	Meerwein-Ponndorf-Verley

NMR	Nuclear magnetic resonance
OA	Oxidative addition
pin	Pinacolato
PMHS	Poly(methylhydrosiloxane)
RE	Reductive elimination
ROP	Ring-opening-polymerisation
RSM	Recovered starting material
sc-XRD	Single crystal X-ray diffraction
SEC	Size exclusion chromatography
SFC	Supercritical fluid chromatography
ssNMR	Solid-state nuclear magnetic resonance
TGA	Thermogravimetric analysis
THD	Transfer hydrodeuteration
TH	Transfer hydrogenation
TMP	2,2,6,6-Tetramethylpiperidine
TMS	Tri- or tetramethylsilane
TNA	Time normalisation analysis
TOF	Turnover frequency
TON	Turnover number
TS	Transition state

Do not spray into eyes

- Alt-J

Chapter 1

Spatial Confinement in Iron- β -Diketiminato Complexes and its Influence on Reactivity and Catalysis

1.1 The β -Diketiminato Ligand

Finding a robust ligand platform for stabilisation of reactive species has been a long-standing endeavour of the inorganic chemist. Hence, the foundations are laid for the exploration of fundamental reactivity. Spatial confinement can provide stability- whilst promoting selectivity, and is achieved by tuning spectator ligand sterics. A commonly deployed scaffold is the β -diketiminato (BDK) ligand- shown in figure 1.1.1, a function of its inherent steric modularity.

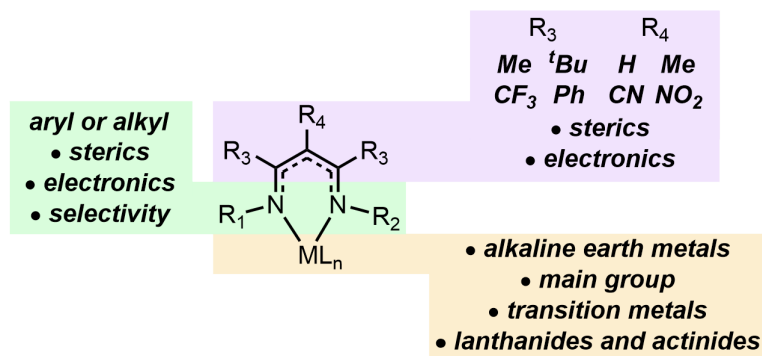


Figure 1.1.1: Modularity of the BDK.

Classically, BDK synthesis is achieved by the condensation of two equivalents of a primary amine with acetylacetone.¹⁻³ This facile synthesis enables the systematic modification of the ligand scaffold. Selection of the N -containing moiety allows the BDK ligand ‘flanking groups’ (R_1 and R_2) to be modified. Likewise, substitution at the acetylacetone α - and β -‘backbone’ positions (R_4 and R_3 , respectively) grant the opportunity for further functionalisation. Deprotonation yields a conjugated, monoanionic ligand that binds to metal centres, typically by a κ^2 -coordination mode. BDK ligand flanking groups are usually derived from aromatic substituents, which adopt a conformation perpendicular to the plane of the BDK ligand backbone. This generates a region of steric confinement, facilitating isolation of many low-coordinate complexes scattered throughout the periodic table.⁴⁻⁹

This modularity means the BDK ligand is tunable.¹⁰ Structural properties of BDK complexes can be modified by altering the steric bulk at R_1 , R_2 and R_3 . Larger substituents at R_3 force the flanking groups towards the metal centre via the ‘buttressing effect’, reducing the M-N bond length. Consequently, the N-M-N bite- and R_3C-N-R_1/R_2 bond angles increase. This is accompanied by lengthening of the M-L bond. Increased steric bulk at the aryl- R_1/R_2 *ortho*-position can also enlongate the M-L bond. In contrast, smaller substituents favour di- or multinuclear complex formation or facilitate the coordination of ancillary ligands. Furthermore, electronic properties can be altered by substitution at R_3 and R_4 - where the π -conjugation is influenced directly. Examples illustrating how structural and electronic modification have influenced reactivity are described in section 1.2.

Because of this tunable confinement, BDK complexes have attracted immense attention in the stabilisation of highly reactive species. Pertinent examples include, but are not limited to; the isolation of magnesium-magnesium and magnesium-boron bonds, reduction of N_2 by calcium-calcium bonds and iron-mediated coupling of N_2 and hydrocarbons.¹¹⁻¹⁴ Beyond featuring a BDK ligand, these reports share a second common attribute- they harness earth-abundant elements.

BDK Nomenclature

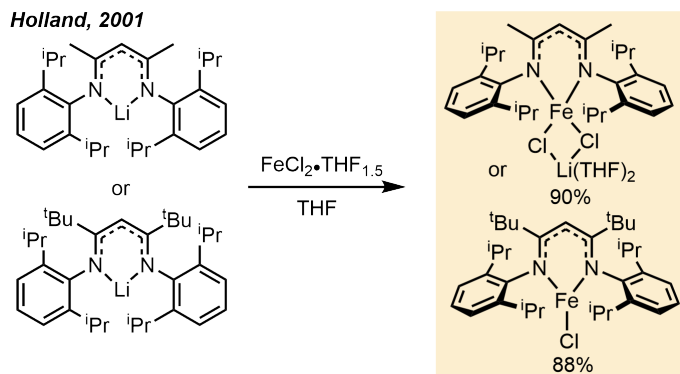
Specific nomenclature is required to denote BDK ligand substitution (refer to figure 1.1.1). In most cases, $R_1 = R_2$. These BDK ligands are termed ‘symmetric’, attributed to conformations with high C_{2v} or C_2 symmetry. Typical notation follows the general form $R_1\text{BDK}^{R_3,R_4}$. Where $R_1 \neq R_2$, the BDK ligand is deemed ‘unsymmetric’, with reduced C_s or C_1 symmetry. In this case, notation follows the form $R_{1,R_2}\text{BDK}^{R_3,R_4}$. Examples where R_3 are inequivalent are not discussed in this instance, and where $R_3 = \text{Me}$ and $R_4 = \text{H}$, notation can follow the form $R_1\text{BDK}^{R_3}$ or $R_1\text{BDK}$ respectively, for clarity.

1.2 Iron β -Diketiminates: Reactivity and Catalysis

Precious metal catalysts are ubiquitous in industry for the synthesis of commodity chemicals (examples include but are not limited to, asymmetric hydrogenation, acetic acid production, cross-coupling, hydroformylation and Wacker-oxidation).¹⁵ However, continued dependence upon these rare and finite elements mean their reserves are diminishing. Estimates suggest precious metal ore deposits could be exhausted in as little as 30-50 years.^{16,17} With this scarcity comes growing economic, geopolitical, and environmental unrest, compounded by the ever-increasing chemical and technological demand for these elements. In the interest of sustainability, alternative catalytic methods must be found. Therefore, uncovering reactivity analogous to that of precious metals, utilising more abundant elements is a desirous objective of chemical research.

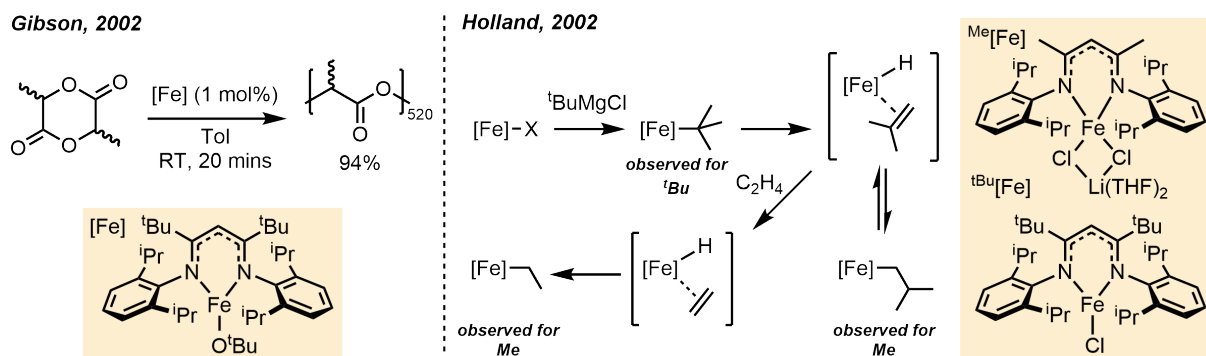
Iron is an inexpensive element being the most abundant transition metal in the Earth’s crust (6% by mass). As of January 2023, the global market price for iron ore was estimated at £0.10 per gram, compared to £13.84, £353.94, £46.59, £131.27 and £28.77 per gram for its precious metal counterparts (Ru, Rh, Pd, Ir and Pt, respectively). Hence, it is an economically viable alternative, whilst circumventing the aforementioned geographical pressures. Iron is routinely utilised within the human body (for example in the active site of proteins/enzymes such as haemoglobin, CO dehydrogenase and hydrogenases)- a function of its high abundance.¹⁸ Thus, it is relatively non-toxic.¹⁹ As of 2019, permitted residual iron impurities for pharmaceutical ingredients were 1300 ppm, compared to only 10 ppm for the precious metals.²⁰ Therefore, iron-mediated processes reduce the demand for downstream purification, limiting the processing costs for fine chemical synthesis. Beyond these inherent advantages, iron has shown wide reactivity-spanning an array of oxidation states (-2 to +6) and partaking in one-, or two-electron processes.¹⁵ Hence, iron has demonstrated its value as an effective catalyst for reductive and oxidative processes alike.^{21–24} Consequently, it is no surprise iron-catalysis is a constantly expanding field of chemical research. Following the aforementioned benefits of iron-catalysis and the modularity of the BDK ligand (section 1.1), it is inevitable the two have been combined to achieve distinctive reactivity. Major discoveries are described herein.

The steric properties of the BDK ligand were harnessed by Holland and co-workers, to synthesise the first three-coordinate iron-BDK complex.²⁵ ($\text{dippBDK}^{\text{Me}}\text{Li}$) pro-ligand was reacted with $\text{FeCl}_2 \cdot (\text{THF})_{1.5}$ yielding four-coordinate LiCl adduct $(\text{dippBDK}^{\text{Me}})\text{FeCl}_2\text{Li} \cdot (\text{THF})_2$. The analogous reaction with $(\text{dippBDK}^{\text{tBu}})\text{Li}$,



Scheme 1.2.1: Synthesis of three- and four-coordinate (BDK)FeCl_n complexes, reported by Holland and co-workers.²⁵

formed three-coordinate (^{dipp}BDK^{tBu})FeCl. The ^tBu backbone buttresses the ^{dipp} flanking groups leading to an 10° increase in C-N-C bond angle, compared to (^{dipp}BDK^{Me})FeCl₂Li·(THF)₂. This change is significant enough to enforce a three-coordinate, planar geometry at iron- an early demonstration of spatial confinement influencing reactivity.

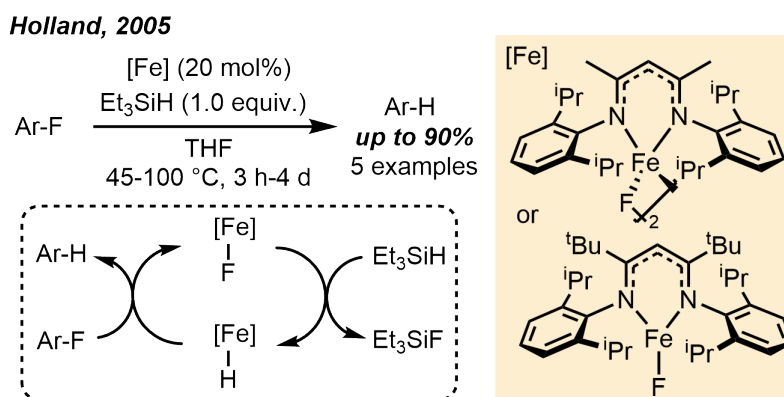


Scheme 1.2.2: (BDK)FeO^tBu-catalysed polymerisation of lactide, reported by Gibson and co-workers (left), and alkyl isomerisation in (BDK)Fe(alkyl) complexes, reported by Holland and co-workers (right).^{26,27}

Gibson and co-workers reported the first catalytic transformation by an (BDK)FeO^tBu complex (scheme 1.2.2).²⁶ Reacting (^{dipp}BDK^{tBu})FeCl with NaO^tBu yielded iron-alkoxide (^{dipp}BDK^{tBu})FeO^tBu. The iron-alkoxide was an effective initiator for the polymerisation of *rac*-lactide. Poly(lactide) was generated in high molecular weight (37500 Da) and narrow dispersity (1.12). High activity was attributed to the electrophilicity of iron, carrying only 12-valence electrons.

Stoichiometric reactivity was reported by Holland and co-workers, demonstrating reversible β -hydride elimination/hydride insertion (scheme 1.2.2).²⁷ Reaction of (^{dipp}BDK^{tBu})FeCl with ^tBuMgCl, yielded the corresponding (^{dipp}BDK^{tBu})Fe^tBu complex. However, in the case of (^{dipp}BDK^{Me})FeCl, isomerised product (^{dipp}BDK^{Me})FeⁱBu was observed. The same reaction under one atmosphere of ethylene yielded ethylene insertion product (^{dipp}BDK^{Me})FeEt and liberated isobutene. This reactivity indicated reversible β -hydride elimination and alkene substitution is occurring at less sterically-congested (^{dipp}BDK^{Me})Fe^tBu/ⁱBu,

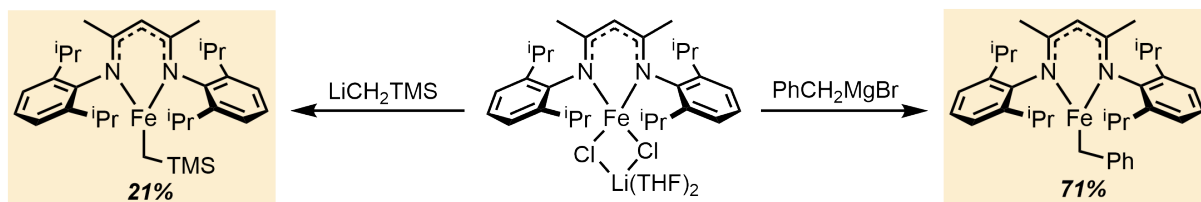
through $(\text{dippBDK}^{\text{Me}})\text{FeH}(\eta^2\text{-alkene})$ intermediates. Only at elevated temperatures was $(\text{dippBDK}^{\text{tBu}})\text{Fe}^{\text{iBu}}$ observed, demonstrating the impact of spatial confinement on reactivity. The proposed $(\text{BDK})\text{FeH}(\eta^2\text{-alkene})$ intermediates underpin mechanistic hypotheses for many later iron-BDK-catalysed alkene hydrofunctionalisation reactions (*vide infra*).



Scheme 1.2.3: (BDK)FeF-catalysed hydrodefluorination of fluorocarbons, reported by Holland and co-workers.²⁸

Hydride intermediates are prevalent in later work by Holland and co-workers (scheme 1.2.3).²⁸ Reaction of $(\text{dippBDK}^{\text{Me}})\text{Fe}(\text{alkyl})$ or $(\text{dippBDK}^{\text{tBu}})\text{Fe}(\text{alkyl})$ complexes with Me_3SnF yielded $[(\text{dippBDK}^{\text{Me}})\text{FeF}]_2$ or $(\text{dippBDK}^{\text{tBu}})\text{FeF}$, respectively. Iron-fluoride complexes catalysed the hydrodefluorination (HDF) of arylfluorides with stoichiometric Et_3SiH co-reagent. Working mechanistic hypothesis was as follows. The catalyst reacts with Et_3SiH yielding $(\text{dippBDK})\text{FeH}$ -type intermediates. Their reaction with arylfluorides yield the HDF product, regenerating the iron-fluoride catalyst. This study demonstrated the catalytic potential of iron-BDK-complexes in challenging HDF, a field frequented by precious-metal catalysts.²⁹

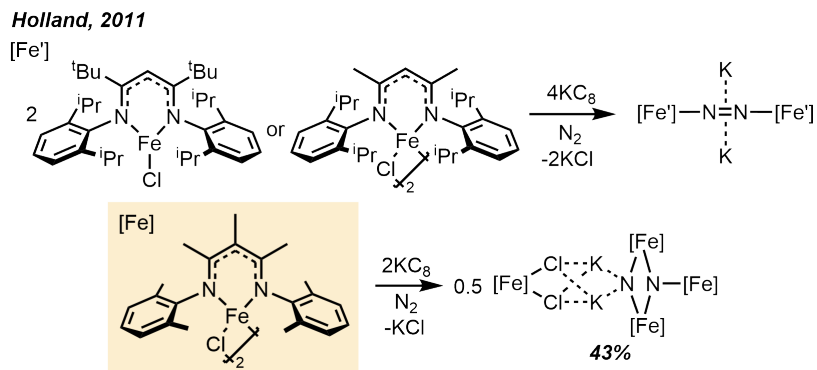
Hessen, 2006



Scheme 1.2.4: Synthesis of three-coordinate (BDK)Fe(alkyl) complexes, reported by Hessen and co-workers.³⁰

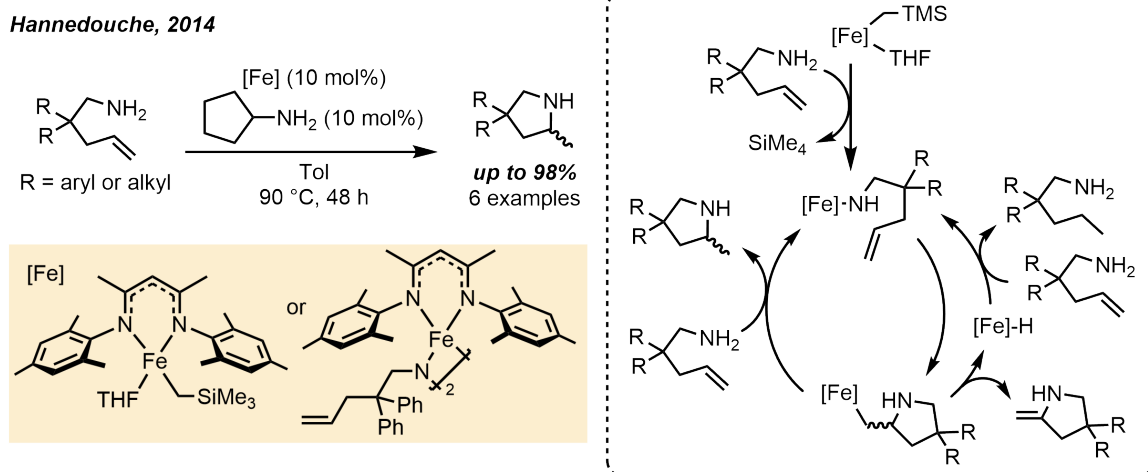
The isolation of three-coordinate iron-alkyl species were described by Hessen and co-workers (scheme 1.2.4).³⁰ Salt-metathesis of $(\text{dippBDK})\text{FeCl}_2\text{Li}(\text{THF})_2$ with LiCH_2TMS or PhCH_2MgBr , yields iron-alkyl complexes $(\text{dippBDK})\text{FeCH}_2\text{TMS}$ and $(\text{dippBDK})\text{FeCH}_2\text{Ph}$, respectively. It was later demonstrated that the iron-carbon bond can be cleaved to access a range of catalytically active species. This activation event underpins mechanistic understanding for many (BDK)Fe(alkyl)-catalysed processes (*vide infra*).

Holland and co-workers later utilised the iron-BDK for the homogeneously-mediated cleavage of N_2 (scheme 1.2.5).³¹ The reaction of potassium graphite (KC_8) with $(\text{dippBDK}^{\text{tBu}})\text{FeCl}$ or $[(\text{dippBDK}^{\text{Me}})\text{FeCl}]_2$ yielded $\text{K}_2(\text{BDK})\text{FeNNFe}(\text{BDK})$ complexes.³² However, reaction of $[(\text{dmpBDK}^{\text{Me,Me}})\text{Fe}(\mu\text{-Cl})]_2$ ($\text{dmp} =$



Scheme 1.2.5: (BDK)Fe-mediated N_2 reduction, reported by Holland and co-workers.³¹

2,6-dimethylphenyl) with KC_8 yielded a tetrameric iron-bis-nitride complex. Exposing this species to excess H_2 generated $[(\text{dmpBDK}^{\text{Me,Me}})\text{Fe}(\mu\text{-H})]_2$ and KCl . Unfortunately, ammonia does not form under these conditions and the nitrogen-based products were not determined. Nevertheless, the reduced steric bulk of the $\text{dmpBDK}^{\text{Me,Me}}$ ligand is required to access the congested tetrameric bis-nitride complex. Thus, this study is a pertinent example of BDK ligand sterics influencing reactivity.

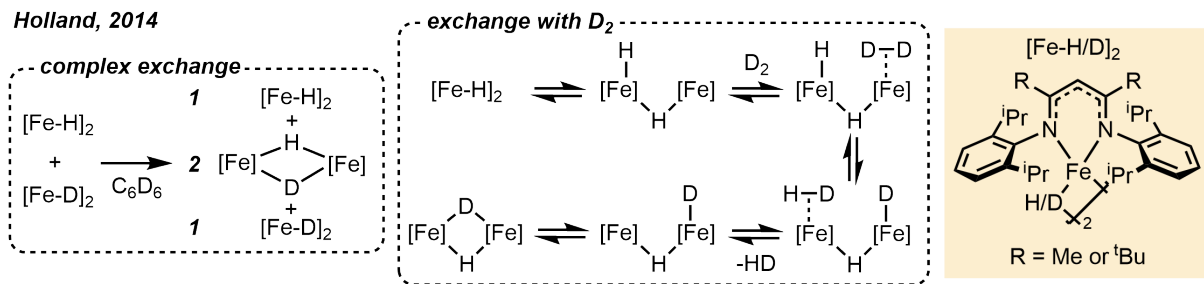


Scheme 1.2.6: $(\text{mes}^{\text{BDK}})\text{FeCH}_2\text{TMS}(\text{THF})$ - and $(\text{mes}^{\text{BDK}})\text{FeNR}$ -catalysed intramolecular hydroamination of primary aliphatic alkenylamines, reported by Hannedouche and co-workers.³³

Another influential synthetic example is the $(\text{mes}^{\text{BDK}})\text{FeCH}_2\text{TMS}(\text{THF})$ -catalysed ($\text{mes} = 2,4,6$ -mesityl) intramolecular hydroamination (HA) of primary aliphatic alkenylamines, reported by Hannedouche and co-workers (scheme 1.2.6).³³ This is attributable to the dominance of late-transition metal catalysts for HA, and is the first example of an iron-BDK catalysing a hydrofunctionalisation reaction.³⁴ A range of primary alkenylamines were tolerated with excellent yield (85-98%). Pre-catalyst and substrate protonolysis yields an iron-amido catalyst and SiMe_4 . Alkene insertion generates an iron-alkyl intermediate which is liberated by protonolysis with a second equivalent of substrate, yielding the HA product. Since then, the iron-BDK has been deployed for other highly atom-efficient hydrofunctionalisation reactions (hydroboration and inter- and intramolecular hydrophosphination).³⁵

The intricacies of (BDK)Fe-H chemistry were examined further by Holland and co-workers (scheme

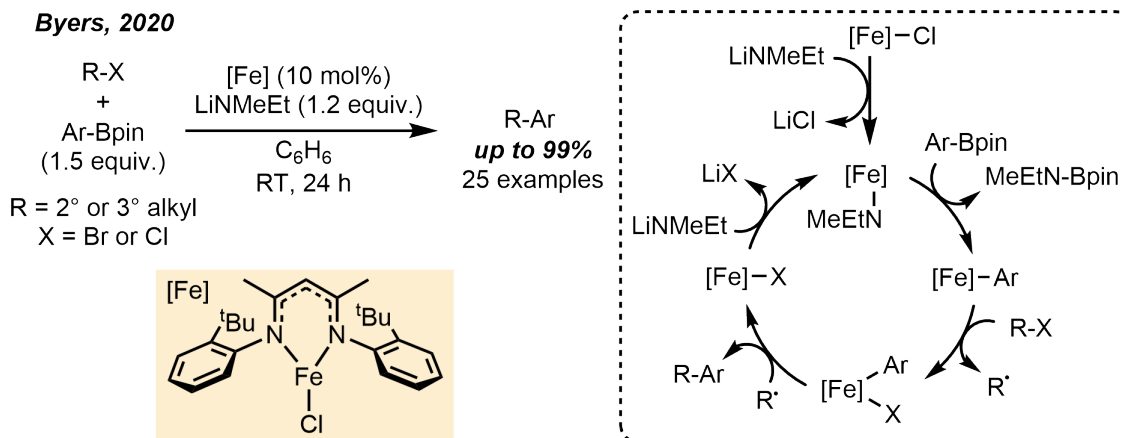
Holland, 2014



Scheme 1.2.7: Hydrogen/deuterium exchange in (BDK)FeH complexes, reported by Holland and co-workers.³⁶

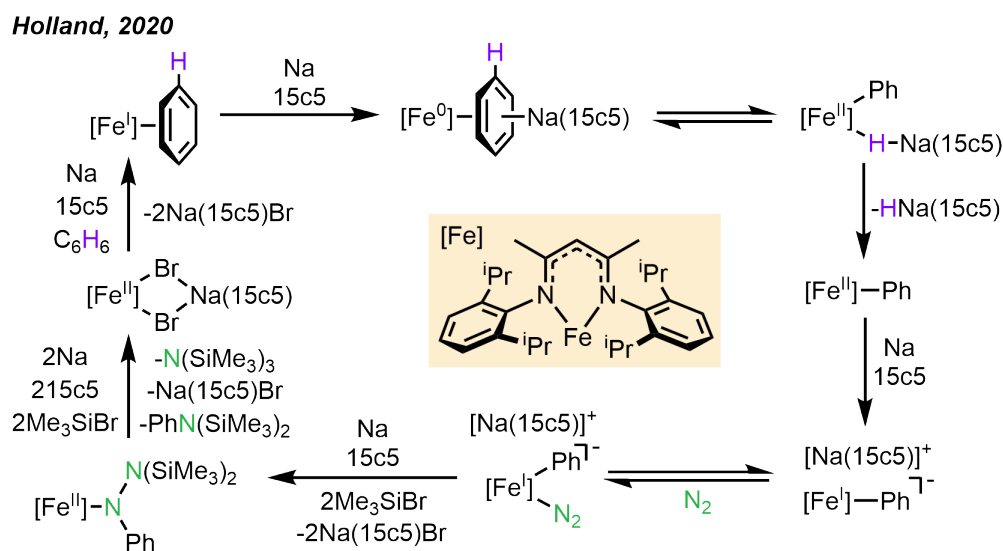
1.2.7.³⁶ [(dippBDK^{Me})Fe(μ -H/D)]₂ and [(dippBDK^{tBu})Fe(μ -H/D)]₂ complexes were synthesised from the corresponding (BDK)FeCl, by reduction with KC₈ followed by H₂/D₂ binuclear oxidative addition.³⁷ At equilibrium, [(dippBDK^{Me})Fe(μ -H)]₂ exists in dimeric form. However, for more spatially confined (dippBDK^{tBu})Fe(μ -H), an approximate 1:1 ratio of mononuclear to dinuclear complex is observed by ¹H NMR spectroscopy. Equilibrium distribution demonstrated yet again the impact of BDK ligand sterics on reactivity. Upon mixing [(dippBDK^{Me/tBu})Fe(μ -H)]₂ and [(dippBDK^{Me/tBu})Fe(μ -D)]₂, three isotopologues were observed in the ¹H NMR spectrum in a 1:2:1 ratio. Peaks were assigned to complexes [(BDK)Fe(μ -H)]₂, [(BDK)Fe(μ -H/D)]₂ and [(BDK)Fe(μ -D)]₂ respectively, products of statistical redistribution. This observation demonstrated the ability of hydride complexes to undergo intermolecular H/D-exchange. When exposing isotopologue [(dippBDK^{Me})Fe(μ -H)]₂ to excess D₂, exclusive formation of [(dippBDK^{Me/tBu})Fe(μ -D)]₂ is observed in the ¹H NMR spectrum. Under excess H₂, [(dippBDK^{Me/tBu})Fe(μ -H)]₂ is regenerated. These experiments demonstrated [(BDK)Fe(μ -H/D)]₂ complexes are able to activate H₂/D₂. This exchange is expected to proceed via an ‘open’ [(BDK)FeH(μ -H)Fe(η^2 -D₂)(BDK)] intermediate. Isotope exchange occurs yielding [(BDK)Fe(η^2 -HD)(μ -H)FeD(BDK)]. HD dissociation forms [(BDK)Fe(μ -H/D)]₂. This mechanistic insight underpins isotope exchange chemistry described in chapter 2.

Byers, 2020



Scheme 1.2.8: (BDK)FeCl-catalysed Suzuki-Miyaura cross-coupling of aromatic boronic esters and 1° and 2° alkyl electrophiles, reported by Byers and co-workers.³⁸

In search for earth-abundant catalysts for Suzuki-Miyaura cross-coupling (CC), Byers and co-workers described the iron-catalysed CC of heteroaromatic boronic esters with 2° and 3° alkyl electrophiles (scheme 1.2.8).³⁸ The modularity of the BDK ligand allowed for systematic design, where a (*o*-*t*BuBDK^{Me})FeCl complex emerged as the leading pre-catalyst for the CC reaction, balancing sterics and activity. (*o*-*t*BuBDK^{Me})FeCl with stoichiometric LiNMeEt, undergoes CC of various sp²-heteroaromatic boronic esters with 2° and 3° alkyl halides (up to 99% and 92%, respectively), scarcely found substrates in CC reactions. On-cycle (BDK)Fe(NMeEt) forms by reaction of the pre-catalyst with LiNMeEt. Transmetalation yields a (BDK)FePh intermediate and MeEtNBpin, which undergoes halogen atom abstraction with alkyl halides forming (BDK)FePh(X) and a carbon-centred radical. The radical is quenched by the iron-phenyl bond, furnishing the CC product and (BDK)FeX. Reaction with a second equivalent of LiNMeEt regenerates the catalyst. This study demonstrated how the tunability of BDKs can be harnessed to achieve reactivity comparable to that of precious metals.



Scheme 1.2.9: (BDK)FePh-mediated N₂ and hydrocarbon coupling, reported by Holland and co-workers (15c5 = 15-crown-5).¹⁴

The final select example, and perhaps the most impressive feat in iron-BDK chemistry to date, Holland and co-workers described the iron-mediated coupling of N₂ and benzene (scheme 1.2.9).¹⁴ Reduction of (^{dipp}BDK^{Me})Fe^I($\eta^6\text{-C}_6\text{H}_6$) with sodium metal in the presence of 15-crown-5 (15c5) yielded (BDK)Fe⁰(C₆H₆)Na(15c5). This species is in equilibrium with a (BDK)Fe^{II}(Ph)(HNa(15c5))- a product of benzene C-H oxidative addition. The latter complex decays into (BDK)Fe^{II}(Ph) and HNa(15c5). A second reduction with sodium metal and 15c5 forms $[(\text{BDK})\text{Fe}^{\text{I}}(\text{Ph})][\text{Na}(15\text{c}5)]$, which can bind N₂, yielding (BDK)Fe^I(Ph)(N₂). Silylation and reduction with Me₃SiBr, sodium metal and 15c5 forms a (BDK)Fe^{II}N(Ph)(N(SiMe₃)₂) hydrazido complex- a product of formal aryl migration. A second silylation and reduction generated a (BDK)Fe^{II}($\mu\text{-Br}$)₂Na(15c5) complex and N₂-activated products- PhN(SiMe₃)₂ and N(SiMe₃)₃. Notably, all intermediates were isolated and crystallographically characterised. This study represented the first example of CC between N₂ and C-H bonds, and is pertinent in the field on nitrogen fixation chemistry. The transformation required the isolation of a range of highly reactive three-

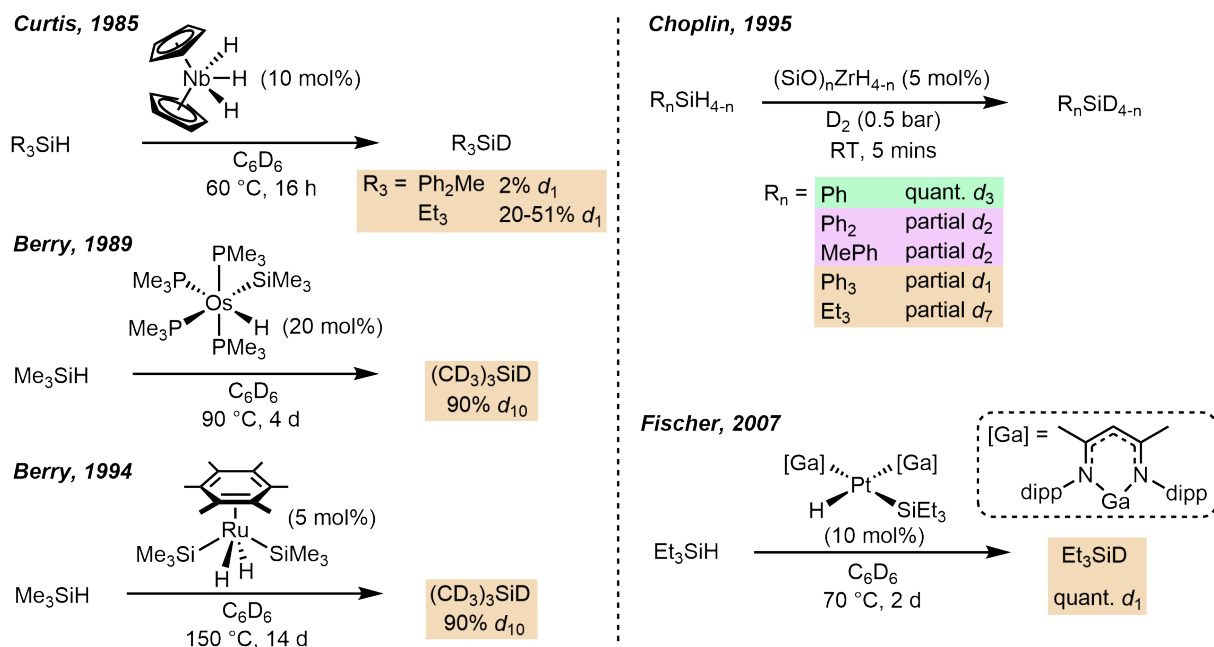
and four-coordinate species, in an array of oxidation states. Such a feat bears testimony to BDK ligand stabilisation.

Regardless of the research motivation (for example, finding sustainable catalytic alternatives, mechanistic understanding of naturally occurring processes or fundamental curiosity-driven research), these examples testify to the ongoing interest in iron-BDK-mediated transformations. Reactivity differences are commonly attributed to the steric properties of the BDK. Because of its inherent modularity, numerous avenues remain for exploring and tuning reactivity in these complexes. This thesis describes the exploration of iron-BDK chemical space through ligand substitution. This led to a broad project encompassing a range of transformations. Hence, each chapter features an independent introduction surveying the chemistry it entails.

Chapter 2

Iron-catalysed H/D Exchange of Primary, Secondary and Tertiary Silanes, Tertiary Siloxanes and Pinacolborane

2.1 Introduction



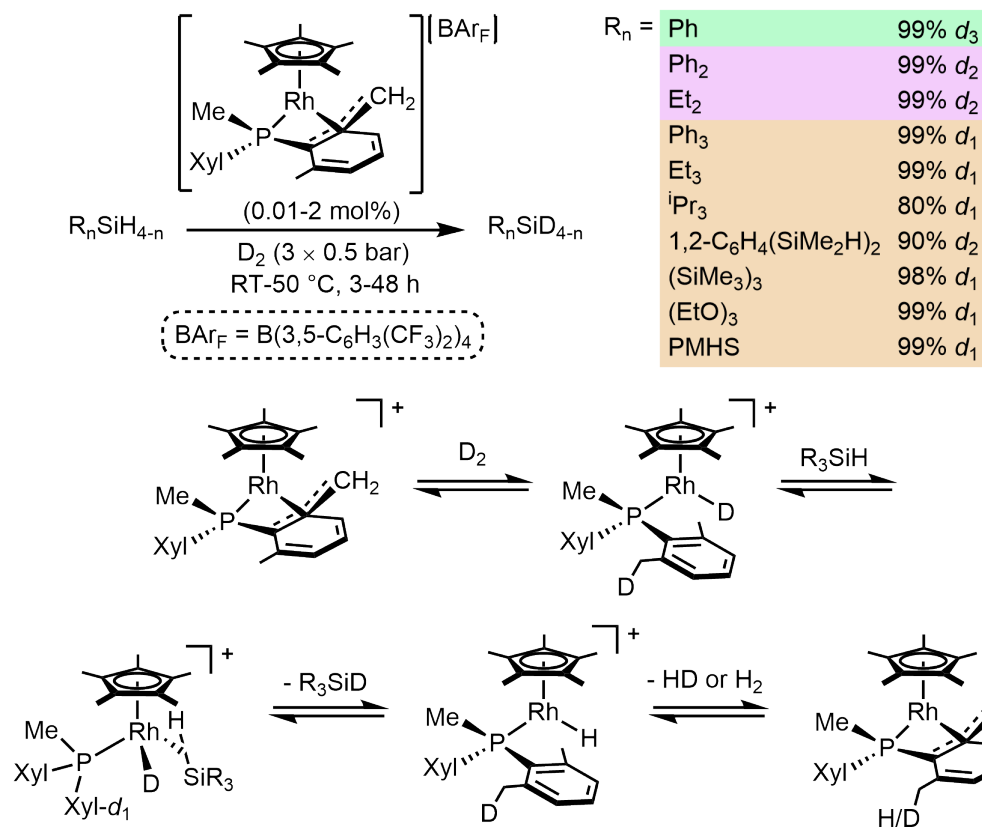
Scheme 2.1.1: Early reports of catalytic H/D exchange of silanes.^{39–43}

Techniques in a chemist's arsenal that uncover precise detail of chemical transformations are vital for mechanistic understanding and reaction design. Isotopic-labelling is such a tool. Qualitative analysis of the distribution of deuterium atoms provide mechanistic evidence, whilst kinetic isotope effect (KIE) provides quantitative detail regarding rate-determining bond-breaking events.⁴⁴ Furthermore, need for deuterium-labelled products extends to the pharmaceutical industry. In 2017, deutetribenzazine (treatment for side effects of Huntington's disease) was approved for use, representing the first example of a deuterium-labelled medicine.⁴⁵ Therefore, methods for facile and selective deuterium-labelling of molecules are in demand.

Deuterosilanes are routinely deployed isotopically-labelled reagents, a function of their ubiquitous use as reducing agents (including but not limited to, hydrosilylation, carbon-halogen bond reduction and synthesis of metal-hydride complexes).^{24,46,47} Despite broad use, methods for their synthesis are few. Deuterosilanes are traditionally prepared by reaction of chlorosilane (Cl_nSiR_{4-n}) with air- and moisture-sensitive, metal-deuteride ($n NaBD_4$ or $LiAlD_4$). This yields the corresponding deuterosilane with stoichiometric quantity of waste metal salt. Furthermore, highly reducing metal-deuterides are associated with poor functional group tolerance. These issues have been circumvented with the emergence of catalytic methods for synthesising deuterosilanes.

Early reports of silane H/D exchange arose from activation of deuterated solvent. The first catalytic silane H/D exchange was discovered by Butler and co-workers in 1985.³⁹ Exposing complex Cp_2NbH_3 to $MePh_2SiH$ or Et_3SiH in a solution of C_6D_6 , $MePh_2SiD$ and Et_3SiD were formed in 2% and 20–51% H/D exchange, respectively. Dehydrocoupling (DHC) of Cp_2NbH_3 with an equivalent of silane forms silyl complex, $Cp_2Nb(SiR_3)H_2$. Reductive elimination forms R_3SiH and Nb(III) complex, Cp_2NbH . This intermediate can reversibly activate a benzene C–D bond, liberating Cp_2NbD , through intermediate $Cp_2NbH(D)(C_6H_5)$. Reversible silane insertion then generates the observed deuterosilane.

Carmona, 2010



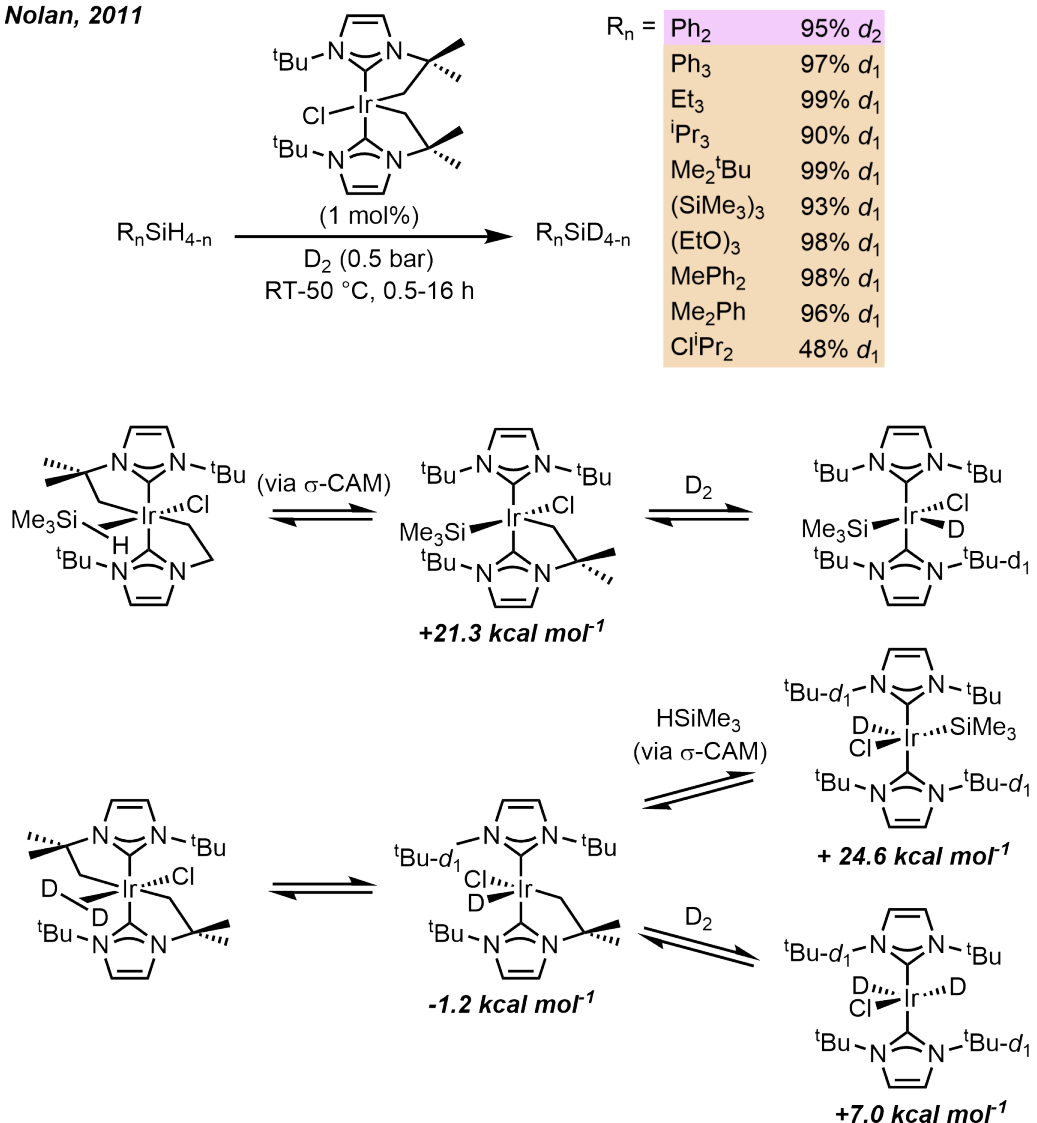
Scheme 2.1.2: The first general method for the catalytic H/D exchange of silanes, reported by Carmona and co-workers.⁴⁸

Similar reactivity was observed for (PMe₃)₄OsH(SiMe₃) and (C₆Me₆)RuH₂(SiMe₃)₂ complexes, reported by Berry and co-workers.^{40,41} Reversible C-D and Si-H bond activation yielded (D₃C)₃SiD with 90% deuterium incorporation at silicon in both cases after reflux for 4 and 14 days, respectively. Notably, the propensity of these complexes to undergo reversible β -hydride elimination of silyl ligands led to poor selectivity for silicon H/D exchange, furnishing trimethylsilane-*d*₁₀.

In search of heterogeneous catalysts for synthesis of poly(silanes), Choplin and co-workers uncovered the first example of catalytic silane H/D exchange from deuterium gas.⁴² A supported zirconium-hydride catalyst facilitated H/D exchange of PhSiH₃. PhSiD₃ was generated with quantitative deuterium incorporation, determined by infrared (IR) spectroscopy and mass spectrometry (MS). Partial H/D exchange was observed for secondary and tertiary silanes, with Et₃SiH undergoing C-H activation, yielding (H₃CD₂C)₃SiD with partial H/D exchange.

The reversible oxidative addition and reductive elimination was demonstrated again by Fischer and co-workers.⁴³ A ((BDK)Ga)₂PtH(SiEt₃) complex facilitates catalytic H/D exchange of Et₃SiH with C₆D₆, forming Et₃SiD in quantitative yield. The authors propose the platinum(II) precursor undertakes C-D activation yielding a platinum(IV)-hydride-deuteride intermediate.

Nolan, 2011



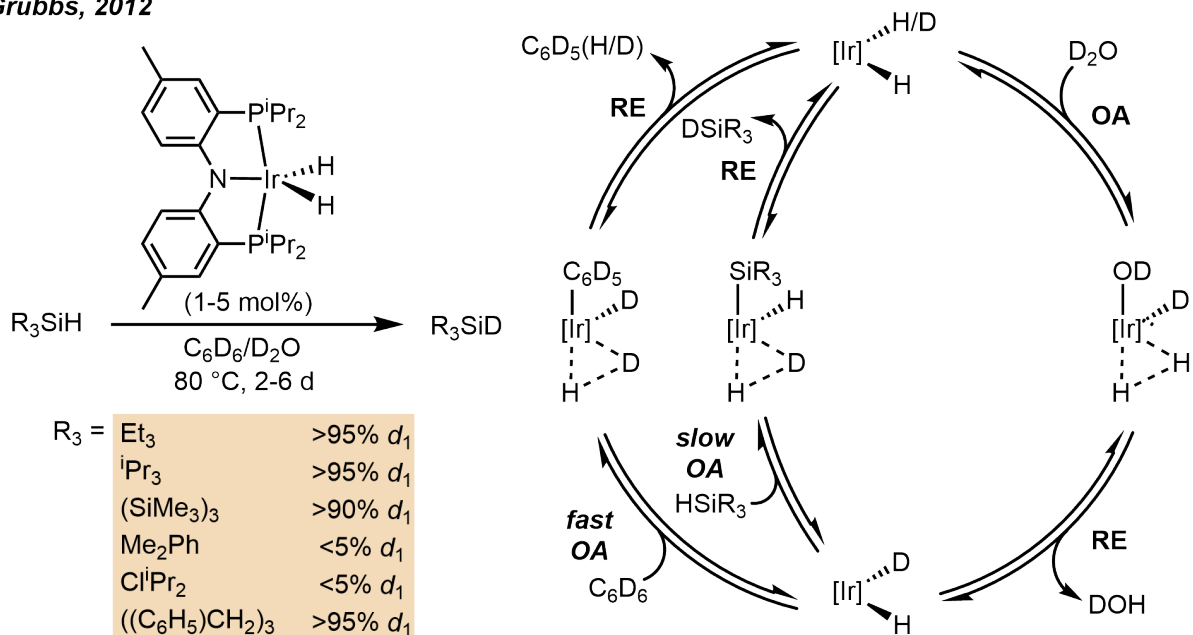
Scheme 2.1.3: The iridium-catalysed H/D exchange of silanes, reported by Nolan and co-workers.⁴⁹

The first general method for the catalytic H/D exchange of silanes was demonstrated by Carmona and co-workers.^{48,50} A $[\text{Cp}^*\text{Rh}(\text{PMe}(\text{Xyl})_2)]^+$ complex catalysed the H/D exchange of primary, secondary and tertiary silanes and siloxanes. At low catalyst loading, near complete D-incorporation was observed for most substrates tested, albeit with three charges of D_2 . Owing to the rare $\kappa^4\text{-P,C,C',C''}$ coordination of the phosphine, metal-ligand cooperation facilitated the activation of D_2 gas, forming rhodium-deuteride, $[\text{Cp}^*\text{RhD}(\text{PMe}(\text{xyl})_2)]^+$. This complex was demonstrated to exchange with Si-H bonds. The authors indicated this proceeds via a σ -silane intermediate. However, theoretical methods suggested coordination of a Si-H bond is not thermodynamically feasible.

In 2011, Nolan and co-workers reported the iridium-catalysed isotopic-labelling of silanes, shown in **2.1.3**.⁴⁹ With a single charge of D_2 gas, excellent deuteration was achieved for a range of secondary and tertiary silanes. By combination of experimental and DFT studies, the authors demonstrate facile reversible activation of D_2 with the catalyst. The authors proposed silane H/D exchange is promoted by σ -complex assisted metathesis (σ -CAM). However, silane addition via σ -CAM to the iridium-carbon

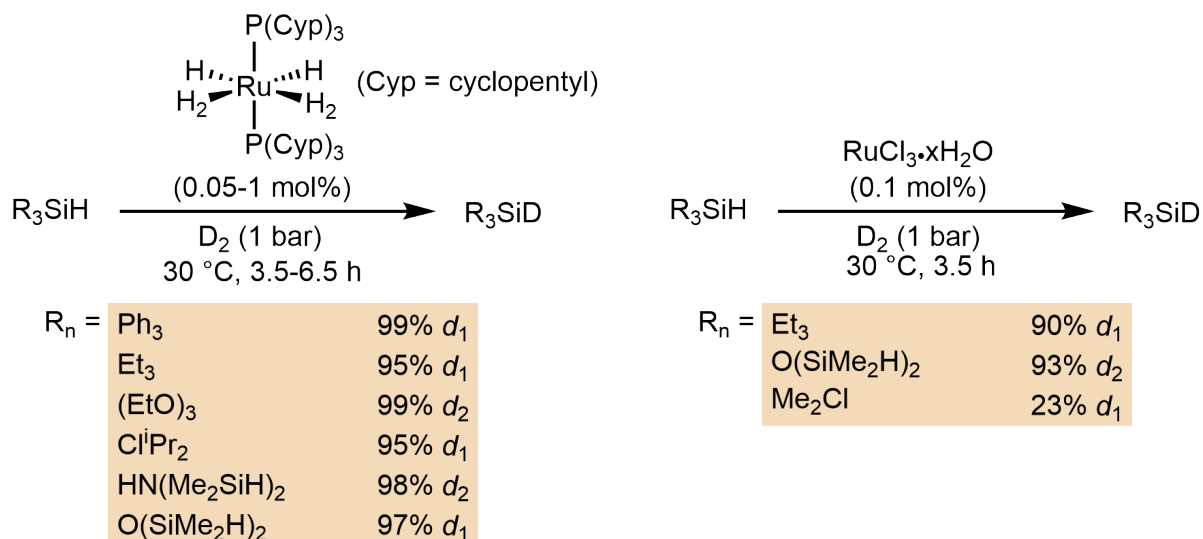
bond of the catalyst is not observed stoichiometrically. This is corroborated by corresponding iridium-silyl intermediates being high in energy. Disproving σ -CAM related mechanisms, the authors recognise silicon H/D exchange at iridium-deuteride centres is complex.

Grubbs, 2012



Scheme 2.1.4: The iridium-catalysed H/D exchange of silanes reported by Grubbs and co-workers.⁵¹

Sabo-Etienne, 2014



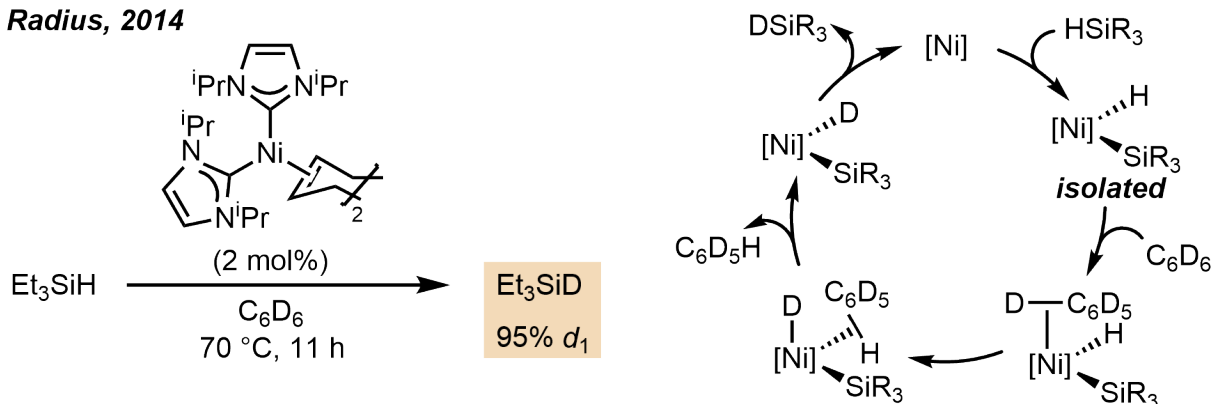
Scheme 2.1.5: The ruthenium-catalysed H/D exchange of silanes, reported by Sabo-Etienne and co-workers.⁵²

In 2012, Grubbs and co-workers reported the iridium-catalysed H/D exchange of aromatic carbon-hydrogen bonds.⁵¹ This method was extended to include deuterium labelling of silanes in a solution of D_2O and C_6D_6 . Only four tertiary substrates were tolerated in up to 95% D-incorporation. Furthermore, exchange requires long reaction times and high temperatures. This is because the rate of C-H insertion

($5.4 \times 10^{-3} \text{ min}^{-1}$) into the iridium-hydride catalyst was estimated as being twice as fast as Si-H ($2.7 \times 10^{-3} \text{ min}^{-1}$). Hence, C-H oxidative addition outcompetes that of Si-H. Therefore, poor selectivity leads to extended reaction times.

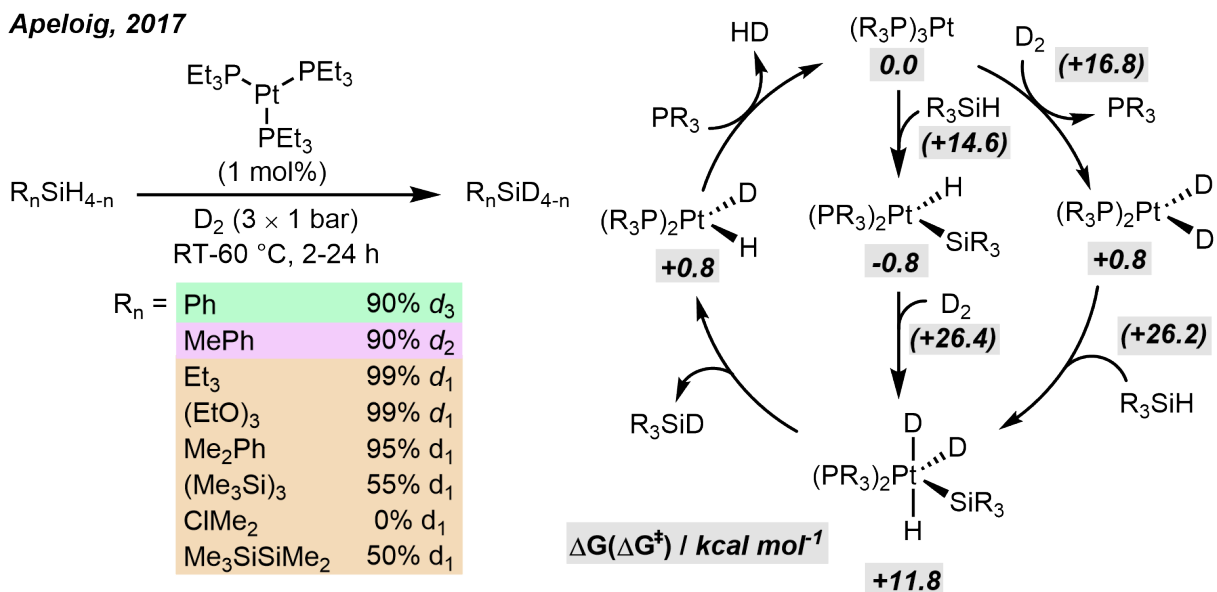
Sabo-Etienne and co-workers followed with a ruthenium-catalysed deuterium-labelling of silanes.⁵² $\text{RuH}_2(\eta^2\text{-H}_2)_2(\text{PCyp}_3)_2$ and $\text{RuCl}_3 \cdot x\text{H}_2\text{O}$ facilitated the H/D exchange of a range of tertiary silanes with D_2 gas. Reaction of analogous $\text{RuH}_2(\eta^2\text{-H}_2)_2(\text{PCyp}_3)_2$ with $\text{O}(\text{SiMe}_2\text{H})_2$, gave chemical shifts in the ^1H and ^{31}P NMR spectrum corresponding to a $\text{RuH}_2((\eta^2\text{-HSiMe}_2)_2\text{O})(\text{PCyp}_3)_2$. Complexes of this type catalysed the H/D exchange of the coordinated silane.⁵³ Despite this evidence for substrate coordination, the mechanism for H/D exchange at silicon is unclear.

Radius, 2014



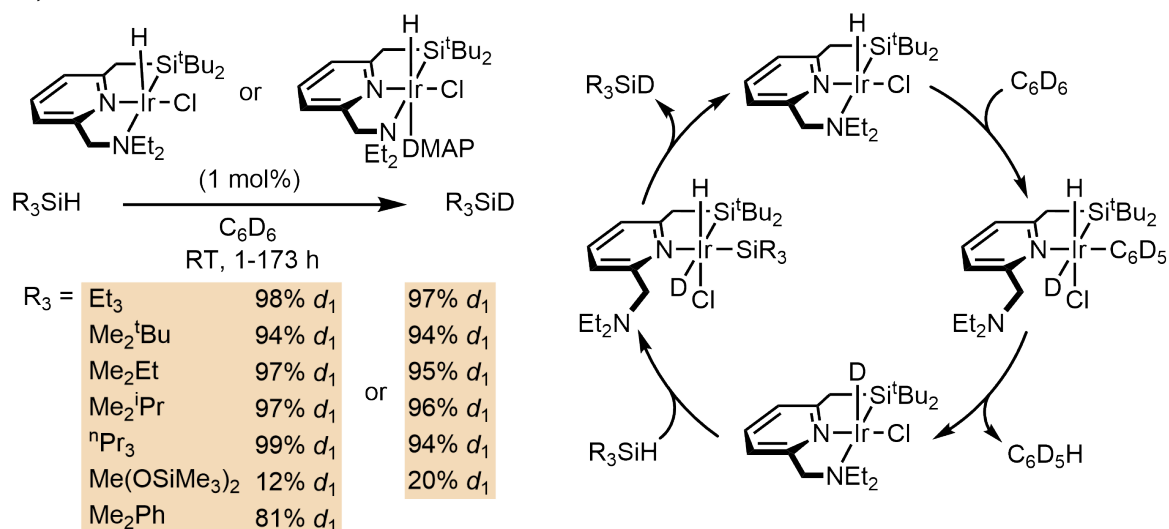
Scheme 2.1.6: The nickel-catalysed deuterium labelling of silanes, reported by Radius and co-workers.⁵⁴

Apeloig, 2017



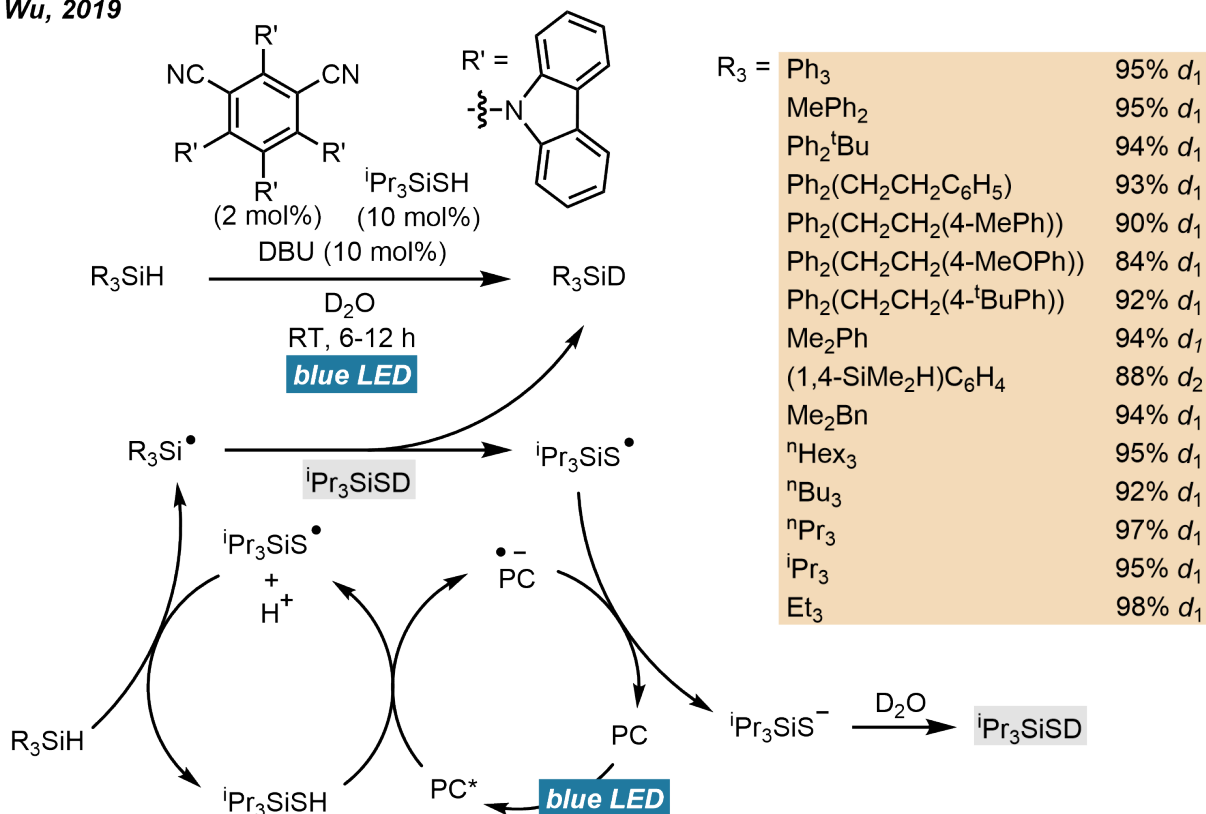
Scheme 2.1.7: The platinum-catalysed deuterium labelling of silanes, reported by Apeloig and co-workers.⁵⁵

Tobita, 2019



Scheme 2.1.8: The iridium-catalysed H/D exchange of silanes, reported by Tobita and co-workers.⁵⁶

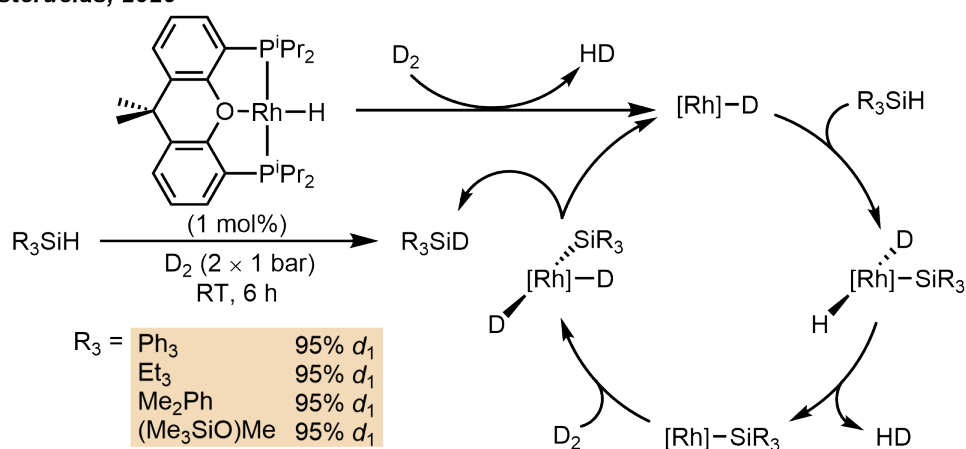
Wu, 2019



Scheme 2.1.9: The photo-catalysed H/D exchange of silanes, reported by Wu and co-workers.⁵⁷

Radius and co-workers described the H/D exchange of Et₃SiH and C₆D₆, catalysed by (Ni(NHC)₂)₂COD with 95% deuterium incorporation.⁵⁴ A range of oxidative addition products with various secondary and tertiary silanes were demonstrated, forming the corresponding *bis-N*-heterocyclic carbene nickel(II)-silyl-hydride complexes. A tentative mechanism described the σ -CAM of a C₆D₆ C-D bond, with said Ni-H bond. Surprisingly, nickel-silyl-hydride complexes were not tested in catalysis to substantiate this claim.

Esteruelas, 2020



Scheme 2.1.10: The rhodium catalysed H/D exchange of silanes reported by Esteruelas and co-workers.⁵⁸

Apeloig and co-workers detail a platinum complex, capable of catalysing the H/D exchange of silanes with D_2 .⁵⁵ Select tertiary silanes were tolerated with near complete deuterium incorporation. Notably, incomplete deuteration was achieved with primary and secondary substrates. A detailed mechanistic investigation revealed oxidative addition of silane with $(\text{Et}_3\text{P})_2\text{Pt}$ is slightly preferred to D_2 , consistent with silane addition being the first step in the catalytic cycle.

Tobita and co-workers report the iridium-catalysed H/D exchange of silanes with C_6D_6 .⁵⁶ The authors propose the hemilability of silyl-pyridine-amine pincer ligand is essential for providing a vacant coordination site for C-D or Si-H oxidative addition. The method tolerated a range of tertiary aryl and alkyl silanes in excellent H/D exchange. Notably, conditions were not tolerant of secondary diethylsilane, where no isotope exchange was observed.

The greatest scope for catalytic deuteration of silanes was described by Wu and co-workers.⁵⁷ The visible-light-mediated process was demonstrated on 15 tertiary silanes with excellent deuterium incorporation. Furthermore, under continuous flow conditions, over 61 grams of Et_3SiD were generated in 100 hours, at reduced D_2O , photocatalyst and hydrogen atom transfer catalyst loadings. Despite the broad scope, primary and secondary silanes were not tolerated under optimised conditions. Furthermore, the equipment required for photocatalysis reduces the generalisability of the method.

Esteruelas and co-workers reported the most recent example of catalytic silane H/D exchange.⁵⁸ POP-pincer ligated rhodium-hydride complex catalysed the H/D exchange of four tertiary silanes in excellent deuterium incorporation. Notably, the method was extended to other substrates, pinacolborane (HBpin), catecholborane (HBCat), triethylgermane (Et_3GeH), triphenylgermane (Ph_3GeH) and triphenylstannane (Ph_3SnH) in near complete H/D exchange.

Despite the emergence of reports into the catalytic H/D exchange of silanes, for all substrates tested, 90% consist of tertiary silanes. Only four reports include primary or secondary silanes, with a total of 9 examples, shown in figure 2.1.1. These show reduced activity in the catalytic H/D exchange reaching incomplete deuterium incorporation or requiring multiple charges of D_2 . The steric contribution from tertiary silanes is larger than primary or secondary silanes. Therefore, sterics are an unlikely culprit for

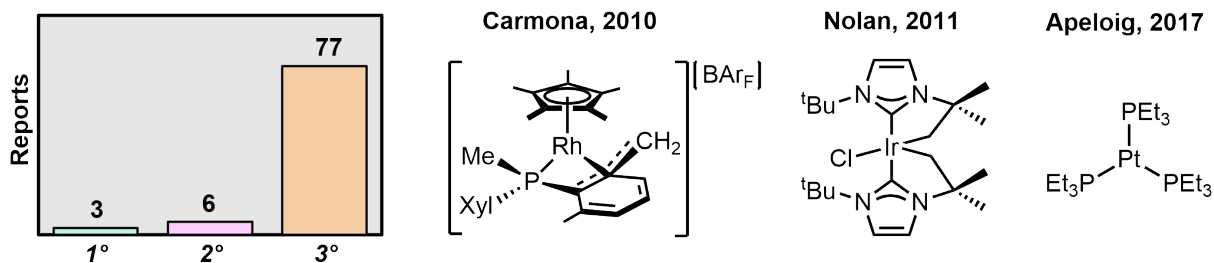
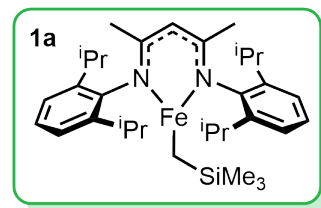
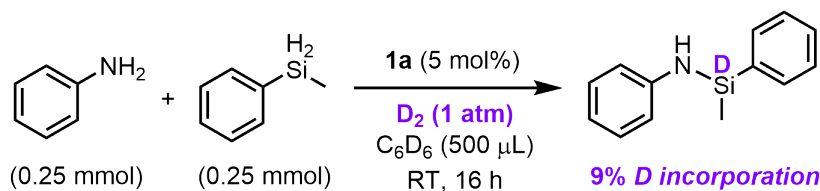
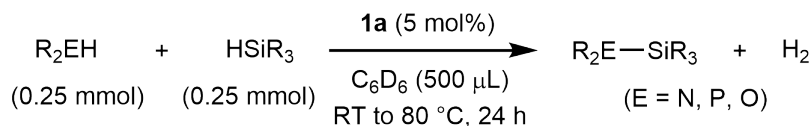


Figure 2.1.1: Number of examples for the catalytic H/D exchange of primary, secondary and tertiary silanes, and homogeneous catalysts that facilitate the H/D exchange of primary and secondary silanes (PhSiH_3 , Et_2SiH_2 , Ph_2SiH_2 and MePhSiH_2).

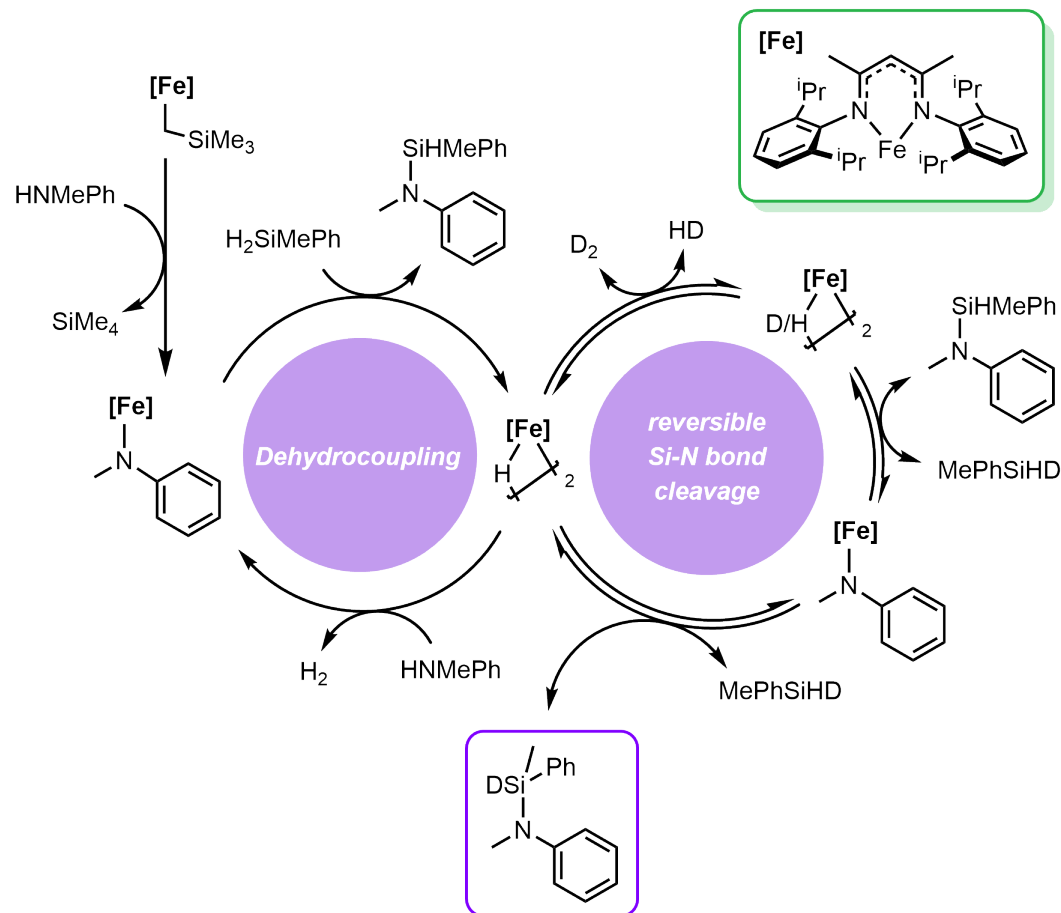
the increased activity observed for tertiary silanes. Instead, electronic factors contribute more significantly. Most reports of catalytic silane H/D exchange described require reversible oxidative addition of a Si-H bond; Silane hydricity strength follows the order $3^\circ > 2^\circ > 1^\circ$, where the developing positive charge at silicon is more inductively stabilised.⁵⁹ Therefore, oxidative addition can be expected to be more facile for weaker, tertiary silane Si-H bonds. Furthermore, the more electron rich silicon will have enhanced σ -donation in the resulting silyl-to-metal bond.⁶⁰ Therefore, it is no surprise that tertiary silanes dominate the catalytic H/D exchange literature.

Webster, 2020:



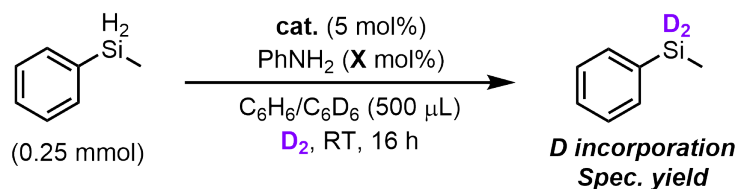
Scheme 2.1.11: Previous work into iron-catalysed DHC of silanes (top) and reversibility investigation (bottom).⁶¹

Previous work by Webster and co-workers demonstrated the facile DHC of silanes with amines, alcohols or phosphines catalysed by pre-catalyst **1a**, shown in scheme **2.1.11**.⁶¹ A mechanistic investigation revealed **1a** reacts with the proton source generating an on-cycle iron-amido species, shown in figure **2.1.12**. Reaction with silane generates the silazane product and a dimeric iron-hydride intermediate. Reaction with a second equivalent of amine regenerates the iron-amido complex and an equivalent of H_2 gas. When the reaction was performed under 1 atmosphere of D_2 gas, some deuterium incorporation was observed at silicon in the generated silazane, shown in figure **2.1.11**. (BDK)FeH complexes have been shown to rapidly exchange with D_2 gas, generating the corresponding iron-deuteride.³⁶ It was hypothesised that the reversible cleavage of the silazane Si-N bond with (BDK)FeD generates deuteriosilane *in situ*. This can dehydrocouple with amines yielding the observed deuteriosilazane.



Scheme 2.1.12: Mechanism for the iron-catalysed DHC and hypothesis for observed deuterium incorporation.

These observations indicate that with co-catalytic amounts of amine and excess D_2 gas, equilibrium could be perturbed to yield the secondary deuteriosilane as the major product. This chapter reports the optimisation, scope and mechanistic investigation into the first iron-catalysed isotope exchange of silanes. Steric tuning facilitates access to a range of primary, secondary and tertiary silanes, tertiary siloxanes and pinacolborane in near quantitative hydrogen/deuterium (H/D) exchange. A combination of experimental and density functional theory (DFT) investigations reveals a plausible mechanism for the transformation based on an iron-hydride intermediate.

Table 2.2.1: H/D exchange of methylphenylsilane and D₂ optimisation.

Entry	cat.	X / mol%	D incorporation ^a (%)	Spec. yield ^b (%)
1 ^c	1a	10	95	n.d.
2	1a	10	94	n.d.
3 ^d	1a	10	89	n.d.
4	1a	5	94	95
5	1a	-	92	93
6	-	-	0	n.d.
7	Fe(acac) ₂	-	0	n.d.
8	FeCl ₂ .THF _{1.5}	-	0	n.d.
9	^{dipp} BDKFe(μ-Cl) ₂ Li(THF) ₂	-	0	n.d.
10	^{dipp} BDK	-	0	n.d.
11 ^e	1a	-	97	95

^aDetermined by ¹H NMR spectra comparing residual Si-H to Si-CH₃ or ^mAr-H after vacuum distillation and ²H NMR spectra. ^bDetermined by ¹H NMR spectra comparing Si-CH₃ or ^mAr-H to 0.25 mmol 1,3,5-trimethoxybenzene after vacuum distillation. ^cStirred for 72 h. ^dReaction performed in 30 mL ampoule instead of 60 mL. ^eD₂ filled over liquid nitrogen (4 atm).

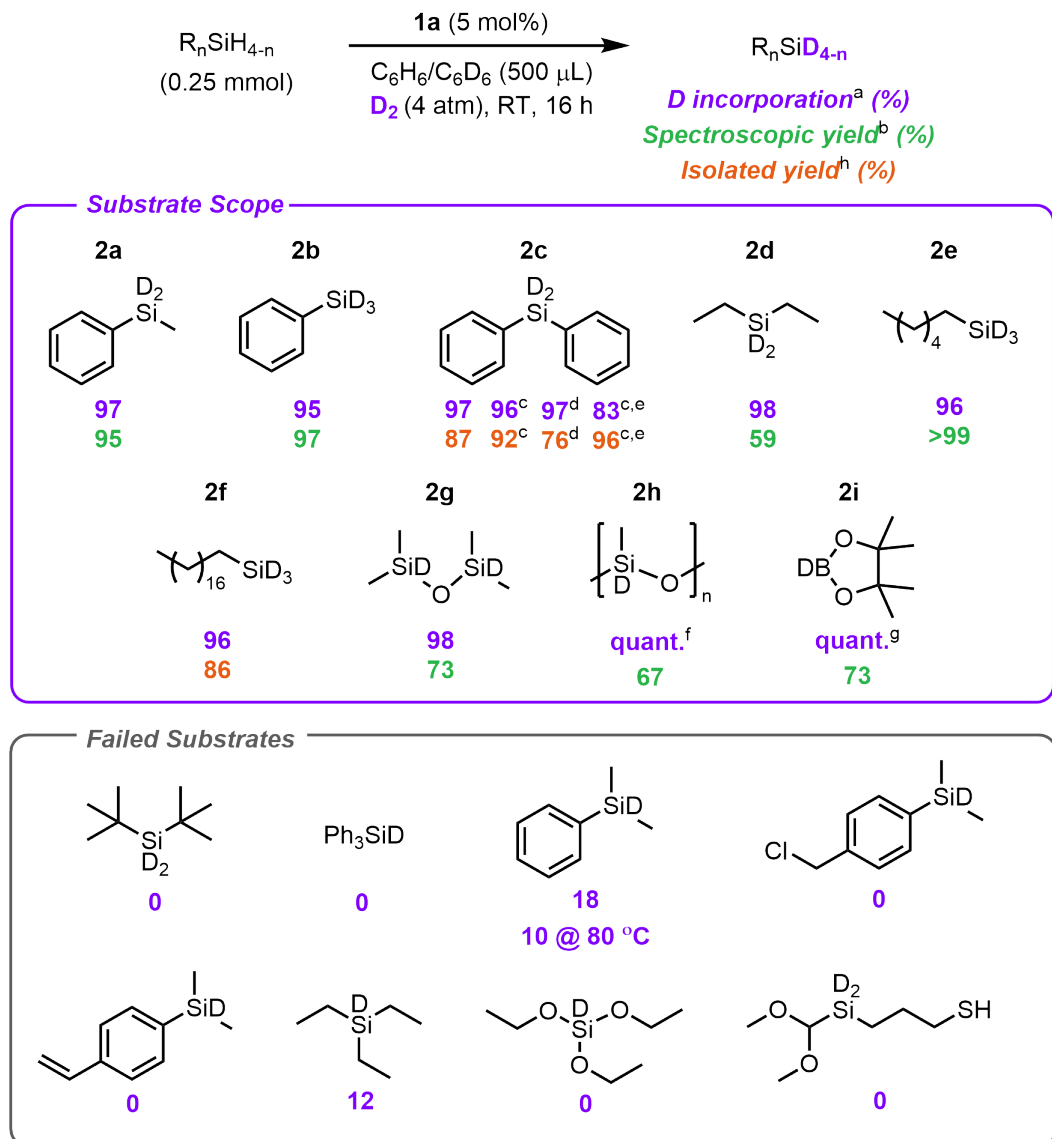
2.2 H/D Exchange of Primary and Secondary Silanes, Tertiary Siloxanes and Pinacolborane

2.2.1 Optimisation

Following the hypothesis proposed in section 2.1, optimisation began by exposing methylphenylsilane to co-catalytic amounts of **1a** (5 mol%) and aniline (10 mol%), under 1 atm of D₂ for 72 hours. Following isolation by vacuum distillation away from the paramagnetic species, deuterium incorporation was determined by ¹H, ²H and ²⁹Si NMR spectroscopy. Near complete loss of the Si-H peak was observed in the ¹H NMR spectrum, with a corresponding peak appearing in the ²H NMR spectrum. Notably, deuterium incorporation was only observed at silicon (by ²H NMR), indicating C-H activation and H/D-exchange is not operating. Deuterium incorporation was further confirmed by the formation of a pentet in the ²⁹Si NMR spectrum, arising from coupling between silicon and two deuterium atoms (I=1). Methylphenyl(silane-*d*₂) was generated in 95% H/D exchange (2.2.1, entry 1). The reaction time could be lowered to 16 hours with no impact on H/D exchange (94%, 2.2.1, entry 2). Reducing the volume of the reaction vessel from 60 mL, to 30 mL had a small impact on isotope exchange, reducing to 89% (2.2.1, entry 3). Based on these volumes and using the ideal gas equation ($pV = nRT$), approximately 4.90 and 2.45 mmol of deuterium atoms are present at 1 atmosphere, respectively. At equilibrium, this creates a maximum theoretical H/D exchange of 91% and 83%, respectively. The observed deuteration is higher than the theoretical maximum. This is attributed to error in ¹H NMR spectrum integration (despite baseline correction and resolved peaks) and the estimated flask volume. The reaction proceeds in the absence of aniline, indicating a proton source is not required to access the active catalytic species (2.2.1, 5). Hence, an alternative

mechanism is operating to that proposed in section **2.1**. Complex **1a** is required for reactivity to occur (**2.2.1**, entry 6). An alternative Lewis-acid, Fe(acac)₂, was inactive in catalysis (**2.2.1**, entry 7). Precursors to **1a** showed no activity in the isotope exchange (**2.2.1**, entries 8-10). Finally, maximum H/D exchange was observed when the ampoule was filled and sealed at 1 atmosphere over liquid nitrogen, in 97% H/D exchange (**2.2.1**, entry 11). This method generates approximately 4 atmospheres of deuterium gas at room temperature and a corresponding theoretical maximum H/D exchange of 98%. The reaction proceeds in deuterated and protonated solvent, confirming deuterium gas is the source of the deuterium atoms.

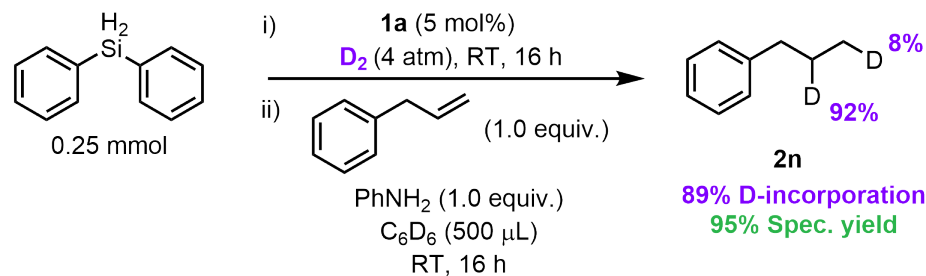
2.2.2 Substrate Scope



^aDetermined by 1H NMR spectra comparing residual Si-H to C-H. ^bDetermined by 1H NMR spectra using 1,3,5-trimethoxybenzene (0.25 mmol). ^c2.5 mmol scale. ^dReaction in pentane. ^eNeat. ^fDetermined by 2H NMR spectra comparing Si-D to toluene- d_8 (0.25 mmol). ^gDetermined by 1H , ^{11}B and $^{11}B\{^1H\}$ NMR spectra. ^hFCC (SiO_2 , pentane).

Figure 2.2.1: Substrate scope for silane, siloxane and pinacolborane H/D exchange, catalysed by **1a**.

With the optimised conditions found, investigation into the substrate scope for the silane isotope exchange was undertaken, shown in figure 2.2.1. Conditions tolerate a range of primary and secondary silanes in excellent isotope exchange and yield. Activity is maintained for activated arylsilanes, generating phenyl(silane- d_3) (**2b**) and diphenyl(silane- d_2) (**2c**) in 95% and 97% H/D exchange, respectively. Substrate **2c** tolerates a ten-fold scale-up with no impact on isotope exchange and isolated yield, at 96% and 92% respectively. Substrate **2c** forms in apolar aliphatic solvent (pentane) with no depletion in deuterium incorporation (97%). The reaction proceeds under solvent-free conditions, with **2c** isolated with 83% deuterium incorporation and 96% yield. The reduced deuterium incorporation can be attributed to



Scheme 2.2.1: 'One-pot, two-step' deuterium labelling of propylbenzene.

the poor solubility of **1a** in diphenylsilane and poor mixing in the large reaction vessel. Aliphatic primary and secondary silanes underwent isotope exchange generating diethyl(silane- d_2) (**2d**), hexyl(silane- d_3) (**2e**) and octadecyl(silane- d_3) (**2f**) in 98%, 96% and 96% H/D exchange, respectively. Two tertiary siloxanes were tolerated, yielding 1,1,3,3-tetramethyldi(siloxane- d) (**2g**) and poly(methyldeuteriosiloxane) (**2h**) in 98% and quantitative deuterium incorporation, respectively. An isolated yield for **2h** could not be obtained because the polymeric substrate blocks the silica or alumina column. Instead, deuterium incorporation was determined by the qualitative loss of Si-H peak in the 1H NMR spectrum and by comparison to internal standard in the 2H NMR spectrum.

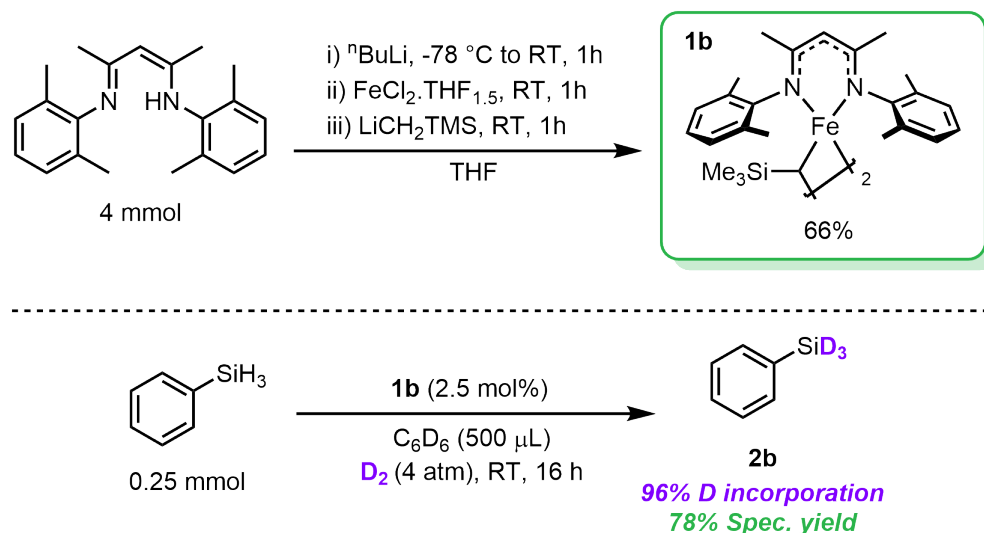
Alternative hydride source pinacolborane (**2i-H**) underwent H/D exchange with quantitative deuterium incorporation. Typically the synthesis of **2i** is challenging, requiring the generation of BD_3 from iodine and sodium borodeuteride and bubbling this through a solution of pinacol.⁶² The new procedure for H/D exchange simplifies this reaction set-up. Alternatively, D_2 deuteriumolysis of B_2pin_2 over catalytic Raney nickel at 80 °C, represents a more forcing method.⁶³ Homogeneous catalytic H/D exchange of HBpin is uncommon, typically requiring precious metal catalysts.⁶⁴⁻⁶⁷ Only two examples are known utilising earth-abundant metals. Huang and co-workers demonstrate the (^{tBu}PNN) $CoCl_2$ -catalysed synthesis of DBpin from B_2pin_2 and D_2 .⁶⁸ Thomas and co-workers describe the (^{Et}BIP) $CoCl_2$ - or (^{tBu}PNN) $FeCl_2$ -catalysed formation of DBpin by an analogous method.⁶⁹

Complimentary to the literature, bulky secondary silanes and tertiary silanes were not well tolerated under optimised conditions, even at elevated temperatures. This is tentatively attributed to the use of bulky 2,6-diisopropylphenyl, derived flanking groups on the BDK ligand. An investigation into ligand sterics on the H/D exchange of tertiary silanes is outlined in section **2.3**.

Next, the activity of pre-catalyst **1a** was investigated in the 'one-pot, two-step' deuterium labelling of allylbenzene, shown in scheme **2.2.1**. Previous work has shown that **1a** can catalyse the selective transfer hydrodeuteration of alkenes with diphenylsilane and aniline- d_2 , leading to selective deuterium incorporation at the alkene β -position.⁷⁰ Following the generation of diphenyl(silane- d_2) under standard H/D exchange conditions *in situ*, allylbenzene and aniline were added. After 16 hours, (propyl-2- d)benzene is generated with 89% deuterium incorporation, with a 92:8 ratio of deuterium atoms across the propyl 2- and 3-position, respectively (scheme **2.2.1**). This suggests that **1a** remains active following the silane H/D exchange step and is able to undergo onward reactivity. The high selectivity for the 'one-pot, two-step' hydrodeuteration is worthy of future investigation for the facile access to complex deuterium labelled products.

2.2.3 Mechanistic Investigation

Experimental Investigation



Scheme 2.2.2: Synthesis of pre-catalyst **1b** (top) and activity in H/D exchange of phenylsilane (bottom).

Outlined in section 2.1, previous work hypothesised a proton-source is required to access an on-cycle iron-amido species. Optimisation showed this is not required to facilitate silane H/D exchange. Therefore, an alternative mechanism must be invoked. Mechanistic investigation began by synthesising alternative pre-catalyst **1b**, shown in scheme 2.2.2. Complex **1b** is derived from 2,6-dimethylphenyl (DMP) flanking groups. With the intention of modelling the system using density functional theory (DFT), a smaller ligand scaffold reduces the associated computational cost. Pre-catalyst **1b** was synthesised following modified literature procedure, in 66% crystalline yield from a saturated solution in pentane at $-20\text{ }^\circ\text{C}$.⁷¹ The solid-state structure of **1b** is shown in figure 2.2.3. The structure reveals **1b** is dimeric in the solid-state, with two CH_2TMS ligands bridging the two iron centres in a 3-centre, 2-electron-type interaction.

The solution ^1H NMR spectrum of **1a** is shown in figure 2.2.2. Previous work by Holland describes the electronic structure of three-coordinate Fe(II)-BDK complexes.⁷² The distorted trigonal-planar geometry leads to z^2 and yz having similar energies. This causes orbital mixing. Spin-orbit coupling between these orbitals increases the orbital angular momentum along the x -axis (the axis of rotation that aligns these orbitals). Therefore, protons aligned with the x -axis are shifted downfield, whereas those aligned with the yz -plane are shifted upfield. The same trends in chemical shift are observed for **4a**. BDK backbone protons **d** and **e**, and CH_2SiMe_3 protons **g** are shifted upfield with chemical shifts of 78.86, 98.09 and 34.41 ppm, respectively. Protons orthogonal to the yz plane (**a-c**) are shifted downfield with chemical shifts of -68.73, -4.58 and -60.28, respectively. These trends in chemical shift suggest **4a** is monomeric, distorted trigonal-planar in solution. Diffusion-ordered spectroscopy (DOSY) could be deployed to estimate complex molecular weight in solution to deduce speciation.

Previously, **1b** had only been synthesised as the THF adduct and showed poor catalytic activity (presumed that THF blocks substrate coordination).⁷¹ **1b** was subjected to standard H/D exchange con-

ditions, scheme **2.2.2** (bottom). Activity is retained for pre-catalyst **1b** with phenyl(silane- d_3) generated in 96% deuterium incorporation. Complex **1b** is therefore a suitable model for mechanistic investigation, with analogous reactivity to **1a**.

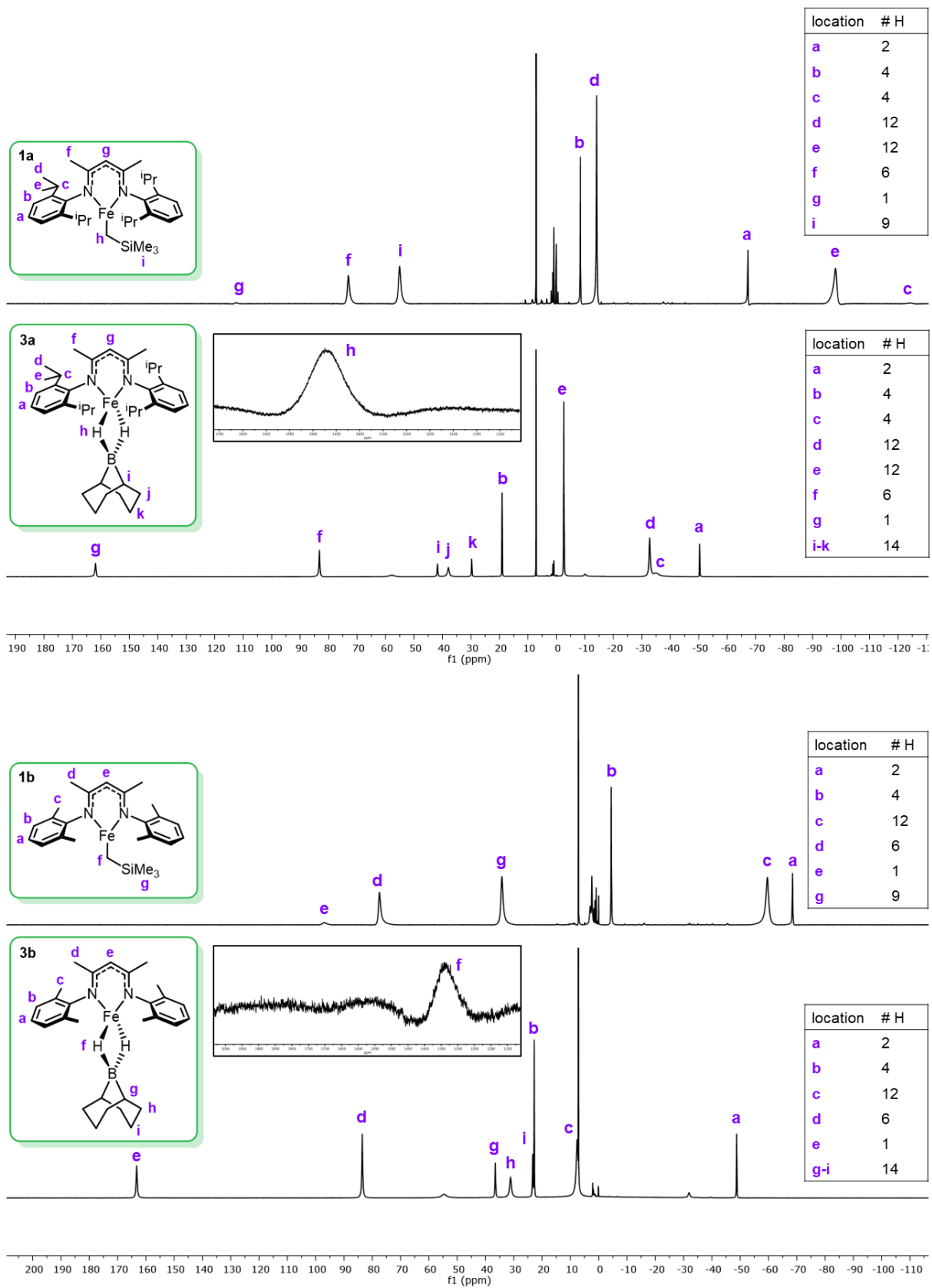


Figure 2.2.2: ^1H NMR spectra of **1a**, **3a**, **1b** and **3b** (400 MHz, C_6D_6 , 298 K).

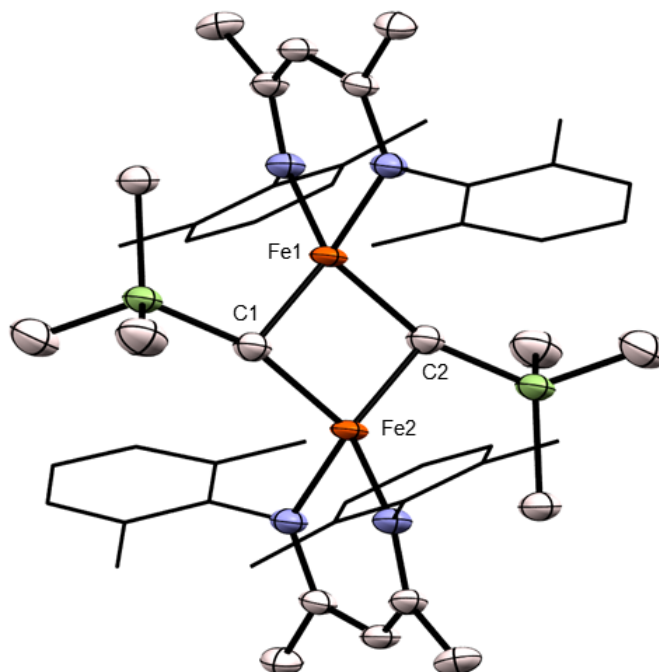
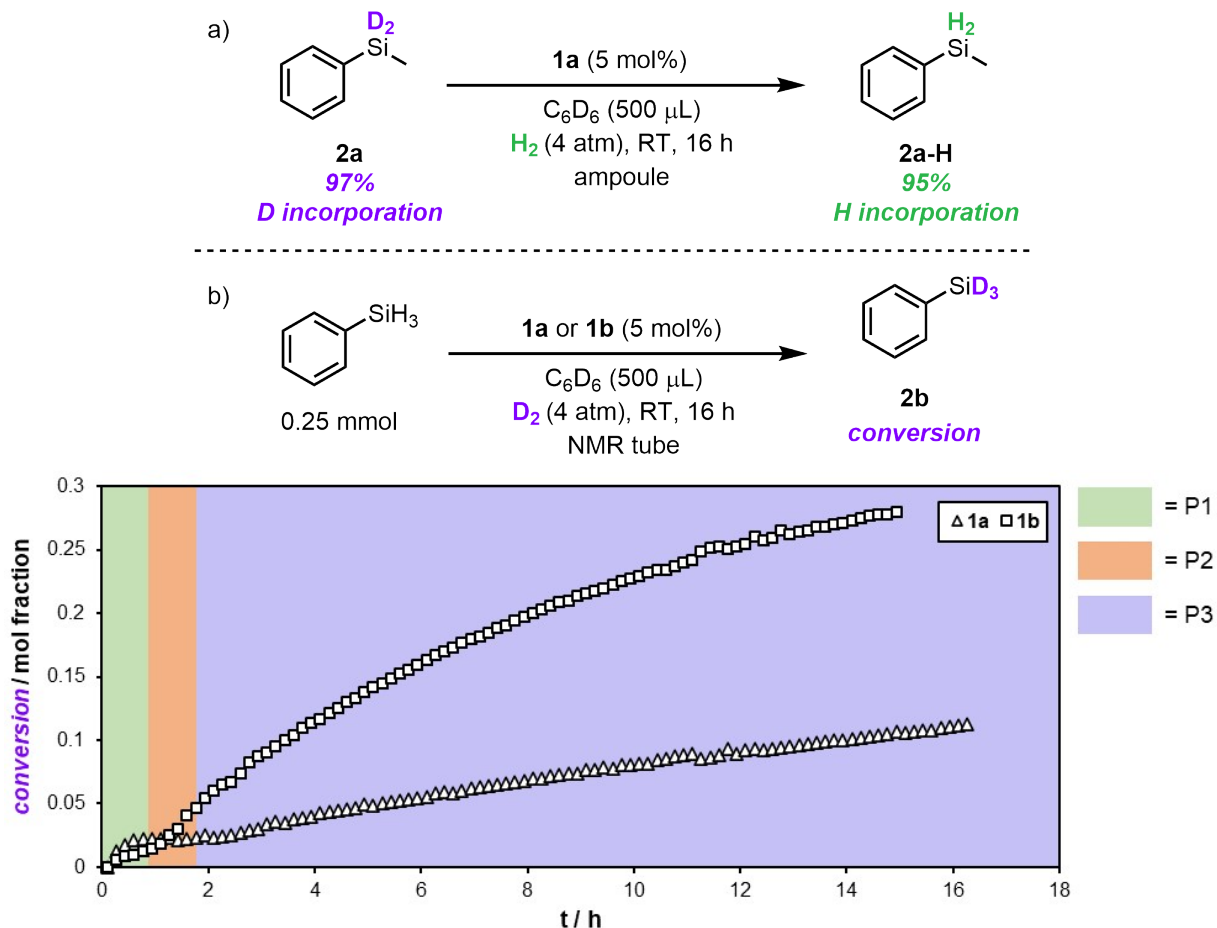


Figure 2.2.3: Single-crystal XRD structure of pre-catalyst **1b**. Ellipsoids are represented at 50% probability and hydrogen atoms omitted for clarity.

The reversibility of the reaction was investigated (scheme **2.2.3**). Subjecting methylphenyl(silane- d_2) to pre-catalyst **1a** under 4 atmospheres of H_2 yields methylphenylsilane (**2a-H**) with 95% H-incorporation after 16 hours. This suggests the reaction is reversible and H/D exchange requires an excess of deuterium source to achieve excellent deuterium incorporation. Furthermore, these findings indicate no isotope effects are contributing to the H/D exchange equilibrium, as the same degree of isotope exchange is observed in the reverse reaction, within error based on 1H NMR spectroscopy.

Stoichiometric reactions between complexes **1a** and **1b** and a range of silanes showed no reactivity. However, under catalytic conditions in a large excess of silane, reactivity is observed. *In situ* reaction monitoring experiments were undertaken using 1H NMR spectroscopy, reacting pre-catalysts **1a** and **1b** with phenylsilane and D_2 , shown in scheme **2.2.3**. The volume of the high-pressure J-Young NMR tube was estimated as $3.83 \times 10^{-6} m^3$. From the ideal gas equation, this suggests 0.627 mmol of D_2 gas in the reaction vessel at 4 atmospheres at 298 K and a theoretical maximum H/D exchange of 63% at equilibrium. Therefore, significantly reduced conversion is expected under NMR conditions. Nevertheless, three distinct phases are consistently seen in the reaction monitoring traces for both pre-catalysts. In the case of **1a**, initial uptake of silane is observed between 0-1 hours, P1. A lag phase then follows between 1-2 hours, P2. Finally, silane uptake continues and is gradually consumed over the observed reaction time, P3. While the reaction is ongoing, formation of a new peak at 0.04 ppm is observed. This resonance is assigned to the $SiMe_3$ protons of $PhSiH_2(CH_2SiMe_3)$, also noted in previous reports.^{73,74} This is the expected product of a reaction across the pre-catalyst Fe-C bond with an equivalent of silane, by σ -bond metathesis. By measuring the peak integral versus time, this gives an estimate for percentage catalyst activation, shown in figure **2.2.4**. Notably, $PhSiH_2(CH_2SiMe_3)$ is already present at the start of reaction monitoring. This suggests that catalyst activation is ongoing during the freeze-pump-thaw cycles, prior



Scheme 2.2.3: D/H exchange of methylphenyl(silane- d_2) and H₂ catalysed by **1a** (a) and reaction monitoring for the H/D exchange of phenylsilane and D₂ catalysed by **1a** and **1b** (b).

to charging the system with D₂ gas. Furthermore, previous work has described that pre-catalyst **1a** does not react with H₂ gas at pressures as high as 10 atmospheres.⁷⁰ This indicates that D₂ is not involved in catalyst activation. Figure 2.2.4 shows pre-catalyst **1a** only reaches 20% activation after 16 hours. In contrast, **1b** activated more readily reaching 75% after 14 hours. This degree of activation is mirrored in rate of reaction shown in scheme 2.2.3b. Conversion of PhSiH₃ to PhSiD₃ is more rapid for **1b** than **1a**. This indicates catalyst activation and catalytic turnover is faster for sterically less demanding BDK flanking groups. This is discussed further in section 2.3.

For PhSiH₂(CH₂SiMe₃) to be the product of catalyst activation, the concurrent formation of an iron-hydride complex is expected. Although stoichiometric reactions of **1a** or **1b** with silanes showed no reactivity, evidence for hydride formation was observed for alternative hydride source, 9-borabicyclo[3.3.1]nonane (9-BBN). During the substrate scope for the H/D exchange, some further boranes were tested. In the case of catecholborane, no deuterium incorporation was observed. However, for 9-BBN a bright pink solution formed. The stoichiometric reaction between 9-BBN dimer and **1a** and **1b** forms a new species by ¹H NMR spectroscopy. The spectra of **3a** and **3b** are shown in figure 2.2.2. Using **3b** as an example, new chemical shifts for diagnostic ligand protons **a-e** are observed. Loss of the peak at the 34.41 ppm (proton **g**) is indicative of the cleavage of the Fe-C bond in **1b**. This is accompanied by a new peak at 85.3 ppm in

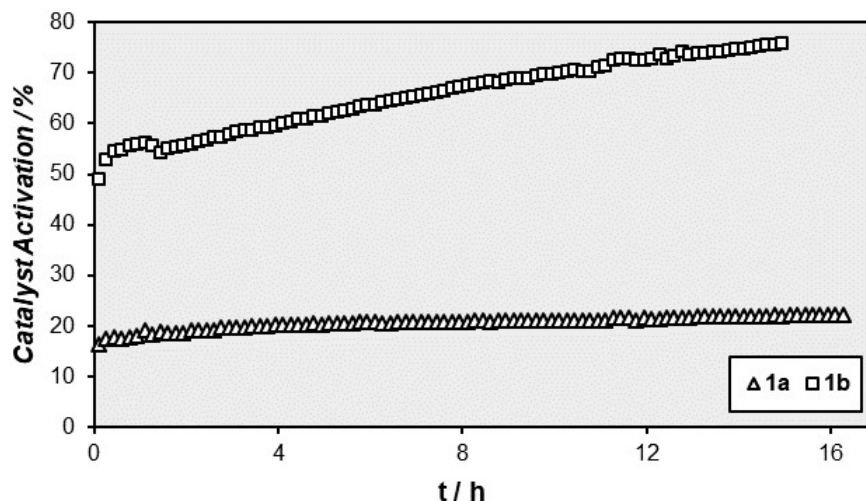
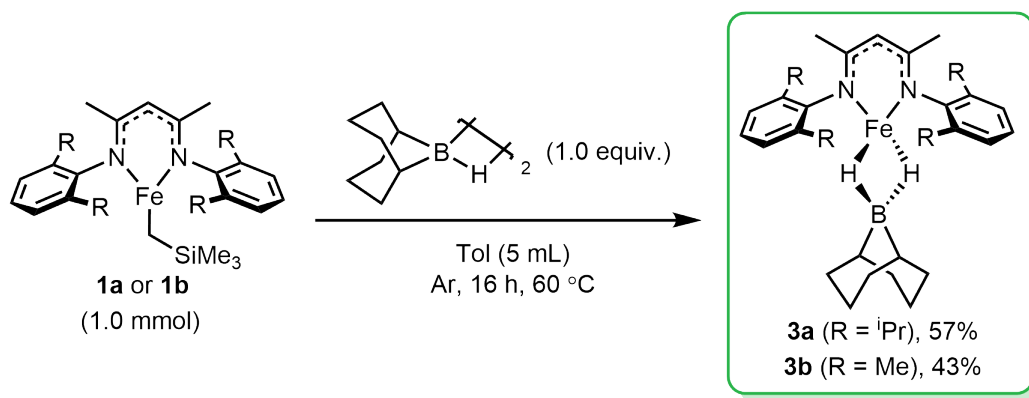


Figure 2.2.4: Percentage catalyst activation for **1a** and **1b** by monitoring the formation of $\text{PhSiH}_2(\text{CH}_2\text{SiMe}_3)$.



Scheme 2.2.4: Synthesis of $(\text{BDK})\text{Fe}-\kappa^2$ -9-borabicyclo[3.3.1]nonane complexes, **3a** and **3b**.

the ^{11}B NMR spectrum, indicative of a tertiary alkylborane. This peak is assigned to Me_3SiCH_2 -9-BBN, formed from borylation of the Fe-C bond of complexes **1a** and **1b**. Crystallisation from appropriate solvents yields pink crystals of **3a** and **3b**. ^{11}B NMR spectroscopy of these solids reveals no peak between 100 and -100 ppm, indicating Me_3SiCH_2 -9-BBN has been removed following recrystallisation. These crystals were suitable for single crystal XRD and their solid-state structures are shown in figure 2.2.5. Single-crystal XRD reveals the formation of $(\text{BDK})\text{Fe}-\kappa^2$ -9-borabicyclo[3.3.1]nonane complexes, **3a** and **3b**. Surprisingly, crystalline **3a** and **3b** show some air and moisture-stability, decolourising after 3 days. The ^1H NMR spectra of **3a** and **3b** are shown in figure 2.2.2. The spin state of four-coordinate **3a** was investigated by NMR spectroscopy using the Evan's method:⁷⁵

$$\chi_g = -\frac{3\Delta f}{2\pi f m} + \chi_o + \frac{\chi_o(d_o - d_s)}{m} \quad (2.1)$$

where χ_g = solute mass susceptibility ($\text{cm}^3 \text{g}^{-1}$), Δf = reference solvent shift (Hz), f = spectrometer frequency (500×10^8 Hz), m = mass of compound per cm^3 (0.0238 g), χ_o = solvent mass susceptibility ($-5.48 \times 10^{-5} \text{ cm}^3 \text{g}^{-1}$), d_o = solvent density (0.95 g cm^{-3}) and d_s = solution density (0.974 g cm^{-3}). A

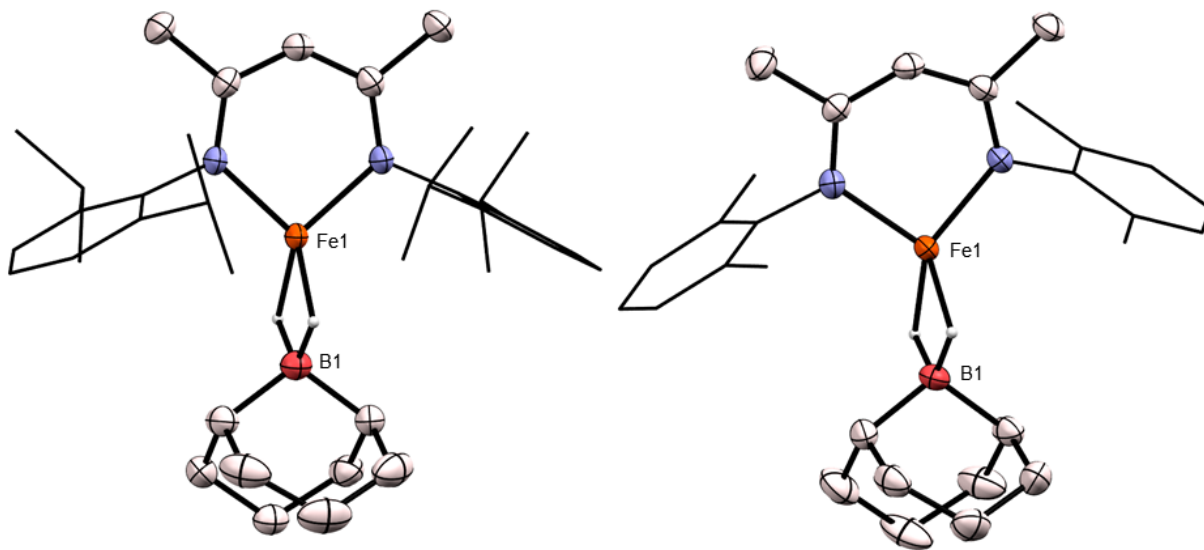
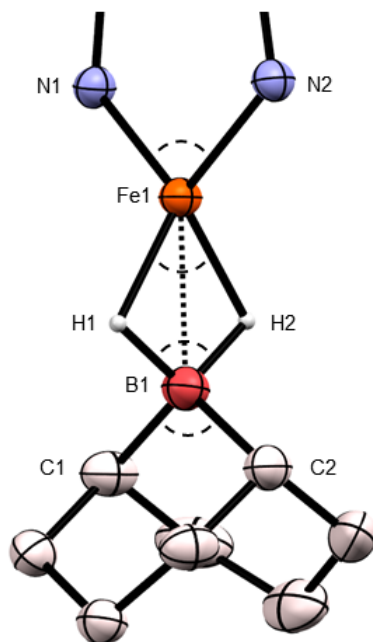


Figure 2.2.5: Single-crystal XRD structures of (BDK)Fe- κ^2 -9-borabicyclo[3.3.1]nonane complexes, **3a** (left) and **3b** (right). Ellipsoids are represented at 50% probability and non Fe-H hydrogen atoms omitted for clarity.

0.04 mM solution in benzene gives Δf of 818 Hz, therefore $\chi_g = 1.64 \times 10^{-5} \text{ cm}^3 \text{ g}^{-1}$. Multiplying χ_g by solute molecular weight (596.53 g mol $^{-1}$) gives molar solute mass susceptibility, $\chi_M = 9.79 \times 10^{-3} \text{ cm}^3 \text{ mol}^{-1}$. Following diamagnetic correction ($\chi_A = \chi_M + \chi_D$, $\chi_D = -3.85 \times 10^{-4}$), $\mu_{\text{eff}} = 4.69 \mu_B$ ($\mu_{\text{eff}} = 2.828\sqrt{\chi_A T}$, T = 293 K).⁷⁶ This is in good agreement with high-spin tetrahedral iron(II) complexes in the quintet spin-state (from spin-only formula, $\mu_{\text{eff}} = 4.90 \mu_B$ ($\mu_{\text{eff}} = \sqrt{n(n+2)} \mu_B$, where n = number of unpaired electrons)).

Resonances at 1474 and 1346 ppm (295 K) were detected in the ^1H NMR spectra of **3a** and **3b**, respectively. These are assigned to the iron-hydride environments (**h** and **f**, respectively). These represent a rare example of detection of paramagnetic metal-hydride resonance by ^1H NMR spectroscopy. Enders and co-workers recorded the first and only other example.⁷⁷ The upfield hydride resonance for a carbazole-based PNP-iron-hydride was detected at -3560 ppm (295 K). Hydrides **3a** and **3b** represent the most downfield ^1H NMR chemical shift to date. Clearly, there is a wide possible shift-range for iron-hydride nuclei, accompanied by significant line-broadening as hydrides are neighbouring the paramagnetic centre. Therefore, finding hydride resonances is challenging, requiring a vast number of scans across a wide spectral range. Work is ongoing to develop a theoretical method to accurately predict paramagnetic hydride resonances, for more facile experimental detection.

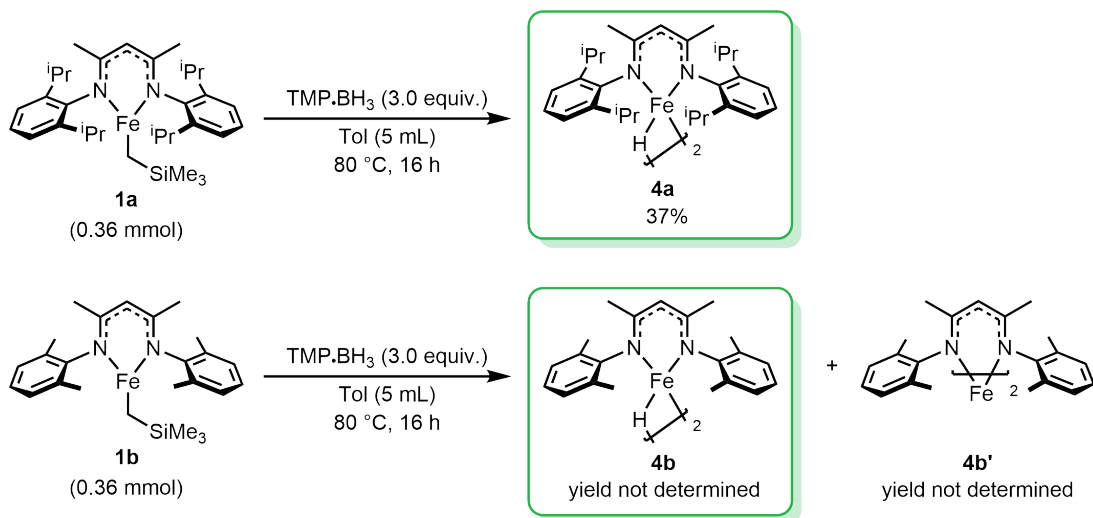
Complex **1b** was tested as a catalyst for H/D exchange with all failed tertiary silanes. It was hypothesised that **1b** (with reduced steric bulk), would be more active than **1a**. However, no deuteration was observed for all tertiary silanes tested. Complexes **1a** and **1b** crystallise in different geometries at the iron-centre (distorted trigonal planar and tetrahedral, respectively). Isolation of complexes **3a** and **3b** provides the first insight into structural differences between 2,6-dipp and 2,6-dmp iron-BDKs. Relevant bond lengths and angles are shown in table 2.2.2. Complexes **3a** and **3b** show similar Fe-N (1.9562(14) Å and 1.9562(14) Å, and 1.9596(12) Å and 1.9599(12) Å, respectively), Fe-H (1.73(3) Å and 1.77(3) Å,

Table 2.2.2: List of bond lengths and bond angles for complexes **3a** and **3b**.


Bond Length / Å	3a	3b
N1-Fe1	1.9562(14)	1.9596(12)
N2-Fe2	1.9562(14)	1.9599(12)
Fe1-H1	1.73(3)	1.75(2)
Fe1-H2	1.77(3)	1.75(2)
Fe1-B1	2.177(3)	2.186
H1-B1	1.25(4)	1.24(2)
H2-B1	1.29(3)	1.24(2)
C1-B1	1.605(3)	1.601(2)
C2-B1	1.605(3)	1.606(2)

Bond Angle / °	3a	3b
N1Fe1N1	97.077	96.48(5)
H1Fe1H2	71.344(16)	68.9(9)
H1B1H2	107(2)	106.5(13)
C1B1C2	108.516	108.30(13)

and 1.75(2) Å and 1.75(2) Å, respectively) and B-H (1.25(4) Å and 1.29(3) Å, 1.24(2) Å and 1.24(2) Å, respectively) bond lengths. The Fe-B atom distance is slightly smaller in **3a** than **3b**, at 2.177(3) Å and 2.186 Å, respectively. This is accompanied by a larger associated HFeH bond angle in **3a** compared to **3b**, at 71.344(16)° and 68.9(9)°, respectively. This is unexpected as the larger steric bulk of the 2,6-diisopropylphenyl ligand would be expected to hinder the approach of the 9-BBN fragment more strongly, enforcing a larger Fe-B atom distance and smaller HFeH bond angle. However, this is not the case in the solid-state structure. Generally, the structural differences between **3a** and **3b** are small. Therefore, it is no surprise that both **1a** and **1b** show no activity towards the catalytic H/D exchange of tertiary silanes, as ligand substitution leads to minimal structural difference in this case.

**Scheme 2.2.5:** Synthesis of iron-hydride dimers **4a** (top) and **4b** (bottom), and homoleptic complex **4b'** (bottom).

Complexes **3a** and **3b** provide experimental evidence for the cleavage of the Fe-C bond in pre-catalysts **1a** and **1b** by a hydride source. In the case of 9-BBN, the formed iron-hydride is trapped as the corresponding κ^2 -complex, providing evidence for iron-hydride formation under catalytic conditions. To investigate whether an iron-hydride may be the active species in catalysis, its synthesis was attempted directly.

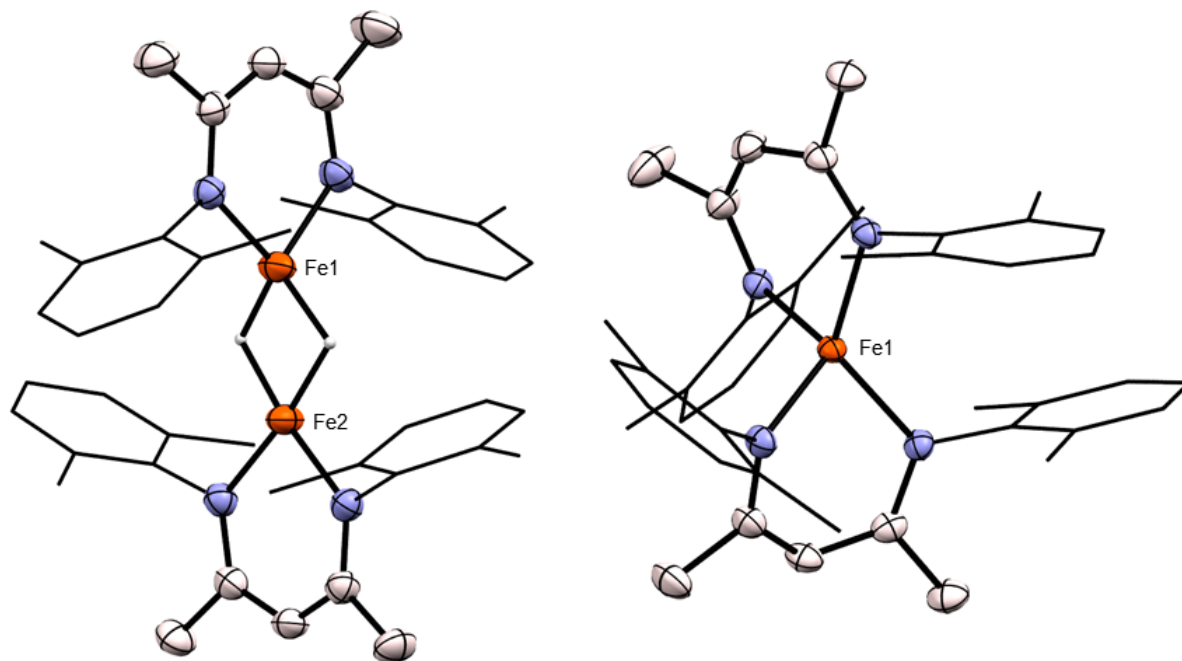
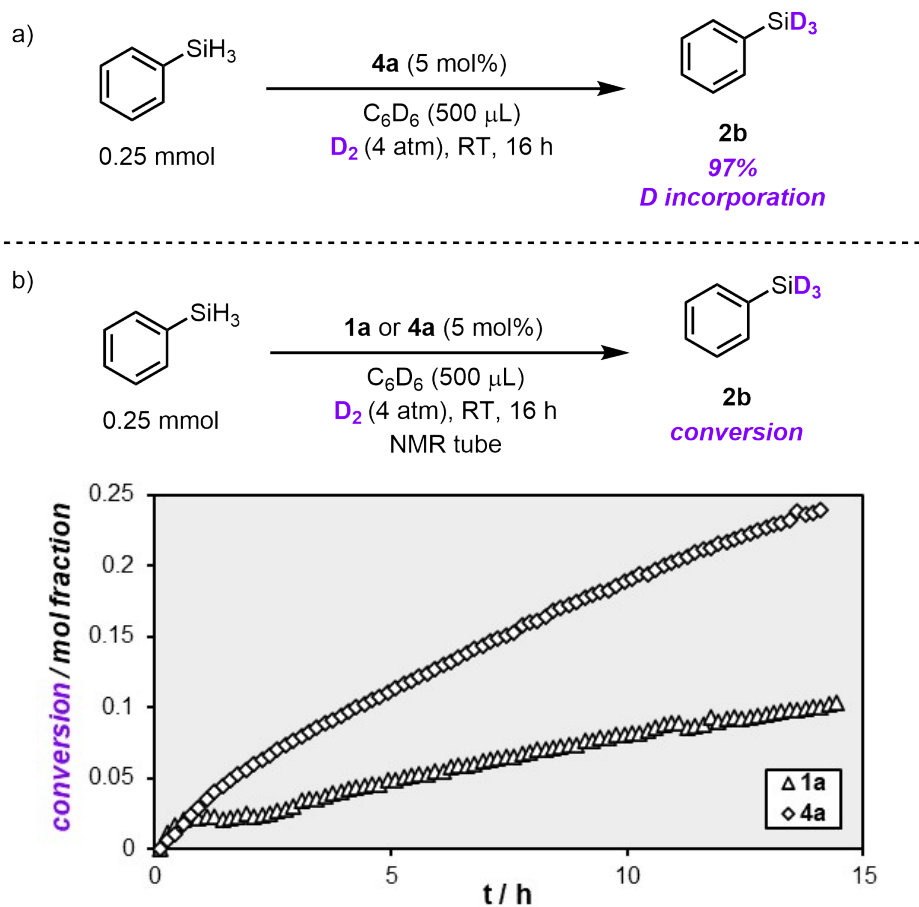


Figure 2.2.6: Single-crystal XRD structures of iron-hydride dimer **4b** (left) and homoleptic complex **4b'** (right). Ellipsoids are represented at 50% probability and non Fe-H hydrogen atoms omitted for clarity.

Iron-hydride dimer, **4a**, was synthesised following a known literature procedure, shown in scheme 2.2.5.⁶¹ Reaction of complex **1a** and $\text{TMP}\cdot\text{BH}_3$ yields **4a** in 37% yield. The identity of **4a** was confirmed by ^1H NMR spectroscopy and unit cell check. The analogous reaction between **1b** and $\text{TMP}\cdot\text{BH}_3$ is unreported. The reaction forms a significant amount of black precipitate, presumed to be iron(0) deposits. Subsequent filtration and crystallisation from pentane at $-20\text{ }^\circ\text{C}$ yields a mixture of black and red crystals. These crystals were suitable for single crystal XRD and their solid-state structures are shown in figure 2.2.6. Black crystals of desired iron-hydride dimer, **4b**, were observed in the solid-state. However, these were inseparable from homoleptic complex **4b'**. Hydride dimer, **4b**, is suspected to decompose into homoleptic complex **4b'**, H_2 and $\text{Fe}(0)$ under reaction conditions. Repeating the reaction at room temperature yielded no change in the product distribution, thus efforts to synthesise a pure sample of **4b** were unsuccessful. Nevertheless, synthesis of **4a** was achieved for investigation into the active species in the catalytic H/D exchange.



Scheme 2.2.6: a) H/D exchange of phenylsilane, catalysed by **4a** under standard conditions and b) reaction monitoring trace for the H/D exchange of phenylsilane and D_2 , catalysed by **1a** and **4a** (conversion of starting material reported).

Complex **4a** was subjected to standard H/D exchange conditions, shown in scheme **2.2.6a**. Activity is maintained under standard conditions, generating phenyl(silane- d_3) with 97% D incorporation after 16 hours. This indicates **4a** is an active catalyst for the H/D exchange process. Previously, Holland and co-workers have reported **4a** is able to facilitate H/D exchange (see section **1.2**, scheme **1.2.7**).³⁶ In their study, exposing **4a-H** to one atmosphere of D_2 forms an equilibrium between **4a-H** and **4a-D** in less than one minute. Charging the system with a second atmosphere of D_2 yields **4a-D** exclusively. This process is reversible, returning to **4a-H** with two sequential charges of H_2 (1 atmosphere). Therefore, it is assumed **4a-D** forms under these catalytic conditions and is responsible for the silane H/D exchange. Notably, the authors suggest dimeric **4a** is the major species in solution and therefore responsible for the H/D exchange, based on 1H NMR spectroscopy.

Kinetic investigation was undertaken to gain insight into the speciation of **4a** during catalysis (figure **2.2.7**). First, the reaction between phenylsilane and D_2 was performed at various concentrations of **4a**. By analysing the initial rates of reaction, the reaction is approximately half-order in **4a**. This was corroborated using time normalisation analysis (TNA).^{78,79} When time normalisation is performed, reasonable overlap is observed in the 0.4th, 0.5th and 0.6th order TNA plots (experimental figure **2.7.1**). Typically, TNA requires a full reaction profile for fitting to be reliable. Unfortunately, given the reduced

headspace of the high-pressure J-Young NMR tube, full conversion was never achieved. Thus, the exact order in catalyst cannot be deduced with certainty. Nevertheless, these traces are in agreement with initial rate analysis, suggesting off-cycle dimer dissociation to monomeric **4a** is required to participate in the turnover-limiting step. Performing the reaction at varying temperatures and plotting $\ln \frac{k}{T}$ against $\frac{1}{T}$, generates an Eyring plot of the following form:

$$\ln \frac{k}{T} = \frac{-\Delta H^\ddagger}{R} \frac{1}{T} + \ln \frac{k_B}{h} + \frac{\Delta S^\ddagger}{R} \quad (2.2)$$

where intercept $c = \ln \frac{k_B}{h} + \frac{\Delta S^\ddagger}{R}$ and negative gradient $m = \frac{-\Delta H^\ddagger}{R}$. This allows determination of ΔS^\ddagger as $-146 (\pm 28.2)$ J mol⁻¹ K⁻¹ and ΔH^\ddagger as $39.6 (\pm 8.94)$ kJ mol⁻¹. The large and negative ΔS^\ddagger suggests the transition state associated with the turnover-limiting step is highly ordered. Combining the kinetic investigations, this suggests dissociation of off-cycle dimer **4a** is required to participate in the turnover-limiting step. This monomer then reacts through a highly ordered transition state. Deuterium exchange between **4a-H** and **4a-D** is rapid (equilibrates within seconds³⁶). Thus, the highest energy step is expected to be σ -bond metathesis between monomeric **4a-D** and PhSiH₃. This would generate a highly constrained 4-membered transition state, in agreement with the observed ΔS^\ddagger .

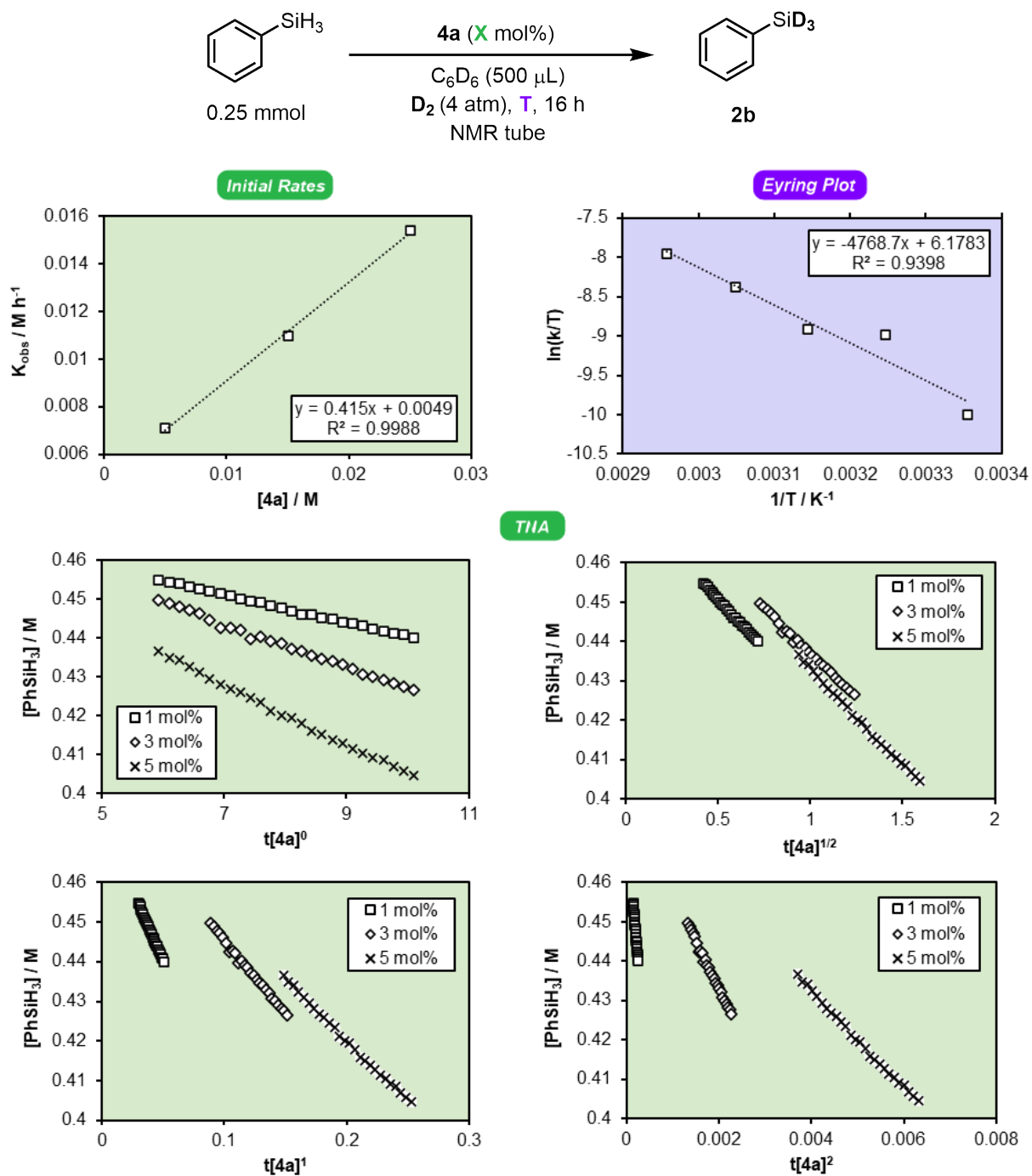


Figure 2.2.7: Kinetic investigation for the H/D exchange of phenylsilane and D₂, catalysed by **4a**, initial rates (top left), Eyring plot (top right) and TNA (bottom, demonstrating [4a]⁰, [4a]¹ and [4a]² are unlikely orders in **4a**).

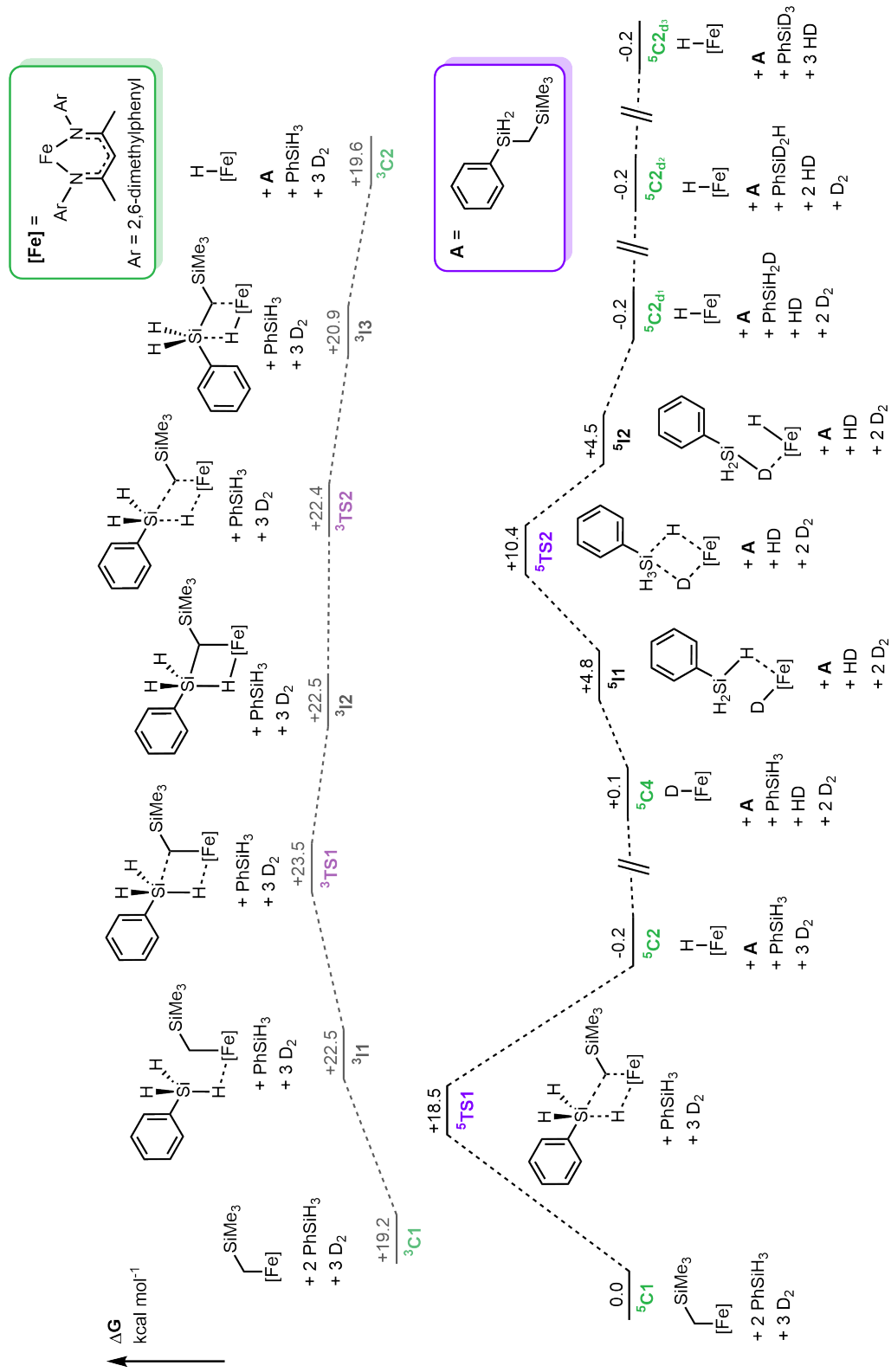
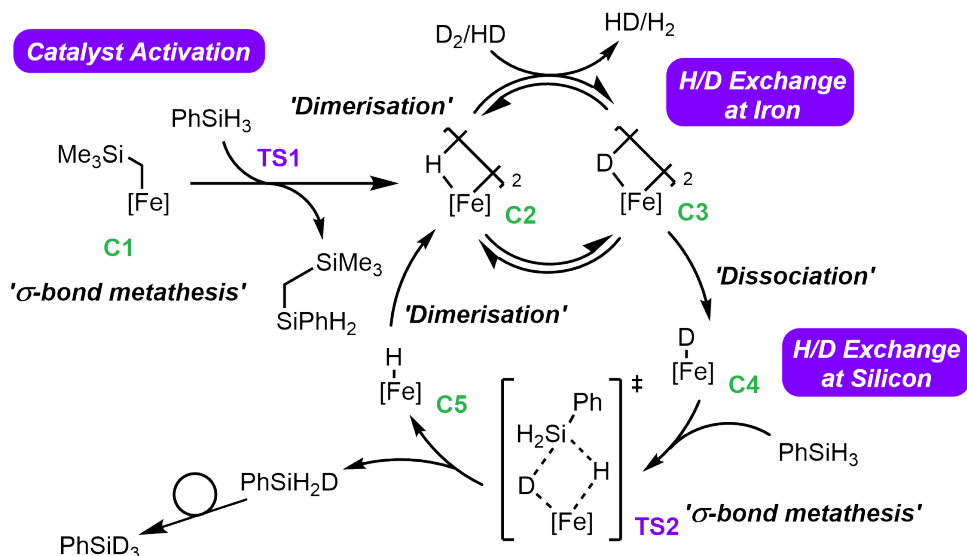


Figure 2.2.8: DFT-derived energy level diagram for catalyst activation and H/D exchange. Energies are calculated at the B3PW91-D3BJ/Def2-TZVP/IEF-PCM(C₆H₆)//BP86/BS1 level of theory. All energies are reported in kcal mol⁻¹ and referenced to **5C1** and reactants.



Scheme 2.2.7: Proposed mechanism for the iron-catalysed H/D exchange.

Computational Modelling

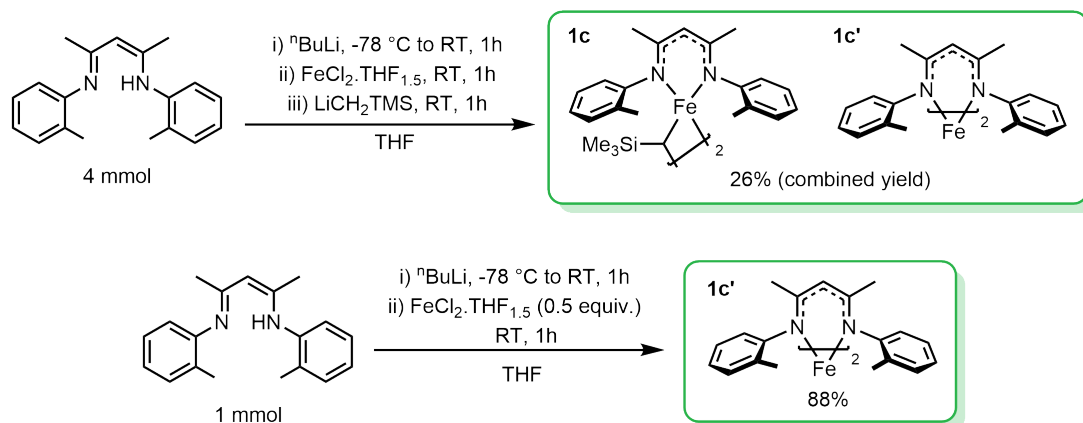
Density functional theory (DFT) was used to examine the ease of catalyst activation and H/D exchange. Transition states (TSs) and intermediates on the triplet energy surface were consistently larger in energy than the quintet. Therefore, the transformation is suggested to proceed on the quintet energy surface. A TS for the deuterium exchange could not be found for the triplet energy surface. Given the consistently larger energy for the triplet spin-state, this was discounted as a potential pathway. Pre-catalyst ${}^5\mathbf{C1}$ reacts with phenylsilane through ${}^5\mathbf{TS1}$. This has a relatively large associated activation barrier of $+18.5 \text{ kcal mol}^{-1}$. This is anticipated given the lack of stoichiometric reactivity observed between pre-catalysts **1a** and **1b** and silanes. Notably, there is negligible thermodynamic gain for the reaction of ${}^5\mathbf{C1}$ with phenylsilane, with ${}^5\mathbf{C2}$ generated in $-0.2 \text{ kcal mol}^{-1}$. This is in agreement with experimental findings as a large excess of silane is required to force equilibrium to ${}^5\mathbf{C2}$. These results indicate that catalyst activation is reversible. Intermediate ${}^5\mathbf{C2}$ readily dimerises and exchanges with D_2 . Dissociation is required to form monomeric ${}^5\mathbf{C4}$, determined from kinetic investigation. DFT on dimeric ${}^5\mathbf{C2}$ or ${}^5\mathbf{C4}$ was not attempted because the system is large and carries huge computational cost. Intermediate ${}^5\mathbf{C4}$ reacts with a second equivalent of phenylsilane through highly ordered four-membered TS, ${}^5\mathbf{TS2}$. This has an associated energy barrier of $+10.3 \text{ kcal mol}^{-1}$. The reduced energy barrier compared to ${}^5\mathbf{TS1}$ is in agreement with experimental studies as **4a** reacts more readily than **1a** (see figure 2.2.6). This reforms ${}^5\mathbf{C2}$, generating PhSiH_2D . Subsequent H/D exchanges to yield PhSiHD_2 and PhSiD_3 proceed with negligible thermodynamic gain. This is in good agreement with equilibrium being dictated by a large excess of D_2 in the system.

Proposed Mechanism

With concurrent experimental and theoretical insight, the following mechanism is proposed, shown in scheme 2.2.7. The slow activation of pre-catalyst **C1**, by reaction with silane, generates an on-cycle iron-hydride. Activation is evidenced by formation of $\text{PhSiH}_2\text{CH}_2\text{TMS}$ under catalytic conditions. Literature precedent suggests **C1** dimerises in solution forming **C2**. Complex **C2** can exchange with deuterium

forming iron-deuteride dimer, **C3**.³⁶ Under the reaction monitoring conditions used for kinetic studies, the reaction appears to be approximately half-order in **4a** (demonstrated by analysis of initial rates and TNA), therefore dissociation of off-cycle dimer to monomeric **C4** is required in the on-cycle turn-over limiting step. Intermediate **C4** reacts with a second equivalent of silane by highly-ordered four-membered TS, **TS2** (evidenced through Eyring analysis and DFT). This regenerates catalyst **C2** and singly deuterated silane. The monodeuterosilane can re-enter the catalytic cycle until full deuteration is achieved.

2.3 H/D Exchange of Tertiary Silanes



Scheme 2.3.1: Synthesis of pre-catalyst **1c** and homoleptic complex **1c'**.

The new silane H/D exchange method using **1a** and **1b** complements the literature. Primary and secondary deuteriosilanes are readily accessible. However, the reaction is incompatible with tertiary silanes. Large substituents on the BDK flanking groups are required to stabilise these three-coordinate iron(II) complexes. It is therefore unsurprising that for sterically demanding substrates, di-*tert*-butylsilane and tertiary silanes, little or no H/D exchange is observed. Reducing the ligand steric demands further could improve catalytic activity for such substrates.

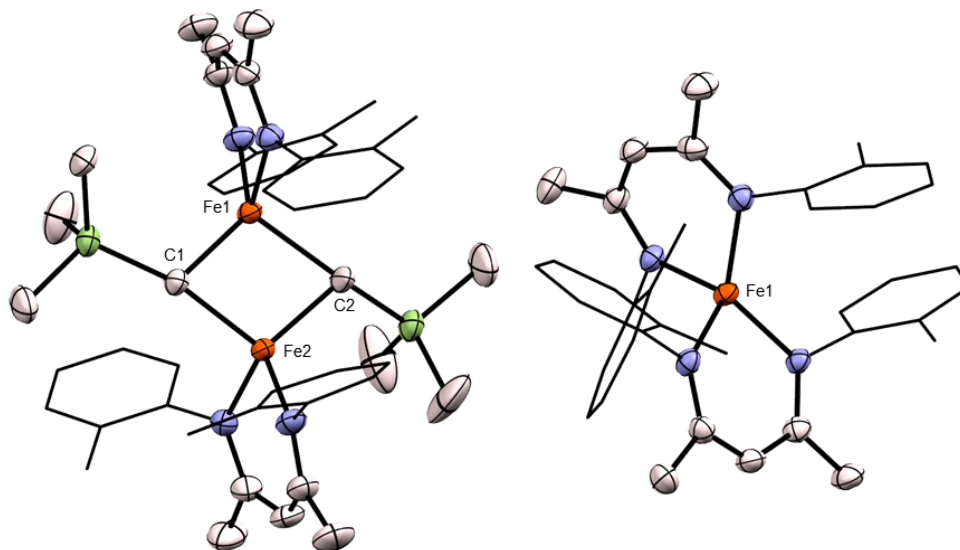


Figure 2.3.1: Single-crystal XRD structure of pre-catalyst **1c** (left) and homoleptic complex **1c'** (right). Ellipsoids are represented at 50% probability and hydrogen atoms omitted for clarity.

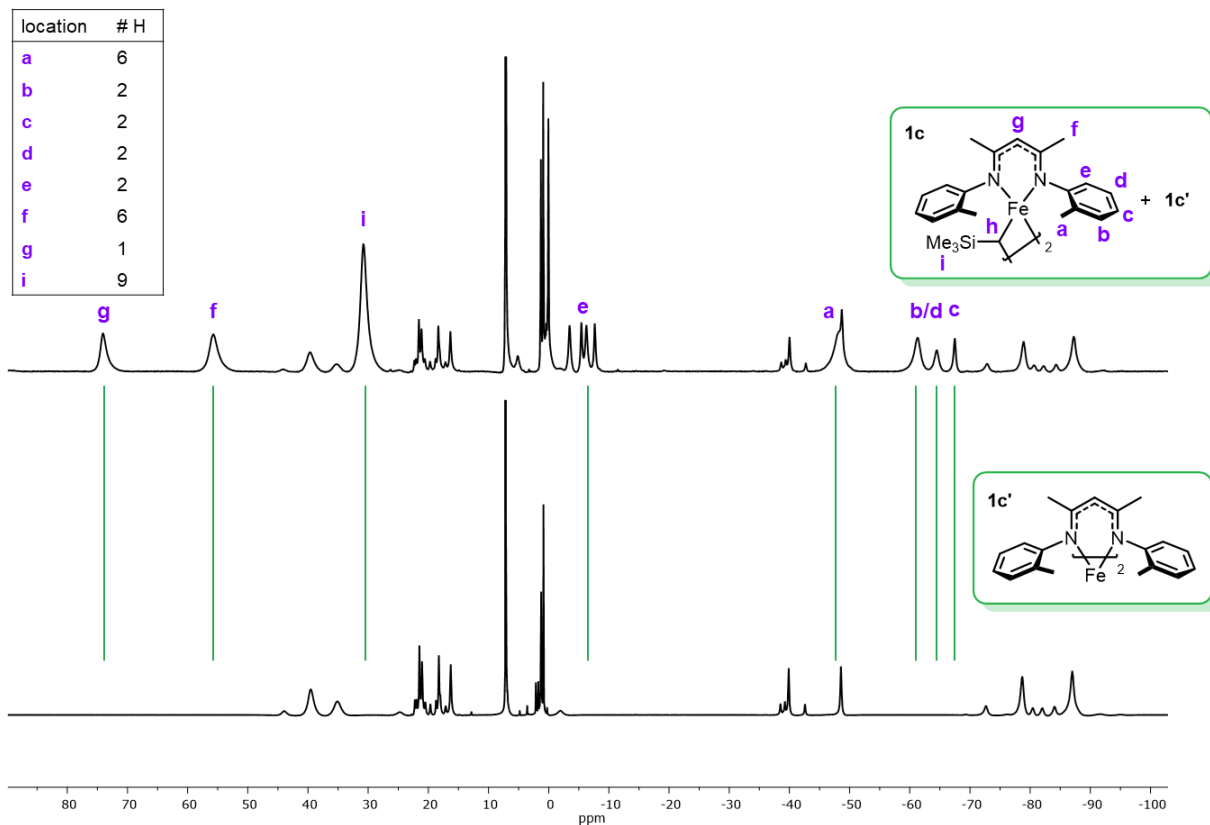
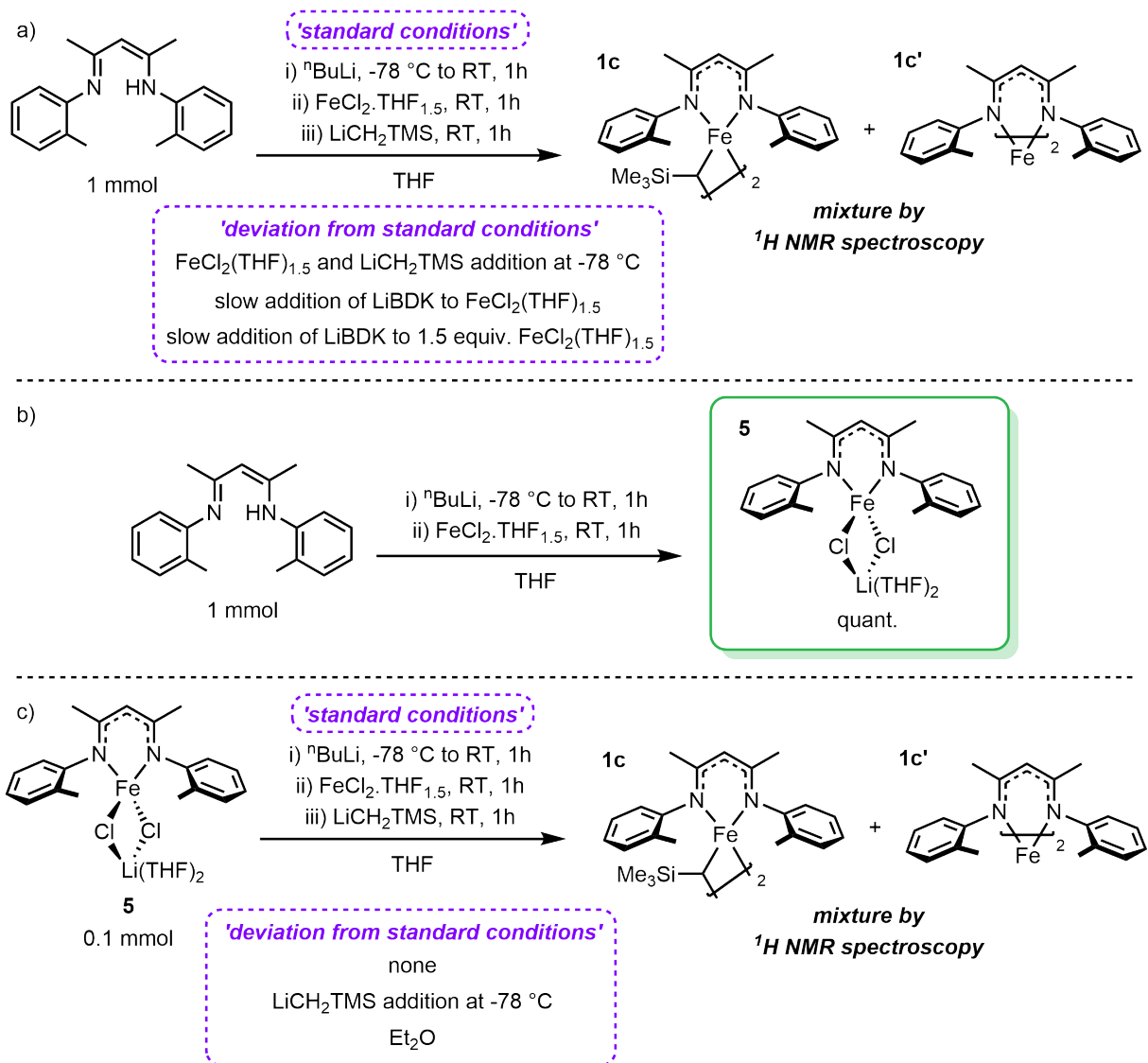


Figure 2.3.2: ¹H NMR spectra of **1c** and **1c'** crystal mixture (top) and **1c'** crystals (bottom, 400 MHz, C₆D₆, 298 K).

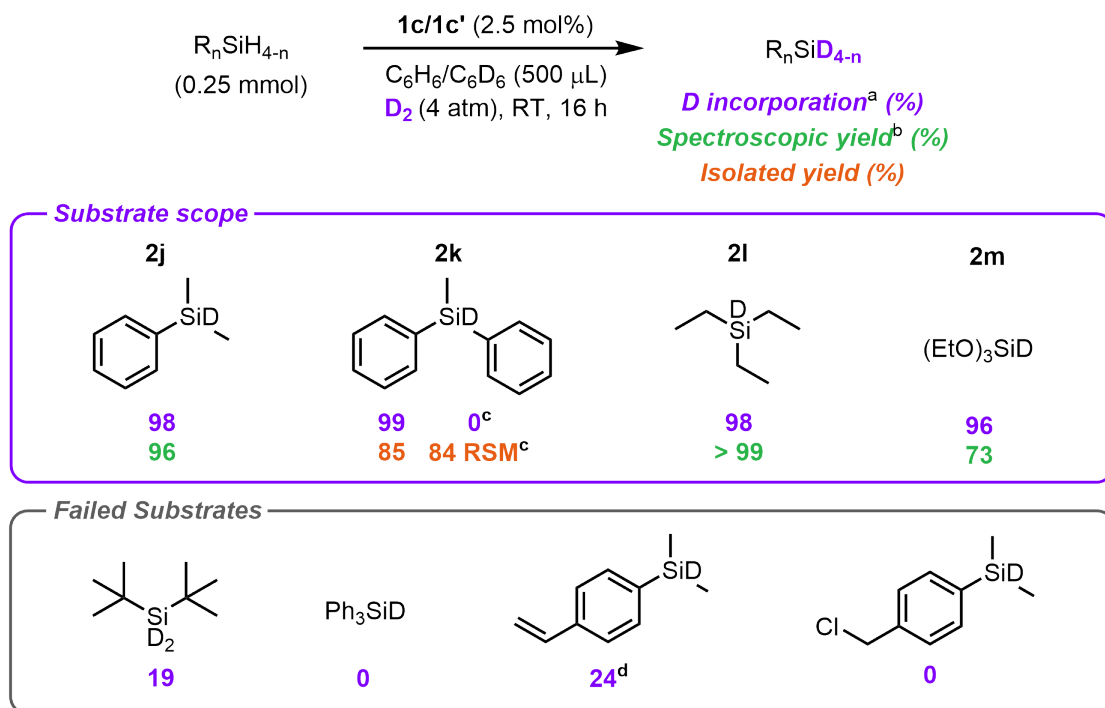
Synthesis of 2-methylphenyl substituted pre-catalyst **1c** was attempted by analogous method to **1a** and **1b**, shown in figure **2.3.1**. Synthesis of (BDK)FeCH₂TMS complexes of this type are unreported. Upon extraction of the crude mixture with pentane, a large amount of black solid was observed. Crystallisation of the filtrate from pentane at -20 °C yielded a mixture of yellow and pink crystals suitable for solid-state characterisation, albeit in low combined yield of 26%. Their solid-state structures are shown in figure **2.3.1**. The yellow crystals were revealed to be the desired complex **1c**, with 3-centre-2-electron bonding as observed in **1b**. The pink crystals were revealed to be four-coordinate homoleptic complex **1c'**. It can be presumed that decomposition of **1c** or ligand redistribution following disproportionation, leads to formation of homoleptic complex **1c'**. Importantly, isolated complex **1c**, (as a mixture with **1c'**), remains stable in benzene solution and could be analysed by ¹H NMR spectroscopy. Synthesis of **1c'** was also undertaken for direct comparison (figure **2.3.1**) with its purity confirmed by elemental analysis (EA).



Scheme 2.3.2: a) Attempts to improve synthesis of pre-catalyst **1c**, b) synthesis of **5** and c) synthesis of **1c** from **5**.

The stacked ^1H NMR spectra of the **1c** and **1c'** crystal mixture and analytically pure **1c'** is shown in figure 2.3.2. Peaks observed in the spectrum for **1c** and **1c'** do not appear in the spectrum of crystalline **1c'**. By integration of these peaks, they can be assigned to complex **1c**. Notably, proton **e** (figure 2.3.2) is observed as multiple peaks, suggesting that the BDK aryl groups have restricted rotation, leading to *cis/trans* isomerism with respect to the 2-methyl groups. This is also observed in the solid-state with, 75:25 disorder between the *cis/cis* and *cis/trans* BDK ligand isomers in dimer **1c**. The ^1H NMR spectrum of homoleptic **1c'** is complex, this is again attributed to multiple possible *cis/trans* isomers being present in solution. Both samples were dissolved in toluene and spectra measured up to $80\text{ }^\circ\text{C}$. However, no coalescence was observed for either sample.

Further methods were attempted to synthesise **1c** cleanly, shown in scheme 2.3.2a. Salt-metatheses were performed at $-78\text{ }^\circ\text{C}$ and the reaction cooled throughout. However, **1c'** remained the dominant species by ^1H NMR spectroscopy. Order of addition was investigated to reduce formation of **1c'**. However,



^aDetermined by ¹H NMR spectra comparing residual Si-H to C-H. ^bDetermined by ¹H NMR spectra using 1,3,5-trimethoxybenzene (0.25 mmol). ^cCatalysed by **1c**. ^dReduction of double bond. RSM = recovered starting material.

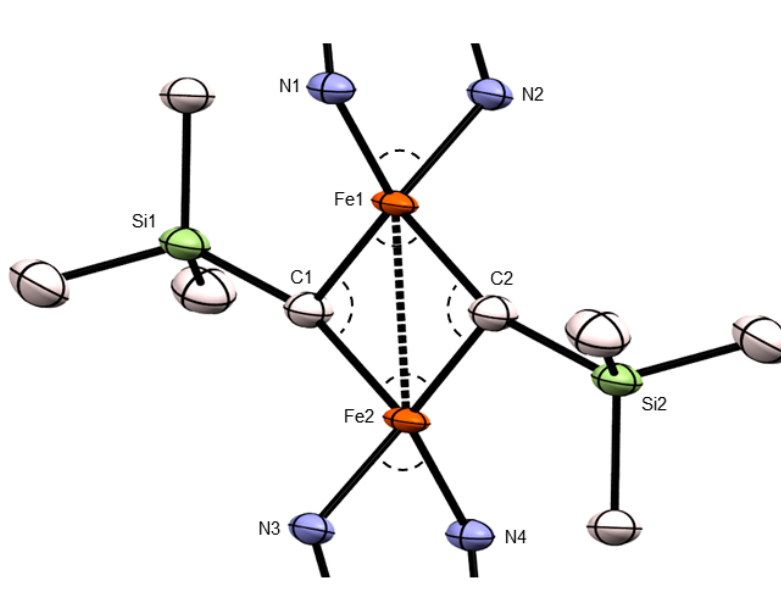
Figure 2.3.3: Substrate scope for tertiary silanes and siloxanes H/D exchange, catalysed by **1c** and **1c'**.

slow addition of lithiated ligand into 1.0 or 1.5 equivalents of FeCl₂·(THF)_{1.5} again furnished **1c'** as the dominant product. To check the iron-chloride intermediate was forming its direct synthesis was undertaken (figure 2.3.2b), following reports by Byers and co-workers.⁸⁰ Complex **5** was subjected to salt-metathesis, shown in figure 2.3.2c. Complex **1c'** is observed under both standard conditions and reduced temperature, when reacting **5** with LiCH₂TMS. These results indicate decomposition occurs during the final synthetic step. Finally, the reaction was undertaken in Et₂O. Dissociation of dimer **1c** with THF could facilitate complex decomposition. However, performing the reaction in Et₂O also yielded **1c'**. Clean synthesis of **1c** remains elusive.

Although **1c** could not be isolated cleanly, by combination of ¹H NMR spectroscopy, single-crystal X-ray diffraction (XRD) and EA, the products can be confidently assigned as desired **1c** and homoleptic **1c'**. Therefore, the mixture of **1c** and **1c'** was tested under standard H/D exchange conditions, shown in figure 2.3.3. H/D exchange is observed for tertiary silanes and siloxanes in excellent isotope exchange and yield. Activity is maintained for tertiary arylsilanes, generating dimethylphenyl(silane-*d*) (**2j**) and methyl-diphenyl(silane-*d*) (**2k**) in 98% and 99% H/D exchange, respectively. Tertiary alkylsilane, triethyl(silane-*d*) (**2l**) forms in 98% isotope exchange and quantitative yield. Finally, triethoxysilane now tolerates deuteration, generating triethoxy(silane-*d*) (**2m**) in 96% deuterium incorporation, albeit with contamination of homocoupled hexaethoxydisilane (**2m'**), by dehydrogenative coupling. Notably, isolated complex **1c'** is not an effective catalyst for the H/D exchange of methyl-diphenylsilane, with 0% deuterium incorporation and 84% recovered starting material. Outlined in section 2.2.3, metathesis of a pre-catalyst

Fe-C bond is required, furnishing an iron-hydride as the active catalyst. Therefore, it is expected that homoleptic complex **1c'** cannot facilitate H/D exchange. Large di-*tert*-butylsilane and triphenylsilane remain incompatible. Reduction of the dimethyl(4-vinylphenyl)silane occurs with poor H/D exchange observed. Finally, the solution turns black upon addition of dimethyl(4-chloromethylphenyl)silane to the pre-catalyst solution with no H/D exchange observed.

Table 2.3.1: List of bond lengths and bond angles for complexes **1b** and **1c**.

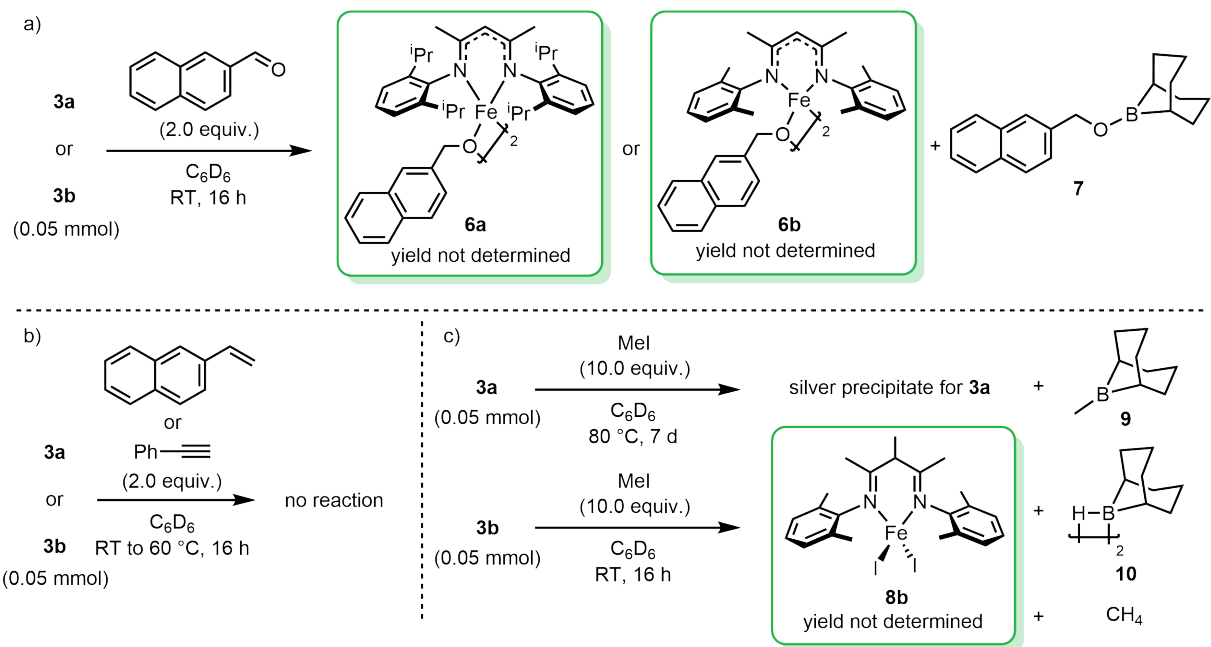


Bond Length / Å	1b	1c
N1-Fe1	2.0396(18)	2.0233(19)
N2-Fe1	2.0396(18)	2.0175(19)
Fe1-C1	2.058(4)	2.107(2)
Fe1-C2	2.275	2.249(2)
Fe1-Fe2	2.634	2.660
C1-Fe2	2.275	2.248(2)
C2-Fe2	2.058(4)	2.090(3)
Fe2-N3	2.0396(18)	2.0176(19)
Fe2-N4	2.0396(18)	2.0245(19)
Bond Angle / °		
N1Fe1N2	95.436	89.28(8)
C1Fe1C2	105.299	103.65(9)
Fe1C1Fe2	74.701	75.21(7)
Fe1C2Fe2	74.701	75.52(8)
C1Fe2C2	105.299	104.25(9)
N3Fe2N4	95.436	91.33(8)

Like complex **1b**, **1c** crystallises in a dimeric tetrahedral geometry. Therefore, the direct structural comparison of the two pre-catalysts could be made. Relevant bond lengths and bond angles are shown in table **2.3.1**. Notably, the asymmetric unit of **1b** contains a quarter of the dimer, so most bond lengths and angles are symmetry derived. Similar Fe-N bond lengths are observed, 2.0396(18) Å for **1b**, and 2.0233(19) Å, 2.0175(19) Å, 2.0176(19) Å and 2.0245(19) Å for **1c**. Fe-C bond lengths are also comparable at 2.058(4) Å and 2.275 Å in **1b**, and 2.107(2) Å, 2.249(2) Å, 2.248(2) Å and 2.090(3) Å in **1c**. In the solid-state, structural differences between **1b** and **1c** are insignificant. This suggests that ligand substitution causes negligible electronic change in the resulting pre-catalyst geometry. Therefore, their differences in reactivity for 1°, 2° and 3° silane H/D-exchange is likely a steric argument (larger 3° silane coordination is more facile in reduced bulk **1c**).

2.4 Reactivity of (BDK)Fe- κ^2 -9-borabicyclo[3.3.1]nonane Complexes

Owing to the stability of (BDK)Fe- κ^2 -9-borabicyclo[3.3.1]nonane complexes **3a** and **3b**, their stoichiometric reactivity was investigated. Complexes **3a** and **3b** were reacted with a selection of unsaturated compounds to investigate insertion into carbon-carbon or carbon-heteroatom multiple bonds, summarised



Scheme 2.4.1: Reactions of **3a** and **3b** with, a) 2-naphthaldehyde, b) 2-vinylnaphthalene and phenylacetylene, and c) methyl iodide.

in scheme **2.4.1**. The reaction of **3a** and **3b** with 1.0 equivalent of 2-naphthaldehyde (scheme **2.4.1**) forms a new peak at 57.7 ppm in the ^{11}B NMR spectrum, accompanied by complete loss of the 2-naphthaldehyde α -proton in the ^1H NMR spectrum. This new shift in the ^{11}B NMR spectrum is characteristic of primary boronic esters ($\text{R}_2\text{BOR}'$).⁸¹ Notably, only partial consumption of **3a** and **3b** is observed in the ^1H NMR spectrum. It is likely that **3a** or **3b** reacts with one equivalent of aldehyde furnishing hydroboration product **7**. This would yield iron-hydride **4a** or **4b**, which can rapidly insert into a second equivalent of aldehyde. When **3a** and **3b** are reacted with 2.0 equivalents of 2-naphthaldehyde, full consumption of starting materials were observed accompanied by formation of a yellow precipitate. Recrystallisation from vapour diffusion of pentane into a saturated solution of THF, yields yellow crystals suitable for solid-state characterisation. Single-crystal XRD reveals iron-alkoxide dimers **6a** and **6b** in the solid-state, shown in figure **2.4.1**. **6a** and **6b** indicate *in situ* formation of an iron-hydride intermediate. Reacting **6a** with one equivalent of 9-BBN dimer reforms **3a**, indicating **3a** could be active in catalytic hydroboration. Complexes **3a** and **3b** were unable to reduce more challenging carbon-carbon multiple bonds. No reaction is observed for either 2-vinylnaphthalene or phenylacetylene, with starting materials observed by ^1H and ^{11}B NMR spectroscopy. This is likely attributable to the boron-oxygen bond being stronger than boron-carbon bond (806 kJ mol^{-1} and 448 kJ mol^{-1} , respectively).⁸²

Next, **3a** and **3b** were reacted with alternative electrophile iodomethane. No reaction is observed between **3a** and iodomethane at room temperature. Upon heating for seven days at $80 \text{ }^\circ\text{C}$, a peak at 88.6 ppm is observed in the ^{11}B NMR spectrum, accompanied by formation of black precipitate and liberated ligand by ^1H NMR spectroscopy. The boron resonance is assigned to 9-methyl-9-BBN, **9**.⁸³ **9** is likely a by-product of decomposition of **3a** with iodomethane. The formation of **9** is surprising, suggesting a nucleophilic boryl species forms under reaction conditions. Nucleophilic boryls are of interest

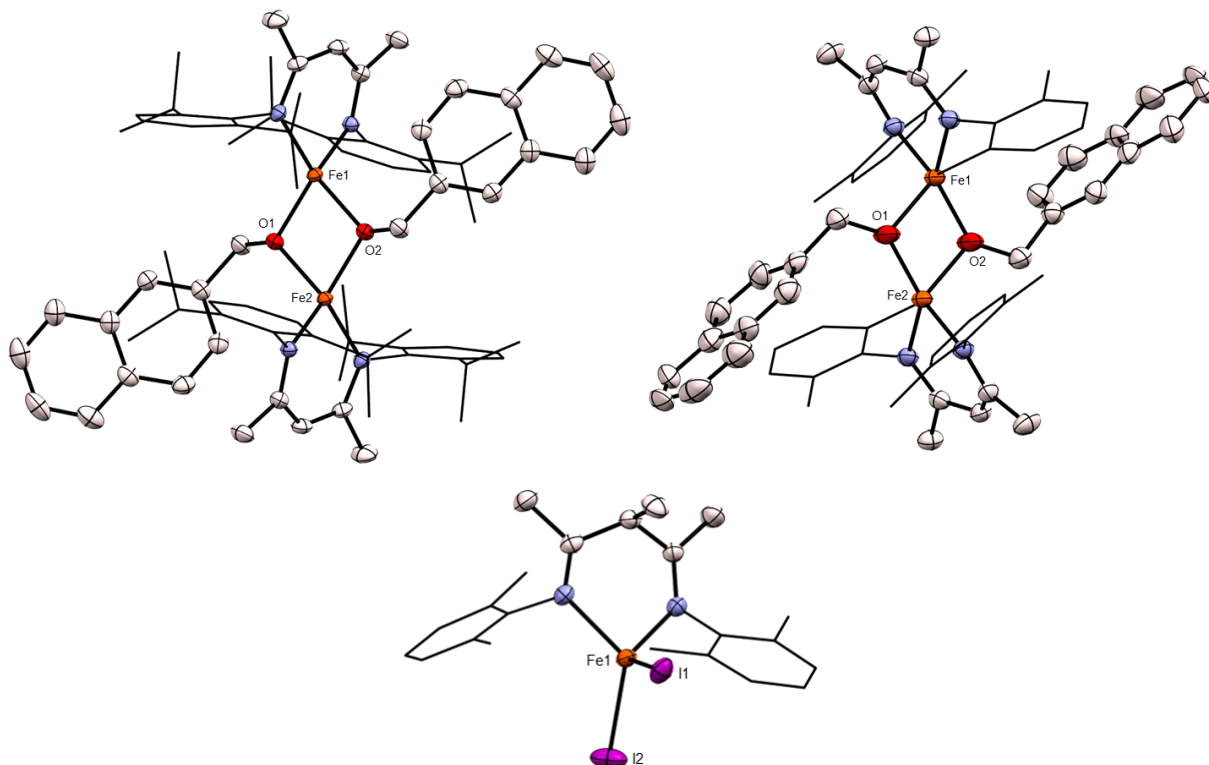
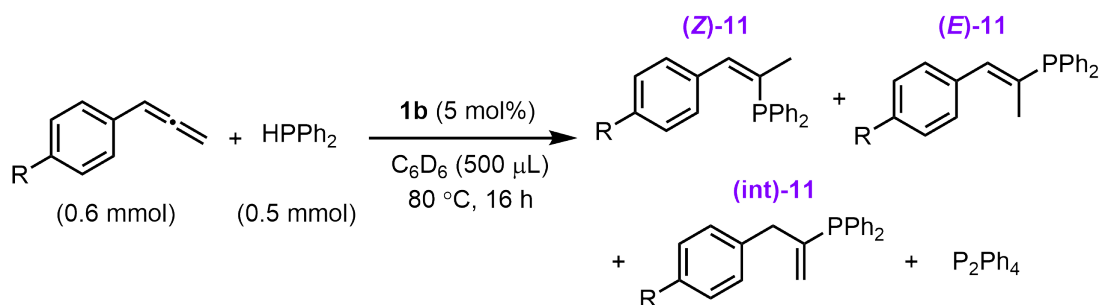


Figure 2.4.1: Single-crystal XRD structure of iron-alkoxides **6a** (top left) and **6b** (top right), and iron-diiodide complex **8b** (bottom). Ellipsoids are represented at 50% probability and hydrogen atoms omitted for clarity.

as unique reagents for C-B bond forming reactions.^{12,84} The unusual reactivity of **3a** is worthy of further investigation. Reaction of **3b** with iodomethane proceeds in an opposing manner. After 16 hours at room temperature, complete consumption of **3b** is observed by ¹H NMR spectroscopy. A ¹¹B NMR resonance at 27.9 ppm appears assigned as 9-BBN dimer, **10**. The reaction is accompanied by quantitative formation of yellow crystals, suitable for solid-state characterisation. Single-crystal XRD reveals crystals as iron-diiodide complex, **8b**. Reduction of the BDK backbone is observed forming a methylated 1,3-dimine ligand, presumably formed via reaction with excess iodomethane. An equivalent of methane is expected to form, assigned by a peak at 0.14 ppm in the ¹H NMR spectrum. Reaction of **3b** with one equivalent of iodomethane is required to access monoiodinated **8b** and investigate ease of ligand reduction.

2.5 Hydrophosphination of Allenes

Table 2.5.1: Substrate scope for allene hydrophosphination, catalysed by **1b**.



Entry	R		Relative Conversion ^a				P ₂ Ph ₄
			(Z)	(E)	(int)		
1	H	(11a)	trace (8)	86 (51)	11 (23)	trace (2)	
2	Me	(11b)	9 (6)	15 (48)	60 (27)	trace (2)	
3	OMe	(11c)	5 (15)	77 (60)	13 (11)	3 (7)	
4	Cl	(11d)	trace (6)	13 (70)	79 (1)	trace (18)	

^aDetermined by ³¹P NMR spectroscopy. ^bConversions in parenthesis catalysed by **1a**.

Ongoing work by C. R. Woof and R. L. Webster detailed the catalytic hydrophosphination of allenes, shown in table 2.5.1.⁸⁵ Hydrophosphination of allenes remains an underexplored synthetic tool for atom-economic routes to new phosphorus containing molecules.^{86–88} Previous work demonstrated **1a** was an effective pre-catalyst for alkene and alkyne hydrophosphination in high regioselectivity.^{89,90} However, using allenes as substrates for hydrophosphination introduces a second reactive site. Therefore (*E*)-, and (*Z*)-, and internally hydrophosphinated isomers are accessible. Furthermore, **1a** has been shown to catalyse the DHC of secondary phosphines to produce undesired product, P₂Ph₄.⁹¹ Therefore, controlling the chemo- and regio-selectivity of allene hydrophosphination is challenging. Table 2.5.1 shows **1a** is an active pre-catalyst for allene hydrophosphination. However, this method shows only moderate selectivity towards the (*E*)-isomer. The mechanism for allene hydrophosphination is expected to proceed via insertion of an iron-phosphide into the allene. Under reduced steric strain, this step becomes more facile. Given the influence of ligand size on catalytic activity of iron-BDK complexes, outlined in section 2.3, **1b** was investigated as a catalyst for allene hydrophosphination. The results are shown in table 2.5.1. Substrates **11b** and **11d** show good selectivity for the internally hydrophosphinated product at 60% and 79%, respectively. A rise from 27% and 1% when catalysed by **1a**. In contrast, for allenes **11a** and **11c**, high selectivity for the (*E*)-isomer is observed at 86% and 77%, respectively, compared to 51% and 60% when catalysed by **1a**. The hypothesis that **1b** will preferentially undergo insertion at the internal position holds for substrates **11b** and **11d**. However, this is not the case for **11a** and **11c**. Understanding the regioselectivity of allene hydrophosphination remains challenging, extending beyond simple steric and electronic reasoning. Nevertheless, pre-catalyst **1b** leads to improved selectivity for each substrate tested.

The stoichiometric reaction of **1b** and diphenylphosphine gives new paramagnetic signals by ¹H NMR spectroscopy. Recrystallisation from pentane at -20 °C yields red crystals suitable for solid-state charac-

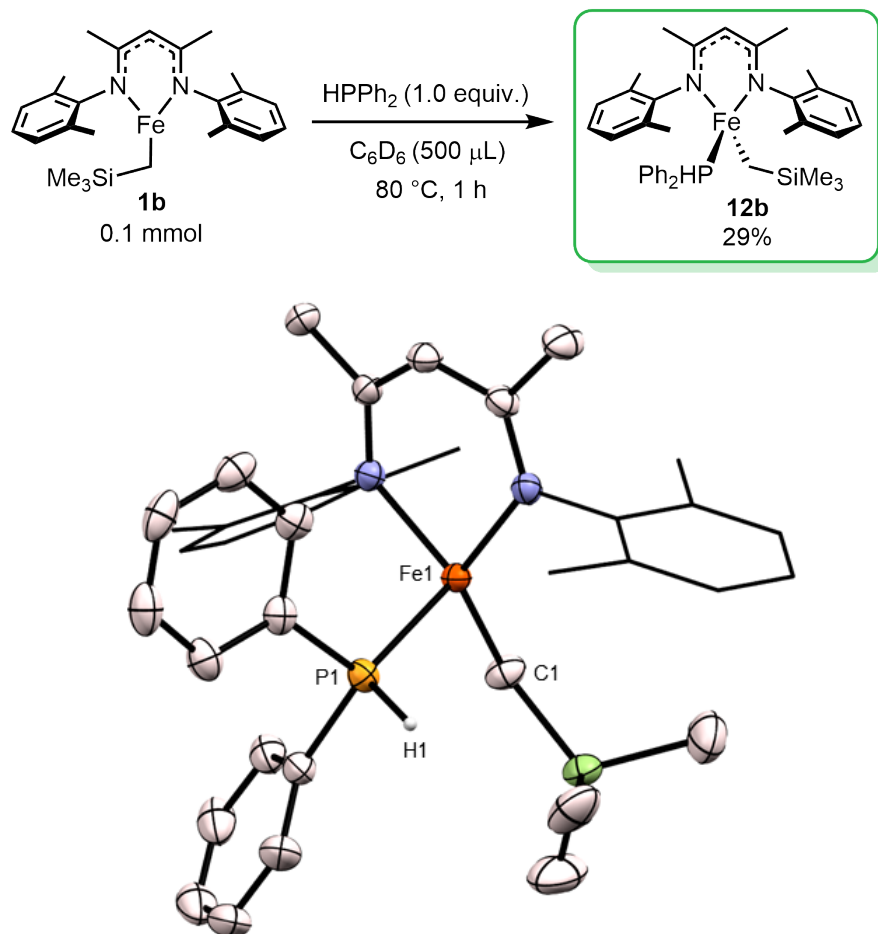


Figure 2.5.1: Synthesis and single-crystal XRD structure of **12b**. Ellipsoids are represented at 50% probability and hydrogen atoms, except P-H, omitted for clarity.

terisation. Single-crystal XRD reveals phosphine adduct **12b** was formed. Efforts to synthesise catalytic intermediates derived from **1a** were, thus far, unsuccessful. Complex **12b** represents the first step in the proposed allene hydrophosphination. Efforts to furnish a proposed iron-phosphide by release of SiMe_4 were unsuccessful and no further intermediates were discovered.

2.6 Conclusions and Future Work

The first example of iron-catalysed H/D exchange of silanes is described, facilitated by pre-catalysts **1a** and **1b**. The method provides the broadest scope to date for isotope exchange of primary and secondary silanes, and tertiary siloxanes. Eight examples were demonstrated in 95-99% deuterium incorporation and activity extends to alternative hydride source, pinacolborane. For laboratories where D₂ gas is available, the method offers clean access to deuterium-labelled species with facile purification. A detailed mechanistic study was undertaken. 1) Reaction monitoring experiments with iron-hydride dimer **4a**, reveal rate of H/D exchange is enhanced compared to **1a**. Catalyst activation is averted indicating **4a** is the active on-cycle species. 2) Analysis of initial rates and TNA show the reaction is approximately half-order in **4a**. Therefore, dissociation of dimeric **4a** is required in the rate determining step. 3) Eyring analysis delivers a large and negative ΔS^\ddagger ($-146 (\pm 28.2) \text{ J mol}^{-1} \text{ K}^{-1}$), indicating the associated transition state is highly ordered. 4) DFT concurs with these findings as catalyst activation by **⁵TS1** has a large associated energy barrier ($+18.5 \text{ kcal mol}^{-1}$). Once the iron-hydride/deuteride forms, σ -bond metathesis is more facile, accessed through four-membered **⁵TS2** ($+10.4 \text{ kcal mol}^{-1}$). Less bulky **1c** affects the H/D exchange of tertiary silanes, expanding the scope to include 4 further substrates. Unfortunately, a clean synthesis of **1c** remains elusive. Nevertheless, the by-product of its synthesis was identified (**1c'**) and is inactive in H/D exchange.

To report the complete set of 1°, 2° and 3° deuteriosilanes, a clean synthesis of **1c** is required. ¹H NMR spectroscopy suggests that once **1c** forms it is stable in a solution of toluene up to 80 °C. The decomposition product- homoleptic **1c'**- was observed when synthesis was attempted in THF and Et₂O. Given that these are coordinating solvents, **1c** dimer likely dissociates, leading to decomposition and formation of **1c'**. Synthesis of **1c** should be attempted from its iron-chloride precursor (**5**) in non-coordinating solvents at various temperatures to improve the yield of **1c**. Contamination of homoleptic **1c'** remains a barrier to a comprehensive substrate scope for catalytic H/D exchange of silanes.

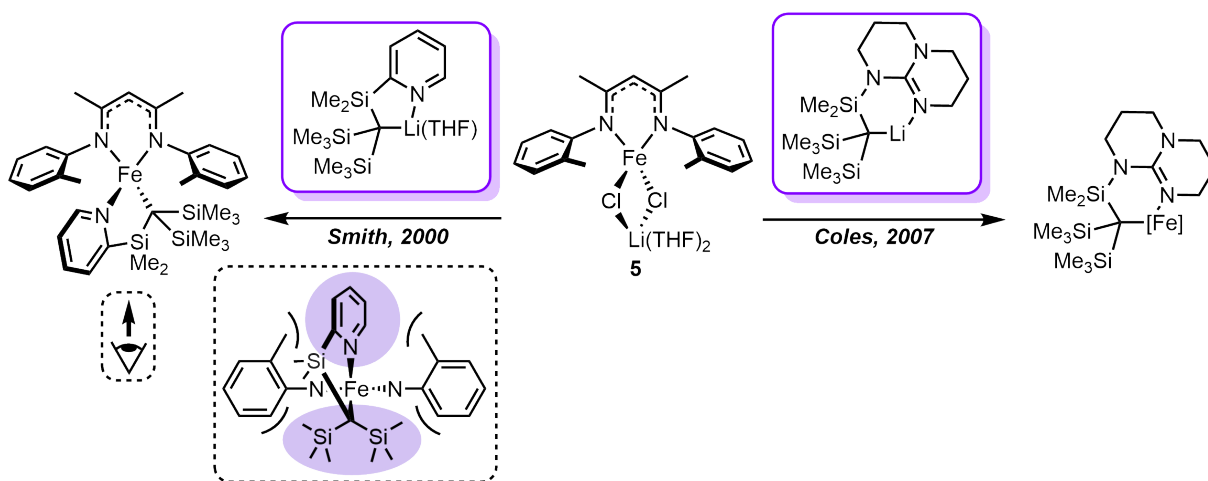


Figure 2.6.1: Stabilisation of 2-methylphenyl iron-BDK complexes with bulky trisyl ligands.

Alternatively, a larger leaving group could be introduced at the iron-centre to stabilise **1c**. Maintaining a relatively weak Fe-C bond in the pre-catalyst is essential. As such, it can still be cleaved by Si-H σ -bond

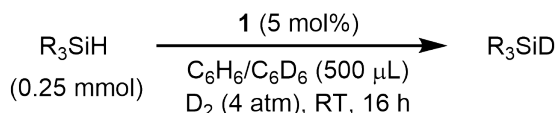
metathesis during catalyst activation. Ligands derived from tertiary carbon centres are prevalent in the literature. Trisyl ligands are an example of this.⁹²⁻⁹⁴ Larger than CH_2SiMe_3 currently deployed, ligands of this type can better supplement the steric deficiency of the 2-methylphenyl flanking groups. Furthermore, large SiMe_3 groups offer pre-catalyst stability, filling the void provided by the (*cis*)-orientation of the BDK flanking groups observed crystallographically. This idea is demonstrated in figure **2.6.1**. Denticity of these ligands could be problematic as a second-coordination is likely from pendant nitrogen containing moieties. Catalyst activation will therefore be reliant on iron-carbon bond metathesis and iron-nitrogen dissociation.

2.7 Experimental

2.7.1 General Considerations

Reagents were purchased from Fisher Scientific or Merck and dried and distilled prior to use. Laboratory grade pentane was purchased from Fisher Scientific and used without further purification. THF, C₆H₆ and C₆D₆ were dried over Na/benzophenone and distilled prior to use. DCM was dried over CaH₂ and distilled prior to use. Pre-catalyst **1a** was synthesised following literature procedure.⁹¹ (diⁱppBDK)Fe(μ-Cl)₂Li(THF)₂ was synthesised following literature procedure.⁷² NMR spectra were collected at 300, 400 or 500 MHz on Agilent or Bruker instruments in C₆D₆, C₆H₆ or CDCl₃ at 298 K and referenced to the residual solvent peak. Reactions were undertaken using standard glovebox (Ar, 0.1 ppm H₂O and 0.1 ppm O₂) and Schlenk line (N₂) techniques unless otherwise stated. All reactions were undertaken in 60 mL Teflon-sealed J-Young ampoules unless otherwise stated. D₂ cylinder was purchased from BOC.

2.7.2 General Method for Deuteration of Silanes

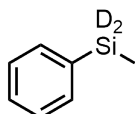


All reactions were performed in duplicate in protonated and deuterated solvent. To a flame-dried 60 mL Teflon-sealed J-Young ampoule (unless otherwise stated) containing pre-catalyst **1a**, **1b** or **1c** (5 mol%), C₆H₆ or C₆D₆ (500 μL) and silane (0.25 mmol) were added. The vessel was sealed, removed from the glovebox and subjected to freeze-pump-thaw cycles until a continuous vacuum was achieved. The ampoule was cooled in liquid nitrogen and backfilled with D₂ gas. The mixture was warmed to room temperature and stirred for 16 hours, turning from yellow to dark yellow after 30 minutes. Reactions containing volatile silanes in deuterated solvent were transferred to a H-distillation tube and separated from **1** by vacuum distillation. 1,3,5-Trimethoxybenzene (0.25 mmol) was added as a stock solution and spectroscopic yield and D-incorporation were determined by ¹H NMR spectroscopy. Reactions containing non-volatile silanes in deuterated solvent were isolated by FCC (SiO₂, pentane). Reactions in protonated solvent were transferred to the glovebox, toluene-*d*₈ (26.6 μL, 0.25 mmol) was added and D-incorporation was determined by ²H NMR spectroscopy.

2.7.3 Substrate Scope Spectroscopic Data

Catalysed by 1a

Methylphenyl(silane-*d*₂), **2a**

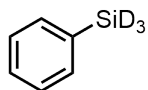


Deuterium incorporation: 97%

Spectroscopic yield: 95%

$^1\text{H NMR}$ (C_6D_6 , 400 MHz) δ 7.47-7.44 (m, 2H, ^mArH), 7.16-7.12 (m, 3H, $^{o,p}\text{ArH}$), 4.49-4.46 (m, 0.1H, SiH), 0.18 (s, 3H, CH_3); $^{13}\text{C}\{^1\text{H}\}$ NMR (C_6D_6 , 100 MHz) δ 135.2 ($^{\text{ArC}}$), 133.4 ($^{\text{ArC}}$), 129.8 ($^{\text{ArC}}$), 129.6 ($^{\text{ArC}}$), -7.81 (CH_3); $^{29}\text{Si NMR}$ (C_6D_6 , 125 MHz) δ -36.7 (p, $J=29.6$ Hz); $^2\text{H NMR}$ (C_6H_6 , 77 MHz) δ 4.58. NMR data consistent with a sample of the commercially available hydrosilane starting material.

Phenyl(silane- d_3), 2b

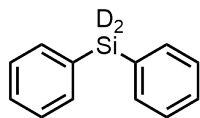


Deuterium incorporation: 95%

Spectroscopic yield: 97%

$^1\text{H NMR}$ (C_6D_6 , 400 MHz) δ 7.40-7.37 (m, 2H, ^mArH), 7.12-7.05 (m, 3H, $^{o,p}\text{ArH}$), 4.21 (s(br), 0.15H, SiH); $^{13}\text{C}\{^1\text{H}\}$ NMR (C_6D_6 , 100 MHz) δ 136.1 ($^{\text{ArC}}$), 130.0 ($^{\text{ArC}}$), 128.4 ($^{\text{ArC}}$); $^{29}\text{Si NMR}$ (C_6D_6 , 125 MHz) δ -61.0 (hept, $J=30.5$ Hz); $^2\text{H NMR}$ (C_6H_6 , 77 MHz) δ 4.29. NMR data consistent with a sample of the commercially available hydrosilane starting material.

Diphenyl(silane- d_2), 2c



0.25 mmol scale

Deuterium incorporation: 97%

Isolated yield: 87%

Isolated as a colourless oil (40.3 mg, 0.217 mmol, 87%). $^1\text{H NMR}$ (C_6D_6 , 400 MHz) δ 7.55-7.53 (m, 4H, ^mArH), 7.19-7.13 (m, 6H, $^{o,p}\text{ArH}$), 5.10 (s(br), 0.06H, SiH); $^{13}\text{C}\{^1\text{H}\}$ NMR (C_6D_6 , 125 MHz) δ 136.1 ($^{\text{ArC}}$), 131.7 ($^{\text{ArC}}$), 130.1 ($^{\text{ArC}}$), 128.5 ($^{\text{ArC}}$); $^{29}\text{Si NMR}$ (C_6D_6 , 125 MHz) δ -34.3 (p, $J=30.3$ Hz); $^2\text{H NMR}$ (C_6H_6 , 77 MHz) δ 5.10. NMR data consistent with a sample of the commercially available hydrosilane starting material.

2.5 mmol scale

Deuterium incorporation: 96%

Isolated yield: 92%

Reaction undertaken in a 375 mL ampoule. Isolated as a colourless oil (430 mg, 2.31 mmol, 92%). $^1\text{H NMR}$ (C_6D_6 , 400 MHz) δ 7.55-7.53 (m, 4H, ^mArH), 7.19-7.12 (m, 6H, $^{o,p}\text{ArH}$), 5.11 (s(br), 0.08H, SiH); $^{13}\text{C}\{^1\text{H}\}$ NMR (C_6D_6 , 125 MHz) δ 136.1 ($^{\text{ArC}}$), 131.7 ($^{\text{ArC}}$), 130.1 ($^{\text{ArC}}$), 128.5 ($^{\text{ArC}}$); $^{29}\text{Si NMR}$ (C_6D_6 , 125 MHz) δ -34.3 (p, $J=30.3$ Hz); $^2\text{H NMR}$ (C_6H_6 , 77 MHz) δ 5.09. NMR data consistent with a sample of the commercially available hydrosilane starting material.

0.25 mmol in pentane

Deuterium incorporation: 97%

Isolated yield: 76%

Isolated as a colourless oil (35.5 mg, 0.190 mmol, 76%). $^1\text{H NMR}$ (C_6D_6 , 400 MHz) δ 7.55-7.53 (m, 4H, ^mArH), 7.19-7.12 (m, 6H, $^{o,p}\text{ArH}$), 5.11 (s(br), 0.07H, SiH); NMR data consistent with a sample of the commercially available hydrosilane starting material.

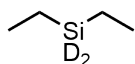
2.5 mmol scale neat

Deuterium incorporation: 83%

Isolated yield: 96%

Reaction undertaken in a 375 mL ampoule. Isolated as a colourless oil (446 mg, 2.39 mmol, 96%). $^1\text{H NMR}$ (C_6D_6 , 400 MHz) δ 7.53-7.51 (m, 4H, ^mArH), 7.18-7.11 (m, 6H, $^{o,p}\text{ArH}$), 5.10 (s(br), 0.07H, SiH₂) 5.09 (s(br), 0.26H, SiHD); $^{29}\text{Si NMR}$ (C_6D_6 , 125 MHz) δ -34.0 (t, $J=30.4$ Hz, SiHD), -34.2 (p, $J=30.3$ Hz, SiD₂); $^2\text{H NMR}$ (C_6H_6 , 77 MHz) δ 5.09. NMR data consistent with a sample of the commercially available hydrosilane starting material.

Diethyl(silane- d_2), 2d

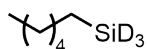


Deuterium incorporation: 98%

Spectroscopic yield: 59%

$^1\text{H NMR}$ (C_6D_6 , 400 MHz) δ 3.84 (s(br), 0.04H, SiH), 0.95 (t, $J=7.9$ Hz, 6H, CH₃), 0.52 (q, $J=7.9$ Hz, 4H, CH₂); $^{13}\text{C}\{^1\text{H}\}$ NMR (C_6D_6 , 125 MHz) δ 9.2 (CH₃), 1.1 (CH₂); $^{29}\text{Si NMR}$ (C_6D_6 , 125 MHz) δ -23.7 (p, $J=28.0$ Hz); $^2\text{H NMR}$ (C_6H_6 , 77 MHz) δ 3.89. NMR data consistent with a sample of the commercially available hydrosilane starting material.

Hexyl(silane- d_3), 2e

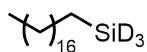


Deuterium incorporation: 96%

Spectroscopic yield: >99%

$^1\text{H NMR}$ (C_6D_6 , 400 MHz) δ 3.64-3.61 (m, 0.13H, SiH), 1.32-1.10 (m, 8H), 0.87 (t, $J=7.0$ Hz, 3H, CH₃), 0.51 (t, $J=7.7$ Hz, 2H, SiCH₂); $^{13}\text{C}\{^1\text{H}\}$ NMR (C_6D_6 , 125 MHz) δ 32.5 (CH₂), 31.8 (CH₂), 26.6 (CH₂), 22.9 (CH₂), 14.3 (CH₃), 5.9 (CH₂SiD₃); $^{29}\text{Si NMR}$ (C_6D_6 , 125 MHz) δ -60.6 (hept, $J=29.3$ Hz); $^2\text{H NMR}$ (C_6H_6 , 77 MHz) δ 3.67. NMR data consistent with a sample of the commercially available hydrosilane starting material.

Octadecyl(silane- d_3), 2f

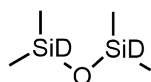


Deuterium incorporation: 96%

Isolated yield: 86%

Isolated as a colourless solid (61.8 mg, 0.215 mmol, 86%). $^1\text{H NMR}$ (C_6D_6 , 400 MHz) δ 3.64 (s(br), 0.12H, SiH), 1.34-1.25 (m, 32H), 0.93-0.88 (m, 3H, CH_3), 0.56 (t, $J=7.0$ Hz, 2H, SiCH_2); $^{13}\text{C}\{^1\text{H}\}$ NMR (C_6D_6 , 125 MHz) δ 33.0 (CH_2), 32.4 (CH_2), 30.3 (CH_2), 30.2 (CH_2), 30.2 (CH_2), 30.0 (CH_2), 29.9 (CH_2), 29.7 (CH_2), 26.7 (CH_2), 23.2 (CH_2), 14.4 (CH_2), 6.0 (CH_3), 1.4 (CH_2SiD_3); $^{29}\text{Si NMR}$ (C_6D_6 , 125 MHz) δ -60.8 (hept, $J=29.3$ Hz); $^2\text{H NMR}$ (C_6H_6 , 77 MHz) δ 3.64. NMR data consistent with a sample of the commercially available hydrosilane starting material.

1,1,3,3-Tetramethyldi(siloxane-*d*), 2g

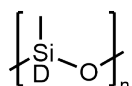


Deuterium incorporation: 98%

Spectroscopic yield: 73%

$^1\text{H NMR}$ (C_6D_6 , 400 MHz) δ 4.97-4.94 (m, 0.05H, SiH), 0.13 (s, 12H, CH_3); $^{13}\text{C}\{^1\text{H}\}$ NMR (C_6D_6 , 125 MHz) δ 0.55 (m, CH_3); $^{29}\text{Si NMR}$ (C_6D_6 , 125 MHz) δ -4.94 (t, $J=31.4$ Hz); $^2\text{H NMR}$ (C_6H_6 , 77 MHz) δ 5.00. NMR data consistent with a sample of the commercially available hydrosilane starting material.

Poly(methyldeuterosiloxane), 2h

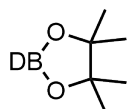


Deuterium incorporation: quant.

Spectroscopic yield: 67% (based on $^2\text{H NMR}$)

Analysed with no further purification. $^1\text{H NMR}$ (C_6D_6 , 400 MHz) δ 0.27 (s(br), 3H); $^2\text{H NMR}$ (C_6H_6 , 77 MHz) δ 5.14. NMR data consistent with a sample of the commercially available hydrosilane starting material.

4,4,5,5-Tetramethyl-1,3,2-dioxaborolane-*d*, 2i



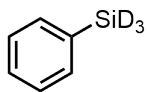
Deuterium incorporation: quant.

Spectroscopic yield: 73%

$^1\text{H NMR}$ (C_6D_6 , 400 MHz) δ 1.00 (s, 12H); $^{13}\text{C}\{^1\text{H}\}$ NMR (C_6D_6 , 125 MHz) δ 83.1 (CH), 24.9 (CH_3); $^{11}\text{B NMR}$ (C_6D_6 , 128 MHz) δ 28.3 (s). NMR data consistent with a sample of the commercially available pinacol borane starting material.

Catalysed by 1b

Phenyl(silane-*d*), 2b



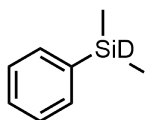
Deuterium incorporation: 96%

Spectroscopic yield: 78%

$^1\text{H NMR}$ (C_6D_6 , 400 MHz) δ 7.40-7.38 (m, 2H, ^mArH), 7.14-7.05 (m, 3H, $^{o,p}\text{ArH}$), 4.21 (s(br), 0.11H, SiH); $^2\text{H NMR}$ (C_6H_6 , 77 MHz) δ 4.26. NMR data consistent with a sample of the commercially available hydrosilane starting material.

Catalysed by 1c

Dimethylphenyl(silane-*d*), 2j

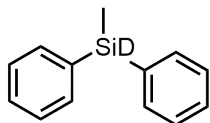


Deuterium incorporation: 96%

Spectroscopic yield: 98%

$^1\text{H NMR}$ (C_6D_6 , 400 MHz) δ 7.48-7.45 (m, 2H, ^mArH), 7.20-7.18 (m, 3H, $^{o,p}\text{ArH}$), 4.62 (m, 0.02H, SiH), 0.21 (s, 6H, CH_3); $^{13}\text{C}\{^1\text{H}\}$ NMR (C_6D_6 , 100 MHz) δ 137.5 ($^{\text{ArC}}$), 134.4 ($^{\text{ArC}}$), 129.5 ($^{\text{ArC}}$), 128.2 ($^{\text{ArC}}$), -3.81 (CH_3); $^{29}\text{Si NMR}$ (C_6D_6 , 125 MHz) δ -17.6 (t, $J=28.7$ Hz, SiD); $^2\text{H NMR}$ (C_6H_6 , 77 MHz) δ 4.63. NMR data consistent with a sample of the commercially available hydrosilane starting material.

Methyldiphenyl(silane-*d*), 2k

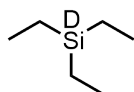


Deuterium incorporation: 99%

Isolated yield: 85%

$^1\text{H NMR}$ (C_6D_6 , 400 MHz) δ 7.52-7.49 (m, 4H, ^mArH), 7.19-7.13 (m, 6H, $^{o,p}\text{ArH}$), 5.14 (q, $J=3.8$ Hz, 0.01H, Si-H), 0.46 (s, 3H, CH_3); $^{13}\text{C}\{^1\text{H}\}$ NMR (C_6D_6 , 100 MHz) δ 135.6 ($^{\text{ArC}}$), 135.2 ($^{\text{ArC}}$), 129.8 ($^{\text{ArC}}$), 128.3 ($^{\text{ArC}}$), -5.0 (CH_3); $^{29}\text{Si NMR}$ (C_6D_6 , 125 MHz) δ -18.0 (t, $J=29.6$ Hz, SiD); $^2\text{H NMR}$ (C_6H_6 , 77 MHz) δ 5.15. NMR data consistent with a sample of the commercially available hydrosilane starting material.

Triethyl(silane-*d*), 2l



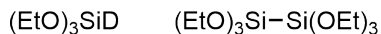
Deuterium incorporation: 98%

Spectroscopic yield: >99%

^1H NMR (C_6D_6 , 400 MHz) δ 3.90-3.86 (m, 0.03H, SiH), 0.97 (t, $J=7.9$ Hz, 9H, CH_3), 0.54 (q, $J=7.9$ Hz, 6H, CH_3); $^{13}\text{C}\{^1\text{H}\}$ NMR (C_6D_6 , 100 MHz) δ 8.4 (CH_3), 2.7 (CH_2); ^{29}Si NMR (C_6D_6 , 125 MHz) δ -0.5 (t, $J=27.2$ Hz, SiD); ^2H NMR (C_6H_6 , 77 MHz) δ 3.90. NMR data consistent with a sample of the commercially available hydrosilane starting material.

Triethoxy(silane-*d*) and hexamethoxydisilane, **2m** and **2m'**

0.7 : 0.3 Mixture



2m

Deuterium incorporation: 96%

Spectroscopic yield: 73%

^1H NMR (C_6D_6 , 400 MHz) δ 4.59 (s, 0.05H, SiH) 3.77 (q, $J=7.0$ Hz, 6H, CH_2), 1.13 (t, $J=7.0$ Hz, 9H, CH_3); ^{29}Si NMR (C_6D_6 , 125 MHz) δ -59.3 (t, $J=43.7$ Hz, SiD); ^2H NMR (C_6H_6 , 77 MHz) δ 4.60. NMR data consistent with a sample of the commercially available hydrosilane starting material.

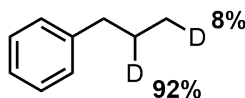
2m'

Spectroscopic yield: 31%

^1H NMR (C_6D_6 , 400 MHz) δ 3.87 (q, $J=7.0$ Hz, 6H, CH_2), 1.18 (t, $J=7.0$ Hz, 9H, CH_3); ^{29}Si NMR (C_6D_6 , 125 MHz) δ -82.0.

2.7.4 Method for Deuterium Labelling of Propylbenzene

Title compound was synthesised by modified literature procedure.⁷⁰ To a flame-dried 60 mL Teflon-sealed J-Young ampoule containing pre-catalyst **1a** (5 mol%), C_6D_6 (500 μL) and diphenylsilane (46.3 μL , 0.25 mmol, 1.0 equiv.) were added. The vessel was sealed, removed from the glovebox and free-pump-thawed until a continuous vacuum was achieved. The ampoule was cooled in liquid nitrogen and backfilled with D_2 gas. The mixture was warmed to room temperature and stirred for 16 hours. The vessel was depressurised and returned to the glovebox. Allyl benzene (33.1 μL , 0.25 mmol, 1.0 equiv.) and aniline (22.8 μL , 0.25 mmol, 1.0 equiv.) were added. The tube was sealed and the reaction was allowed to proceed for 16 hours at room temperature. The solution was transferred to a H-distillation tube and separated from **1a** by vacuum distillation. 1,3,5-Trimethoxybenzene (0.25 mmol) was added as a stock solution and spectroscopic yield and D-incorporation were determined by ^1H and ^2H NMR spectroscopy.



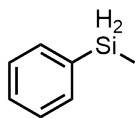
Spectroscopic yield: 95%

^1H NMR (C_6D_6 , 400 MHz) δ 7.18-7.15 (m, 2H, ^mArH), 7.09-7.04 (m, 3H, $^{o,p}\text{ArH}$), 2.44-2.40 (m, 2H, ArCH_2), 1.53-1.43 (m, 1.1H, CHD), 0.84-0.80 (m, 2.9H, CH_3). ^2H NMR (C_6H_6 , 77 MHz) δ 1.50 (s, 0.92D), 0.82 (s, 0.08D). $^{13}\text{C}\{^1\text{H}\}$ NMR (CDCl_3 , 125 MHz) δ 142.4 ($^{\text{Ar}}\text{C}$), 128.4 ($^{\text{Ar}}\text{C}$), 128.2 ($^{\text{Ar}}\text{C}$), 125.6 ($^{\text{Ar}}\text{C}$), 37.9 (CH_2), 24.1 (t, $J=19.5$ Hz, CDH), 13.4 (CH_3). NMR data consistent with a sample of the commercially available protonated starting material.

2.7.5 Method for Hydrogenation of Methylphenyl(silane- d_2)

Methylphenyl(silane- d_2 (98%)) was prepared according to general procedure for deuteration of silanes. To a flame-dried 60 mL Teflon-sealed J-Young ampoule containing pre-catalyst **1a** (5 mol%), a solution of methylphenyl (silane- d_2 (98%)) in C_6D_6 (500 μL) was added. The vessel was sealed, removed from the glovebox and subjected to freeze-pump-thaw cycles until a continuous vacuum was achieved. The ampoule was cooled in liquid nitrogen and backfilled with H_2 gas. The mixture was warmed to room temperature and stirred for 16 hours. The solution was transferred to a H-distillation tube and separated from **1a** by vacuum distillation. 1,3,5-Trimethoxybenzene (0.25 mmol) was added as a stock solution and spectroscopic yield and D-incorporation were determined by ^1H NMR spectroscopy.

Methylphenylsilane, **2a-H**



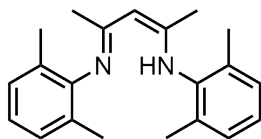
Hydrogen incorporation: 95%

Spectroscopic yield: 69%

^1H NMR (C_6D_6 , 400 MHz) δ 7.47-7.44 (m, 2H, ^mArH), 7.19-7.12 (m, 3H, $^{o,p}\text{ArH}$), 4.48 (q, $J=4.3$ Hz, 1.9H, SiH), 0.18 (t, $J=4.3$ Hz, 3H, CH_3). NMR data consistent with a sample of the commercially available protonated starting material.

2.7.6 Ligand and Complex Syntheses

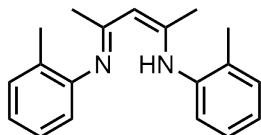
2,6-dimethylphenylBDK



Title compound was synthesised by modified literature procedure.⁹⁵ To a 20 mL microwave reactor vial, 2,6-dimethylaniline (6.05 g, 50.0 mmol, 2.0 equiv.), acetylacetone (2.50 g, 25.0 mmol, 1.0 equiv.) and conc. HCl (2.5 mL) were added. The vial was sealed and heated to 85 $^\circ\text{C}$ under 150 W microwave irradiation with stirring for 30 minutes. The mixture was cooled to room temperature and a solution of Na_2CO_3 (4.00 g) in water (100 mL) was added. The mixture was extracted with DCM (3×100 mL).

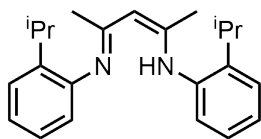
The organic extracts were combined, dried over MgSO₄, filtered and concentrated under reduced pressure. The crude product was dissolved in methanol (100 mL) and cooled to -20 °C, yielding white crystals of 2,6-dimethylphenylBDK (3.59 g, 11.7 mmol, 47%). **¹H NMR** (CDCl₃, 400 MHz) δ 12.21 (s (br), 1H, NH), 7.05 (d, *J*=7.5 Hz, 4H, ^mArH), 6.96 (dd, *J*=8.1, 6.8 Hz, 2H, ^pArH), 4.90 (s, 1H, CH), 2.18 (s, 12H, CH₃), 1.71 (s, 6H, CH₃); **¹³C{¹H} NMR** (CDCl₃, 125 MHz) δ 160.9 (CN), 143.9 (^{Ar}C), 132.3 (^{Ar}C), 127.9 (^{Ar}C), 124.4 (^{Ar}C), 93.5 (^{backbone}CH), 20.5 (CH₃), 18.5 (CH₃); **HRMS**(ESI) predicted: 307.2174, found: 307.2176 [M+H]⁺. Analytical data in agreement with previous report.⁹⁵

2-methylphenylBDK



Title compound was synthesised following modified literature procedure.⁹⁶ To a stirred solution of 2-methylaniline (10.8 mL, 0.1 mol, 2.0 equiv.) and p-toluenesulfonic acid (9.6 g, 0.05 mol, 1.0 equiv.) in toluene (250 mL), acetylacetone (5.2 mL, 0.05 mol, 1.0 equiv.) was added. The solution was heated to 140 °C with the incorporation of a Dean-Stark trap and refluxed for 16 hours. The reaction was cooled and yellow precipitate was filtered before being suspending in diethyl ether (250 mL) and water (100 mL). Sodium carbonate (12 g) was added and the mixture was stirred until dissolution was observed. The organic phase was separated and washed with brine (50 mL). The organic phase was separated, dried over magnesium sulfate, filtered and concentrated. Yellow oil was dissolved in ethanol (100 mL) and cooled to -20 °C yielding yellow crystals of ^{2-Me}BDK (9.03 g, 32.4 mmol, 65%). **¹H NMR** (CDCl₃, 400 MHz) δ 12.5 (s, 1H, NH), 7.14 (dd, *J*=17.5, 7.7 Hz, 4H, ArH), 6.99-6.90 (m, 4H, ArH), 4.89 (s, 1H, CH), 2.19 (s, 6H, CH₃), 1.89 (s, 6H, CH₃). **¹³C{¹H} NMR** (CDCl₃, 100 MHz) δ 159.7 (CN), 144.7 (^{Ar}C), 130.8 (^{Ar}C), 130.4 (^{Ar}C), 126.2 (^{Ar}C), 123.7 (^{Ar}C), 123.1 (^{Ar}C), 96.7 (^{backbone}C), 20.9 (CH₃), 18.4 (CH₃). **HRMS**(ESI) predicted: 279.1861, found: 279.1860 [M+H]⁺. Analytical data in agreement with previous report.⁹⁶

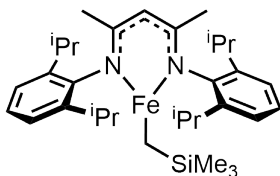
2-isopropylphenylBDK



Title compound was synthesised following modified literature procedure.⁹⁷ To a stirred solution of 2-isopropylaniline (5.0 mL, 35.4 mmol, 2.0 equiv.) and p-toluenesulfonic acid (609 mg, 3.20 mmol, 0.2 equiv.) in toluene (100 mL), acetylacetone (1.64 mL, 16.0 mmol, 1.0 equiv.) was added. The solution was heated to 140 °C with the incorporation of a Dean-Stark trap and refluxed for 16 hours. The mixture was cooled and concentrated. Saturated NaHCO₃ solution (100 mL) was added and extracted with DCM (3 × 50 mL). The organic phases were combined, dried over MgSO₄, filtered and concentrated. Yellow oil was dissolved in methanol and cooled to -20 °C yielding off-white crystals of ^{2-isopropylphenyl}BDK (4.12g, 12.3

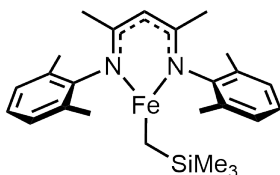
mmol, 77%). **¹H NMR** (C₆D₆, 400 MHz) δ 12.46 (s(br), 1H, NH), 7.26 (m, 2H, ArH), 7.11 (m, 4H, ArH), 6.89 (m, 2H, ArH), 4.91 (s, 1H, ^{backbone}CH), 3.19 (hept, $J=6.9$ Hz, 2H, ⁱPrCH), 1.90 (s, 6H, ^{backbone}CH₃), 1.16 (d, $J=6.9$ Hz, 12H, ⁱPrCH₃). **¹³C{¹H} NMR** (CDCl₃, 100 MHz) δ 160.1 (CN), 143.5 (^{Ar}C), 141.7 (^{Ar}C), 125.9 (^{Ar}C), 125.7 (^{Ar}C), 124.4 (^{Ar}C), 124.1 (^{Ar}C), 96.4 (^{backbone}CH), 28.2 (CH), 23.4 (CH₃), 21.0 (CH₃). **HRMS**(ESI) predicted: 335.2487, found: 335.2448 [M+H]⁺. Analytical data in agreement with previous report.⁹⁷

(2,6-diisopropylphenyl)BDK)Fe(CH₂TMS), **1a**



Title compound was synthesised following literature procedure.⁷¹ To a flame dried ampoule containing a solution of 2,6-diisopropylphenylBDK (2.21 g, 5.28 mmol, 1.0 equiv.) in THF (100 mL) at -78 °C, ⁿbutyllithium (2.5 M solution in hexanes, 2.11 mL, 5.28 mmol, 1.0 equiv.) was added dropwise. The solution was warmed to room temperature and stirred for 1 hour. FeCl₂·(THF)_{1.5} (1.24 g, 5.28 mmol, 1.0 equiv.) was added and the mixture was stirred for a further 45 minutes. LiCH₂TMS (497 mg, 5.28 mmol, 1.0 equiv.) was added and the mixture was stirred for a further 45 minutes. Volatiles were removed under reduced pressure. The mixture was suspended in pentane (2 × 20 mL) and concentrated to remove residual coordinating THF. Pentane (50 mL) was added and the solution isolated by cannula filtration through a celite plug. The filtrate was concentrated to 20 mL and cooled to -20 °C, yielding yellow crystals of (2,6-diisopropylphenylBDK)Fe(CH₂TMS) (1.84 g, 3.28 mmol, 62%). ¹H NMR (C₆D₆, 400 MHz) δ 111.77 (s(br), 1H, backbone CH), 72.80 (s(br), 6H, backbone CH₃), 54.88 (s(br), 9H, SiMe₃), -8.29 (s(br), 4H, ^mArH), -14.04 (s(br), 12H, ⁱPr-CH₃), -67.02 (s(br), 2H, ^pArH), -97.74 (s(br), 12H, ⁱPr-CH₃), -124.14 (s(br), 4H, ⁱPr-CH). NMR data in agreement with previous report.⁷¹

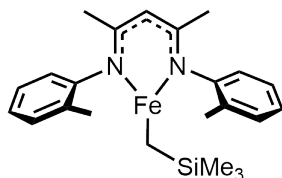
(2,6-dimethylphenyl)BDK)Fe(CH₂TMS), **1b**



Title compound was synthesised following literature procedure.⁹⁸ To a flame dried ampoule containing a solution of 2,6-dimethylphenylBDK (2.03 g, 6.62 mmol, 1.0 equiv.) in THF (40 mL) at -78 °C, ⁿbutyllithium (2.5 M solution in hexanes, 1.6 mL, 6.62 mmol, 1.0 equiv.) was added dropwise. The solution was warmed to room temperature and stirred for 1 hour. FeCl₂·(THF)_{1.5} (1.56 g, 6.62 mmol, 1.0 equiv.) was added and the mixture was stirred for a further 45 minutes. LiCH₂TMS (623 mg, 6.62 mmol, 1.0 equiv.) was added and the mixture was stirred for a further 45 minutes. Volatiles were removed under reduced pressure and the remaining yellow solid was left under vacuum (2 × 10⁻² mbar) for 2 hours to remove residual coordinating THF. The mixture was suspended in pentane (2 × 5 mL) and concentrated to remove residual coordinating THF. Pentane (20 mL) was added and the solution isolated by cannula filtration. The filtrate was concentrated to 5 mL and cooled to -20 °C, yielding red crystals of (2,6-dimethylphenylBDK)Fe(CH₂TMS) (2.50 g, 5.57 mmol, 84%). ¹H NMR (C₆D₆, 400 MHz) δ 98.09 (s(br), 1H, backbone CH), 78.86 (s(br), 6H, backbone CH₃), 34.41 (s(br), 9H, SiMe₃), -4.58 (s(br), 4H, ^{Ar}CH), -60.28 (s(br), 12H, ^{Ar}CH₃), -68.73 (s(br), 2H, ^{Ar}CH). **CHN** calculated for C₂₅H₃₆FeN₂Si: C, 66.95; H, 8.09; N, 6.25; found: C, 66.89; H, 8.22; N, 6.08. **MP** 79-81 °C. **UV/vis** (pentane) 321 nm. **sc-XRD**

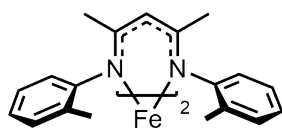
relevant crystallographic data are reported in the X-ray crystallography section. Screening of multiple crystals revealed a mixture of monomeric and dimeric $(^{2,6\text{-dmp}}\text{BDK})\text{Fe}(\text{CH}_2\text{TMS})$.

$(^{2\text{-methylphenyl}}\text{BDK})\text{Fe}(\text{CH}_2\text{TMS})$ and $(^{2\text{-methylphenyl}}\text{BDK})_2\text{Fe}$, **1c and **1c'****



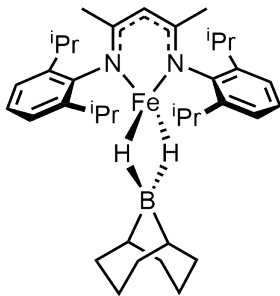
Title compounds were synthesised by modified literature procedure.⁹⁸ To a flame dried schlenk containing a solution of $^{2\text{-methylphenyl}}\text{BDK}$ (1.00 g, 3.59 mmol, 1.0 equiv.) in THF (20 mL) at $-78\text{ }^\circ\text{C}$, n butyllithium (2.5M solution in hexanes, 1.44 mL, 3.59 mmol, 1.0 equiv.) was added dropwise. The solution was warmed to room temperature and stirred for 45 mins. $\text{FeCl}_2\cdot(\text{THF})_{1.5}$ (843 mg, 3.59 mmol, 1.0 equiv.) was added and the mixture was stirred for a further 45 minutes. LiCH_2TMS (338 mg, 3.59 mmol, 1.0 equiv.) was added and the mixture was stirred for a further 45 minutes. Volatiles were removed under reduced pressure and the remaining yellow solid was left under vacuum (2×10^{-2} mbar) for 2 hours to remove residual coordinating THF. Pentane (20 mL) was added and the solution isolated by cannula filtration. The filtrate was concentrated to 5 mL and cooled to $-20\text{ }^\circ\text{C}$, yielding a mixture of yellow and red crystals of $(^{2\text{-Me}}\text{BDK})\text{Fe}(\text{CH}_2\text{TMS})$ dimer and homoleptic $(^{2\text{-Me}}\text{BDK})_2\text{Fe}$, respectively (396 mg, 0.942 mmol, 26%). Peaks associated with **1c**: $^1\text{H NMR}$ (C_6D_6 , 400 MHz) δ 73.97, 55.70, 30.75, -3.40, 5.41, -6.33, -7.71, -48.10, -61.37, -64.53, -67.44. **sc-XRD** relevant crystallographic data are reported in the X-ray crystallography section. Screening of multiple crystals revealed a mixture of $(^{2\text{-Me}}\text{BDK})\text{Fe}(\text{CH}_2\text{TMS})$ dimer and homoleptic $(^{2\text{-Me}}\text{BDK})_2\text{Fe}$.

$(^{2\text{-methylphenyl}}\text{BDK})_2\text{Fe}$, **1c'**



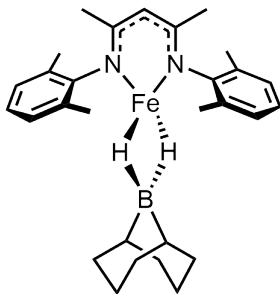
To a flame dried schlenk containing a solution of $^{2\text{-methylphenyl}}\text{BDK}$ (278 mg, 1.00 mmol, 1.0 equiv.) in THF (10 mL) at $-78\text{ }^\circ\text{C}$, n butyllithium (2.5M solution in hexanes, 400 μL , 1.00 mmol, 1.0 equiv.) was added dropwise. The solution was warmed to room temperature and stirred for 45 mins. $\text{FeCl}_2\cdot(\text{THF})_{1.5}$ (118 mg, 0.50 mmol, 0.5 equiv.) was added and the mixture was stirred for a further 45 minutes. Volatiles were removed under reduced pressure. Pentane (10 mL) was added and the filtrate isolated by cannula filtration. The solution was concentrated yielding $(^{2\text{-Me}}\text{BDK})_2\text{Fe}$ as a pink powder (270 mg, 0.442 mmol, 88%). $^1\text{H NMR}$ (C_6D_6 , 400 MHz) δ 44.02, 39.49, 34.99, 24.77, 22.26, 21.98, 21.49, 21.06, 20.50, 19.66, 18.74, 18.26, 18.04, 17.11, 16.30, -38.52, -39.25, -39.89, -42.59, -48.56, -72.67, -78.73, -80.52, -82.10, -84.10, -87.06. **CHN** calculated for $\text{C}_{38}\text{H}_{42}\text{FeN}_4$: C, 74.75; H, 6.93; N, 9.18; found: C, 73.96; H, 6.29; 8.81. **MP** 96-100 $^\circ\text{C}$. **UV/vis** (hexane) 218.40, 341.20 nm. **sc-XRD** Crystals suitable for X-ray diffraction were grown from a saturated solution in pentane at $-20\text{ }^\circ\text{C}$ and identity was confirmed by unit cell check.

(2,6-diisopropylphenylBDK)Fe- κ^2 -9-BBN, **3a**



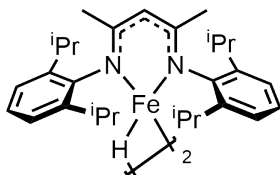
Title compound was synthesised following literature procedure.⁹⁸ To a flame dried schlenk containing **1a** (561 mg, 1.0 mmol, 1.0 equiv.) dissolved in toluene (5 mL), 9-borabicyclo [3.3.1]nonane (244 mg, 1.0 mmol, 1.0 equiv.) was added. The vessel was heated to 60 °C and stirred for 16 hours. The solution was concentrated under reduced pressure. The solid was dissolved in a minimum amount of pentane and cooled to -20 °C, yielding pink crystals of (2,6-diⁱppBDK)Fe- κ^2 -9-BBN (337 mg, 0.565 mmol, 57%). ¹H NMR (C₆D₆, 400 MHz) δ 1474.4 (FeH), 161.88, 83.25, 57.93, 41.76, 37.95, 29.76, 19.08, -2.60, -10.19, -32.75, -35.03, -50.31. CHN calculated for C₃₇H₅₇BFen₂: C, 74.50; H, 9.63; N, 4.70; found: C, 74.51; H, 9.44; N, 4.63. MP 130-131 (decomposition), 188-190 (melt) °C. UV/vis (pentane) 397, 296 nm. sc-XRD relevant crystallographic data are reported in the X-ray crystallography section.

(2,6-dimethylphenylBDK)Fe- κ^2 -9-BBN, **3b**



Title compound was synthesised following literature procedure.⁹⁸ To an ampoule containing **1b** (449 mg, 1.0 mmol, 1.0 equiv.) dissolved in toluene (5 mL), 9-borabicyclo[3.3.1]nonane (244 mg, 1.0 mmol, 1.0 equiv.) was added. The vessel was heated to 60 °C and stirred for 16 hours. The solution was concentrated under reduced pressure. The solid was dissolved in a minimum amount of toluene and cooled to -20 °C, yielding pink crystals of (2,6-dmpBDK)Fe- κ^2 -9-BBN (210 mg, 0.433 mmol, 43%). ¹H NMR (C₆D₆, 400 MHz) δ 163.25 (FeH), 83.55, 54.67, 36.53, 31.15, 23.33, 22.80, 7.62, -31.95, -48.75. CHN calculated for C₂₉H₄₁BFen₂: C, 71.92; H, 8.53; N, 5.78; found: C, 71.98; H, 8.57; N, 5.74. MP 156-158 (decomposition), 208-212 (melt) °C. UV/vis (pentane) 393, 293 nm. sc-XRD relevant crystallographic data are reported in the X-ray crystallography section.

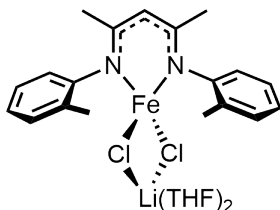
[(diisopropylphenylBDK)FeH]₂, **4a**



Title compound was synthesised according to literature procedure.⁶¹ To a solution of **1a** (200 mg, 0.36 mmol, 1.0 equiv.) in toluene (1 mL), TMP.BH₃ (167 mg, 1.08 mmol, 3.0 equiv.) was added. The vessel was sealed and stirred at 80 °C for 16 hours. The mixture was concentrated under reduced pressure and pentane (5 mL) was added. The mixture was filtered and cooled to -20 °C yielding red crystals of [(diⁱPrP)BDK)FeH]₂ (63.5 mg, 0.134 mmol, 37%). ¹H NMR (C₆D₆, 400 MHz) δ 13.0 (s(br), 12H, 8H, CH₃, ^mArH), 7.15 (s(br), 24H, ⁱPrCH₃), -24.0 (s(br), 4H, ^pArH), -24.9 (s(br), 24H, ⁱPrCH₃), -56.1 (s(br), 2H, ⁱPrCH). **sc-XRD** confirmed by unit cell check. Data in agreement with the literature.^{36,61}

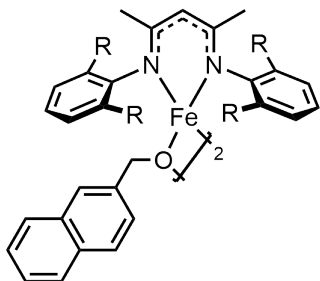
The synthesis of [(^{2,6}-dimethylphenylBDK)FeH]₂ (**4b**) was also attempted by an analogous method. A mixture of complexes [(^{2,6}-dimethylphenylBDK)FeH]₂ and Fe(^{2,6}-dimethylphenylBDK)₂ were isolated. The relevant crystallographic data are reported in the X-ray crystallography section. Thus far, a direct and selective synthesis of these complexes has not been achieved.

(²-methylphenylBDK)FeCl₂Li(THF)₂, **5**



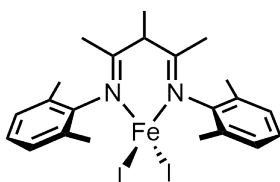
Title compound synthesised following modified literature procedure.⁸⁰ To a flame dried schlenk containing a stirred solution of ²-methylphenylBDK (278 mg, 1.0 mmol, 1.0 equiv.) in THF (10 mL) at -78 °C, ⁿbutyllithium (2.5 M in hexanes, 400 μL, 1.0 mmol, 1.0 equiv.) was added dropwise. The solution was warmed to room temperature and stirred for 1 hour. FeCl₂·(THF)_{1.5} (235 mg, 1.0 mmol, 1.0 equiv.) was added and stirred for 1 hour. The solution was concentrated, washed with pentane (3 × 5 mL) and dried yielding the title compound as a yellow powder in quantitative yield. Spectroscopic data in agreement with the literature.⁸⁰ Single crystals were grown from vapour diffusion of pentane into a saturated solution of THF and identity confirmed by unit cell check. ¹H NMR (THF, 500 MHz) δ 15.47, 9.12, -40.39, -53.34, -67.05, -101.96, -107.83.

(BDK)FeOCH₂C₁₀H₇ Complexes, **6a** and **6b**



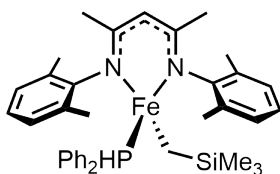
To a J-Young NMR tube containing (BDK)Fe-9-BBN complex (**3a** or **3b**, 0.125 mmol) dissolved in C₆D₆ (500 μL), 2-naphthaldehyde (39.0 mg, 0.25 mmol, 2.0 equiv.) was added. The reaction proceeded for 16 hours where a yellow precipitate forms. The precipitate was filtered, washed with pentane (3 × 2 mL) and dried. Solid was crystallised from vapour diffusion of pentane into a saturated solution of THF, yielding the title compound (yield not determined).

(2,6-dimethylphenyl)**3**-methylpentanediimine)FeI₂, **8b**



To a J-Young NMR tube containing **3b** (40.0 mg, 0.0826 mmol, 1.0 equiv.) dissolved in C₆D₆ (500 μL), iodomethane (51.4 μL, 0.826 mmol, 10.0 equiv.) was added. Reaction proceeded for 16 hours forming yellow single-crystals of the title compound (yield not determined).

(2,6-dimethylphenylBDK)FeCH₂TMS(PHPh₂), **12b**



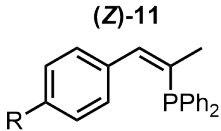
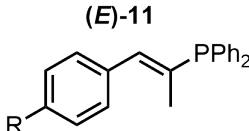
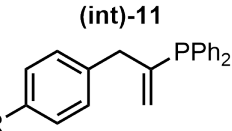
To a J-Young NMR tube containing **1b** (44.9 mg, 0.1 mmol, 1.0 equiv.) dissolved in C₆D₆ (500 μL), diphenylphosphine (17.4 μL, 0.1 mmol, 1.0 equiv.) was added. The tube was sealed and heated at 60 °C for 1 hour. The solution was concentrated, dissolved in pentane (1 mL) and cooled to -20 °C, yielding the title compound as orange crystals (18.7 mg, 0.0295 mmol, 29%). ¹H NMR (C₆D₆, 400 MHz) δ 28.18 (6H, backboneCH₃), 9.19 (6H, ^o-MeArCH₃), 6.80 (12H, ^o-MeArCH₃ and P-ArH), 6.38 (2H, ArH), 4.64 (2H, ArH), 3.28 (2H, ArH), -25.16 (9H, SiMe₃), -56.37 (1H, backboneCH). MP 91-94 °C (melt/decomposition). UV/vis 261.0, 316.6 nm. CHN Expected: C: 70.02, H: 7.46, N: 4.41, Found: C: 70.08, H: 7.11, N: 4.35.

2.7.7 Reaction Monitoring Method

To a high-pressure J-Young NMR tube containing [Fe] (5 mol%) and 1,3,5-trimethoxybenzene (0.25 mmol), C₆D₆ (500 μ L) and silane (0.25 mmol) were added. The tube was sealed, removed from the glovebox and subjected to freeze-pump-thaw cycles until a continuous vacuum was achieved. The tube was cooled in liquid nitrogen and backfilled with D₂ gas. The mixture was warmed to room temperature and the reaction was monitored for 16 hours. D-incorporation was determined by ¹H NMR spectroscopy.

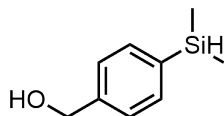
2.7.8 General Method for Hydrophosphination of Allenes

To a J-Young NMR tube containing pre-catalyst **1b** (11.2 mg, 0.025 mmol, 5 mol%) dissolved in C₆D₆ (600 μ L), allene (0.6 mmol, 1.2 equiv.) and diphenylphosphine (87.0 μ L, 0.5 mmol, 1.0 equiv.) was added. The tube was sealed and heated at 80 °C for 16 hours. Relative conversion of hydrophosphinated products was determined by ³¹P NMR spectroscopy.⁸⁵

			
R	³¹ P NMR Chemical Shift / ppm		
H	-13.3	8.9	-2.2
Me	-12.3	9.3	-2.4
OMe	-12.8	10.0	-2.8
Cl	-13.4	8.1	-2.6

2.7.9 Substrate Syntheses

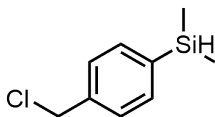
(4-(Dimethylsilyl)phenyl)methanol



Title compound was synthesised according to literature procedure.⁹⁹ To a solution of (4-bromophenyl)methanol (2.81 g, 15.0 mmol, 1.0 equiv.) in THF (50 mL) at -78 °C, ⁿbutyllithium (2.5 M solution in hexanes, 15.0 mL, 37.5 mmol, 2.5 equiv.) was added dropwise over 30 minutes. The mixture was stirred at this temperature for 2 hours before the dropwise addition of chlorodimethylsilane (2.25 mL, 20.0 mmol, 1.3 equiv.). The solution was warmed to room temperature and stirred for 16 hours. The reaction was quenched with saturated aqueous NH₄Cl solution (50 mL) and extracted with DCM (3 \times 50 mL). The organic extracts were combined, washed with water (50 mL) and brine (50 mL), dried over MgSO₄, filtered and concentrated under reduced pressure. The crude product was purified by column chromatography

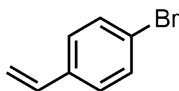
(SiO₂, pet. ether/EtOAc (4:1)) yielding (4-(dimethylsilyl)phenyl)methanol as a colourless oil (1.19 g, 7.14 mmol, 48%). ¹H NMR (CDCl₃, 400 MHz) δ 7.55 (d, *J*=7.8 Hz, 2H), 7.37 (d, *J*=7.8 Hz, 2H), 4.69 (s, 2H), 4.44 (hept, *J*=3.7 Hz, SiH), 0.35 (d, *J*=3.7 Hz, 6H); ¹³C{¹H} NMR (CDCl₃, 125 MHz) δ 142.0 (ArC), 137.0 (ArC), 134.4 (ArC), 126.6 (ArC), 65.4 (COH), -3.6 (SiCH₃); ²⁹Si NMR (CDCl₃, 125 MHz) δ -17.3. NMR data in agreement with the literature.⁹⁹

(4-(Chloromethyl)phenyl)dimethylsilane



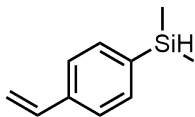
Title compound was synthesised according to literature procedure.⁹⁹ To a stirred solution of (4-(dimethylsilyl)phenyl)methanol (1.00 g, 6.01 mmol, 1.0 equiv.) in DCM (10 mL), triethylamine (1.01 mL, 7.22 mmol, 1.2 equiv.) was added dropwise. 4-Methylbenzenesulfonyl chloride (1.26 g, 6.61 mmol, 1.1 equiv.) was added and the solution was stirred for 16 hours. The mixture was diluted in DCM (10 mL) and washed with water (10 mL) and brine (10 mL). Organic extract was dried over MgSO₄, filtered and concentrated under reduced pressure. Crude product was purified by FCC (SiO₂, pentane) yielding (4-(chloromethyl)phenyl)dimethylsilane as a colourless oil (394 mg, 2.13 mmol, 36%). ¹H NMR (CDCl₃, 400 MHz) δ 7.55 (d, *J*=7.9 Hz, 2H), 7.39 (d, *J*=7.9 Hz, 2H), 4.59 (s, 2H), 4.43 (hept, *J*=3.7 Hz, SiH), 0.35 (d, *J*=3.7 Hz, 6H); ¹³C{¹H} NMR (CDCl₃, 125 MHz) δ 138.5 (ArC), 138.1 (ArC), 134.6 (ArC), 46.3 (CCl), -3.7 (SiCH₃); ²⁹Si NMR (CDCl₃, 125 MHz) δ -17.0. NMR data in agreement with the literature.⁹⁹

4-Bromostyrene



Title compound was synthesised according to literature procedure.¹⁰⁰ To a stirred suspension of methyltriphenylphosphonium iodide (5.33 g, 13.2 mmol, 1.1 equiv.) in THF (50 mL) at 0 °C, ⁿbutyllithium (2.5 M solution in hexanes, 6.6 mL, 16.5 mmol, 1.4 equiv.) was added dropwise over 30 minutes and left stirring for a further 2 hours. A solution of 4-bromobenzaldehyde (2.22 g, 12.0 mmol, 1.0 equiv.) in THF (10 mL) was added dropwise, warmed to room temperature and stirred for 16 hours. Et₂O (100 mL) was added and the solution was washed with water (100 mL) and brine (100 mL), dried over MgSO₄, filtered and concentrated under reduced pressure. Crude product was purified by FCC (SiO₂, pentane) yielding 4-bromostyrene as a colourless oil (739 mg, 4.04 mmol, 34%). ¹H NMR (CDCl₃, 400 MHz) δ 7.37 (d, *J*=8.4 Hz, 2H), 7.20 (d, *J*=8.5 Hz, 2H), 6.58 (dd, *J*=17.6, 10.9 Hz, 1H), 5.66 (d, *J*=18.1 Hz, 1H), 5.20 (d, *J*=10.9 Hz, 1H); ¹³C{¹H} NMR (CDCl₃, 100 MHz) δ 136.6 (ArC), 135.9 (ArC), 131.8 (ArC), 127.9 (ArC), 121.7 (CH), 114.8 (CH₂). NMR data in agreement with the literature.¹⁰⁰

Dimethyl(4-vinylphenyl)silane

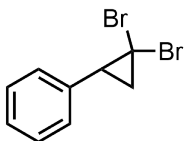


Title compound was synthesised by modified literature procedure.⁹⁹ To a solution of 4-bromostyrene (719 mg, 3.93 mmol, 1 equiv.) in THF (10 mL) at -78 °C, ⁿbutyllithium (2.5 M solution in hexanes, 1.89 mL, 1.2 equiv.) was added dropwise over 30 minutes. The mixture was stirred at this temperature for 2 hours before the dropwise addition of chlorodimethylsilane (873 μL, 7.86 mmol, 2.0 equiv.). The solution was warmed to room temperature and stirred for 16 hours. The reaction was quenched with saturated aqueous NH₄Cl solution (10 mL) and extracted with diethylether (3 × 10 mL). The organic extracts were combined, washed with water (20 mL) and brine (20 mL), dried over MgSO₄, filtered and concentrated under reduced pressure. The crude product was purified by FCC (SiO₂, pentane) yielding dimethyl(4-vinylphenyl)silane as a colourless oil (495 mg, 3.05 mmol, 78%). ¹H NMR (CDCl₃, 400 MHz) δ 7.53 (d, *J*=8.0 Hz, 2H), 7.42 (d, *J*=7.9 Hz, 2H), 6.73 (dd, *J*=17.6, 10.9 Hz, 1H), 5.80 (d, *J*=17.6 Hz, 1H), 5.28 (d, *J*=10.9 Hz, 1H), 4.44 (hept, *J*=3.8 Hz, 1H), 0.36 (d, *J*=3.8 Hz, 6H); ¹³C{¹H} NMR (CDCl₃, 125 MHz) δ 138.5 (ArC), 137.2 (ArC), 137.0 (ArC), 134.4 (ArC), 125.8 (CH), 114.4 (CH₂), -3.62 (SiCH₃); ²⁹Si NMR (CDCl₃, 125 MHz) δ -17.3. NMR data in agreement with the literature.⁹⁹

General method for synthesis of (2,2-dibromocyclopropyl)benzenes

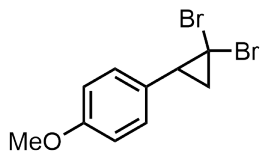
Compounds were synthesised by modified literature procedure.¹⁰¹ To a stirred mixture of alkene (1.0 equiv.), bromoform (1.5 equiv.) and BnNEt₃Cl (1 mol%), NaOH (50 wt% in water, 4.0 equivs.) was added dropwise. The mixture was stirred for 3 hours at room temperature. Water was added and the solution was extracted with DCM. Organic phases were combined, washed with brine, dried over MgSO₄ and filtered. Filtrate was concentrated and purified by FCC (SiO₂, pentane).

(2,2-dibromocyclopropyl)benzene



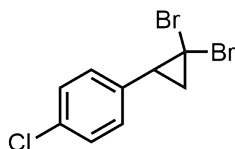
Title compound isolated as a colourless oil (2.97 g, 10.7 mmol, 54%). Spectroscopic data in agreement with previous literature.¹⁰² ¹H NMR (CDCl₃, 400 MHz) δ 7.45-7.37 (m, 3H, ArH), 7.33-7.7.30 (m, 2H, ArH), 3.03 (dd, *J*=10.5, 8.4 Hz, 1H, CH), 2.20 (dd, *J*=10.5, 7.7 Hz, 1H, CH₂), 2.08 (dd, *J*=8.4 Hz, 7.7 Hz, 1H, CH₂); ¹³C{¹H} NMR (CDCl₃, 100 MHz) δ 136.1 (ArC), 129.0 (ArC), 128.4 (ArC), 127.8 (ArC), 36.1 (ArCH), 28.6 (CBr₂), 27.4 (CH₂).

(2,2-dibromocyclopropyl)-4-methoxybenzene



Title compound isolated as a colourless oil (2.25 g, 7.35 mmol, 37%). Spectroscopic data in agreement with previous literature.¹⁰¹ $^1\text{H NMR}$ (CDCl_3 , 400 MHz) δ 7.18-7.16 (m, 2H, ArH), 6.88 (dd, $J=8.7$, 2.0 Hz, 2H, ArH), 3.81 (s, 3H, OCH_3), 2.89 (dd, $J=10.7$, 8.5 Hz, 1H, CH), 2.09 (m, 1H, CH), 1.94 (td, $J=8.5$, 1.9 Hz, 1H, CH); $^{13}\text{C}\{^1\text{H}\}$ NMR (CDCl_3 , 100 MHz) δ 159.2 (ArC), 130.1 (ArC), 128.3 (ArC), 113.8 (ArC), 55.4 (OCH_3), 35.5 (ArCH), 29.4 (CBr_2), 27.5 (CH_2).

(2,2-dibromocyclopropyl)-4-chlorobenzene

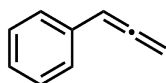


Reaction heated at 90 °C for 48 hours. Title compound isolated as a colourless oil (6.81 g, 21.9 mmol, 64%). Spectroscopic data in agreement with previous literature.¹⁰¹ $^1\text{H NMR}$ (CDCl_3 , 400 MHz) δ 7.35-7.31 (d, $J=8.5$ Hz, 2H, ArH), 7.19 (d, $J=8.1$ Hz, 2H, ArH), 2.91 (dd, $J=10.5$, 8.1 Hz, 1H, CH), 2.15 (dd, 10.5, 7.8 Hz, 1H, CH), 1.97 (t, $J=8.0$ Hz, 1H, CH).

General method for synthesis of Phenylallenes

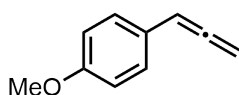
Compounds were synthesised by modified literature procedure.¹⁰¹ To a stirred solution of dibromocyclopropylbenzene (1.0 equiv.) dissolved in THF at 0 °C, EtMgBr (3M solution, 1.2 equiv.) was added dropwise. The solution was warmed to room temperature and stirred for 1 hour. The solution was cooled to 0 °C and slowly quenched with water. Excess 1M HCl was added and the solution extracted with petroleum ether. Organic phases were combined, dried over MgSO_4 , filtered and concentrated. Crude mixture was purified by FCC (pentane, SiO_2).

Phenylallene



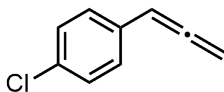
Title compound isolated as a colourless oil (yield not determined). Spectroscopic data in agreement with previous literature.¹⁰² $^1\text{H NMR}$ (CDCl_3 , 400 MHz) δ 7.33-7.19 (m, 5H, ArH), 6.17 (td, $J=7.0$, 1.9 Hz, 1H, CH), 5.15 (d, $J=7.0$ Hz, 2H, CH_2); $^{13}\text{C}\{^1\text{H}\}$ NMR (CDCl_3 , 100 MHz) δ 209.9 (C), 134.0 (ArC), 128.7 (ArC), 127.0 (ArC), 126.8 (ArC), 94.1 (CH), 78.9 (CH_2).

4-Methoxyphenylallene



Title compound isolated as a colourless oil (878 mg, 6.54 mmol, 89%). Spectroscopic data in agreement with previous literature.¹⁰¹ ^1H NMR (CDCl_3 , 400 MHz) δ 7.26 (d, $J=8.7$ Hz, 2H, ArH), 6.86 (d, $J=8.7$ Hz, 2H, ArH), 6.13 (t, $J=6.8$ Hz, 1H, CH), 5.12 (d, $J=6.8$ Hz, 2H, CH_2), 3.80 (s, 3H, OCH_3); $^{13}\text{C}\{^1\text{H}\}$ NMR (CDCl_3 , 100 MHz) δ 209.5 (C), 158.9 (ArC), 127.9 (ArC), 126.3 (ArC), 114.3 (ArC), 93.4 (CH), 78.9 (CH_2), 55.5 (OCH_3).

4-Chlorophenylallene



Title compound isolated as a colourless oil (2.45 g, 17.6 mmol, 82%). Spectroscopic data in agreement with previous literature.¹⁰¹ ^1H NMR (CDCl_3 , 400 MHz) δ 7.28-7.21 (m, 4H, ArH), 6.12 (t, $J=6.8$ Hz, 1H, CH), 5.16 (d, $J=6.8$ Hz, 2H, CH_2); $^{13}\text{C}\{^1\text{H}\}$ NMR (CDCl_3 , 100 MHz) δ 260.9 (C), 183.5 (ArC), 179.8 (ArC), 178.9 (ArC), 144.2 (CH), 130.3 (CH_2).

0.4th, 0.5th and 0.6th Order TNA Plots

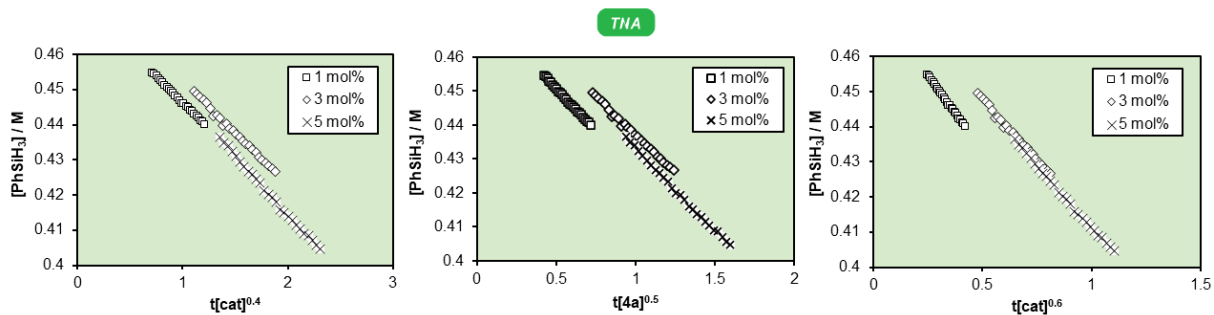


Figure 2.7.1: TNA plot for the catalytic H/D-exchange of phenylsilane and D_2 by **4a**, simulated in the 0.4th, 0.5th and 0.6th order in catalyst.

2.7.10 Computational Method

Density functional theory calculations were executed using Gaussian 16, A.03.¹⁰³ All geometry optimizations were computed with the BP86 functional, accompanied by the ultrafine integral grid option 'int=grid=ultrafine'. Iron atoms were defined using the Stuttgart-Dresden Effective Core Potentials and basis sets (SDDAll).¹⁰⁴ Other atoms were described with double- ζ plus polarization 6-31G** basis sets, defined as 'BS1'.^{105,106} Frequency calculations at the same level of theory were used to generate free energies, with energy minima (confirmed with no imaginary frequencies), corresponding to the relevant intermediate species along the reaction coordinate and saddle points (confirmed with one imaginary frequency), corresponding to the relevant TS. Single point energy corrections were calculated at the B3PW91-D3BJ/Def2-TZVP/IEF-PCM(C₆H₆) level, with Ahlrichs triple- ζ basis set deployed on all atoms.¹⁰⁷ This method follows that employed by Webster and co-workers, following successful benchmarking against an experimental β -hydrogen transfer with an analogous iron-BDK system.⁶² Free-energy profiles are valued in kcalmol⁻¹ at the B3PW91-D3BJ/Def2-TZVP/IEF-PCM(C₆H₆)/BP86/BS1 theory level described above.¹⁰⁸

Following Webster and co-workers study,⁶² empirical dispersion corrections were calculated with Grimme's D3¹⁰⁹ addition to KS-DFT, with the Becke-Johnson damping function.¹¹⁰ Benzene solvent corrections were deployed using the IEF-PCM implemented in Gaussian 16, using optimised geometries at the BP86/BS1 level.¹¹¹ All corrections and scaling factors were applied using the GoodVibes programme, frequency cut-off 100.0 cm⁻¹ (T = 298.15 K, C = 1.0 mol L⁻¹, vibrational scale factor = 1.0).¹¹²

All iron containing structures for catalyst activation were optimised in both the quintet (denoted ⁵X) and triplet (denoted ³X) spin states to identify whether any spin-crossover mechanism is operable, again following preceding work by Webster and co-workers.⁶² TSs for the H/D exchange on the triplet energy surface did not converge. Given the triplet state is consistently higher in energy than the quintet, these structures were omitted from the mechanistic investigation.

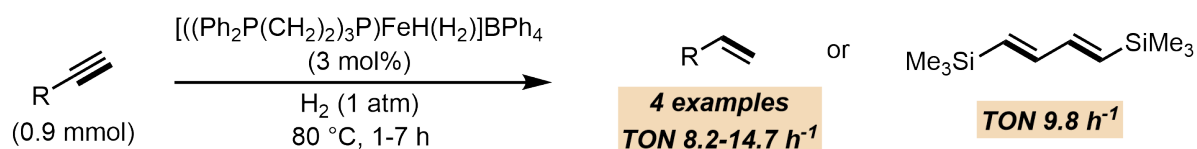
Chapter 3

Room Temperature Iron-catalysed Transfer Hydrogenation Using ⁿButanol and Poly (methylhydrosiloxane)

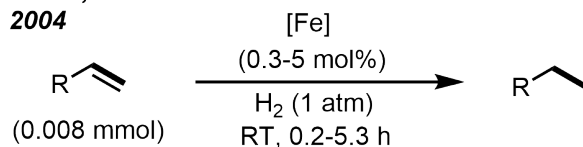
3.1 Introduction

Catalytic hydrogenation is one of the most widely explored chemical transformations in synthetic chemistry.¹¹³ Commonly implemented examples in industry include heterogeneous catalysts based on palladium (10% Pd/C and Lindlar's catalyst) highly regarded as the cleanest methods for hydrogenation of alkenes. Homogeneous methods are also widely established, merited for stereo- and functional group selectivity whilst operating under relatively low H₂ pressure. Therefore, these methods are better suited to the production of fine chemicals. Famous examples include Wilkinson's (RhCl(PR₃)₃) and Noyori's (Ru((*R*)/(*S*)-BINAP)Cl₂) catalysts- for which the later author received the Nobel Prize in Chemistry in 2001.^{114,115} With the current trends to shift towards catalysts made from abundant elements, iron has attracted attention in hydrogenation chemistry. The same valence as ruthenium, there is potential for iron to display analogous reactivity.

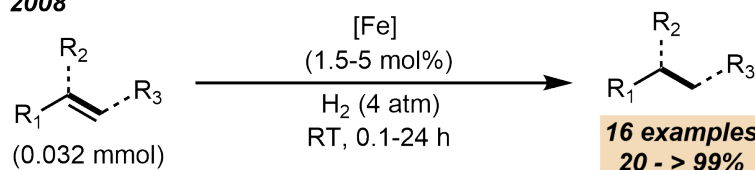
Bianchini, 1989 & 1992



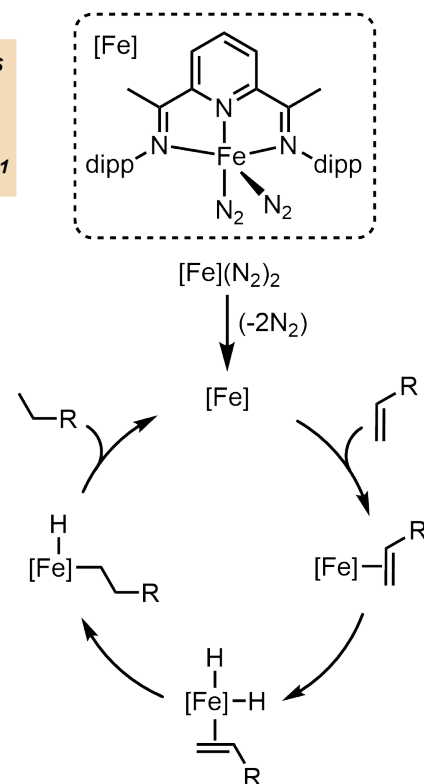
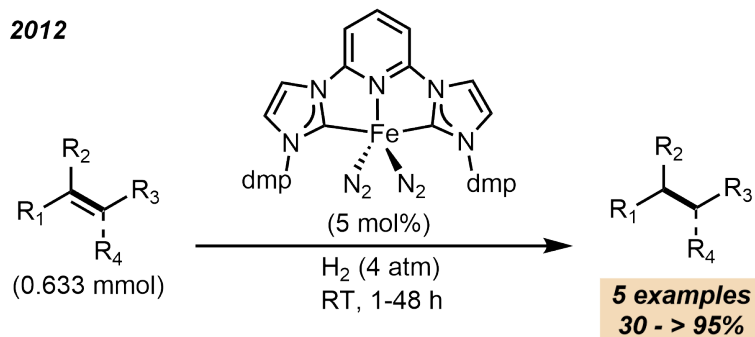
Chirik, 2004



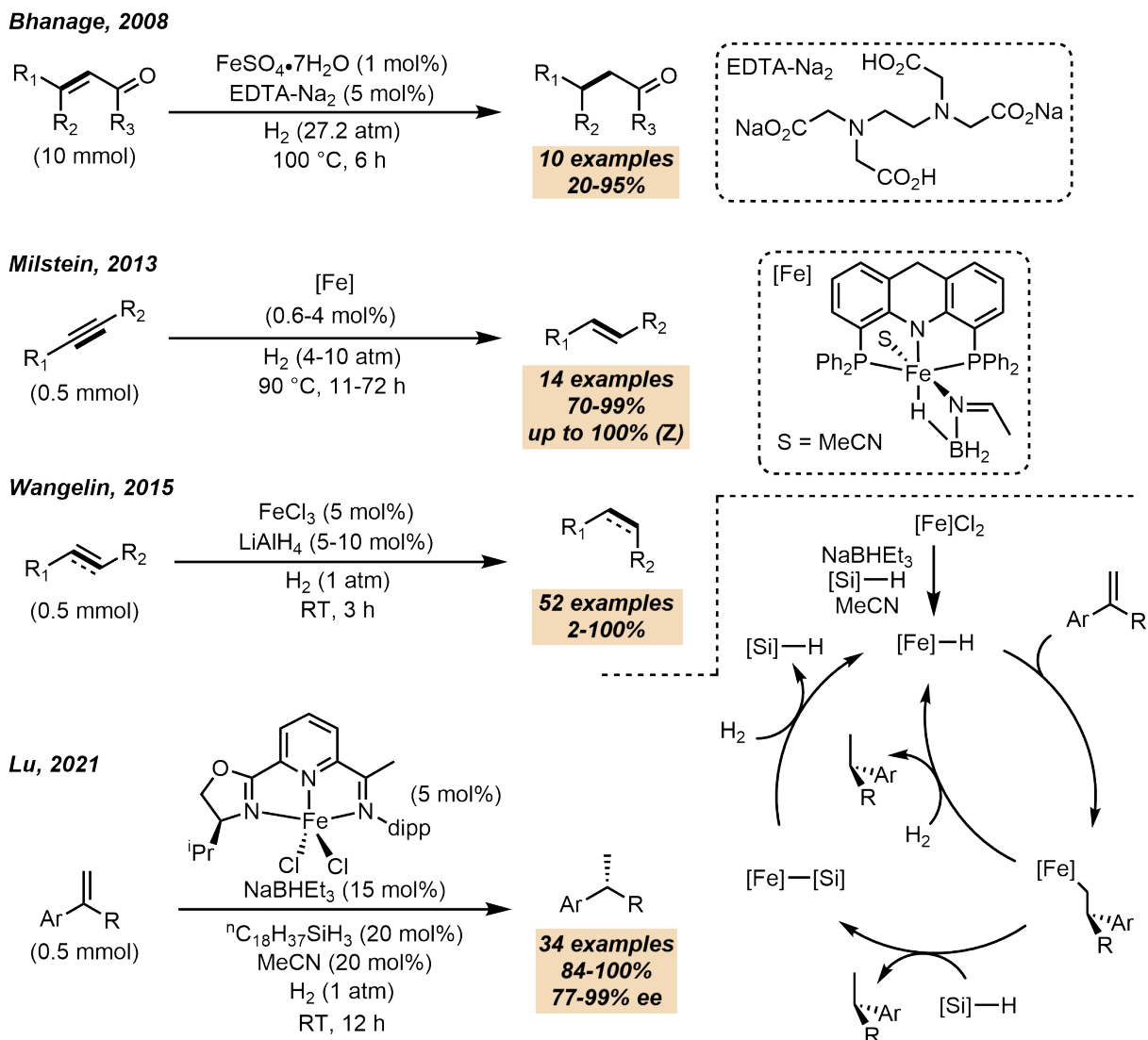
2008



2012



Scheme 3.1.1: Previous reports of iron-catalysed classical hydrogenation of alkenes and alkynes, and simplified mechanism reported by Chirik and co-workers.¹¹⁶⁻¹²⁰



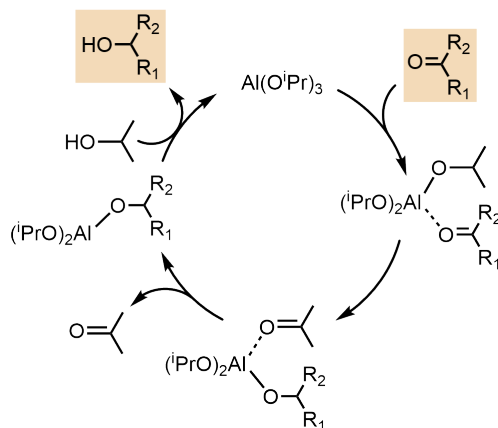
Scheme 3.1.2: Previous reports of iron-catalysed classical hydrogenation of alkenes and alkynes, and simplified mechanism reported by Lu and co-workers.¹²¹⁻¹²⁴

The activity of iron complexes in hydrogenation of carbon-heteroatom multiple bonds is well documented, likely arising from the polarised nature of these unsaturated bonds.¹²⁵ The more challenging carbon-carbon unsaturated bond is scarcer with less than 40 examples.²⁴ The state-of-the-art in iron-catalysed classical hydrogenation are described herein. The earliest report by Butterfield and co-workers detailed the hydrogenation/isomerisation of methyl linoleate, catalysed by $\text{Fe}(\text{CO})_5$ under highly forcing conditions (180 °C and 27.2 atm) forming a mixture of isomers.¹²⁶ However, Bianchini and co-workers demonstrated reduction could be achieved under milder conditions, shown in scheme 3.1.1.^{116,117} Hydride complex, $[\text{((Ph}_2\text{P}(\text{CH}_2)_2)_3\text{P)FeH}(\text{H}_2)]\text{BPh}_4$ catalysed the semi-reduction of phenylacetylene, 1-pentyne, 1-heptyne and 1-methoxy-1-buten-3-yne to their corresponding terminal alkenes under 1 atmosphere of H_2 . In the absence of H_2 , reaction of $[\text{((Ph}_2\text{P}(\text{CH}_2)_2)_3\text{P)FeH}(\text{H}_2)]\text{BPh}_4$ and 3 equivalents of phenylacetylene, yielded iron- σ -alkynyl complexes along with 2 equivalents of alkene, providing some early mechanistic insight. With excess H_2 , $[\text{((Ph}_2\text{P}(\text{CH}_2)_2)_3\text{P)FeH}(\text{H}_2)]\text{BPh}_4$ is replenished after each alkene insertion and metathesis event, permitting catalytic turn-over.

Possibly the strongest contribution, Chirik and co-workers developed bis(imino)pyridine iron bis(nitrogen) (Fe(PDI)(N₂)₂) complexes that facilitated hydrogenation of various mono-, di-, and tri-substituted alkenes under very mild conditions with remarkable activity (shown in scheme **3.1.1**).^{118,119} The method shows good functional group tolerance, with amines, ketones, esters and amides evading reduction. Boasting a TOF of 1814 mol h⁻¹, iron is superior to common hydrogenation catalysts under their conditions; 10% Pd/C (366 mol h⁻¹), (PPh₃)₃RhCl (10 mol h⁻¹) and [(COD)Ir(PCy₃py)]PF₆ (75 mol h⁻¹). Catalysis proceeds by η^2 -alkene coordination to the iron-centre, followed by H₂ oxidative addition. Alkene insertion into the iron-hydride bond and reductive elimination furnishes the reduced product. Chirik and co-workers later developed a bis(arylimidazol-2-ylidene)-pyridine iron dinitrogen ((CNC)Fe(N₂)₂) analogue, which was able to hydrogenate challenging tri- and tetra-substituted olefins (shown in scheme **3.1.1**).¹²⁰ Broad activity and scope of these complexes make them the most active iron-catalysts to date for alkene hydrogenation.

Credible efforts by Bhanage and co-workers detail the selective hydrogenation of α,β -unsaturated carbonyl carbon-carbon double-bonds (shown in scheme **3.1.2**).¹²¹ Simple FeSO₄ pre-catalyst and co-catalytic EDTA-Na₂ affect hydrogenation, with 10 examples up to 95% yield, albeit at high H₂ pressure (27.2 atm). The origin of selectivity was not disclosed. Milstein and co-workers later developed a pincer iron iminoborohydride complex ((PNP)Fe(MeCN)(N(=CHMe)BH₃)) that catalysed the semi-hydrogenation of internal alkynes to (*E*)-alkenes at low catalyst loadings (0.6-4 mol%).¹²² Again, origin of selectivity and the influence of the iminoborohydride ligand were not disclosed. A milder hydrogenation was later reported by Wangelin and co-workers.¹²³ FeCl₃ and co-catalytic LiAlH₄ reduce various alkenes and alkynes in excellent yields and broad scope, under 1 bar of H₂. A complex mechanism was suggested. Hydrogenation commences homogeneously, catalysed by an iron(0) species following pre-catalyst reduction with LiAlH₄ and subsequent H₂ release. Absence of a stabilising ligand leads to catalyst decomposition and nanoparticle formation after 1 hour. Fortunately, these nanoparticles then catalyse heterogeneous hydrogenation allowing full conversion to be reached. Lastly, a long-awaited enantioselective hydrogenation was reported by Lu and co-workers.¹²⁴ An unsymmetric, chiral oxazoline derivative of Chirik's PDI complex was disclosed. The isopropylimidazol-2-ylidene-imino-pyridine iron dichloride ((C*NN)FeCl₂) complex catalysed the enantioselective hydrogenation of 1,1-disubstituted styrenes with expansive scope and excellent percentage enantioexcess (%*ee*). The transformation is selective toward styrene reduction, with a precursor to (*R*)-xanthorrhizol (anti-cancer, anti-microbial and anti-inflammatory biologically active molecule extracted from turmeric) synthesised with no reduction observed for the non-styrenyl olefin. *In situ* reduction of the pre-catalyst with NaBHET₃ generates an iron-hydride intermediate. Alkene insertion into the iron-hydride is the enantio-determining step, yielding a diastereomeric iron-alkyl complex. Iron-carbon bond cleavage proceeds by reaction with silane or H₂, to furnish the chiral alkane.

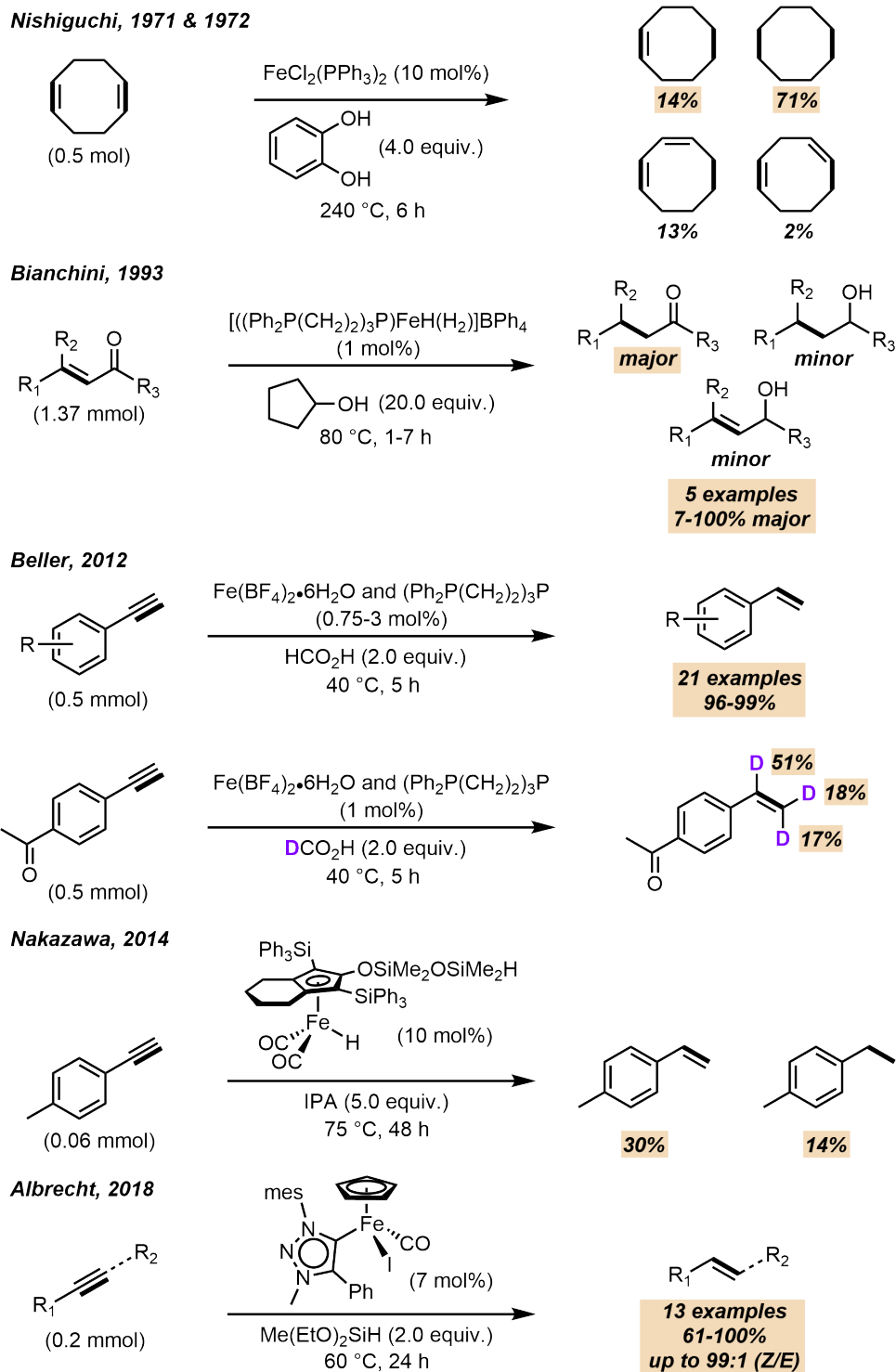
Despite its vast use in both academia and industry, classical hydrogenation can be disadvantageous; 1) Handling of highly explosive, pressurised and diffusive H₂ require relatively honerous safety protocols. Consequently, experimental set-up is non-trivial. On an industrial scale, this creates significant processing costs.¹²⁷ 2) Classical hydrogenation often requires highly forcing conditions (high pressure and temperature). Therefore, functional group selectivity is poor.¹²⁷ Between 1925 and 1926, Meerwein and Schmidt,



Scheme 3.1.3: General mechanism for MPV-reduction.

Verley, and Ponndorf individually uncovered a method to circumvent these issues.^{128–130} The Meerwein-Ponndorf-Verley (MPV) reduction described the aluminium alkoxide-catalysed reaction of ketones with a sacrificial hydrogen donor (ethanol or isopropanol), to form the desired alcohol and ketone by-product. A general mechanism is shown in scheme **3.1.3**. The reaction proceeds by transfer of an aluminium-alkoxide α -proton to the coordinated carbonyl-carbon. Hydroxyl product is furnished by protonolysis from the solvent, reforming the starting aluminium alkoxide.¹³¹ This represented the first example of transfer hydrogenation (TH). Other developments from Doering and Young, detail the first enantioselective MPV reduction using a sacrificial chiral alcohol hydrogen source, albeit in poor %*ee* (up to 22%*ee*).¹³² The first highly enantioselective TH was reported by Noyori and co-workers.¹³³ Chiral (TsDPEN)RuCl(mes) (TsDPEN = (1*S*,2*S*)-*N*-(*p*-tolylsulfonyl)-1,2-diphenylethylenediamine) complex catalysed the enantioselective TH of 20 ketones in up to >99% yield and 98%*ee*. With unprecedented activity (0.5 mol% catalyst loading) and selectivity for its time, research into ruthenium-based catalysts remains the most widely explored area of carbonyl TH. This activity has been extended to more challenging olefin reduction by *N*-heterocyclic carbene (NHC) containing analogues and Grubbs' type catalysts.^{134–136} However, reports of this type are scarce.

Beyond its inherent simplicity, TH has further benefits making it a more available method for reduction of unsaturated bonds;¹²⁷ 1) Hydrogen donors are usually benign. 2) The hydrogen source can be tailored for facile separation and to perturb equilibrium. For example, formic acid forms carbon dioxide when oxidised during the TH process, which readily boils from the reaction providing an entropic driving force. 3) Conditions are less forcing. Thus, many reports of functional group selectivity have emerged. 4) Deuterium labelled TH reagents can lead to regioselective hydrodeuteration. 5) Many catalysts have emerged for TH, derived from abundant first-row transition metals.^{24,125,137} Outlined in chapter 1, substituting precious metals for inexpensive, more abundant first-row transition metals is important. Given the activity of ruthenium demonstrated in TH, iron- in the same group as ruthenium, could serve as a promising alternative. Indeed, select reviews demonstrate the broad scope of iron-catalysed (enantioselective) TH of ketones, aldehydes and imines.^{24,125,137} However, compared to classical hydrogenation, reports of iron-catalysed TH of carbon-carbon multiple bonds are rare.

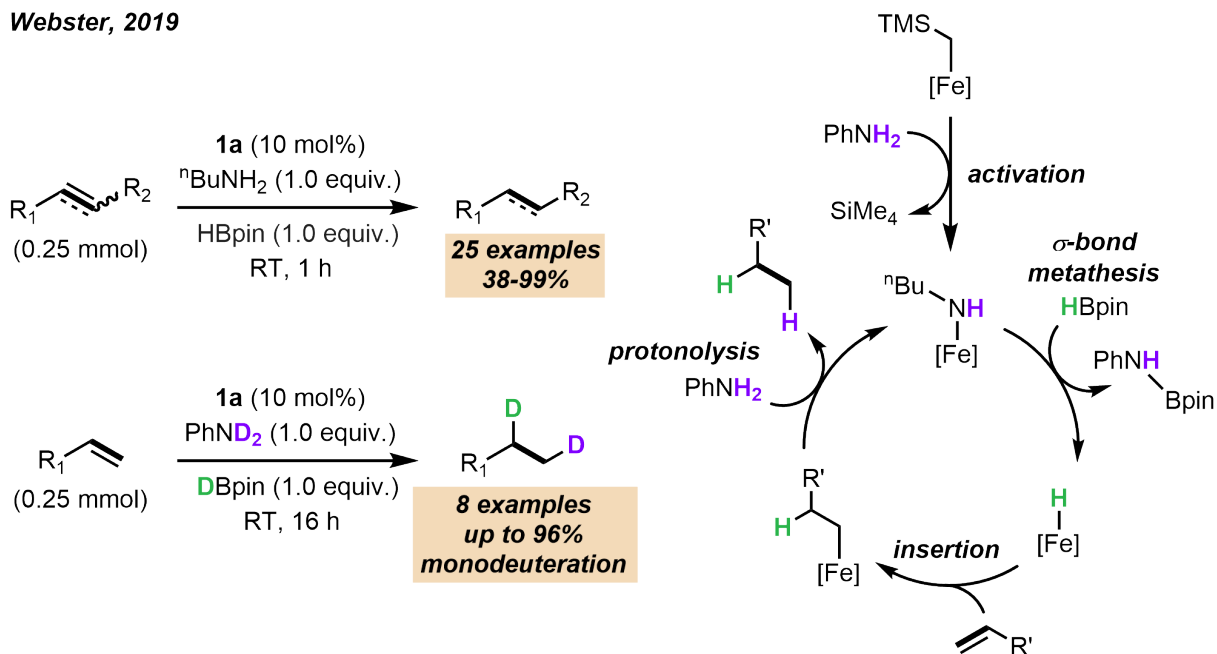


Scheme 3.1.4: Previous reports of iron-catalysed transfer hydrogenation of alkenes and alkynes. ^{138–143}

The first example of iron-catalysed TH was reported by Nishiguchi and Fukuzumi across two reports, shown in scheme **3.1.4**.^{138,139} Heating a mixture of $\text{FeCl}_2(\text{PPh}_3)_2$, 1,5-cyclooctadiene and *p*-dihydroxybenzene at 240 °C for 6 hours, forms cyclooctane as the major product along with cyclooctene, 1,3- and 1,4-cyclooctadiene. Chemoselectivity was demonstrated by Bianchini and co-workers.¹⁴⁰ $[(\text{Ph}_2\text{P}(\text{CH}_2)_2)_3\text{P}]\text{FeH}(\text{H}_2)\text{BPh}_4$ catalysed the TH of α,β -unsaturated ketones with cyclopentanol. Of the 16 substrates tested, 5 furnished the saturated ketone as the major product. Chemoselectivity was in-

consistent, with saturated- and unsaturated alcohol products often being the dominant product after reduction. Bianchini and co-workers probed the mechanism in more detail. Dissociation of a H_2 ligand leaves a vacant coordination site at the iron-centre. Substrate alkene or carbonyl coordination, followed by iron-hydride insertion determined the observed selectivity for the TH. Where the ketone is sterically protected, improved selectivity to the saturated ketone was observed. In 2012, Beller and co-workers demonstrated the iron-catalysed selective semi-hydrogenation of alkynes.¹⁴¹ Spectroscopic yields of 96–>99% for the corresponding alkenes were observed for 21 out of 22 substrates tested, using $Fe(BF_4)_2 \cdot 6H_2O$ catalyst, co-catalytic $(Ph_2P(CH_2)_2)_3P$ and formic acid. D-labelled TH reagent DCO_2H led to deuterium scrambling across the styrene α - and β -positions. Authors suggest pre-catalyst activation generates an $[(Ph_2P(CH_2)_2)_3P]FeF^+$ species. Intermediate $[(Ph_2P(CH_2)_2)_3P]FeF(HD)^+$ forms by reaction of the active species with formic acid, producing CO_2 and is the origin for the observed deuterium scrambling. An Fe(IV) intermediate is hypothesised by sequential H_2 oxidative addition, followed by hydride insertion into the coordinated alkyne. Reductive elimination furnishes the styrenyl product and reforms the $[(Ph_2P(CH_2)_2)_3P]FeF^+$ catalyst. Nakazawa and co-workers reported bifunctional iron-complexes for the TH of 4-methylphenylacetylene with isopropylalcohol. A mixture of 4-methylstyrene and 1-ethyl-4-methylbenzene forms in 30% and 14% yields, respectively. Albrecht and Johnson reported the iron-catalysed semi-reduction of acetylenes, generating corresponding (*Z*)-alkenes in high stereoisomeric ratio across all substrates tested.¹⁴³

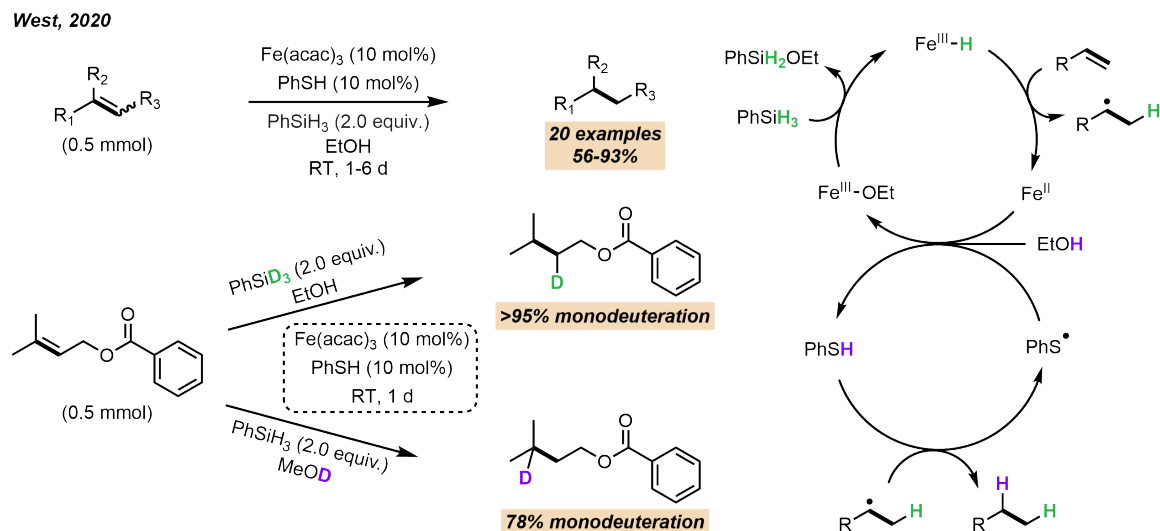
Webster, 2019



Scheme 3.1.5: Transfer hydrogenation and deuterium labelling of alkenes and alkynes catalysed by **1a**, reported by Webster and co-workers.⁶²

Not until 2019, was a general method for the iron-catalysed TH of alkenes reported. Previously described methods were limited by poor scope and selectivity.^{138–140} Webster and co-workers demonstrated the rapid reduction of alkenes and alkynes using **1a**, $nBuNH_2$ and HBpin (scheme 3.1.5).⁶² By substituting the proton source for aniline, selective monodeuteration could be achieved. Careful selection of

DBpin or PhND₂ yielded α - or β -monodeuterated products in high regioselectivities. These findings, combined with DFT insight, suggested a redox innocent catalytic cycle. Pre-catalyst activation occurs by protonolysis with ⁿBuNH₂ or PhNH₂ generating an iron-amido catalyst. σ -Bond metathesis with HBpin yields an iron-hydride (**4a**) and amine-borane by-product. This can insert into alkenes forming an iron-alkyl intermediate. A second protonolysis regenerates the iron-amido catalyst, and furnishes the reduced product.



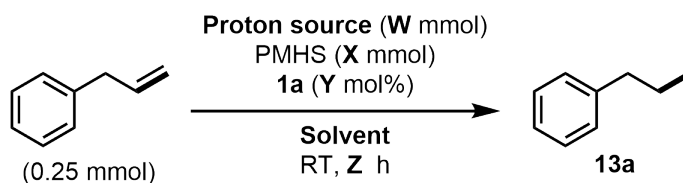
Scheme 3.1.6: Iron-catalysed cooperative hydrogen atom transfer hydrogenation and deuterium labelling of alkenes, reported by West and Kattamuri.¹⁴⁴

In 2020, West and Kattamuri developed a method for iron-catalysed cooperative hydrogen atom TH (cHATH) (scheme 3.1.6).¹⁴⁴ Arguably the most benign method to date, cHATH of olefins occurs at room temperature, catalysed by commercially available air- and moisture-stable $\text{Fe}(\text{acac})_3$ with co-catalytic HAT reagent (thiophenol). Ethanol and phenylsilane are the proton and hydride source for the transformation, respectively. 20 examples were demonstrated in good to excellent yields. The method demonstrated some functional group tolerance with olefin reduction preferred over esters and amides. Regioselective monodeuteration was achieved when introducing PhSiD_3 or MeOD . A detailed mechanistic investigation indicated reduction occurs by cooperative metal-mediated HAT and radical trapping HAT.

Despite the mechanistic differences between the works of Webster and West, the conditions and species required to facilitate TH are similar. In Webster and co-workers' case, the method benefits from fast reaction times (1 hour). In comparison, West and Kattamuri require long reaction times (1-6 days), but boast a simple iron-catalyst, more benign proton source (alcohols instead of amines) and more stable hydride source (PhSiH_3 instead of HBpin). Combining ideals from both studies presents an opportunity to develop a more sustainable method for TH. This chapter describes the optimisation and scope for a more benign TH of alkenes catalysed by **1a**. TH reagents include the cheapest commercially available silane derived from by-products of the silicon industry and a bio-derived alcohol.^{145,146} TH is demonstrated on a range of olefins and product distribution reveals competing side-reactions arising from isomerisation and DHC. Finally, combining amines and silanes leads to complete, regioselective hydrodeuteration of alkenes.

3.2 Optimisation

Table 3.2.1: Transfer hydrogenation of allylbenzene optimisation.



Entry	Proton Source	W (mmol)	X (mmol)	Y (mol%)	Solvent	Z (h)	Conversion ^a (%)	Spec. Yield ^b (%)
1	H ₂ NPh	0.25	0.25	10	C ₆ D ₆	24	60	52
2	H ₂ NPh	0.25	0.50	10	C ₆ D ₆	24	85	76
3	H ₂ NPh	0.25	0.75	10	C ₆ D ₆	24	quant.	>99
4	H ₂ NPh	0.25	0.75	5	C ₆ D ₆	24	quant.	99
5	H ₂ NPh	0.25	0.75	5	C ₆ D ₆	16	quant.	90
6	H ₂ NPh	0.25	0.75	5	Tol-d ₈	24	quant.	82
7	H ₂ NPh	0.25	0.75	10	2-MeTHF	24	-	9 ^c
8	H ₂ NPh	0.25	0.75	5	CPME	24	-	16 ^g
9	D-(-)-fructose	0.25	0.25	10	C ₆ D ₆	24	39 ^d	-
10	D-(+)-glucose	0.25	0.25	10	C ₆ D ₆	24	2 ^d	-
11	sucrose	0.25	0.25	10	C ₆ D ₆	24	0 ^d	-
12	D-(-)-fructose	0.25	0.75	10	C ₆ D ₆	24	36 ^{d,e}	32 ^{d,e}
13	D-(+)-glucose	0.25	0.75	10	C ₆ D ₆	24	6 ^{d,e}	4 ^{d,e}
14	ⁿ BuOH	0.25	0.25	5	C ₆ D ₆	24	-	70 ^f
15	H ₂ NPh	0.25	-	10	PMHS	24	-	84 ^h
16	H ₂ NPh	0.25	-	5	PMHS	24	-	71 ^h
17	ⁿ BuOH	0.25	-	5	PMHS	24	-	85 ^h
18	MeOH	0.25	-	5	PMHS	24	-	58 ^h
19	EtOH	0.25	-	5	PMHS	24	-	74 ^h
20	ⁿ BuOH	1.00	0.75	5	-	24	-	0 ^h
21	ⁿ BuOH	0.75	0.38	5	-	24	-	0 ^h
22	ⁿ BuOH	0.25	-	-	PMHS	24	-	0 ^h
23	ⁿ BuOH	0.25	-	5	PMHS	24	-	81 ⁱ
24	ⁿ BuOH	0.25	-	5	PMHS	24	quant. ^j	-

^aDetermined by ¹H NMR spectroscopy versus allylbenzene. ^bDetermined by ¹H NMR spectroscopy using 0.1 mmol DCE internal standard. ^cSolvent removed under a stream of N₂. ^dJ-Young NMR-tube agitated at 10 rpm. ^eSolution filtered in glovebox before NMR analysis. ^fSolution passed through a silica plug. ^gSolvent removed under reduced pressure. ^hProduct isolated by vacuum distillation. ⁱ2.5 mol% PMe₃ added. ^j1 drop of Hg added.

Optimisation commenced by following the iron-catalysed TH method carried out by Webster and co-workers, substituting hydride donor HBpin, for poly(methylhydrosiloxane) (PMHS).⁶² PMHS is the cheapest commercially available silane because it is derived from by-products of the silicone industry.¹⁴⁵ During the Müller-Rochow process for synthesising Me₂SiCl₂ from Si and CH₃Cl, by-product MeSiHCl₂ forms. Reaction of MeSiHCl₂ with water generates PMHS on an industrial scale.¹⁴⁷ PMHS serves as a suitable alternative hydride source to HBpin as it is cheap, air- and moisture-stable, and non-toxic. PMHS has previously been combined with iron catalysts for the reduction of less challenging substrates.²⁴ Many reports exist for the iron-catalysed hydrosilylation of carbonyls with PMHS.^{148–154} Notably, Beller and co-workers report the enantioselective catalytic hydrosilylation of ketones with PMHS as the hydride source.¹⁵⁵ More challenging transformations have been achieved. Tandem reductive amination/hydrosilylation to furnish secondary and tertiary amines was disclosed by Enthaler, and Darcel and co-workers.^{156,157} PMHS has also been deployed in iron-catalysed isomerisation/hydrosilylation of allylic alcohols with amines, and reduction of amides, esters and sulfoxides.^{158–163} Several examples are known where PMHS is used in copper-catalysed alkyne semi-reduction.^{164–167} However, a thorough literature search revealed only two examples of PMHS in catalytic carbon-carbon double-bond reduction. In Werner and Longwitz study, reduction with PMHS was demonstrated on one highly activated α,β -unsaturated carbonyl, diethylfumarate.¹⁶⁸ In Albrecht and Johnson's work outlined in scheme **3.1.4**, phenyl acetylene was reduced to styrene in 43% conversion during reaction optimisation.¹⁴³ In this case, a 1.0:1.0:1.0 ratio of allyl benzene, aniline and PMHS, with 10 mol% **1a** generates target product phenylpropane (**13a**) in 52% spectroscopic yield. This result demonstrates the first example of PMHS being used in the transfer hydrogenation of unactivated carbon-carbon double-bonds. Increasing the silane loading to 2.0 and 3.0 equivalents yielded **13a** in 76% and >99%, respectively (table **3.2.1**, entries 2 and 3). Catalyst loading could be reduced from 10 to 5 mol% with no impact on spectroscopic yield of **13a** (table **3.2.1**, entry 4). Reducing the reaction time from 24 to 16 hours saw a small decline in spectroscopic yield, to 90% (table **3.2.1**, entry 5). In search of a more benign TH method, alternative solvents to benzene were tested. Reaction in toluene-*d*₈ led to reduced yields of **13a**. Biomass derived 2-methyltetrahydrofuran (2-MeTHF) and safer alternative cyclopentyl methyl ether (CPME) also formed **13a** in reduced yields of 9% and 16%, respectively. Historically, coordinating polar solvents led to poor activity for pre-catalyst **1a**.⁹¹ Therefore, it might be expected that 2-MeTHF and CPME are incompatible.

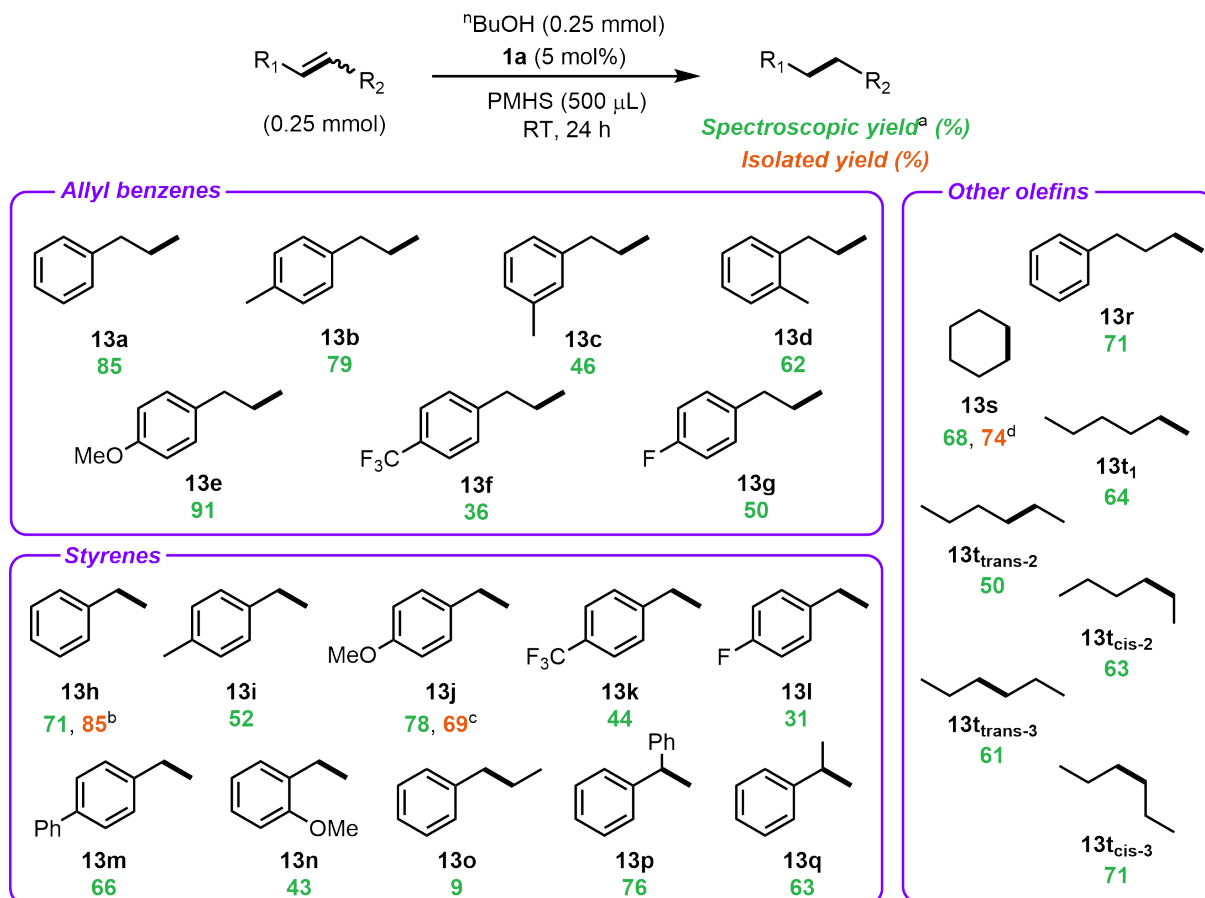
D-(-)-fructose and D-(+)-glucose show some activity as TH reagents. Two examples are known using bioderived compounds as reducing reagents. Thananattananachon and co-workers demonstrated the transfer hydrogenation of carbonyls by α -D-glucose catalysed by an iridium-dii-amido complex (Cp*Ir(TsDPEN)).¹⁶⁹ Scope was limited to 4 aldehydes; benzaldehyde, furfural, hexanal and 5-hydroxymethylfurfural in 89-100% conversion. Carbon-carbon double-bond reduction was achieved by Matsunaga and co-workers. The authors detail the cobalt-salen/photoredox-catalysed hydrogen atom transfer hydrogenation of alkenes using vitamin C.¹⁷⁰ 34 substrates were tolerated in up to 95% yield. Under the new conditions D-(-)-fructose and D-(+)-glucose generate **13a** in 32% and 4% yield, respectively (table **3.2.1**, entries 9 and 10). This is unexpected given their insolubilities in apolar organic solvents and demonstrates the first example of use of sugars in carbon-carbon double bond reduction. Unfortunately, yields could not be improved by

increasing the loading of sugars to 3.0 equivalents (table **3.2.1**, entries 12 and 13).

Inspired by work of Kattamuri and West, ⁿBuOH was tested as TH proton-source in this study.¹⁴⁴ ⁿBuOH can be derived from the acetone-butanol-ethanol fermentation of sugar, glycerol or lignocellulose.¹⁴⁶ Compared to aniline used in the previous report, ⁿBuOH has reduced acute toxicity. Therefore, it is considered a suitable alternative as proton source in the TH. Substrate **13a** was generated in 70% yield (table **3.2.1**, entry 14). Gratifyingly, **1a** is soluble in PMHS, allowing the reaction to be performed neat in excess PMHS (table **3.2.1**, entries 15 and 16). 5 mol% and 10 mol% **1a** yields **13a** in 84% and 71% spectroscopic yield, respectively. Substituting ⁿBuOH into these conditions yields **13a** in 85%. Alternative alcohols- methanol and ethanol- have diminished returns with **13a** forming in 58% and 74%, respectively (table **3.2.1**, entries 18 and 19). Notably, raising the ⁿBuOH to PMHS ratio shuts down reactivity. Substrate-to-proton source-to-hydride source ratios of 1:4:3 and 1:3:1.5 (table **3.2.1**, entries 20 and 21) show no reactivity. Significant gas evolution is observed under these conditions suggesting DHC between proton and hydride source becomes the dominant process. Qualitative determination of hydrogen evolution is discussed in section **3.4**. Pre-catalyst **1a** is required to facilitate the reaction (table **3.2.1**, entry 22). With a co-catalytic amount of PMe₃, **13a** forms in slightly depleted yield of 81% (table **3.2.1**, entry 23). Furthermore, the reaction proceeds in the presence of a drop of mercury (table **3.2.1**, entry 24). These results are strong evidence for the reaction being homogeneously catalysed. After thorough optimisation, conditions shown in table **3.2.1**, entry **17** were selected for the substrate scope investigation. Under solvent free conditions using cheap, industrial by-product PMHS and bioderived ⁿBuOH, the new method serves as a greener alternative to the previous report. These conditions prove advantageous as the reduced product can be cleanly distilled away from remaining non-volatiles: PMHS, poly(methylⁿbutoxysiloxane) and iron-complex.

3.3 Substrate Scope

Figure 3.3.1: Substrate scope for alkene transfer hydrogenation, catalysed by **1a**.



^aDetermined by ¹H NMR spectra using DCE or mesitylene (0.25 mmol). ^b2.5 mmol, 48 hrs. ^c0.5 mmol.

^d2.5 mmol.

Under newly optimised conditions, a further 23 substrates were tested in the transfer hydrogenation (shown in figure 3.3.1). 4-, 3- and 2-allyl-1-methylbenzene undergo TH generating **13b**, **13c** and **13d** in 79%, 46% and 62% yield, respectively. Electron donating substrates favour TH with 4-methoxyphenylpropane (**13e**) generated in 91% yield. In contrast, electron deficient substrates 4-allyl-trifluoromethylbenzene and 4-allyl-fluorobenzene show diminished returns yielding reduced products **13f** and **13g** in 36% and 50% yield, respectively. Conditions tolerate styrenyl substrates. Styrene undergoes TH in 71% spectroscopic yield (**13h**). Notably, yield is improved following a ten-fold scale-up with **13h** isolated in 85% yield, after 48 hours. 4-Methylstyrene undergoes TH generating **13i** in 52% spectroscopic yield. Electron rich 4-methoxystyrene is reduced in good spectroscopic yield of 78%. Substrate **13j** was isolated by FCC in 69% yield on a 0.5 mmol scale, demonstrating non-volatile products can be separated from remaining polymeric material. Electron deficient substrates 4-trifluoromethylstyrene and 4-fluorostyrene show poor activity, forming **13k** and **13l** in 44% and 31%, respectively. 4-Phenylstyrene and 2-methoxystyrene undergo TH generating **13m** and **13n** in 66% and 43% spectroscopic yield, respectively. 1,2-Substituted trans- β -methylstyrene is not tolerated under optimised conditions, with **13o** forming in 9% spectroscopic

yield. 1,1-Substituted α -phenylstyrene and α -methylstyrene are tolerated yielding **13p** and **13q** in 76% and 63% yield, respectively. Other non-activated alkenes were tested. 4-Phenyl-1-butene undergoes TH yielding **13r** in 71%. Internal alkene, cyclohexene undergoes reduction at 0.25 mmol and 2.5 mmol scale, in 68% spectroscopic and 74% isolated yields, respectively. TH works for all isomers of hexene, with **13t₁**, **13t_{trans-2}**, **13t_{cis-2}**, **13t_{trans-3}**, **13t_{cis-3}** forming in 64%, 50%, 63%, 61% and 71% spectroscopic yield, respectively. Incompatible substrates include (*E*)-cinnamyl chloride, acrylonitrile, allyl acetate, allyl acetone, (*E*)-cinnamyl alcohol, allyl trifluoroacetate, 1,2-epoxy-5-hexene and 1-bromo-5-hexene, where no conversion was observed.

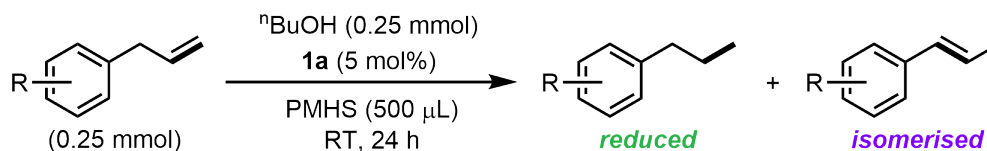
Compared to previous work by Webster and co-workers, use of ⁿBuOH and PMHS as proton and hydride sources in the TH led to enhanced activity in some cases. Yield of **13t_{cis-2}** and **13t_{cis-3}** are raised from 28% and 48%, to 63% and 71% spectroscopic yield, respectively.⁶² Styrenyl substrates performed similarly to previous studies, but marked improvements are seen for **13h**, increasing from 45% spectroscopic yield to 85% isolated yield. Similar spectroscopic yields were observed for **13a**, 81% and 85%. No isomerisation of allyl substrates to the corresponding internal alkene was observed under the previous conditions (a discussion into isomerisation products is outlined in section 3.4.1). Given that **13o** was generated in 99% spectroscopic yield, it is possible the internal alkenes were never identified in the previous study if TH continues unperturbed. Under new TH conditions, **13o** was reduced in 9% spectroscopic yield.

Some improvements are observed compared to West and Kattamuri's iron-catalysed cHATH.¹⁴⁴ α -Substituted styrenes were not well tolerated with trace **13p** forming by ¹H NMR spectroscopy. This was suggested to arise from stabilisation of benzylic radicals through π -conjugation, making the final radical reduction challenging. In contrast, **13p** forms in 76% spectroscopic yield under new conditions and the scope includes a range of different styrenes. In the cHATH process, **13e** and **13r** were tolerated in 83% and 93% yields. Yields are comparable under new TH methodology (91% and 71%, respectively). However, **13e** is generated in 24 hours instead of 4.5 days. An advantage of the cHATH process is hydroxyl groups are tolerated. This is unexpected given EtOH is the proton source for the transformation. Under new TH conditions, this is unlikely to be the case. When acetophenone was tested under TH conditions, full conversion was observed by ¹H NMR spectroscopy. However, TH product 1-phenylethanol was uncovered in 9% spectroscopic yield. It can be suggested that the TH product (1-phenylethanol) undergoes DHC with PMHS and cannot be distilled.

3.4 Mechanistic Investigation

3.4.1 Alkene Isomerisation

Table 3.4.1: Substrate scope for alkene transfer hydrogenation, catalysed by **1a**.



R (substrate)	spectroscopic yield ^a	
	reduced (%)	isomerised (%)
4-H (13a)	85	2
4-Me (13b)	79	-
3-Me (13c)	46	2
2-Me (13d)	62	25
4-MeO (13e)	91	-
4-CF ₃ (13f)	36	34
4-F (13g)	50	30
4-phenylbutene (13r)	71	9

^aDetermined by ¹H NMR spectra using DCE or mesitylene (0.25 mmol).

Not all allyl benzenes were well tolerated under optimised TH conditions (**13c**, **13f** and **13g**). Upon close inspection, substrates that performed poorly have trace amounts of starting material remaining by ¹H NMR spectroscopy. Instead, their styrenyl derivatives are observed, shown in table 3.4.1. These products are expected to arise from a competing isomerisation side-reaction. Previously, work by Webster and co-workers demonstrated the iron-catalysed isomerisation of alkenes, mediated by **1a**.¹⁷¹ In the presence of co-catalytic HBpin, on-cycle **4a** can disproportionate generating a (BDK)Fe(I) complex with substrate η^2 -alkene coordination filling the vacant site. Oxidative addition generates a (BDK)Fe(III)H(η^3 -allyl) intermediate. Reductive elimination reforms the Fe(I) species and the thermodynamically preferred internal (*E*)-alkene. During optimisation, it was shown that co-catalytic MePhSiH₂ and **1a** slowly isomerises allylbenzene forming **13o** with 15% conversion after 48 hours at 80 °C. Therefore, it is unsurprising internal alkenes are observed under TH conditions, where a large excess of PMHS is used as a hydride source. Notably, electron withdrawing substrates **13f** and **13g** have the largest yield of isomerised product. Oxidative addition of the (BDK)Fe(I) intermediate into electron deficient alkenes can be expected to be more facile, favouring the competing redox-active Fe(I)/Fe(III) isomerisation. Indeed, this is observed for electron-deficient **13f** and **13g**, and the opposite is true for electron rich **13e**. *trans*- β -Methylstyrene is not tolerated under TH conditions (**13o**). Therefore, once the internal alkene forms, TH cannot proceed.

3.4.2 Gas Evolution Experiments

During optimisation, significant gas evolution was observed when the proton source loading was increased (table 3.2.1 entries 20 and 21). Based on previous work by Webster and co-workers, this is likely to

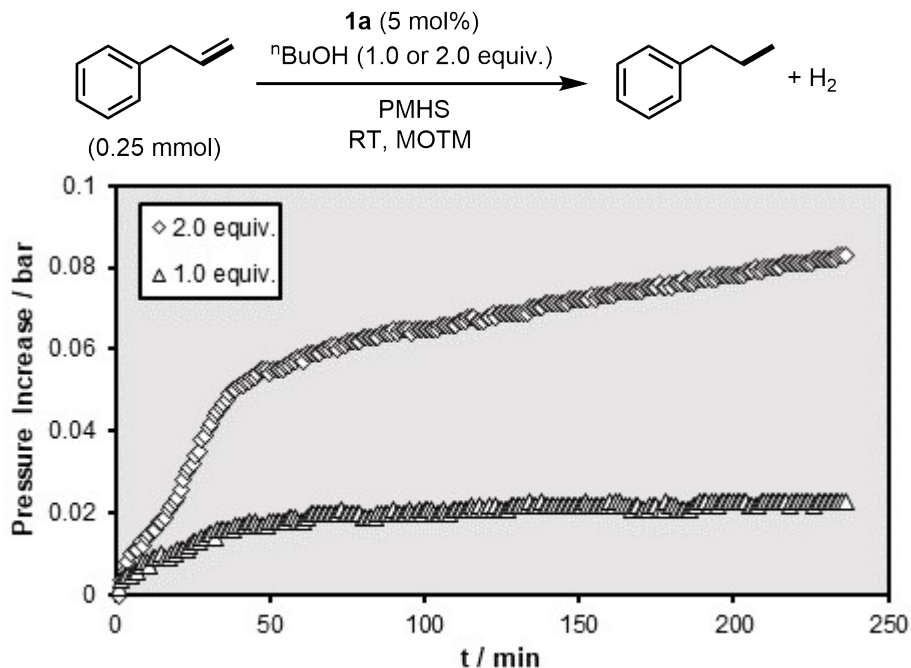
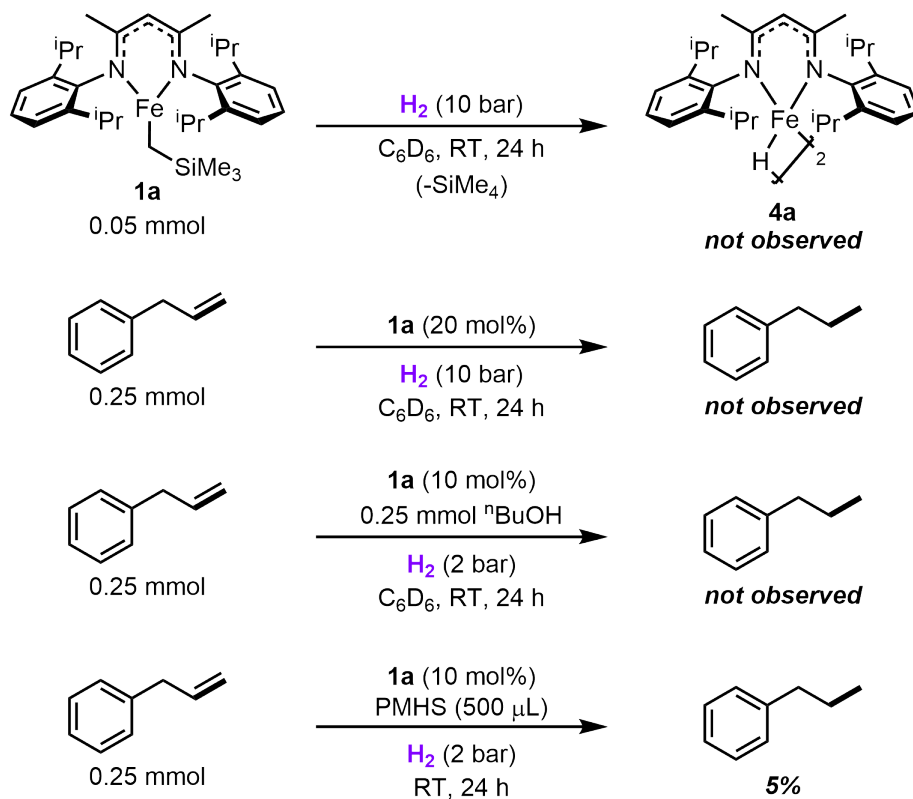


Figure 3.4.1: Hydrogen production at different ⁿBuOH loading.

arise from direct DHC of ⁿBuOH and PMHS. Previous work demonstrates **1a** catalyses the DHC of alcohols or diols with hydrosilanes to generate siloxanes and poly(siloxanes).^{61,172} Competing DHC is problematic for the TH method as TH reagents (proton and hydride sources) are removed from the system. Furthermore, with H₂ present in the reaction mixture, TH may not be operating and instead classical hydrogenation occurs by tandem DHC and hydrogenation.^{173–175} If this is the case, an initial rise in H₂ pressure is anticipated where DHC dominates. Pressure is then expected to drop while hydrogenation occurs. Reaction conditions make *in situ* monitoring by NMR spectroscopy impractical (viscous mixture requiring vigorous stirring). Instead, gas evolution was measured using Man on the Moon (MOTM) apparatus. This method provides quantitative determination of gas evolution during the course of the reaction, by measuring the change in pressure of the reaction headspace (figure 3.4.1). Under standard conditions, with a 1.0:1.0 ratio of allyl benzene to ⁿBuOH in an excess of PMHS, a small pressure increase is observed. After 4 hours, 0.023 bar of H₂ is generated. From the ideal gas equation, this equates to 0.0121 mmol of H₂ and assumes 5% of TH reagents are used in DHC. With 2.0 equivalents of ⁿBuOH, gas evolution proceeds for the entire observed reaction time, reaching 0.0402 mmol of H₂ after 4 hours. This corresponds to 18% of TH reagents being involved in DHC. From optimisation, high ⁿBuOH loadings yield 0% **13a** (table 3.2.1 entries 20 and 21). This is understandable knowing that DHC becomes more favourable under these conditions. Clearly, greater rate of DHC leads to reduced yield of **13a**, suggesting DHC is in direct competition for the proton and hydride sources. Finally, no fluctuation in pressure is observed indicating reduction proceeds by TH and not DHC followed by classical hydrogenation.



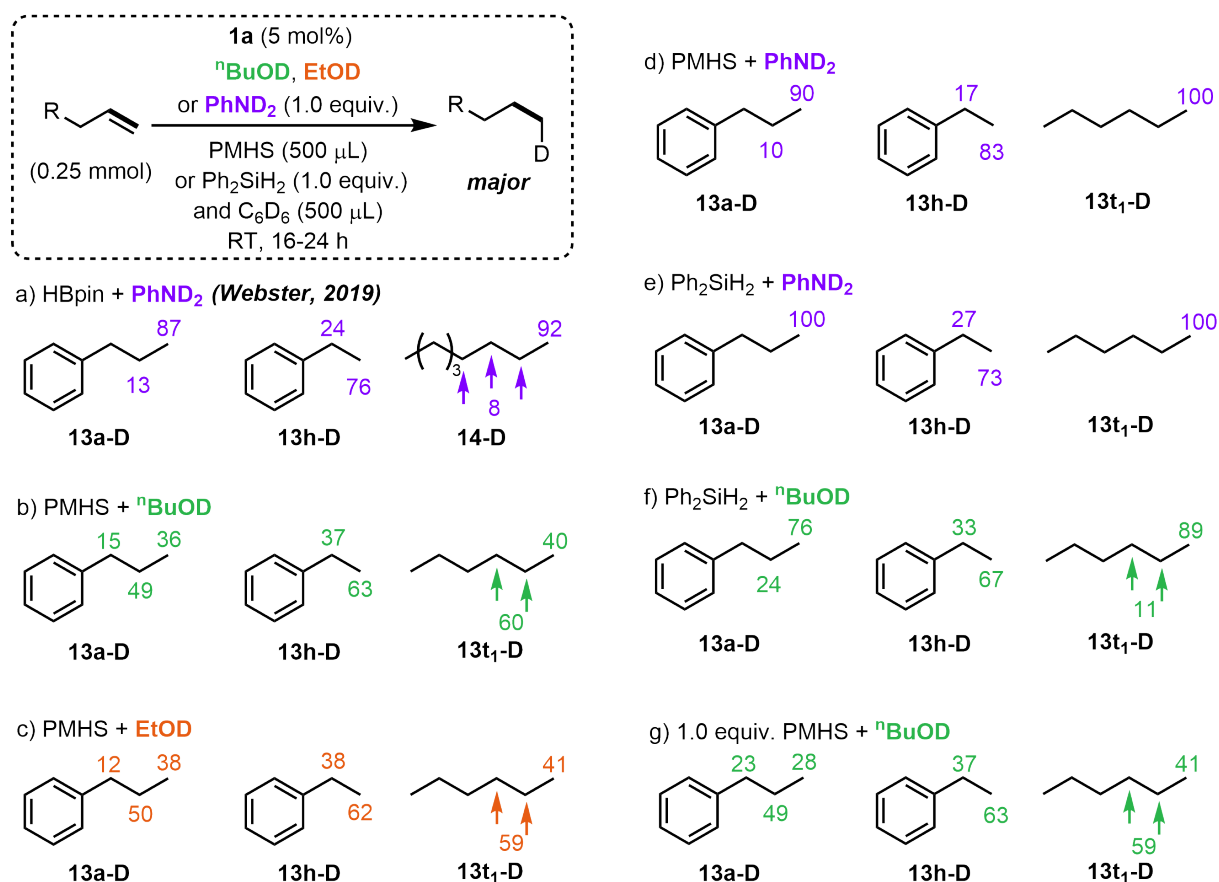
Scheme 3.4.1: Investigation into activation of **1a** with H₂.

3.4.3 Hydrogenation Experiments

Gas evolution experiments suggest H₂ is not involved in alkene hydrogenation (section 3.4.2). Nevertheless, test reactions were undertaken with **1a** and H₂ gas for further insight, shown in scheme 3.4.1. Theoretically, H₂ could react with the iron-carbon bond of **1a** yielding an iron-hydride (**4a**) and SiMe₄. Unpublished work by N. Coles demonstrates that **1a** does not react under 10.0 bar of H₂.¹⁷⁶ Therefore, it is unlikely catalyst activation arises from advantageous H₂ under TH conditions. Next, the role of H₂ was investigated under catalytic conditions. No reaction is observed when allyl benzene is subjected to 20 mol% **1a** and 10.0 bar H₂, with exclusive recovery of starting material. Complex **1a** readily reacts with alcohols generating iron-alkoxides and SiMe₄.⁶¹ Activation of (BDK)FeCH₂SiTMS complexes by σ -bond metathesis with N-H, O-H and P-H bonds to form Fe-N, Fe-O and Fe-P species is widely reported.^{33,62,89,90,177} Therefore, reaction of allyl benzene, ⁿBuOH and 10 mol% **1a** under 2.0 bar H₂ was undertaken. 2.0 bar was selected as a sufficient pressure to simplify reaction set-up. The theoretical maximum that can be achieved under TH conditions is 0.65 bar if complete DHC between proton and hydride sources occurs. No reduction was observed suggesting H₂ is not a substitute for the hydride source in the TH. Reaction of allyl benzene, PMHS and 10 mol% **1a** under 2.0 bar H₂ yields 5% reduced product (**13a**). In chapter 1, it is suggested **1a** can be activated by silanes to generate **4a**. However, lack of reactivity suggests H₂ is not a substitute for the proton source in the TH. Previous work indicates that catalyst activation arises from pre-catalyst protonolysis with amines.⁶² Furthermore, proposed iron-amide intermediates were synthesised and demonstrated to be active catalysts for TH.⁶² The analogous reaction between **1a** and ⁿBuOH was attempted. However, this yielded insoluble amorphous blue crystals assumed

to be an iron-alkoxide dimer. Their insolubility made them unsuitable for further investigation. Dimer dissociation could be investigated by ligation of strong σ -donors. However, this is not representative of catalytic conditions and was not investigated further.

3.5 Mono-deuteration of Alkenes



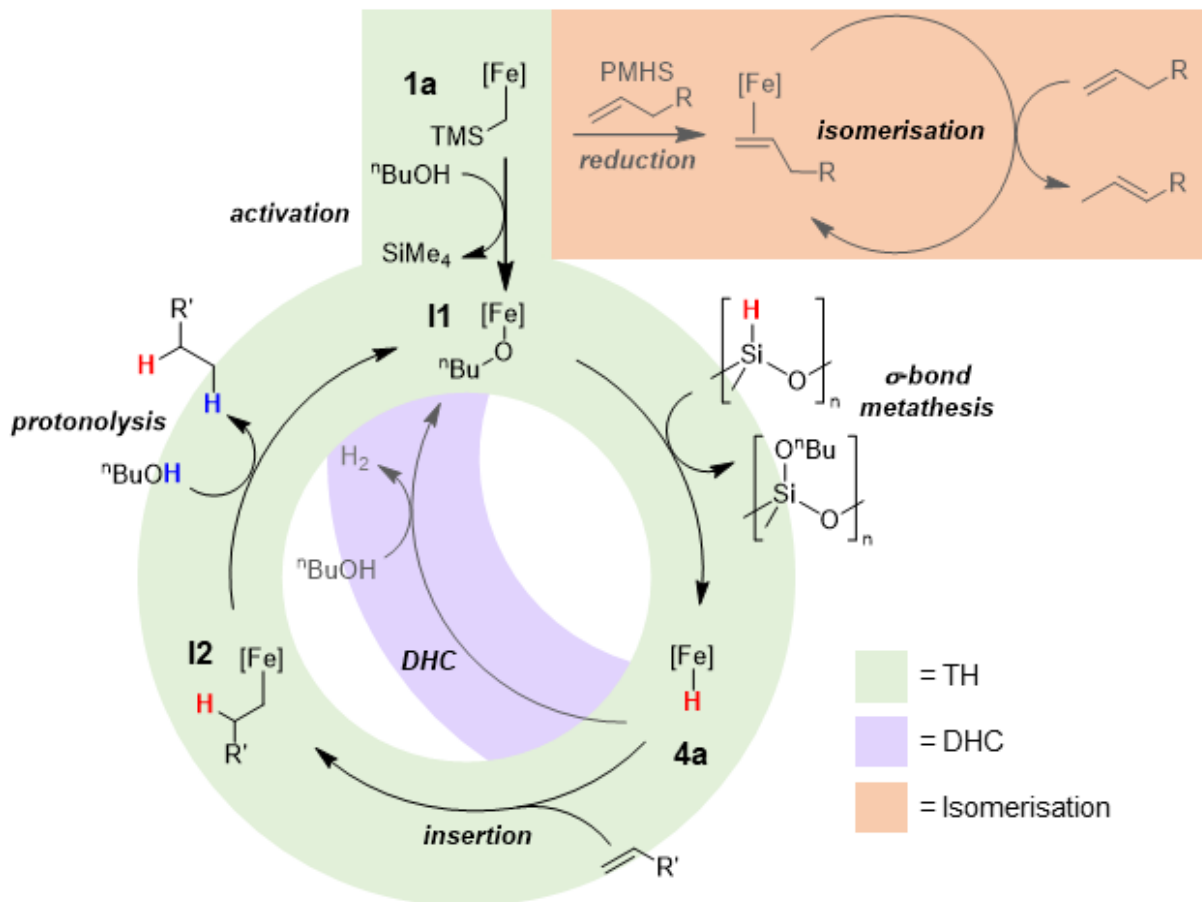
Scheme 3.5.1: Transfer hydrodeuteration using ${}^n\text{BuOD}$, EtOD, PhND_2 , PMHS, HBpin or Ph_2SiH_2 . Reaction a) was extracted from previous report.⁶²

Given the interest in deuterium labelling outlined in chapter 1, new TH conditions were tested for the exclusive regioselective transfer hydrodeuteration (THD) of olefins (scheme 3.5.1). Substrates follow the notation $13\mathbf{x}\text{-D}^a$, where \mathbf{a} corresponds to the position of deuteration on the 1-propylbenzene, ethylbenzene, octyl or hexyl chain. In all cases quantitative incorporation of 1 deuterium atom was determined by ${}^1\text{H}$ and ${}^2\text{H}$ NMR spectroscopy and the relative ratio determined from the ${}^1\text{H}$ NMR spectrum. Under previous TH conditions using **1a**, HBpin and PhND_2 , allyl benzene, styrene and 1-octene were used as model substrates (scheme 3.5.1a). Good regioselectivity was observed, generating the corresponding reduced, monodeuterated products. Substrates $13\mathbf{a}\text{-D}^1$, $13\mathbf{a}\text{-D}^2$ and $13\mathbf{a}\text{-D}^3$ form in 0:13:87 ratio. Slightly reduced regioselectivities were observed for styrene, with $13\mathbf{h}\text{-D}^1$ and $13\mathbf{h}\text{-D}^2$ synthesised in 24:76 ratio. Greatest selectivity was observed for 1-octene, yielding 14-D^1 and 14-D^{2-4} in 92:8 ratio. Under new TH conditions, using PMHS and ${}^n\text{BuOD}$, poor selectivity is observed (scheme 3.5.1b). Substrates

13a-D¹, **13a-D²** and **13a-D³** form in 15:49:36 ratio, **13h-D¹** and **13h-D²** in 37:63 ratio and **13t₁-D¹** and **13t₁-D²⁻³** in 40:60 ratio. The same reactivity was observed with alternative proton source EtOD (scheme **3.5.1c**). For model substrates tested, **13a-D¹**, **13a-D²** and **13a-D³** form in 12:50:38 ratio, **13h-D¹** and **13h-D²** in 38:62 ratio and **13t₁-D¹** and **13t₁-D²⁻³** in 41:59 ratio. Combining PMHS and PhND₂ leads to excellent selectivity (scheme **3.5.1d**). Substrates **13a-D¹**, **13a-D²** and **13a-D³** form in 0:10:90 ratio, **13h-D¹** and **13h-D²** in 17:83 ratio. The completely regioselective THD of 1-hexene occurs with **13t₁-D¹** forming exclusively. The improved selectivity observed for aniline compared to alcohols suggests the proton source is important for determining the regioselectivity of hydrodeuteration. Given the high selectivity observed in West and Kattamuri's study when using a monomeric silane, Ph₂SiH₂ was investigated as the hydride source (scheme **3.5.1e**). Selective terminal monodeuteration was observed for allylbenzene and 1-hexene with **13a-D³** and **13t₁-D¹** forming exclusively. Complete selectivity for styrene was not achieved with **13h-D¹** and **13h-D²** in 27:73 ratio. Evidently, hydride source is a factor in determining the regioselectivity of monodeuteration. Combining Ph₂SiH₂ and ⁿBuOD gives monodeuteration comparable to optimised conditions, when using PMHS and ⁿBuOD (scheme **3.5.1f**). Substrates **13a-D¹**, **13a-D²** and **13a-D³** form in 0:24:76 ratio, **13h-D¹** and **13h-D²** in 33:67 ratio and **13t₁-D¹** and **13t₁-D²⁻³** in 89:11 ratio. No **13a-D¹** is observed indicating no isomerisation to the internal alkene occurs under these conditions. Finally, with 1.0 equivalent on PMHS the same regioselectivity is observed compared to standard conditions (scheme **3.5.1g**). Substrates **13a-D¹**, **13a-D²** and **13a-D³** form in 23:49:28 ratio, **13h-D¹** and **13h-D²** in 37:63 ratio and **13t₁-D¹** and **13t₁-D²⁻³** in 41:59 ratio, albeit in reduced spectroscopic yield. This result demonstrates that 1.0 equivalent of hydride is delivered from PMHS when the reagent is used in excess or in a 1:1:1 ratio with substrate and proton source.

The origin of selectivity in the monodeuteration is complex and depends on multiple reagents. However, some suggestions can be offered for the difference in selectivity. When Ph₂SiH₂ is deployed instead of PMHS, no isomerisation-TH product (**13a-D¹**) is observed (scheme **3.5.1e** and **f**). Tertiary siloxanes are stronger reducing agents and hydride donors than secondary silanes.⁵⁹ Furthermore, PMHS is in much larger excess than Ph₂SiH₂. Therefore, it can be assumed that reaction between on-cycle iron-amide/alkoxide and silane will be more facile with PMHS than Ph₂SiH₂ leading to undesired DHC (scheme **3.1.5**).⁶² Furthermore, a higher concentration of reducing agent will perturb the reduction equilibrium forming more Fe(I)-complex able to catalyse alkene isomerisation.¹⁷¹ TH of the isomerised product would lead to formation of **13a-D¹** when catalysed by PMHS. When PhND₂ is used instead of ⁿBuOH, no isomerisation-TH product (**13a-D¹**) is observed (scheme **3.5.1a**, **d** and **e**). If rate of turn-over from the on-cycle iron-alkyl species is slow, rearrangement can occur forming linear and branched isomers.²⁷ Unfortunately, optimised conditions do not permit *in situ* reaction monitoring to interrogate this further (viscous mixture and vigorous stirring). Therefore, the order in alcohol and amine could not be determined and their exact role in regioselectivity is not disclosed. Nevertheless, conditions were identified for the exclusive monodeuteration of (propyl-3-*d*₁)benzene and hexane-1-*d*₁. This methodology could be combined with silane H/D exchange to yield **13a-D²** and **13a-D¹** in 92:8 ratio by a 'one-pot, two-step' method (see section **2.2.2**).

3.6 Proposed Mechanism



Scheme 3.6.1: Proposed mechanism for the iron-catalyzed transfer hydrogenation, with competing alkene isomerisation and alcohol-silane DHC.

The mechanistic proposal relies significantly on the previous TH methodology demonstrated by Webster and co-workers.⁶² Iron-carbon bond protonolysis of **1a** with $^n\text{BuOH}$ generates on-cycle iron alkoxide, **I1** (evidenced by rapid reaction of **1a** with $^n\text{BuOH}$). σ -Bond metathesis with PMHS forms iron-hydride **4a** and poly(methyl m butoxysiloxane). Alkene insertion yields a linear iron-alkyl species, **I2**. A second iron-carbon bond protonolysis regenerates **I1**, furnishing the TH product, as determined in previous work.⁶² Two competing pathways are identified. DHC quenches intermediate **4a** by reaction with $^n\text{BuOH}$, forming **I1** and H_2 , evidenced by gas evolution experiments. At high loadings of $^n\text{BuOH}$ this process dominates—shutting down TH reactivity.⁶¹ Large excess of PMHS leads to over-reduction and disproportionation of **1a**, to an iron(I)- η^2 -alkene complex that facilitates alkene isomerisation (evidenced by internal alkene products in the ^1H NMR spectra).¹⁷¹

3.7 Dehydrocoupling of Poly(methylhydrosiloxane) and Alcohols

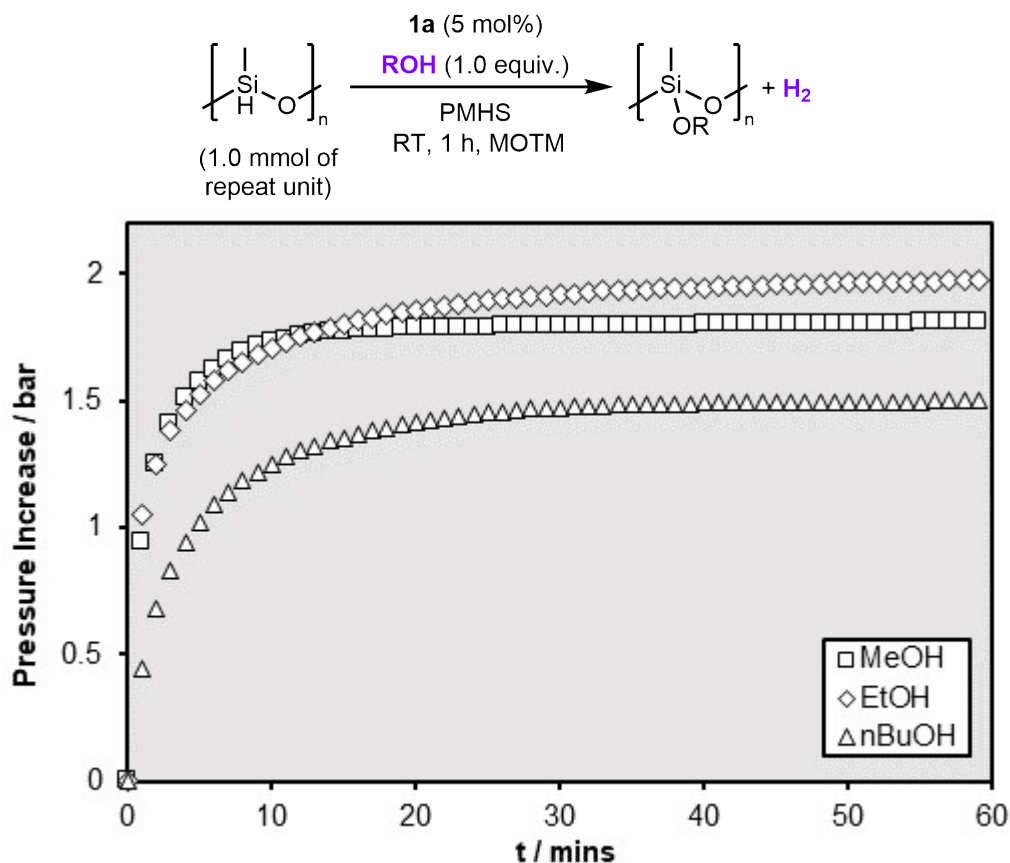


Figure 3.7.1: DHC of alcohols with PHMS, catalysed by **1a**.

Section 3.4.2 demonstrates **1a** can facilitate the DHC of ⁿBuOH and PMHS. Production of hydrogen has interest in the energy sector.¹⁷⁸ With current fossil fuel supply in jeopardy and the detrimental environmental impact of burning these fuels, demand for a sustainable alternative has been an ongoing challenge within the scientific community. Hydrogen is considered a possible green alternative- water being the only product of its combustion. However, safety and practicality concerns around storing large quantities of explosive gas or low boiling liquid are challenging to navigate. Therefore, the chemical storage of hydrogen is considered an alternative. Catalytic DHC of high weight percent hydrogen materials such as ammonia-borane (AB, 19.5 wt % H₂) have attracted interest.¹⁷⁹ These compounds represent a safer and easily manipulated source of hydrogen. Thus, research into catalysts that facilitate AB DHC are well explored.^{177,179–181} Although the DHC of ⁿBuOH and PMHS is unlikely to attract the same interest (1.5 wt % H₂), generation of hydrogen from industrial by-product PMHS, bioderived ⁿBuOH and iron-catalyst **1a** is worthy of further investigation.

DHC of ⁿBuOH and PMHS was performed and the headspace pressure monitored using MOTM apparatus (figure 3.7.1). Within an hour, a pressure increase of 1.5 bar is observed. With a reaction vessel of 12 mL, this corresponds to 0.73 mmol of H₂ and 73% conversion from the ideal gas equation. Alternative alcohols MeOH and EtOH were tested under DHC conditions. In both cases, rapid H₂

evolution is observed reaching 88% and 97% conversion within an hour. In table **3.2.1**, entries 18 and 19, MeOH and EtOH are investigated as proton sources for the TH reaction. Reduced yields of **13a** are observed at 58% and 74%, respectively, compared to 85% with ⁿBuOH. Given EtOH and MeOH led to increased H₂ generation under DHC conditions, it is of no surprise they show diminishing returns in TH. More background DHC occurs during TH with MeOH and EtOH, removing proton and hydride sources from the system. Thus, there are insufficient TH reagents to reach full conversion. Proficiency of MeOH and EtOH to undergo DHC with PMHS is assumed to arise for two reasons: 1) large steric contribution from ⁿBuOH makes DHC comparatively slow, and 2) proton acidity follows the order MeOH > EtOH > ⁿBuOH (p*K*_a values of 15.3, 15.9 and 16.1, respectively), so reaction with the iron-hydride intermediate is more facile for MeOH and EtOH, compared to ⁿBuOH.¹⁸²

3.8 Conclusions and Future Work

The iron-catalysed, solvent-free TH of alkenes is reported, using bioderived ⁿBuOH and industrial by-product PMHS as TH reagents. The method tolerates a range of allylbenzenes, styrenes and other unactivated alkenes in moderate to excellent spectroscopic yields, with isolated yields reported up to 85%. Isomerisation of allylbenzenes to the corresponding internal alkenes is observed suggestive of a competing isomerisation process. Gas evolution experiments indicate that under high concentrations of proton source, DHC becomes favourable, halting the TH process. High pressure H₂ experiments confirm classical hydrogenation is not operating from H₂ generated by background DHC. Conditions were optimised for the completely regioselective THD of allylbenzene and 1-hexene, when PhND₂ and Ph₂SiH₂ are deployed as TH reagents. In the absence of alkene, rapid DHC occurs between PMHS and a variety of alcohols with H₂ generated in up to 97% yield within 1 hour.

Given the emergence of deuterium labelling in drug discovery and its importance in mechanistic investigation, a full scope for regioselective THD of alkenes should be undertaken. A partial scope was demonstrated in work by Webster and co-workers.⁶² However, THD reagents were not fully optimised and complete regioselectivity was not achieved. It is demonstrated that combining **1a**, PhND₂ and Ph₂SiH₂ leads to quantitative *d*₁-incorporation at the terminal position. Selective monodeuteration of alkenes is rare.¹⁸³ Leading examples include copper- and B(C₆F₅)₃-catalysed THD.^{184–186} If the high selectivity demonstrated for **13a-D** and **13t₁-D** is maintained, **1a** will emerge as the leading catalyst for THD.

3.9 Experimental

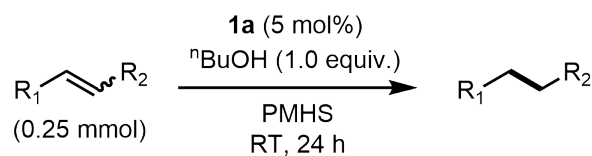
3.9.1 General Considerations

Reagents were purchased from Sigma Aldrich or Alfa Aesar and dried/distilled prior to use. Laboratory grade dichloromethane (DCM) and pentane were purchased from Fisher Scientific and used without further purification. Deuterated benzene was dried over Na/benzophenone and distilled prior to use. Pre-catalyst **1a** was synthesised following literature procedure.⁹¹ NMR spectra were collected at 300, 400 or 500 MHz on Bruker or Agilent instruments in benzene-*d*₆, toluene-*d*₈ or chloroform-*d*₁ at 298 K and referenced to residual protic solvent. Reactions were undertaken using standard glovebox (0.1 ppm H₂O and 0.1 ppm O₂) and Schlenk line techniques, unless otherwise stated. All reactions were undertaken in sealed vessels; Teflon-sealed J-Young NMR tubes, ampoules or 4 dram vials. Gas evolution experiments were undertaken using the Man on the Moon Series X103 apparatus.

3.9.2 Optimisation

Equivalents of PMHS reported correspond to the number of repeat units per equivalent of substrate, determined by the MW of a repeat unit (60.1 g mol⁻¹). For reactions undertaken in deuterated solvent, conversion and spectroscopic yield were determined by *in situ* ¹H NMR spectroscopy comparing starting material allyl benzene and internal standard dichloroethane (0.1 mmol), respectively (table **3.2.1**, entries 1-6 and 11-15). For reactions in protic solvents, volatiles were removed under a stream of nitrogen (table **3.2.1**, entry 7) or under reduced pressure (table **3.2.1**, entry 8). Reactions with sugar derivatives required agitation because of poor solubility in C₆D₆ and the remaining solids were removed by filtration prior to NMR analysis (table **3.2.1**, entries 9-13). When using ⁿbutanol as proton donor, peaks in the ¹H NMR spectra are broad. Therefore, the hydrogenated product was separated from the reaction mixture by dissolving in CDCl₃ and purifying by vacuum distillation before NMR spectroscopic analysis (table **3.2.1**, entries 15-22).

3.9.3 General Method for Hydrogenation of Alkenes

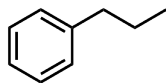


Pre-catalyst **1a** (7.0 mg, 5 mol%) was weighed out into a 5 mL vial equipped with a stirrer bar within the glovebox. ⁿButanol (22.9 μ L, 0.25 mmol, 1.0 equiv.) was added, followed by the corresponding alkene substrate (0.25 mmol, 1.0 equiv.). PMHS (0.5 mL) was added where the vessel was sealed and stirred for 24 hours at room temperature. The vial was removed from the glovebox and exposed to air. For non-volatile products, the mixture was dissolved in DCM (1 mL) and passed through a silica plug to remove the iron complex, before DCM was removed under a stream of nitrogen. As an alternative, ethyl acetate was also shown to be a suitable solvent for further purification. For volatile products, the reaction mixture was

dissolved in CDCl₃ and separated by vacuum transfer. Internal standard (dichloroethane (DCE) and/or mesitylene, 0.25 mmol) was added and spectroscopic yield determined by ¹H NMR spectroscopy.

3.9.4 Substrate Scope Spectroscopic Data

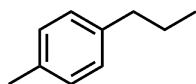
1-Phenylpropane, 13a



Spectroscopic yield: 85%

Spectroscopic data in agreement with previous literature.¹⁸⁷ ¹H NMR (CDCl₃, 400 MHz) δ 7.33-7.29 (m, 2H), 7.22-7.19 (m, 3H), 2.62 (t, $J=7.5$ Hz, 2H), 1.68 (hex, $J=7.5$ Hz, 2H), 0.98 (t, $J=7.5$ Hz, 3H); ¹³C{¹H} NMR (CDCl₃, 100 MHz) δ 142.8 (^{Ar}C), 128.6 (^{Ar}C), 128.3 (^{Ar}C), 125.7 (^{Ar}C), 38.2 (ArCH₂), 24.7 (CH₂), 14.0 (CH₃).

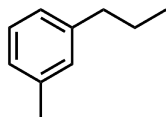
1-Methyl-4-propylbenzene, 13b



Spectroscopic yield: 79%

Spectroscopic data in agreement with previous literature.¹⁸⁸ ¹H NMR (CDCl₃, 400 MHz) δ 7.25-7.20 (m, 4H), 2.70 (t, $J=7.6$ Hz, 2H), 2.47 (s, 3H), 1.78 (m, 2H), 1.09 (m, 3H).

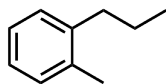
1-Methyl-3-propylbenzene, 13c



Spectroscopic yield: 46%

Spectroscopic data in agreement with commercially available sample. ¹H NMR (CDCl₃, 400 MHz) δ 7.23-7.15 (m, 2H), 7.04-7.00 (m, 2H), 2.59 (t, $J=7.6$ Hz, 2H), 2.37 (s, 3H), 1.68 (hex, $J=7.6$ Hz, 2H), 0.99 (m, 3H).

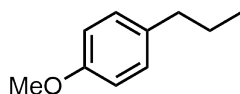
1-Methyl-2-propylbenzene, 13d



Spectroscopic yield: 62%

Spectroscopic data in agreement with previous literature.¹⁸⁹ ¹H NMR (CDCl₃, 400 MHz) δ 7.17-7.10 (m, 5H), 2.61 (t, $J=7.8$ Hz, 2H), 2.34 (s, 3H), 1.65 (h, $J=7.5$ Hz, 2H), 1.02 (t, $J=7.3$ Hz, 3H).

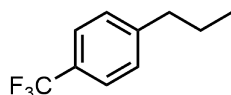
1-Methoxy-4-propylbenzene, 13e



Spectroscopic yield: 91%

Spectroscopic data in agreement with previous literature.¹⁸⁹ $^1\text{H NMR}$ (CDCl_3 , 400 MHz) δ 7.12 (d, $J=8.5$ Hz, 2H), 6.85 (d, $J=8.5$ Hz, 2H), 3.80 (s, 3H), 2.56 (t, $J=7.6$ Hz, 2H), 1.65 (h, $J=7.4$ Hz, 2H), 0.97 (t, $J=7.4$ Hz, 3H).

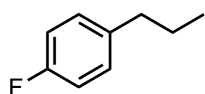
1-Propyl-4-(trifluoromethyl)benzene, 13f



Spectroscopic yield: 36%

Spectroscopic data in agreement with previous literature.¹⁹⁰ $^1\text{H NMR}$ (CDCl_3 , 400 MHz) δ 7.52 (d, $J=8.1$ Hz, 2H), 7.26 (d, $J=8.1$ Hz, 2H), 2.64 (t, $J=7.5$ Hz, 2H), 1.67 (h, $J=7.5$ Hz, 2H), 0.96 (m, 3H); $^{19}\text{F NMR}$ (CDCl_3 , 378 MHz) δ -62.1.

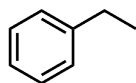
1-Propyl-4-fluorobenzene, 13g



Spectroscopic yield: 50%

Spectroscopic data in agreement with previous literature.¹⁹¹ $^1\text{H NMR}$ (CDCl_3 , 400 MHz) δ 7.13-7.09 (m, 2H), 6.98-6.92 (m, 2H), 2.56 (t, $J=7.5$ Hz, 2H), 1.63 (h, $J=7.5$ Hz, 2H), 0.94 (t, $J=7.5$ Hz, 3H); $^{19}\text{F NMR}$ (CDCl_3 , 378 MHz) δ -118.0.

Ethylbenzene, 13h



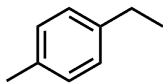
0.25 mmol, 24 h: Spectroscopic yield: 71%

Spectroscopic data in agreement with previous literature.¹⁹² $^1\text{H NMR}$ (CDCl_3 , 400 MHz) δ 7.36-7.28 (m, 2H), 7.24-7.17 (m, 3H), 2.67 (q, $J=7.6$ Hz, 2H), 1.26 (t, $J=7.6$ Hz, 3H).

2.5 mmol, 48 h:

Title compound isolated by vacuum distillation as a colourless oil (225 mg, 2.12 mmol, 85%). Spectroscopic data in agreement with previous literature.¹⁹² $^1\text{H NMR}$ (CDCl_3 , 400 MHz) δ 7.34-7.30 (m, 2H), 7.25-7.19 (m, 3H), 2.69 (q, $J=7.6$ Hz, 2H), 1.28 (t, $J=7.6$ Hz, 3H); $^{13}\text{C}\{^1\text{H}\}$ NMR (CDCl_3 , 100 MHz) δ 144.4 ($^{\text{Ar}}\text{C}$), 128.4 ($^{\text{Ar}}\text{C}$), 128.0 ($^{\text{Ar}}\text{C}$), 125.7 ($^{\text{Ar}}\text{C}$), 29.1 (CH_2), 15.8 (CH_3); FTIR (cm^{-1}) 3084, 3064, 3030, 2967, 2930, 2877, 1603, 1496, 1456.

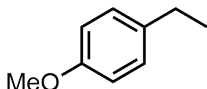
1-Ethyl-4-methylbenzene, 13i



Spectroscopic yield: 52%

Spectroscopic data in agreement with previous literature.¹⁸⁹ **¹H NMR** (CDCl₃, 400 MHz) δ 7.07 (m, 4H), 2.59 (q, $J=7.6$ Hz, 2H), 2.30 (s, 3H), 1.21 (t, $J=7.6$ Hz, 3H).

1-Ethyl-4-methoxybenzene, 13j



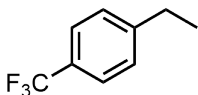
0.25 mmol, 24 h Spectroscopic yield: 78%

Spectroscopic data in agreement with previous literature.¹⁸⁹ **¹H NMR** (CDCl₃, 400 MHz) δ 7.18 (d, $J=8.6$ Hz, 2H), 6.90 (d, $J=8.6$ Hz, 2H), 3.84 (s, 3H), 2.67 (q, $J=7.6$ Hz, 2H), 1.30 (t, $J=7.6$ Hz, 3H).

0.50 mmol, 24 h

Isolated as a colourless oil by FCC (SiO₂, hexane:EtOAc (95:5), 47.0 mg, 0.35 mmol, 69%). Spectroscopic data in agreement with previous literature.¹⁸⁹ **¹H NMR** (CDCl₃, 400 MHz) δ 7.14 (d, $J=8.4$ Hz, 2H), 6.96 (d, $J=8.6$ Hz, 2H), 3.81 (s, 3H), 2.62 (q, $J=7.6$ Hz, 2H), 1.24 (t, $J=7.6$ Hz, 3H); **¹³C{¹H} NMR** (CDCl₃, 100 MHz) δ 157.7 (^{Ar}C), 136.5 (^{Ar}C), 128.8 (^{Ar}C), 113.8 (^{Ar}C), 55.4 (OCH₃), 28.1 (CH₂), 16.1 (CH₃); **FTIR** (cm⁻¹) 2997, 2962, 2934, 2836, 1610, 1583, 1512, 1034.

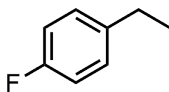
1-Ethyl-4-(trifluoromethyl)benzene, 13k



Spectroscopic yield: 44%

Spectroscopic data in agreement with previous literature.¹⁹³ **¹H NMR** (CDCl₃, 400 MHz) δ 7.57 (d, $J=7.9$ Hz, 2H), 7.33 (d, $J=7.9$ Hz, 2H), 2.75 (q, $J=7.6$ Hz, 2H), 1.31 (t, $J=7.6$ Hz, 3H); **¹⁹F NMR** (CDCl₃, 378 MHz) δ -62.4.

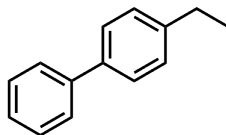
1-Ethyl-4-fluorobenzene, 13l



Spectroscopic yield: 31%

Spectroscopic data in agreement with previous literature.¹⁹⁴ **¹H NMR** (CDCl₃, 400 MHz) δ 7.19-7.16 (m, 2H), 7.02-6.97 (m, 2H), 2.66 (q, $J=7.6$ Hz, 2H), 1.27 (t, $J=7.6$ Hz, 3H); **¹⁹F NMR** (CDCl₃, 378 MHz) δ -118.2.

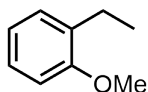
4-Ethyl-1,1'-biphenyl, 13m



Spectroscopic yield: 66%

Spectroscopic data in agreement with previous literature.¹⁹⁵ $^1\text{H NMR}$ (CDCl_3 , 400 MHz) δ 7.58-7.23 (m, 9H), 2.67 (q, $J=7.6$ Hz, 2H), 1.27 (t, $J=7.6$ Hz, 3H).

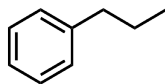
1-Ethyl-2-methoxybenzene, 13n



Spectroscopic yield: 43%

Spectroscopic data in agreement with previous literature.¹⁹⁶ $^1\text{H NMR}$ (CDCl_3 , 400 MHz) δ 7.16-6.82 (m, 4H), 2.83 (s, 3H), 2.64 (q, $J=7.5$ Hz, 2H), 1.19 (t, $J=7.5$ Hz, 3H).

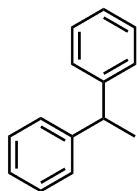
1-Phenylpropane, 13o



Spectroscopic yield: 9%

Spectroscopic data in agreement with previous literature.¹⁸⁷ $^1\text{H NMR}$ (CDCl_3 , 400 MHz) δ 7.16-6.82 (m, 4H), 2.83 (s, 3H), 2.64 (q, $J=7.5$ Hz, 2H), 1.19 (t, $J=7.5$ Hz, 3H).

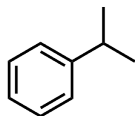
1,1-Diphenylethane, 13p



Spectroscopic yield: 76%

Spectroscopic data in agreement with previous literature.¹⁹⁷ $^1\text{H NMR}$ (CDCl_3 , 400 MHz) δ 7.39-7.19 (m, 10H), 4.20 (q, $J=7.3$ Hz, 1H), 1.69 (d, $J=7.3$ Hz, 3H).

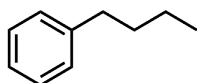
Isopropylbenzene, 13q



Spectroscopic yield: 63%

Spectroscopic data in agreement with commercially available isopropylbenzene. $^1\text{H NMR}$ (CDCl_3 , 400 MHz) δ 7.37-7.16 (m, 5H), 2.94 (hept, $J=6.9$ Hz, 1H), 1.29 (d, $J=6.9$ Hz, 6H).

1-Butylbenzene, 13r



Spectroscopic yield: 71%

Spectroscopic data in agreement with previous literature.¹⁹⁴ $^1\text{H NMR}$ (CDCl_3 , 400 MHz) δ 7.27-7.22 (m, 2H), 7.16-7.10 (m, 3H), 2.59 (t, $J=7.7$ Hz, 2H), 1.63-1.51 (m, 2H), 1.39-1.30 (m, 2H), 0.92 (m, 3H).

Cyclohexane, 13s



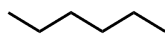
0.25 mmol, 24 h Spectroscopic yield: 68%

Spectroscopic data in agreement with commercially available cyclohexane. $^1\text{H NMR}$ (CDCl_3 , 400 MHz) δ 1.38 (s, 12H).

2.5 mmol, 24 h

Isolated as a colourless oil by vacuum distillation (156 mg, 1.85 mmol, 74%). Spectroscopic data in agreement with commercially available cyclohexane. $^1\text{H NMR}$ (CDCl_3 , 400 MHz) δ 1.38 (s, 12H).

Hexane, 13t



2t₁ Spectroscopic yield: 64%

2t_{trans-2} Spectroscopic yield: 50%

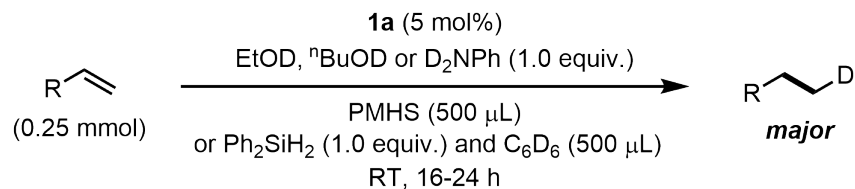
2t_{cis-2} Spectroscopic yield: 63%

2t_{trans-3} Spectroscopic yield: 61%

2t_{cis-3} Spectroscopic yield: 71%

Spectroscopic data in agreement with commercially available hexane. $^1\text{H NMR}$ (CDCl_3 , 400 MHz) δ 1.37-1.29 (m, 8H), 0.94 (t, $J=6.9$ Hz, 6H).

3.9.5 Deuterium Labelling Experiments

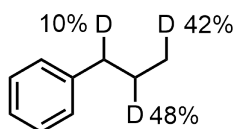


For PMHS experiments, pre-catalyst **1a** (7.0 mg, 5 mol%) was weighed out into a 4 dram vial equipped with a stirrer bar within the glovebox. Ethanol-OD (14.6 μL, 0.25 mmol, 1.0 equiv.), ⁿbutanol-*d*₁₀ (22.9 μL, 0.25 mmol, 1.0 equiv.) or aniline-N,N-*d*₂ (23.1 μL, 0.25 mmol, 1.0 equiv.) was added, followed by the corresponding alkene substrate (0.25 mmol, 1.0 equiv.). PMHS (0.5 mL) was added where the vessel was sealed and stirred for 24 hours at RT. The vial was removed from the glovebox and exposed to air. The mixture was dissolved in CDCl₃ or CHCl₃ and product was separated by vacuum transfer. For Ph₂SiH₂ experiments, pre-catalyst **1a** (7.0 mg, 5 mol%) was weighed into a J-Young NMR tube and dissolved in C₆H₆ (0.5 mL) within the glovebox. Aniline-N,N-*d*₂ (23.1 μL, 0.25 mmol, 1.0 equiv.) or ⁿbutanol-*d*₁₀ (22.9 μL, 0.25 mmol, 1.0 equiv.) was added followed by the corresponding alkene substrate (0.25 mmol, 1.0 equiv.). Ph₂SiH₂ (46.4 μL, 0.25 mmol, 1.0 equiv.) was added where the vessel was sealed for 16 hours. The product was separated by vacuum transfer into a second J-Young NMR tube. Mesitylene (0.25 mmol) and DCM-*d*₂ (0.25 mmol) were added and deuterium incorporation was determined by ¹H and ²H NMR spectroscopy.

3.9.6 Deuterium Labelling Spectroscopic Data

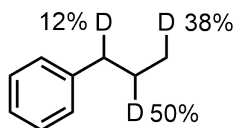
D-1-Phenylpropane, **13a-D**

From ⁿBuOD and PMHS



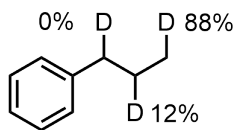
¹H NMR (CDCl₃, 400 MHz) δ 7.32-7.29 (m, 2H), 7.21-7.19 (m, 3H), 2.63-2.60 (m, 1.8H), 1.70-1.64 (m, 1.7H), 0.99-0.97 (m, 2.5H); ²H NMR (CHCl₃, 77 MHz) δ 2.62 (minor, 0.15D), 1.67 (major, 0.49D), 0.98 (minor, 0.36D).

From EtOD and PMHS



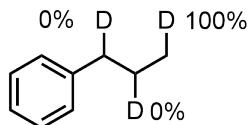
¹H NMR (CDCl₃, 400 MHz) δ 7.29-7.26 (m, 2H), 7.19-7.16 (m, 3H), 2.61-2.58 (m, 1.8H), 1.69-1.61 (m, 1.6H), 0.96-0.91 (m, 2.6H); ²H NMR (CHCl₃, 77 MHz) δ 2.59 (minor, 0.12D), 1.65 (major, 0.50D), 0.96 (minor, 0.38D).

From PhND₂ and PMHS



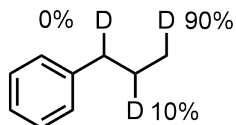
¹H NMR (CDCl₃, 400 MHz) δ 7.32-7.29 (m, 2H), 7.22-7.19 (m, 3H), 2.63-2.60 (m, 2H), 1.72-1.64 (m, 1.9H), 1.00-0.94 (m, 2.1H); ²H NMR (CHCl₃, 77 MHz) δ 1.66 (minor, 0.10D), 0.97 (major, 0.90D).

From PhND₂ and Ph₂SiH₂



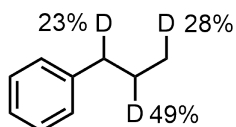
¹H NMR (CDCl₃, 400 MHz) δ 7.17-7.14 (m, 2H), 7.08-7.03 (m, 3H), 2.43-2.40 (m, 1.9H), 1.52-1.46 (m, 1.9H), 0.83-0.78 (m, 2.1H); ²H NMR (CHCl₃, 77 MHz) δ 0.79 (major, 1.00D).

From ⁿBuOD and Ph₂SiH₂



¹H NMR (CDCl₃, 400 MHz) δ 7.16-7.12 (m, 2H), 7.06-7.01 (m, 3H), 2.41-2.38 (m, 1.9H), 1.51-1.45 (m, 1.8H), 0.81-0.76 (m, 2.3H); ²H NMR (CHCl₃, 77 MHz) δ 1.43 (minor, 0.24D), 0.80 (major, 0.76D).

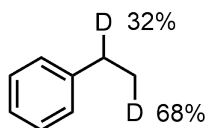
From ⁿBuOD and PMHS (1.0 equiv.)



¹H NMR (CDCl₃, 400 MHz) δ 7.36-7.28 (m, 2H), 7.23-7.20 (m, 3H), 2.63-2.58 (m, 1.7H), 1.71-1.64 (m, 1.6H), 0.99-0.94 (m, 2.7H); ²H NMR (CHCl₃, 77 MHz) δ 2.62 (minor, 0.23D), 1.67 (major, 0.49D), 0.98 (minor, 0.28D).

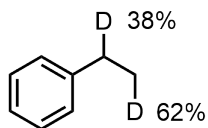
D-1-Phenylthane, 13h-D

From ⁿBuOD and PMHS



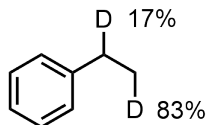
¹H NMR (CDCl₃, 400 MHz) δ 7.35-7.31 (m, 2H), 7.25-7.20 (m, 3H), 2.72-2.66 (m, 1.7H), 1.31-1.25 (m, 2.3H); ²H NMR (CHCl₃, 77 MHz) δ 2.67 (minor, 0.37D), 1.27 (major, 0.63D).

From EtOD and PMHS



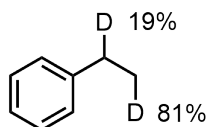
¹H NMR (CDCl₃, 400 MHz) δ 7.35-7.28 (m, 2H), 7.22-7.17 (m, 3H), 2.69-2.64 (m, 1.6H), 1.27-1.24 (m, 2.4H); ²H NMR (CHCl₃, 77 MHz) δ 2.66 (minor, 0.38D), 1.26 (major, 0.62D).

From PhND₂ and PMHS



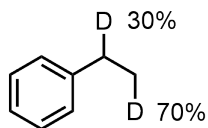
¹H NMR (CDCl₃, 400 MHz) δ 7.32-7.29 (m, 2H), 7.23-7.16 (m, 3H), 2.70-2.65 (m, 1.8H), 1.28-1.23 (m, 2.2H); ²H NMR (CHCl₃, 77 MHz) δ 2.66 (minor, 0.17D), 1.26 (major, 0.83D).

From PhND₂ and Ph₂SiH₂



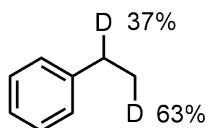
¹H NMR (CDCl₃, 400 MHz) δ 7.17-7.14 (m, 2H), 7.07-7.04 (m, 3H), 2.46-2.42 (m, 1.7H), 1.09-1.04 (m, 2.3H); ²H NMR (CHCl₃, 77 MHz) δ 2.39 (minor, 0.27D), 1.04 (major, 0.73D).

From ⁿBuOD and Ph₂SiH₂



¹H NMR (CDCl₃, 400 MHz) δ 7.15-7.12 (m, 2H), 7.08-7.01 (m, 3H), 2.44-2.40 (m, 1.7H), 1.06-1.02 (m, 2.3H); ²H NMR (CHCl₃, 77 MHz) δ 2.39 (minor, 0.33D), 1.04 (major, 0.67D).

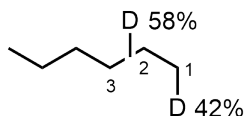
From ⁿBuOD and PMHS (1.0 equiv.)



¹H NMR (CDCl₃, 400 MHz) δ 7.31-7.25 (m, 2H), 7.21-7.16 (m, 3H), 2.68-2.62 (m, 1.6H), 1.27-1.21 (m, 2.4H); ²H NMR (CHCl₃, 77 MHz) δ 2.68 (minor, 0.37D), 1.28 (major, 0.63D).

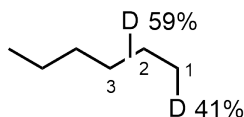
D-1-Hexane, 13t-D

From ⁿBuOD and PMHS



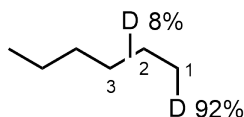
¹H NMR (CDCl₃, 400 MHz) δ 1.37-1.33 (m, 7.4H), 0.96-0.94 (m, 5.6H); ²H NMR (CHCl₃, 77 MHz) δ 1.34 (0.60D), 0.95 (0.40D).

From EtOD and PMHS



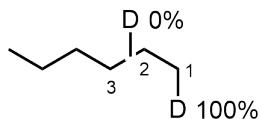
¹H NMR (CDCl₃, 400 MHz) δ 1.31-1.23 (m, 7.5H), 0.90-0.87 (m, 5.5H); ²H NMR (CHCl₃, 77 MHz) δ 1.28 (0.59D), 0.89 (0.41D).

From PhND₂ and PMHS



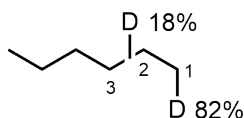
¹H NMR (CDCl₃, 400 MHz) δ 1.37-1.33 (m, 8H), 0.96-0.93 (m, 5H); ²H NMR (CHCl₃, 77 MHz) δ 0.93 (1.00D).

From PhND₂ and Ph₂SiH₂



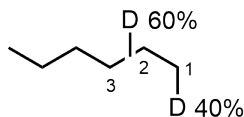
¹H NMR (CDCl₃, 400 MHz) δ 1.25-1.18 (m), 0.87-0.84 (m, 5.1H); ²H NMR (CHCl₃, 77 MHz) δ 1.21 (0.11D), 0.85 (0.89D).

From ⁿBuOD and Ph₂SiH₂



¹H NMR (CDCl₃, 400 MHz) δ 1.28-1.23 (m, 8.0H), 0.90-0.86 (m, 5.0H); ²H NMR (CHCl₃, 77 MHz) δ 0.89 (1.00D).

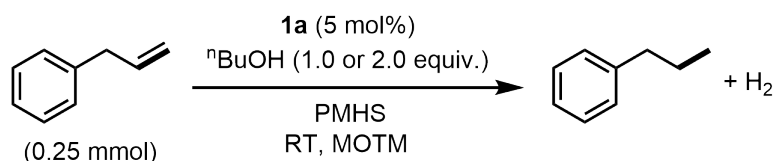
From ⁿBuOD and PMHS (1.0 equiv.)



¹H NMR (CDCl₃, 400 MHz) δ 1.36-1.31 (m, 7.3H), 0.95-0.90 (m, 5.7H); ²H NMR (CHCl₃, 77 MHz) δ 1.30 (0.59D), 0.91 (0.41D).

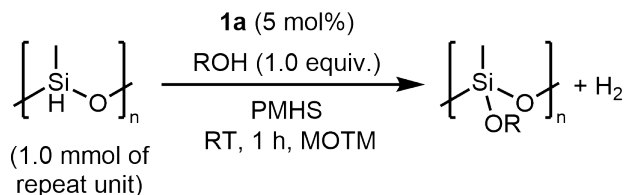
3.9.7 Gas Evolution Experiments

Transfer Hydrogenation



Pre-catalyst **1a** (7.0 mg, 5 mol%) was weighed out into the Man on the Moon (MOTM) reaction flask within the glovebox. The corresponding quantity of ⁿbutanol and allyl benzene (33.1 μL, 0.25 mmol, 1.0 equiv.) were added and the flask was sealed with a septum. The flask was removed from the glovebox and connected to the Schlenk line and pressure sensor under N₂ atmosphere. PMHS (500 μL) was added via syringe and hydrogen evolution was monitored until the reaction reached completion.

Dehydrocoupling Experiments



Pre-catalyst **1a** (28.0 mg, 5 mol%) was weighed out into the MOTM reaction flask within the glovebox. The flask was sealed with a septum, removed from the glovebox and connected to the Schlenk line and pressure sensor under N₂ atmosphere. The corresponding alcohol (1.0 mmol, 1.0 equiv.) and PMHS (60.1 mg, 1.00 mmol, 1.0 equiv.) were added via syringe, and hydrogen evolution was monitored until the reaction reached completion.

3.9.8 H₂ Experiments

Pre-catalyst **1a** was weighed into the Parr bomb reactor within the glovebox. Allyl benzene (33.1 μL, 0.25 mmol, 1.0 equiv.) and PMHS (500 μL) or ⁿbutanol (22.0 μL, 0.25 mmol, 1.0 equiv.) and C₆D₆ (500 μL) were added. The vessel was sealed, removed from the glovebox and charged with the corresponding

pressure of H₂ gas. The mixture was stirred for 24 hours at RT. The vessel was depressurised and reaction progress determined by ¹H NMR spectroscopy. For ⁿbutanol reactions, the mixture was filtered through a short silica plug with DCM and volatiles removed under a stream of N₂ prior to NMR analysis.

Chapter 4

2nd Generation Chiral

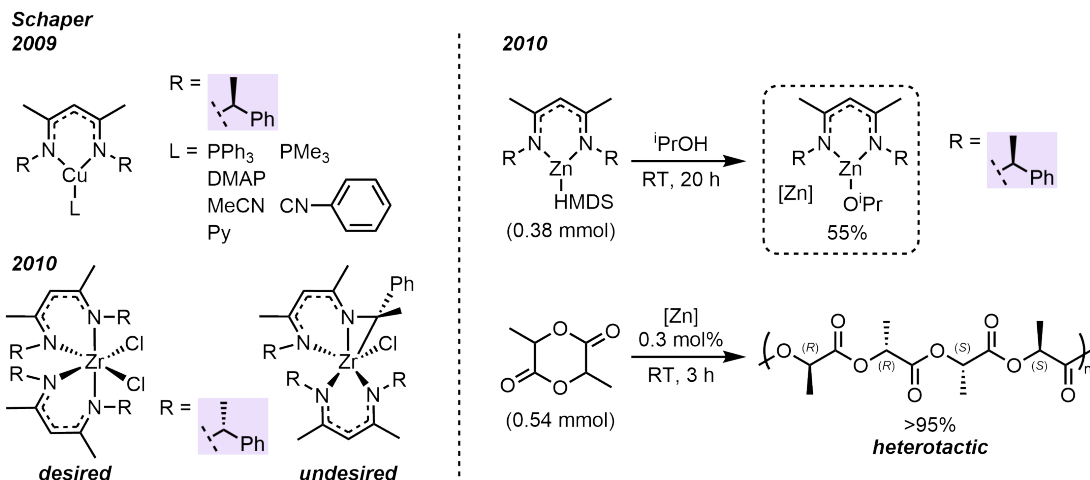
β -Diketiminates: Towards

Enantioenriched Main-Group

Compounds

4.1 Introduction

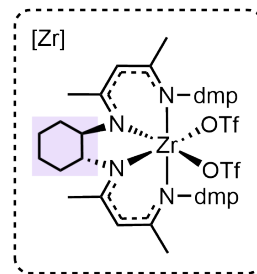
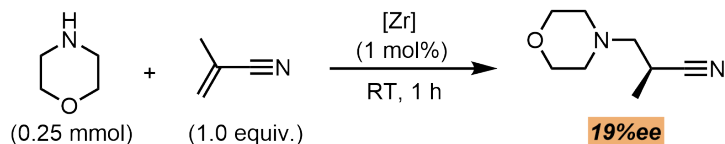
Thus far, this thesis describes the iron-catalysed deuterium-labelling of silanes (chapter 2), followed by the regioselective delivery of this deuterium, via an iron-catalysed transfer hydrodeuteration reaction (chapter 3). As a logical progression, consideration turned towards the regio- and stereoselective delivery of deuterium. To achieve this using our catalytic regime, a chiral BDK ligand is required.



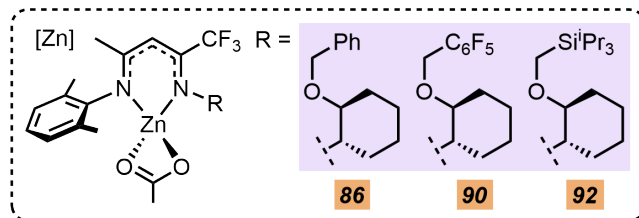
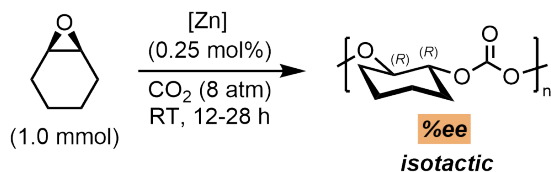
Scheme 4.1.1: BDK* complexes and their activity in ring-opening-polymerisation of (*rac*)-lactide, reported by Schaper and co-workers.^{198–200}

Reports of chiral BDK (BDK*) complexes and their application in catalysis are limited. The earliest examples were disclosed by Schaper and co-workers, shown in scheme 4.1.1. The inaugural chiral BDK ligand was synthesised by condensation of commercially available (*S*)-2-phenylethylamine with acetylacetone, forming pro-ligand bis-*N,N'*-((*S*)-2-phenylethyl)-2,4-diiminopentane.¹⁹⁸ A variety of (BDK*)CuL complexes were synthesised by reaction of the pro-ligand and CuO^tBu in the presence of coordinating ligands (L = PPh₃, DMAP, MeCN, pyridine, PMe₃ and 2,6-xylylisonitrile). Chromium and aluminium analogues bearing the same ligand were later described.^{201,202} The opposite enantiomer was deployed for the synthesis of a (BDK*)₂ZrCl₂ complex, by reaction of Li-BDK* and ZrCl₄.¹⁹⁹ Crystals of (BDK*)₂ZrCl₂ were contaminated with a second species arising from ligand CH-activation, leading to κ^3 -coordination from one of the BDKs. Navigating α -proton acidity and proximity to the metal centre in *N*-alkyl-derived BDKs may lead to undesired reactivity. Such processes are less common in *N*-aryl-derived BDKs, as there is no α -proton available to undergo CH-activation. In the same year, the first example of a BDK* in catalysis was unveiled, using the (*S*)-enantiomer of the same ligand. The reaction of (BDK*)Zn(HMDS) and isopropanol yields zinc-alkoxide complex, (BDK*)ZnOⁱPr. This complex catalysed ring-opening-polymerisation (ROP) of (*rac*)-lactide forming highly heterotactic poly(lactide) (PLA). Heterotactic PLA arises from chain-end control, observed for achiral (diPPBDK)ZnOⁱPr complexes.²⁰³ Therefore, catalyst chirality does not impart any enantioselectivity in this case. There is little evidence for these early *N*-alkyl-derived BDK* complexes being active in catalysis. Furthermore, the potential for ligand CH-activation could lead to unwanted reactivity. A move away from this motif is required to achieve an active and stereoselective catalytic process.

Schaper, 2013



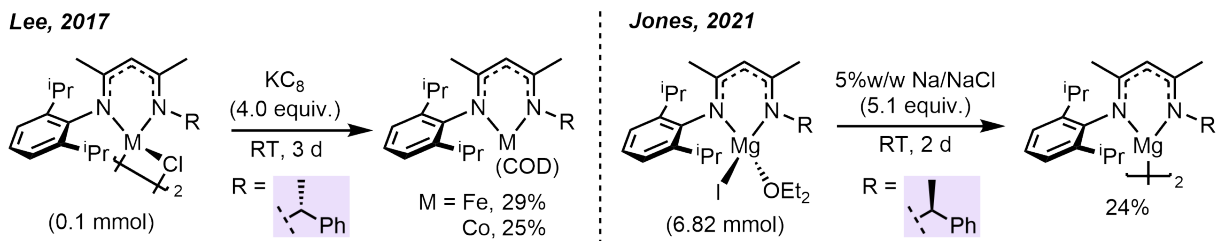
Coates, 2014



Scheme 4.1.2: Chiral zirconium-catalysed hydroamination reported by Schaper and co-workers, and BDK*-zinc complexes and their activity in co-polymerisation of cyclohexene oxide and CO₂, reported by Coates and co-workers.^{204,205}

Examples of enantioselective BDK*-mediated transformations are shown in scheme 4.1.2. Schaper and co-workers were the first to impart any enantioselectivity on the final products.²⁰⁴ A zirconium complex bearing a (*R*),(*R*)-(-)-1,2-cyclohexyl-bridged BDK*, catalysed the hydroamination of morpholine and methacrylonitrile in 19%ee. Poor selectivity was attributed to rapid BDK* $\kappa^2, \eta^2 / \eta^5$ -like' interconversion, leading to a poorly defined coordination environment. The only highly enantioselective transformation was later described by Coates and co-workers.²⁰⁵ A (BDK*)ZnOAc complex catalysed the enantioselective co-polymerisation of cyclohexene oxide and CO₂. Highly isotactic poly(cyclohexyl carbonate) forms in up to 92%ee. The chiral fragments in this case are derived from various (1*S*,2*S*)-cyclohexanaminoethers. The authors suggest that catalyst *C*₁-symmetry is essential for an enantioselective process: 1) the *N*-aryl-derived flanking group prevents inactive dimer formation or ligand redistribution, 2) the chiral *N*-alkyl-derived flanking group enforces TS geometry. Modulation of the chiral R-group geometry allows enantioselectivity to be tuned. Notably, in both Schaper, Coates and co-workers' studies, a *N*-aryl-derived flanking group is retained on one side of the BDK. Chapter 1 described how BDK aromatic flanking groups stabilise reactive centres, by providing a contained steric pocket to control the coordination environment. In Coates and co-workers' example, the chiral cyclohexyl flanking group has an analogous effect in the solid-state. Perhaps the key to a highly stereoselective process, is an ideal balance between chirality and stability.

The ability of unsymmetric *N*-alkyl-*N*-aryl-derived BDKs to stabilise reactive centres is further corroborated in works by Lee, Jones and co-workers (scheme 4.1.3). Chemical reduction of unsymmetric [(BDK*)M(μ -Cl)]₂ complexes with KC₈ in the presence of cyclooctadiene (COD), yielded the corresponding (BDK*)M(COD) complexes (where M = Fe or Co). (BDK*)M^IL complexes of this type are rare, with a few examples all derived from diaryl-substituted BDKs.²⁰⁸⁻²¹⁰ The same ligand scaffold (opposite enantiomer) was employed by Jones and co-workers for the synthesis of a magnesium(I) (BDK*)Mg-Mg(BDK*) complex. Until then, (BDK)Mg-Mg(BDK) complexes were derived from diaryl-substituted BDKs.^{211,212}

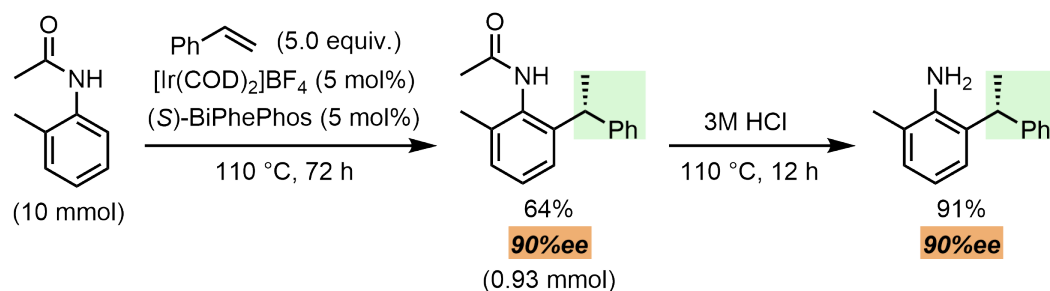


Scheme 4.1.3: BDK*-iron, cobalt and magnesium complexes, reported by Lee, Jones and co-workers.^{206,207}

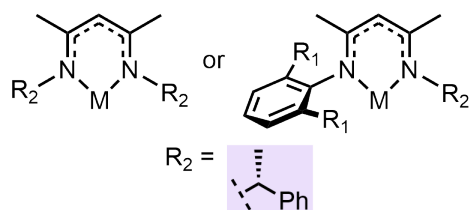
A large ligand scaffold is required to prevent disproportionation to Mg^0 and $Mg^{II}(BDK)_2$. These studies demonstrate how maintaining an aromatic flanking group is beneficial for kinetic stabilisation.

In chapter 1, the capability of iron-BDK-based catalysts to undergo carbon-carbon bond hydrofunctionalisation and heteroatom-heteroatom bond formation is described. In many of these cases, this leads to formation of a stereogenic centre (for example, alkene hydroamination, alkene hydroboration, alkene hydrophosphination, DHC of silanes, alkene transfer hydrogenation).^{33,61,62,89,213} Notably, in these cases, the BDKs are derived from *N*-aryl-derived flanking groups. With a suitable chiral ligand scaffold, these transformations may become enantioselective.

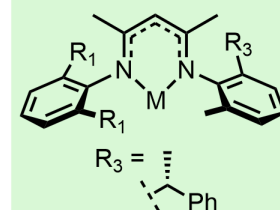
Bower, 2018



1st Gen. Chiral BDK



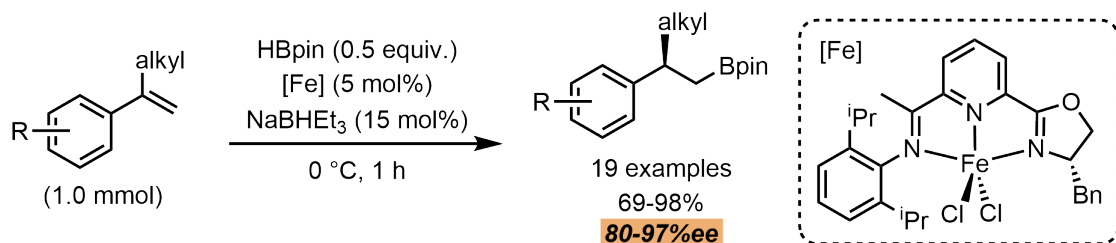
2nd Gen. Chiral BDK



Scheme 4.1.4: Iridium-catalysed enantioselective hydroarylation of styrenes with acetanilides, reported by Bower and co-workers and proposed 2nd generation BDK*s.²¹⁴

A noticeable absence from the BDK* literature are *bis-N*-aryl derived scaffolds. This is because methods for accessing chiral anilines with inert chiral substituents are not well established. An example was described by Coates and co-workers.^{215,216} In this case, a diastereomerically pure (1*S*,1*S*)-*bis*-2,6-(1-phenylethyl)aniline precursor was isolated by semi-preparative high-performance liquid chromatography (HPLC), a time consuming process with limited scope for scale-up. Chiral anilines of this type were used

to synthesise (α -diimine)NiBr₂ complexes, active in the isotactic polymerisation of propylene. Cramer and co-workers later described a synthetic method to access the analogous (1*R*,1*R*)-aniline.²¹⁷ A multi-step method culminates in an enantioselective high-pressure hydrogenation to furnish the chiral aniline. These anilines were incorporated into naphthyridine ligands for the nickel-catalysed asymmetric alkylidenecyclopropanation in up to 92%*ee*. Given the synthetic challenges associated with forming chiral anilines, it might be expected that their use as chiral ligand precursors is under-explored with only the aforementioned examples known. In 2018, a more facile method for the synthesis of chiral anilines was revealed, not reliant on preparative HPLC or a complex multi-step method. Bower and co-workers described the iridium-catalysed, enantioselective alkene hydroarylation of acetanilides, shown in scheme 4.1.4.²¹⁴ (*R*)-(1-Phenylethyl)acetanilides were formed in up to 96%*ee*. Deacetylation yielded the corresponding (*R*)-aniline with no epimerisation. With a viable synthetic method found, incorporation of this fragment into an unsymmetric BDK will form a second generation variant, derived from *bis-N*-aryl flanking groups (shown in scheme 4.1.4). It is anticipated that iron-complexes bearing such a scaffold will be active in enantioselective hydrofunctionalisation reactions, retaining the activity observed for achiral *bis-N*-aryl iron-BDKs. The chiral aromatic flanking group is expected to provide the ideal balance of kinetic stability, required for catalytic turnover, whilst imparting enantioselectivity.

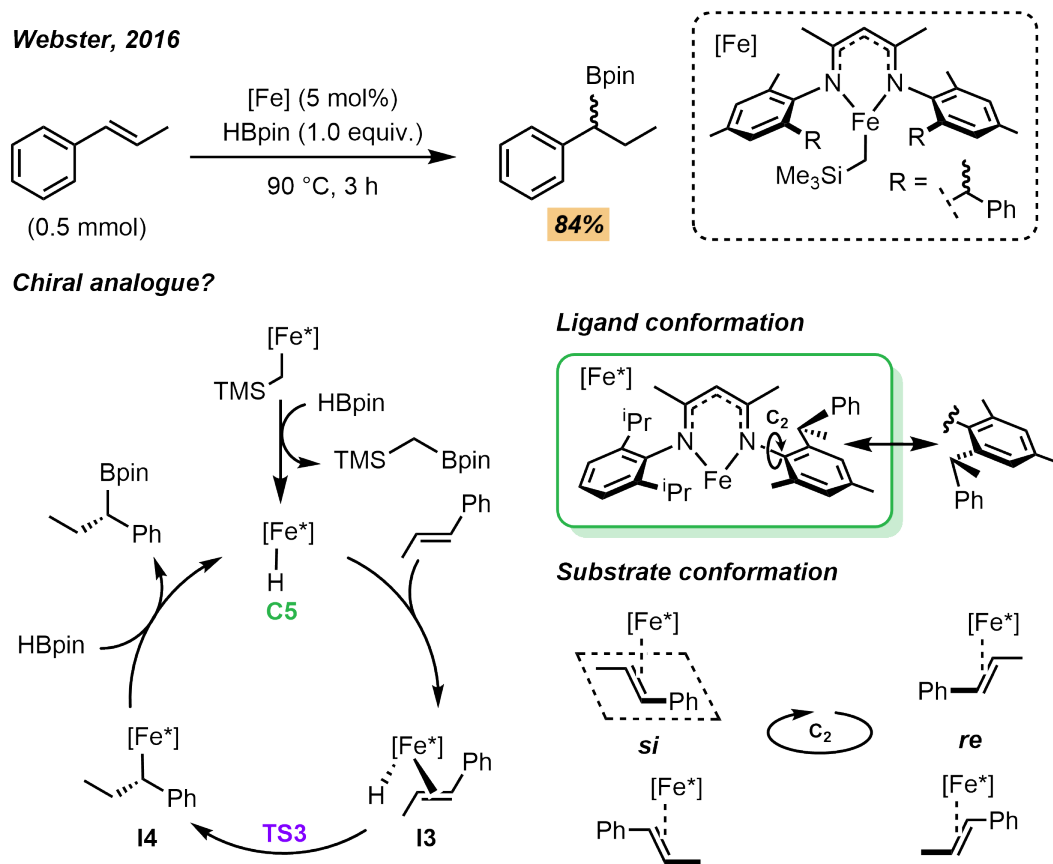


Scheme 4.1.5: Iron-catalysed enantioselective hydroboration of 1,1-disubstituted styrenes, reported by Lu and co-workers.²¹⁸

To investigate the activity of 2nd generation BDK*s in enantioselective catalysis, a model transformation is required. After considering overlap between iron-BDK-catalysed hydrofunctionalisation reactions and literature precedent for their enantioselective analogues, the hydroboration of alkenes was selected. Organoboranes are desirable synthetic building-blocks in organic synthesis, owing to their prowess as cross-coupling reagents and ability to undergo conversion into a vast array of further functionalities.^{219,220} Catalytic hydroboration of alkenes is an attractive method to access organoboranes, as it is 100% atom-efficient and alkene feedstocks are abundant. The synthetic utility of catalytic hydroboration, combined with the inherent sustainability of iron-catalysis, has led to the wide exploration of iron-catalysed hydroboration.^{21,24,221} However, only one asymmetric example is known. Lu and co-workers described the iron-catalysed enantioselective hydroboration of 1,1-disubstituted aryl alkenes, shown in scheme 4.1.5.²¹⁸ The *C*₁-symmetric chiral (IPO)FeCl₂ (IPO = iminopyridine oxazoline) complex yielded enantioenriched organoboranes in excellent yields and %*ee*. The excellent performance of this catalyst means it is the ‘state of the art’ in this field. However, investigation into the reactivity of alternatively substituted alkenes, along with complementary regioselectivity, is required to further navigate this chemical space.

This chapter describes a preliminary investigation into a 2nd generation BDK* ligand, derived from an enantioenriched (*N*)-aryl-derived flanking group. DFT is deployed as a predictive tool, suggesting the associated (BDK*)FeH complex, will undergo the enantioselective insertion of alkenes. Pro-ligand synthesis, along with its associated iron-complexes is discussed, culminating in the asymmetric hydroboration of *trans*- β -methylstyrene.

4.2 DFT-Derived Enantioselective Insertion



Scheme 4.2.1: Suggested mechanism for selective alkene insertion, based on previous work by Webster and co-workers (left) and hypothesised ligand and substrate conformations (right).²¹³

Previous work by Webster and co-workers describes the iron-catalysed hydroboration of styrenes in high regioselectivity, shown in scheme 4.2.1.²¹³ A mechanism for the reaction was proposed. Catalyst activation with HBpin yields an active iron-hydride catalyst (**C5**). Styrene coordination and insertion forms iron-alkyl intermediate (**I4**). Boration with pinacolborane yields the hydroboration product, regenerating **C5**. With the proposed BDK*, an enantioselective styrene insertion may operate by diastereomeric **TS3**.

To investigate the feasibility of enantioselective hydroboration, catalyst **C5** was selected for theoretical investigation, shown in scheme 4.2.1. Catalyst **C5** is derived from a (*R*)-2,4-dimethyl-6-(1-phenylethyl)aniline. The chiral moiety was selected following the high yields and %*ee* demonstrated in Bower and co-workers' enantioselective hydroarylation, so is an accessible ligand scaffold.²¹⁴ Furthermore, Webster and co-workers demonstrated catalytic hydroboration with a symmetric di-(*rac*)-2,4-dimethyl-6-(1-phenylethyl)BDK. Therefore, it is assumed the chiral unsymmetric variant will show analogous activity, serving as a promising complex to model with DFT. Hydroboration of *trans*- β -methylstyrene with this catalyst yielded the Markovnikov product, exclusively. Therefore, *trans*- β -methylstyrene was selected as the model substrate for the investigation.

To estimate the energy barrier associated with *trans*- β -methylstyrene insertion, the energies of **C5** in the triplet and quintet spin-states were first evaluated. Two ligand conformations were investigated, shown

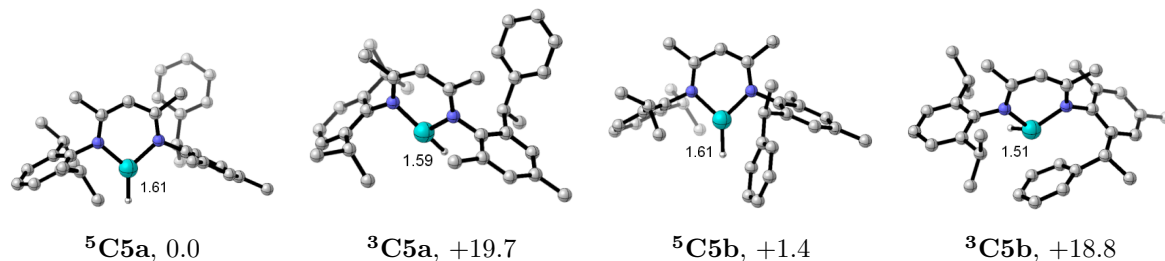


Figure 4.2.1: DFT-derived geometries and ΔG of catalyst **C5**, calculated at the B3PW91-D3BJ/Def2-TZVP/IEF-PCM(C_6H_6)/BP86/**BS1** level, showing Fe-H bond lengths with free energies calculated in kcal mol^{-1} . All energies relative to ${}^5\text{C5a}$. C-H bonds are omitted for clarity.

in figure 4.2.1. In both cases, the quintet spin-states are the lowest in energy, with ${}^5\text{C5a}$ emerging as the lowest energy conformer. These results are consistent with three-coordinate iron(II) species adopting a high-spin ground state.⁷²

To investigate the enantioselective insertion of **C5** into *trans*- β -methylstyrene, **TS3** was calculated in the quintet and triplet spin states for all possible ligand and substrate conformations, shown in scheme 4.2.1. The crystal structures described in section 2.2.3, all show the BDK aryl flanking groups sitting in a perpendicular plane to the ligand backbone. Maintaining this motif, the ligand can adopt two possible conformations via a C_2 rotation about the N- ArC^* bond, shown in scheme 4.2.1. Furthermore, coordination of the alkene can occur as the *re*- and *si*-isomers, each with a possible C_2 rotation, also shown in scheme 4.2.1. These isomers combine to give the eight possible TSs, **a-h**. The Curtin-Hammett principle states that where rate of product formation is slow relative to substrate conformation interconversion, substrate conformations (**I3**) are in rapid equilibrium and the distribution of (*R*)- and (*S*)-products depend on the differences in free energies ($\Delta\Delta G^\ddagger$) of the respective TSs.²²² Therefore, as styrene insertion is suspected to be the rate-determining enantio-inducing step, **I3a-h** are expected to be rapidly interconverting. Thus their energies do not impact the product distribution and relative population can be estimated from $\Delta\Delta G^\ddagger$ of **TS3a-h**.

Following geometry optimisation of ${}^3/{}^5\text{TS3a-h}$, the barrier to insertion (ΔG^\ddagger) is estimated at $+8.1 \text{ kcal mol}^{-1}$, with isomer ${}^5\text{TS3a}$ emerging as the most stable diastereomer, with corresponding (*S*)-configuration. Therefore, $\Delta\Delta G^\ddagger$ values were measured relative to ${}^5\text{TS3a}$. Notably, ${}^3\text{TS3e}$ was optimised using a constrained C-H bond length, and has two imaginary frequencies at -456.66 and -78.55 cm^{-1} . Upon removing the constraint, a single imaginary frequency could not be found. Although bond lengths in ${}^3\text{TS3e}$ are comparable to the other triplet states, a reliable energy comparison cannot be made. Thus, ${}^3\text{TS3e}$ was excluded from enantioexcess calculation. As ${}^3\text{TS3e}$ corresponds to the most populated (*S*)-enantiomer (*vide infra*), its omission will serve to underestimate the final % *ee*.

Calculating $\Delta\Delta G^\ddagger$ values for each TS relative to ${}^5\text{TS3a}$, theoretical equilibrium constant, $k_{i\text{TS}3j}$ (where *i* is the TS spin state and *j* is the isomer **a-h**) can be calculated for each geometry, where $\Delta\Delta G^\ddagger$ is the free-energy difference between ${}^i\text{TS3j}$ and ${}^5\text{TS3a}$ in J mol^{-1} , *R* is the ideal gas constant in $\text{J mol}^{-1} \text{ K}^{-1}$ and *T* is 298.15 K:

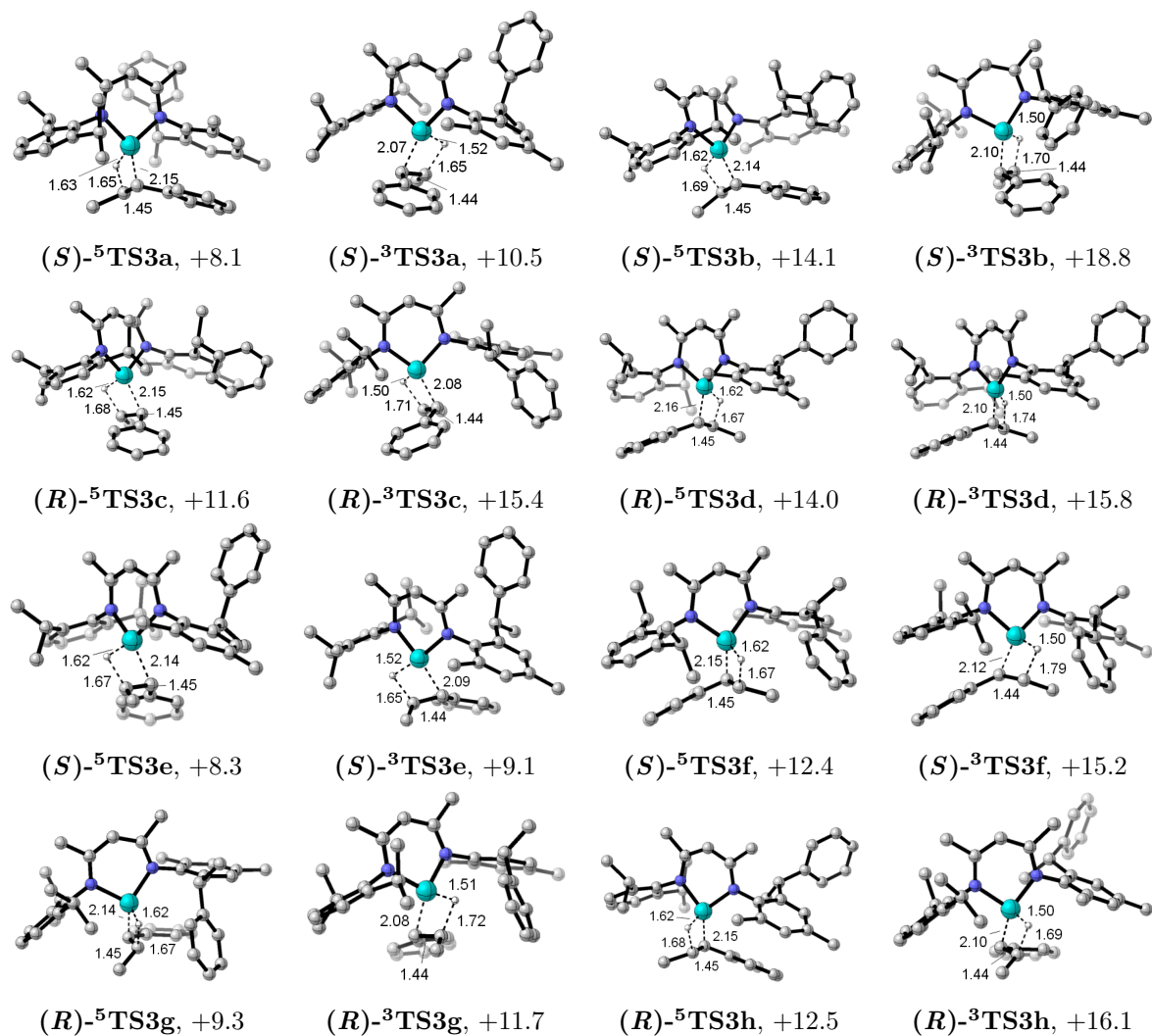


Figure 4.2.2: DFT-derived geometries and ΔG^\ddagger of **TS3**, calculated at the B3PW91-D3BJ/Def2-TZVP/IEF-PCM(C₆H₆)/BP86/BS1 level, showing bond breaking and forming bond lengths with free energies calculated in kcal mol⁻¹. All energies are relative to ⁵C5a and substrates. C-H bonds are omitted for clarity. ³TS3e was optimised with a constrained C-H bond distance.

$$k_{i\text{TS}3j} = e^{\frac{-\Delta\Delta G}{RT}} \quad (4.1)$$

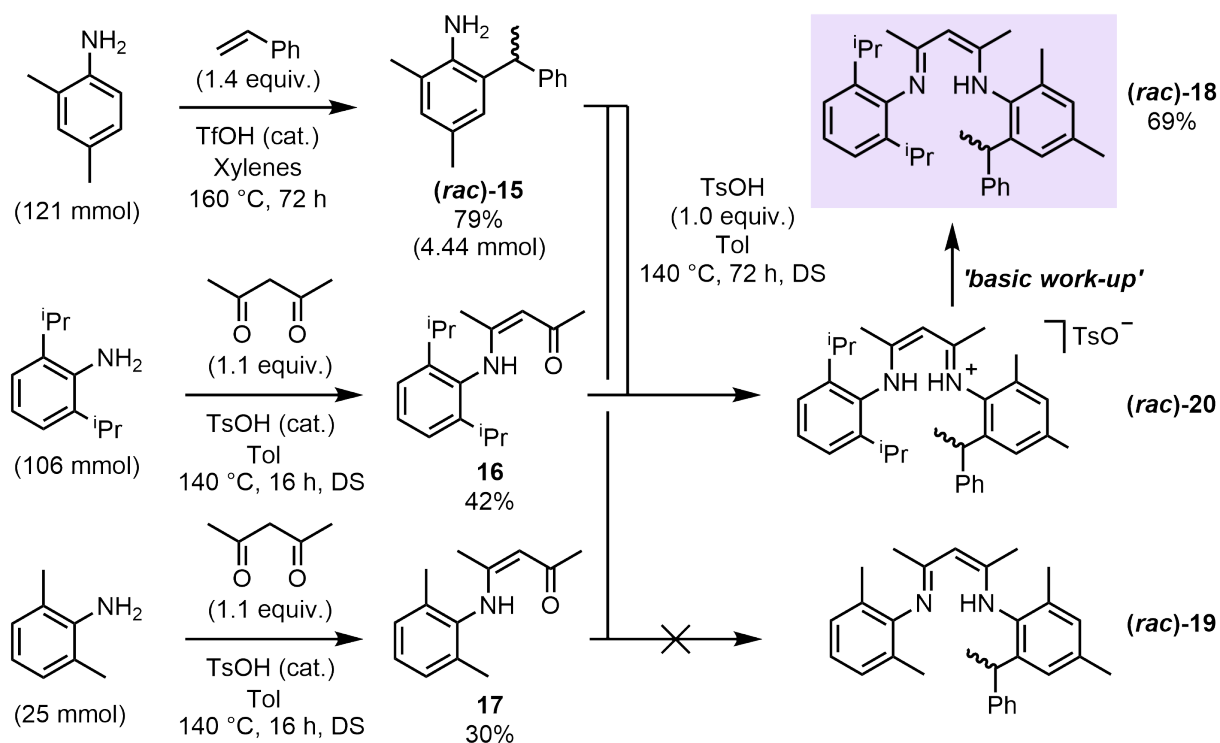
The equilibrium constants can be normalised to estimate their relative populations as a fraction, $N_{i\text{TS}3j}$. To determine %*ee*, populations corresponding to the (*S*)-TSs are subtracted from (*R*)-TSs and presented as a percentage:

$$N_{i\text{TS}3j} = \frac{k_{i\text{TS}3j}}{\sum k_{3\text{TS}3a-h} + \sum k_{5\text{TS}3a-h}} \quad (4.2)$$

$$\begin{aligned} \%ee = 100 & ((N_{5\text{TS}3a} + N_{5\text{TS}3b} + N_{5\text{TS}3e} + N_{5\text{TS}3f} + N_{3\text{TS}3a} + N_{3\text{TS}3b} + N_{3\text{TS}3f}) \\ & - (N_{5\text{TS}3c} + N_{5\text{TS}3d} + N_{5\text{TS}3g} + N_{5\text{TS}3h} + N_{3\text{TS}3c} + N_{3\text{TS}3d} + N_{3\text{TS}3g} + N_{3\text{TS}3h})) \end{aligned} \quad (4.3)$$

Inserting free energies for each TS yields a predicted enantioselectivity of 84% *ee*. Therefore, DFT indicates the proposed chiral scaffold will facilitate enantioinduction with the (*S*)-enantiomer preferred- a promising foundation for experimental investigation.

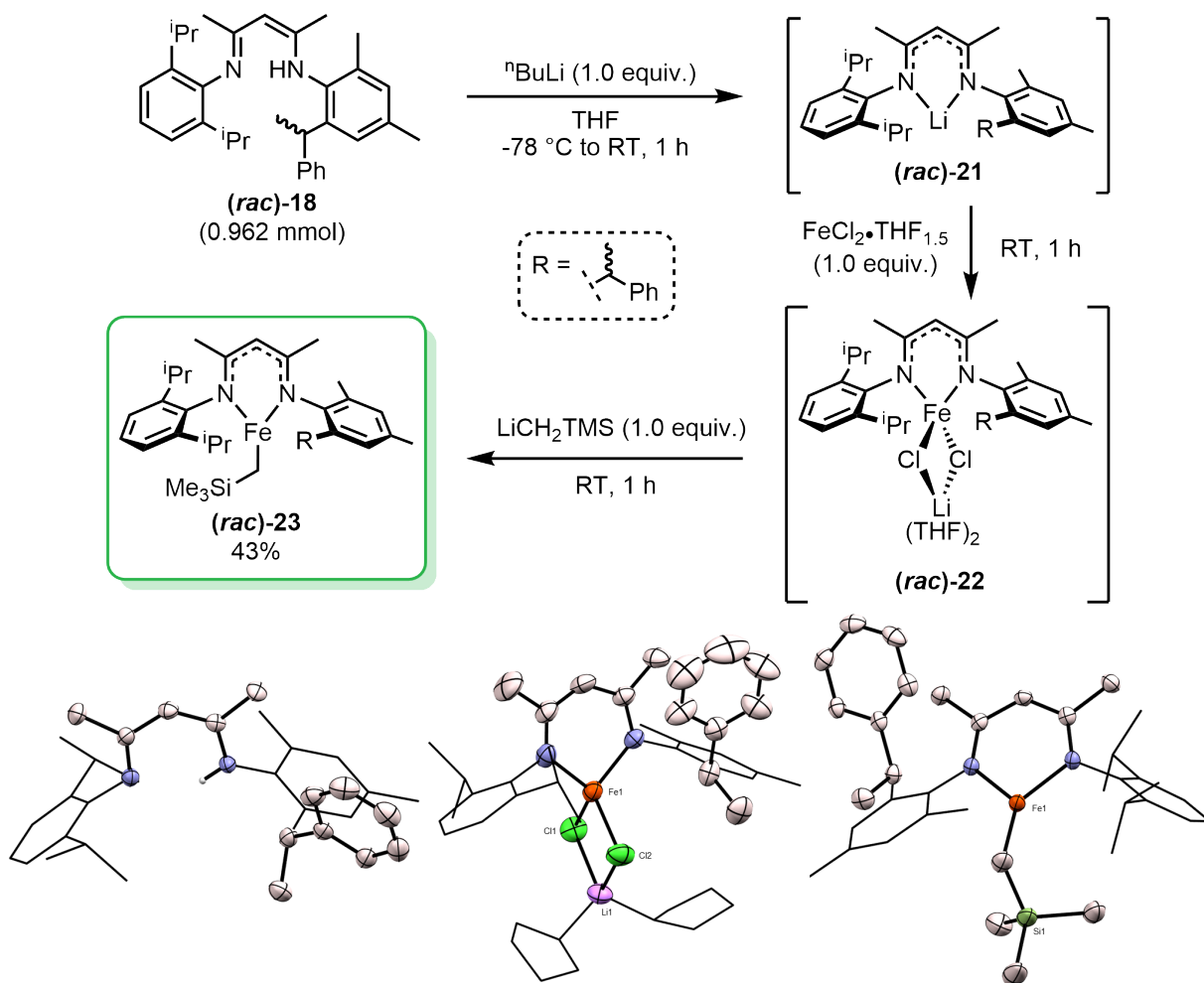
4.3 Optimisation of Unsymmetric (*rac*)-Iron- β -Diketiminato Pre-catalyst



Scheme 4.3.1: Synthesis of pro-ligand (*rac*)-18. DS = Dean-Stark apparatus.

Experimental investigation began with synthesising the racemic analogue of the hypothesised chiral pre-catalyst, to optimise conditions and test its catalytic activity. The racemic ligand synthesis is shown in scheme 4.3.1. The reaction of 2,4-dimethylaniline with styrene, forms (*rac*)-15 in 79% yield. Typically, unsymmetric BDKs are synthesised by sequential condensation of primary amines/anilines with acetyl acetone.⁹ Reaction of 2,6-diisopropylaniline and 2,6-dimethylaniline with acetylacetone, yields ketoimines **16** and **17**, respectively. Refluxing (*rac*)-15 with **17** for 16 hours forms an intractable mixture of products by ¹H NMR spectroscopy, assumed to arise from reversible condensation reactions. However, the reaction of (*rac*)-15 with **16** proceeds more cleanly, generating (*rac*)-18 as the major species after work-up. ¹H NMR spectroscopy reveals a 4:1 ratio of isomers in the solution-state, likely arising from the (*cis*)- and (*trans*)-imine conformations (shown in figure 4.3.1). Notably, symmetric ^{di}ppBDK is observed in the crude ¹H NMR spectrum in 1:9 ratio, with (*rac*)-18. Fortunately, crystallisation from hot methanol isolates (*rac*)-18 cleanly in 39% yield. These crystals were suitable for single-crystal XRD and the solid-state structure is shown in figure 4.3.2. Compound (*rac*)-18 crystallises in the (*cis*)-conformation, thus this isomer is tentatively assigned as the major species in the ¹H NMR spectrum. Clearly, formation of unwanted achiral ^{di}ppBDK must be avoided as ligation to iron will lead to reduced enantiocontrol. Therefore, further optimisation was undertaken to remove this, whilst improving the yield of (*rac*)-18. Crude reaction progress was monitored by conversion to (*rac*)-20. Allowing the reaction between (*rac*)-15 and **16** to proceed for 72 hours generates (*rac*)-20 and ^{di}ppBDK in 94:6 ratio, respectively. Raising

(*rac*)-**15** to 1.2 equivalents has no impact on product ratio, at 94:6 respectively. Finally, under air- and moisture-free conditions for 72 hours, with incorporation of a Dean-Stark trap, optimal conditions were found yielding a 99:1 distribution of products. Recrystallisation formed (*rac*)-**18** cleanly in 69% yield.



Scheme 4.3.2: Synthesis and single-crystal XRD structures of (*rac*)-**18** (left), (*rac*)-**22** (middle) and (*rac*)-**23** (right). Ellipsoids are represented at 50% probability and hydrogen atoms omitted for clarity.

With conditions for the synthesis of (*rac*)-**18** optimised, pre-catalyst synthesis was attempted following the method for **1a** and **1b**, described in chapter 2. Lithiation of (*rac*)-**18** proceeds cleanly generating (*rac*)-**21** *in situ*, as a single isomer by ^1H NMR spectroscopy (shown in figure 4.3.1). Salt metathesis with $\text{FeCl}_2 \cdot (\text{THF})_{1.5}$ follows. An aliquot was removed, concentrated and crystallised by vapour diffusion of pentane into a saturated THF solution. These crystals were suitable for single-crystal XRD and the solid-state structure is shown in figure 4.3.2. XRD reveals lithium chloride adduct (*rac*)-**22** forms *in situ*. A final salt-metathesis with LiCH_2TMS furnishes pre-catalyst (*rac*)-**23**. Recrystallisation of (*rac*)-**23** is challenging because of high solubility in apolar solvents. Nevertheless, (*rac*)-**23** was isolated in 43% yield, as olive green crystals. These crystals were suitable for single-crystal XRD and the solid-state structure is shown in figure 4.3.2. The structure is as expected, revealing the desired pre-catalyst in mononuclear form. The ^1H NMR spectrum of (*rac*)-**23** is shown in figure 4.3.1. Characteristic downfield shifts (protons **e**, **f**, **g** and **s**) were identified, indicative of a three-coordinate iron(II) complex in similar chemical

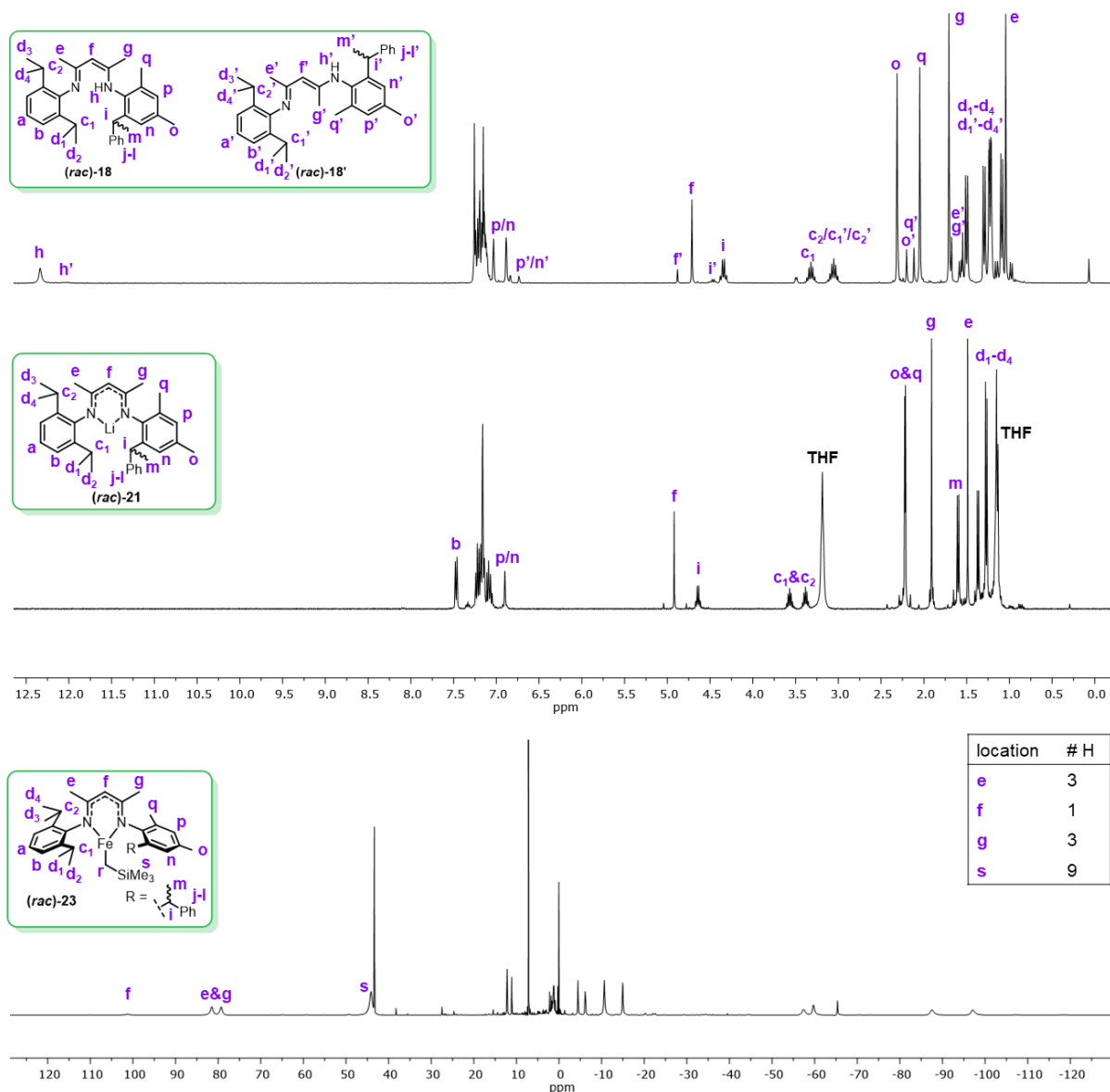
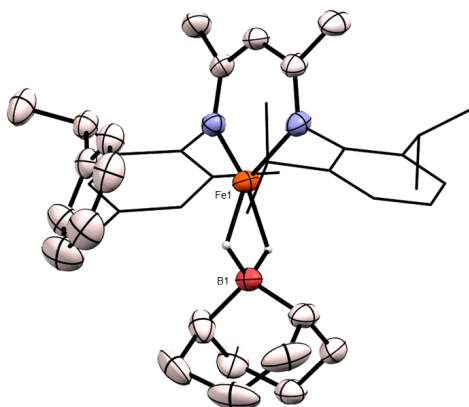
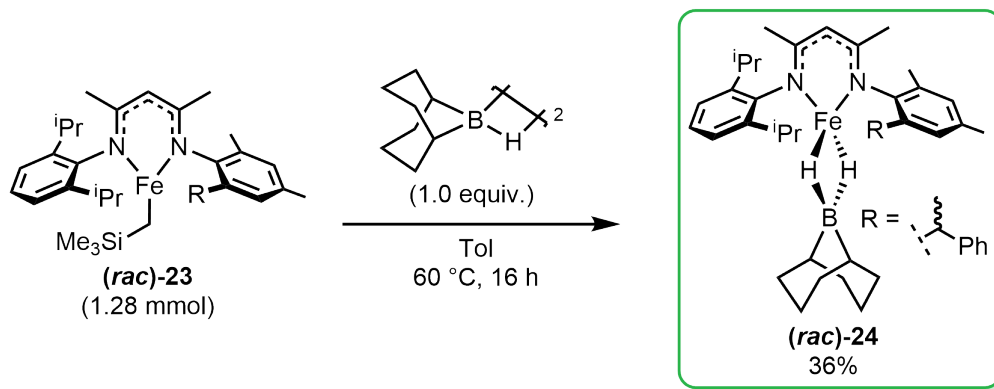


Figure 4.3.1: ^1H NMR spectra of **(rac)-18** (400 MHz, CDCl_3 , 298 K), **(rac)-21** and **(rac)-23** (400 MHz, C_6D_6 , 298 K).

shift range to **1a** and **1b** (see section 2.2.3). Unfortunately, complete assignment is challenging because of the unsymmetric nature of the BDK.

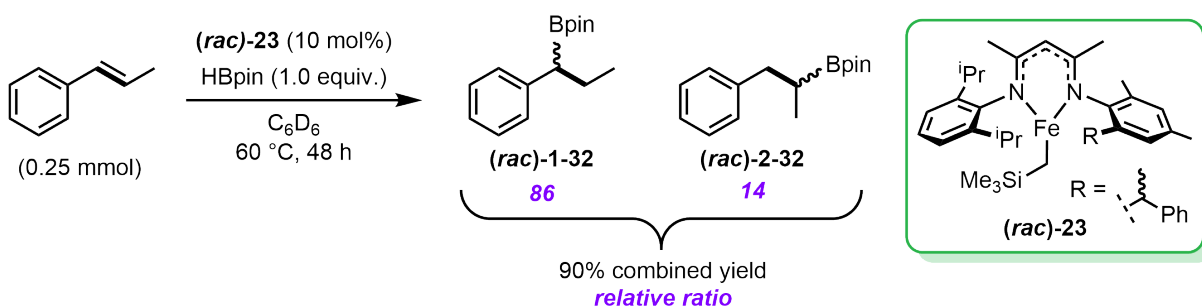
As a proof of concept, complex **(rac)-23** undergoes the same reactivity as **1a** and **1b** with 9-BBN, generating **(rac)-24** as pink crystals. Notably, the yield of **(rac)-24** is lower than the symmetric analogues **3a** and **3b**, 36% compared to 57% and 43%, respectively. Again, this is tentatively ascribed to the high solubility of **(rac)-24**. Crystals of **(rac)-24** were suitable for single-crystal XRD and the solid-state structure is shown in figure 4.3.3. The solid-state structure of **(rac)-24** provides experimental evidence for alternative ligand conformations, with the phenyl flanking group facing the 9-BBN fragment- justifying their exploration in theoretical investigations.

Pre-catalyst **(rac)-23** was tested in the hydroboration of *trans*- β -methylstyrene, shown in scheme 4.3.4. After 48 hours at 60 °C, complete conversion was observed by ^{11}B NMR spectroscopy. Filtration



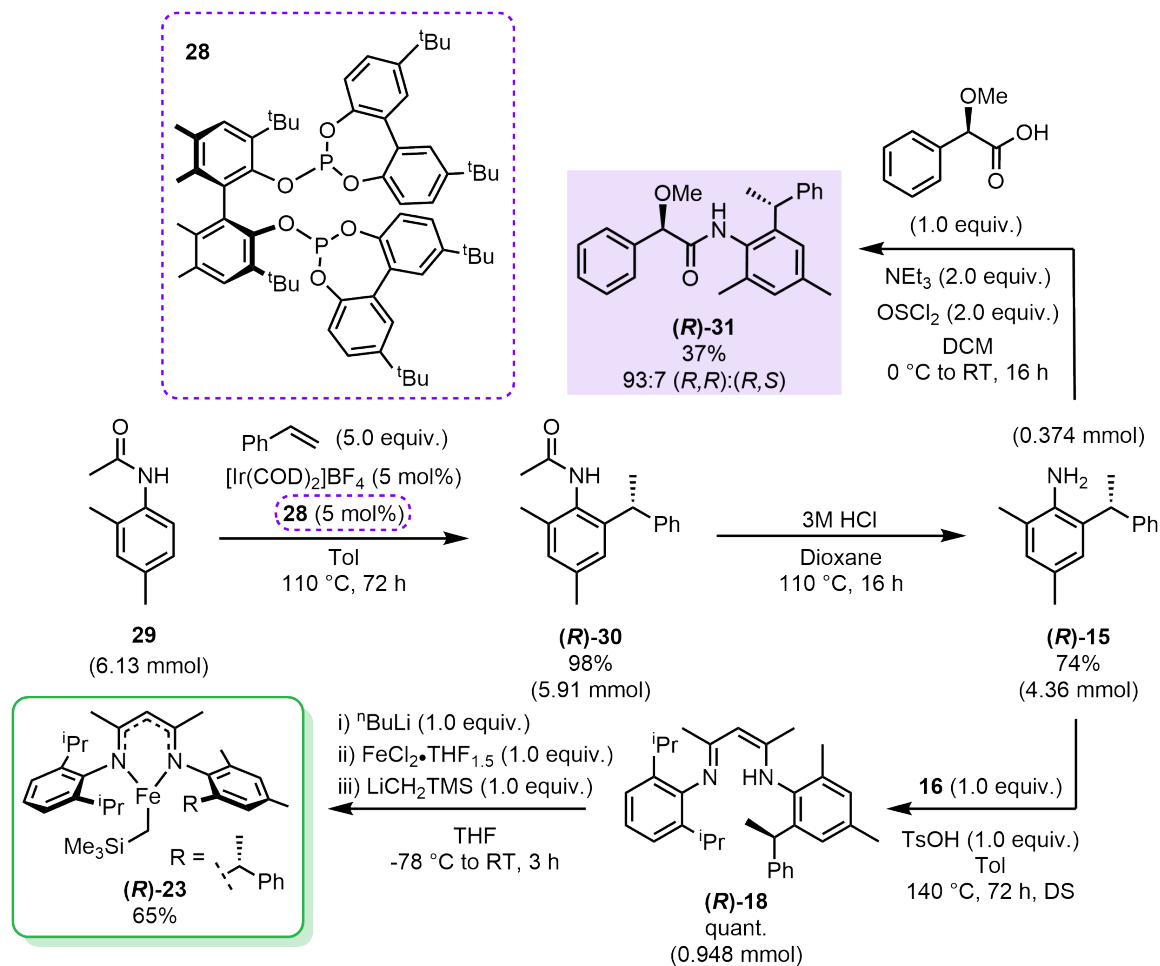
Scheme 4.3.3: Synthesis and single-crystal XRD structure of complex $(rac)\text{-}24$. Ellipsoids are represented at 50% probability and hydrogen atoms, except B-H, omitted for clarity.

through a pad of silica yielded $(rac)\text{-}1\text{-}32$ and $(rac)\text{-}2\text{-}32$ in 90% combined yield and 86:14 regioisomeric ratio, respectively. The previous report by Webster and co-workers detailed the same transformation, catalysed by **1a**.²¹³ In this example, complete regioselectivity was observed yielding $(rac)\text{-}1\text{-}32$, exclusively. Although selectivity is reduced when catalysed by $(rac)\text{-}23$, $(rac)\text{-}1\text{-}32$ forms in good regioisomeric ratio, warranting investigation into enantioselective hydroboration.



Scheme 4.3.4: Hydroboration of *trans*- β -methylstyrene, catalysed by $(rac)\text{-}23$.

4.4 Synthesis of Unsymmetric (*R*)-Iron- β -Diketimate Pre-catalyst



Scheme 4.4.1: Synthesis of pre-catalyst (*R*)-**23**.

With a method to access the desired ligand scaffold found, synthesis of the chiral analogue was undertaken. Section 4.1, describes the iridium-catalysed, enantioselective hydroarylation of styrenes with acetanilides.²¹⁴ Using this method, (*R*)-**30** was synthesised by reaction of acetanilide **29** and styrene, with catalytic [Ir(COD)₂]BF₄ and co-catalytic phosphite **28**. Compound (*R*)-**30** was generated in 98% isolated yield. The acid-mediated deacetylation of (*R*)-**30**, yields chiral aniline (*R*)-**15** in 74% isolated yield. In Bower and co-workers' study, enantiomeric ratios were determined by supercritical fluid chromatography (SFC). With no access to this particular method, determination of the enantiomeric ratios of (*R*)-**30** and (*R*)-**15** were attempted by chiral high-performance liquid chromatography (HPLC) on the same stationary phase. Unfortunately, separation could not be achieved. Instead, the enantiomeric ratio of (*R*)-**15** was inferred by ¹H NMR spectroscopy by condensation with (*R*)-(-)- α -methoxyphenylacetic acid. Amide (*R*)-**31** was synthesised in 37% isolated yield. The ¹H NMR spectrum of (*rac*)-**31** and (*R*)-**31** is shown in figure 4.4.1. A (*R,R*) to (*R,S*) diastereomeric ratio of 93:7 was determined (also corroborated by circular dichroism), suggesting (*R*)-**15** was synthesised in 86 %*ee*. Although complete enantioinduction could not be achieved, incorporation into the BDK scaffold could prove sufficient to observe enantiocontrol in hydrofunctionalisation experiments.

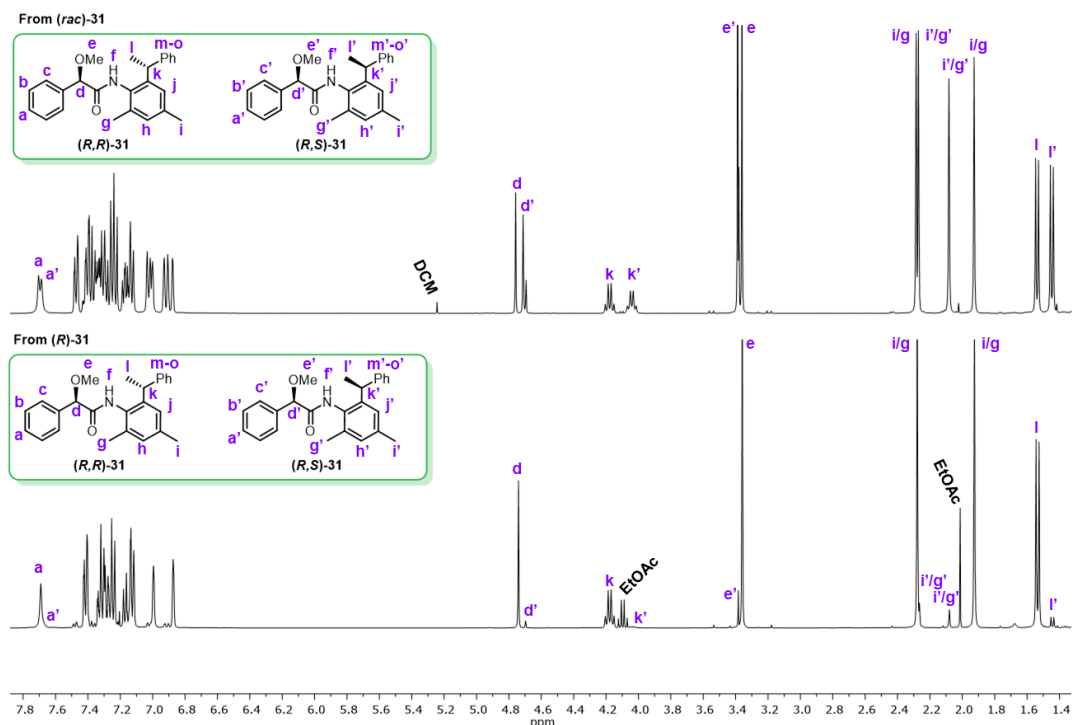


Figure 4.4.1: ^1H NMR spectra of (*rac*)-**31** and (*R*)-**31** (400 MHz, CDCl_3 , 298 K).

Using the conditions optimised for (*rac*)-**18**, synthesis of (*R*)-**18** was attempted by the same method. For compound (*rac*)-**18**, purification by crystallisation was facile, removing contaminating dip^{pp} BDK by-product. However, in the case of the enantioenriched (*R*)-**18**, the product is an oily solid. Therefore, crystallisation could not be achieved despite rigorous testing. Change in physical properties is likely to arise from unequal quantities of enantiomers disrupting crystal packing. Alternative methods to purify (*R*)-**18** by flash column chromatography (FCC, SiO_2 or Al_2O_3) were unsuccessful resulting in ligand decomposition. Therefore, crude (*R*)-**18** was used for complex synthesis. The ^1H NMR spectrum of crude (*R*)-**18** is comparable to crystalline (*rac*)-**18**. Unfortunately, 4% dip^{pp} BDK is present in the crude sample. After ligation to iron, this will lead to small amounts of **1a** being present in the catalyst mixture. Previous work by Webster and co-workers revealed **1a** is active in the anti-Markovnikov selective hydroboration of alkenes.²¹³ Therefore, problems with **1a** contamination are two-fold: 1) it is selective for the opposite regioisomer compared with (*rac*)-**21** and, 2) absence of a chiral-centre will lead to no enantiocontrol. Nevertheless, synthesis of (*R*)-**23** was attempted, anticipating later purification by crystallisation. The ^1H NMR spectra of crude (*R*)-**23** and (*rac*)-**23** crystals are shown in figure 4.4.2. These spectra are in good agreement indicating (*R*)-**23** is the major species by ^1H NMR spectroscopy. Unfortunately, the minor peaks do not compare with the ^1H NMR spectra of **1a** and their assignment remains elusive. Crystallisation of (*R*)-**23**, or the (*R*)-analogues of (*rac*)-**22** and (*rac*)-**24**, could not be achieved. Thus, the solid-state enantioconfiguration could not be determined. Poor crystallinity is likely a continuation of having an enantioenriched sample, as observed for (*R*)-**18**. Clearly, further ligand optimisation is required to improve enantiomeric ratios and overcome purification problems. In the meantime, (*R*)-**23** was tested in enantioselective hydroboration.

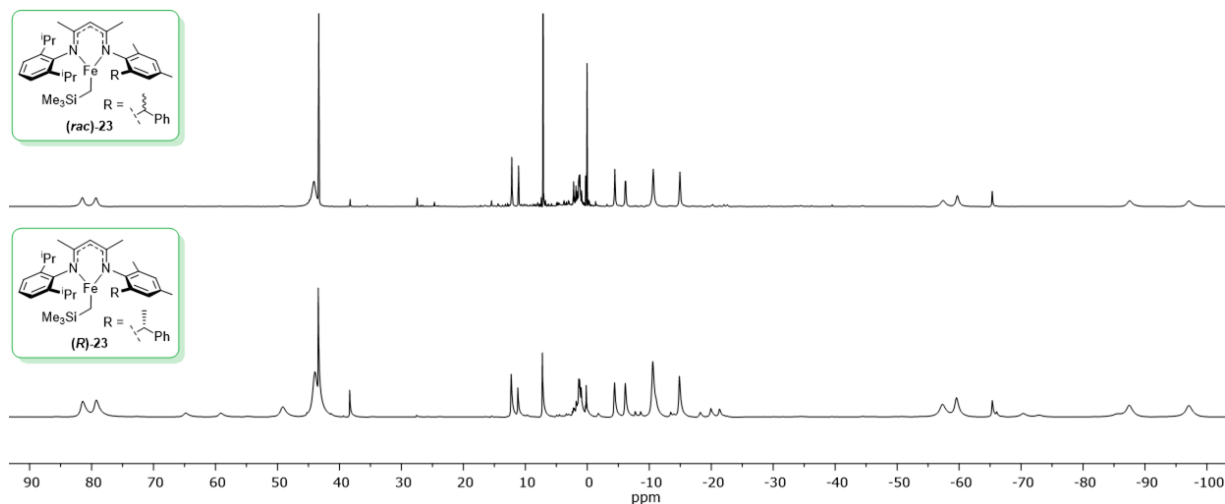
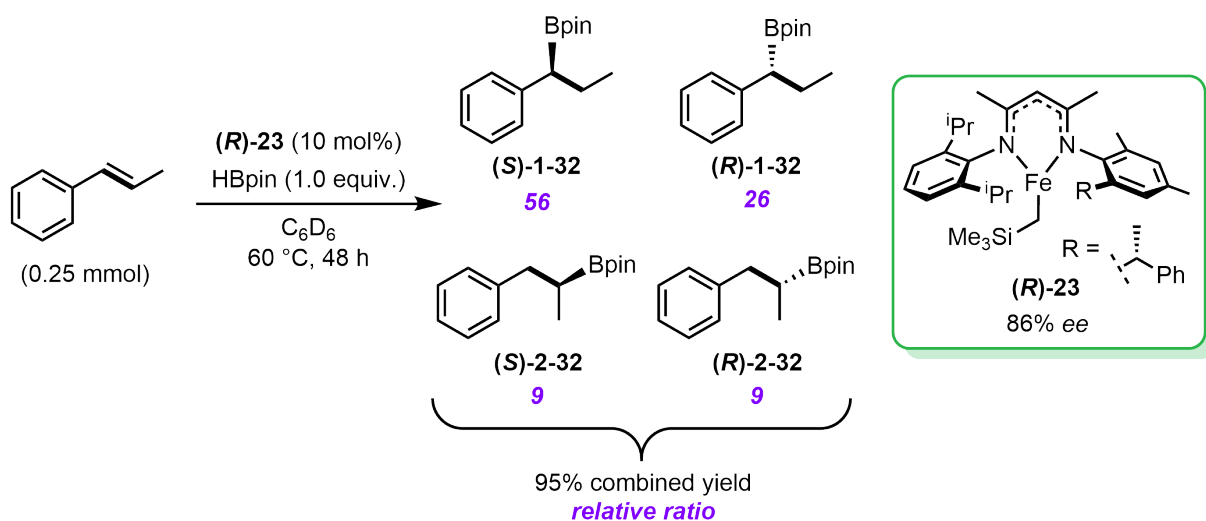


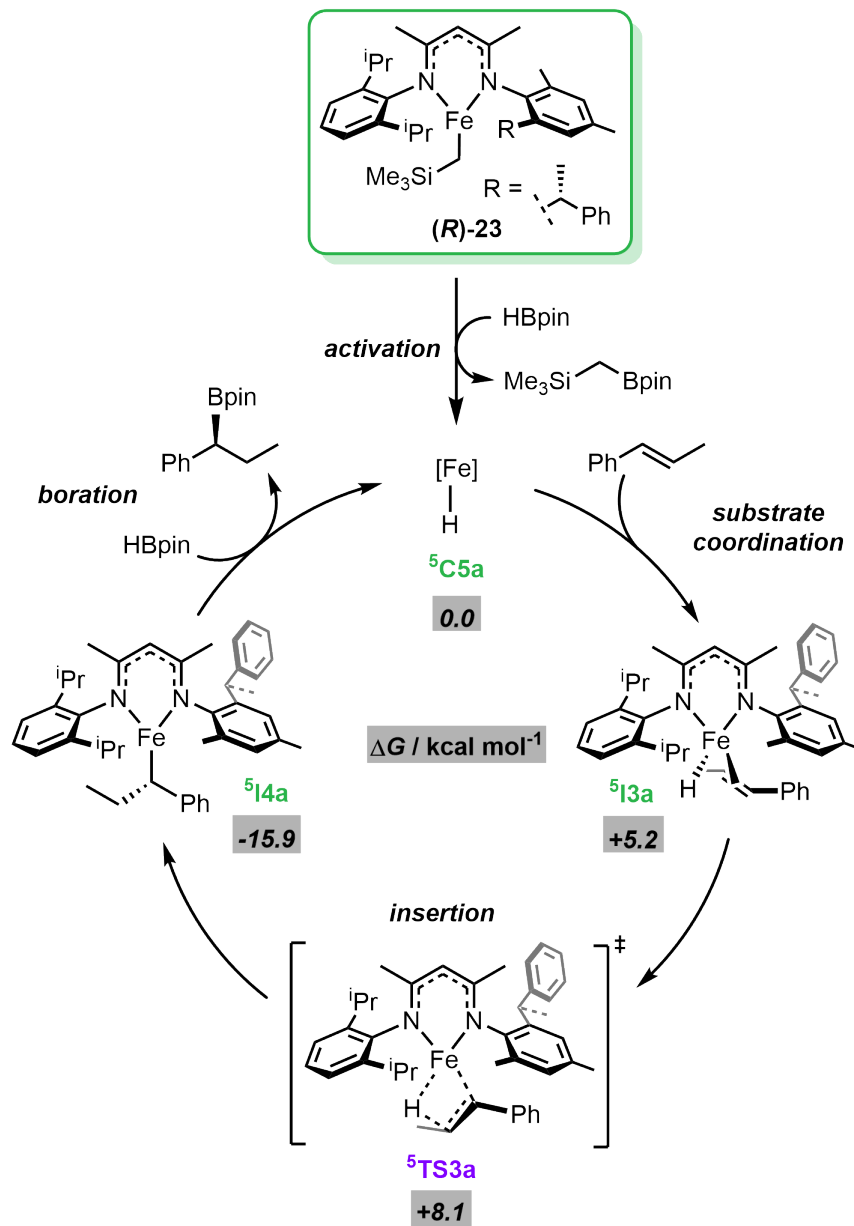
Figure 4.4.2: ^1H NMR spectra of (*rac*)-**23** and (*R*)-**23** (500 MHz, C_6D_6 , 298 K).



Scheme 4.4.2: Hydroboration of *trans*- β -methylstyrene, catalysed by (*R*)-**23**.

Pre-catalyst (*R*)-**23** was tested in the hydroboration of *trans*- β -methylstyrene, shown in scheme 4.4.2. After 48 hours at 60 °C, complete conversion was observed by ^{11}B NMR spectroscopy. Filtration through a pad of silica yielded (*R/S*)-**1-32** and (*R/S*)-**2-32** in 95% combined yield and 82:18 regioisomeric ratio, respectively (confirmed by ^1H NMR spectroscopy). Regioselectivity is slightly depleted compared to the (*rac*)-**23**-catalysed reaction, where a 86:14 ratio was observed, within error. This is expected, as **1a** contaminant favours anti-Markovnikov selectivity. The enantiomeric ratio was determined by chiral HPLC. The (*S*)-**1-32**-to-(*R*)-**1-32** ratio was estimated at 68:32. Pre-catalyst (*R*)-**23** shows enantioselectivity towards the (*S*)-enantiomer agreeing with DFT prediction. However, the extent of that selectivity is depleted at 30-40%*ee* (baseline separation was not achieved so an accurate %*ee* could not be determined, figure 4.6.1), compared to a predicted 84%*ee*. This is anticipated given the pro-ligand is not enantiopure. Nevertheless, pre-catalyst (*R*)-**23** is the first example of a BDK-catalysed enantioselective hydrofunctionalisation reaction.

The mechanism for the enantioselective hydroboration is shown in scheme 4.4.3, based on previous

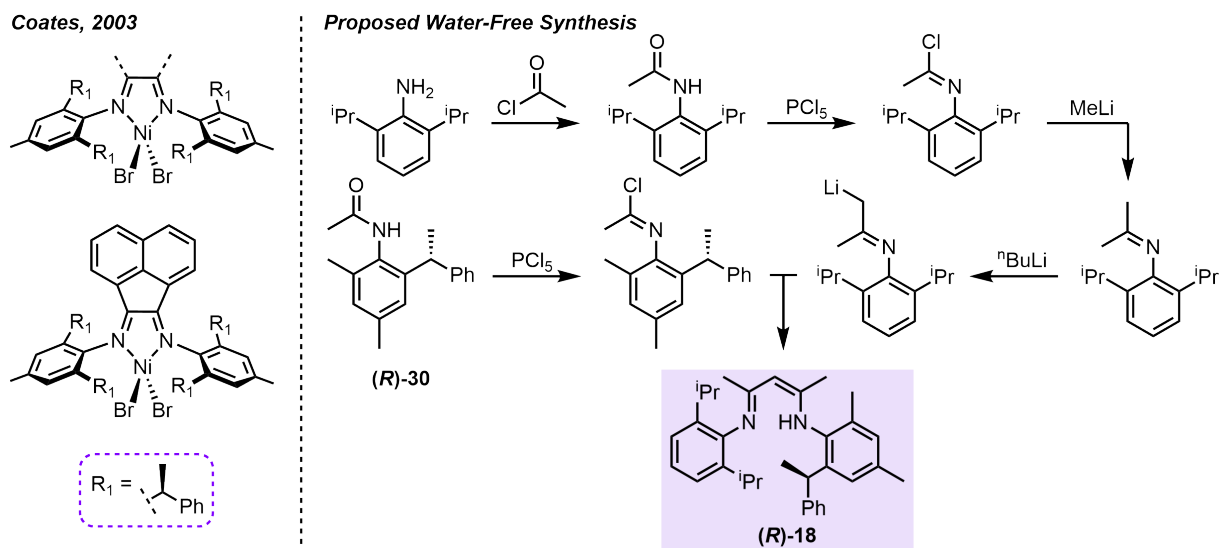


Scheme 4.4.3: Proposed mechanism for the enantioselective hydroboration.

work by Webster and co-workers and DFT-derived free energies.²¹³ Pre-catalyst (**R**)-**23** activation with HBpin yields catalyst **⁵C5a**. Substrate *si*-coordination gives intermediate **⁵I3a**, with free energy of +5.2 kcal mol⁻¹. Substrate insertion yields the most favoured TS, **⁵TS3a**, with free energy of +8.1 kcal mol⁻¹. **⁵TS3a** proceeds to iron-alkyl intermediate **⁵I4a**, with free energy of -15.9 kcal mol⁻¹. Boration with HBpin regenerates the active catalyst **⁵C5a** and (*S*)-**1-32** as the major product.

4.5 Conclusions and Future Work

The first example of an unsymmetric enantioenriched BDK, based on a chiral aniline moiety is described. DFT-derived TSs predict the corresponding iron(II)-hydride, bearing this ligand, will undergo an enantioselective insertion with *trans*- β -methylstyrene towards the (*S*)-enantiomer (84%*ee*). The optimisation of achiral pre-catalyst (**rac**)-**23** is reported. Unsymmetric pro-ligand synthesis leads to trace amounts of undesired ^{dipp}BDK. ^{dipp}BDK contamination can be eradicated under air- and moisture-free conditions, followed by recrystallisation. Pre-catalyst (**rac**)-**23** is active for the hydroboration of *trans*- β -methylstyrene in high yield and good regioselectivity (86:14, α : β). Complex (**rac**)-**23** reacts with 9-BBN, forming (BDK)Fe- κ^2 -9-borabicyclo[3.3.1]nonane complex (**rac**)-**24**. The (*R*)-analogue (**R**)-**23** was synthesised following the optimised method, with the chiral fragment installed by an enantioselective hydroarylation (86%*ee*). The physical properties of the enantioenriched sample made purification and full-characterisation of (**R**)-**23** challenging, as recrystallisation could not be achieved. Nevertheless, pre-catalyst (**R**)-**23** was active in the hydroboration of *trans*- β -methylstyrene with some enantioinduction. (**S**)-**1-32**, (**R**)-**1-32**, (**S**)-**2-32** and (**R**)-**2-32** were formed in 95% combined yield and 56:26:9:9 ratio, respectively.

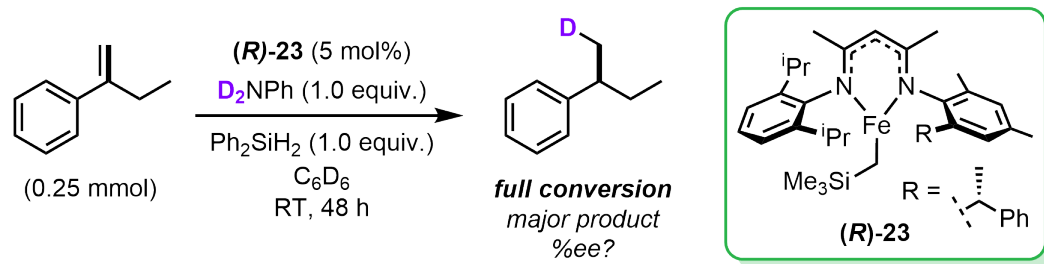


Scheme 4.5.1: Coates and co-workers' 4-methyl-2,6-(di-(*S*)-*sec*-phenylethyl)aniline-derived NiBr₂(α -diimine) complexes, and proposed water-free synthesis of (**R**)-**18**.^{215,223}

Barriers to enhanced enantioselectivity are three-fold: 1) The chiral fragment is not enantiopure ((**R**)-**15** is generated in 86%*ee*). Therefore, this is carried forward leading to trace amounts of the corresponding (*S*)-pre-catalyst, catalysing hydroboration to the undesired (*R*)-enantiomer. This reduces the observed enantioselectivity. 2) Enantioenriched (**R**)-**18** is challenging to crystallise. A method for its purification remains elusive, leading to a poorly defined catalyst (**R**)-**23**. 3) Pro-ligand synthesis is not selective. Reversible condensation/hydrolysis leads to trace amounts of achiral ^{dipp}BDK in the (**R**)-**18** sample. As crystallisation is challenging, ^{dipp}BDK is carried forward leading to trace amounts of achiral **1a** in the sample of (**R**)-**23**, that could not be removed. This reduces the observed catalytic regio- and enantioselectivity. Alternative methods exist for improving the enantiopurity of the chiral fragment. Coates and co-workers synthesised a chiral NiBr₂(α -diimine) complex derived from 4-methyl-

2,6-(di-(*S*)-*sec*-phenylethyl)aniline.^{215,216,224} This complex catalysed the isoselective polymerisation of *trans*-2-butene. The (*S*)-aniline precursor was isolated by semi-prep chiral HPLC. Compound (*rac*)-**15** could be separated into its enantiomers by an analogous method. Alternatively, methods exist for the classical resolution of amines using chiral auxiliaries. Tartaric acid derivatives and camphorsulfonic acid are used in the diastereoselective crystallisation of nitrogen containing molecules.²²⁵ Using such a method, (*R*)-**15** could be separated directly from (*rac*)-**15**. This alleviates need for the challenging enantioselective hydroarylation reaction, whilst increasing the scale at which (*R*)-**15** can be synthesised. Enantiopure (*R*)-**15** is likely to be a solid based on typical physicochemical properties of enantiomeric mixtures ((*rac*)-**15** is solid at room temperature). Therefore, crystallisation of the corresponding proligand (*R*)-**18** and pre-catalyst (*R*)-**23** should become more favourable, leading to a better defined pre-catalyst. Furthermore, a method for crystallisation of (*R*)-**23** will remove trace ^{dipp}BDK, as observed for (*rac*)-**23**, leading to improved regio- and enantioselectivity.

As reversible condensation/hydrolysis leads to undesired ^{dipp}BDK contamination, a water-free method may improve the purity of (*R*)-**18**. Chisholm and co-workers demonstrated an alternative method for synthesising ^tBu-backbone-derived BDks.²²³ The final synthetic step is a salt metathesis between an imidoyl chloride (easily derived from acetanilide (*R*)-**30**) and an organolithium species. Such a method could be used to synthesise (*R*)-**18** and is proposed in scheme 4.5.1. The salt-metathesis step is likely to be irreversible, thus (*R*)-**18** will form more selectively.



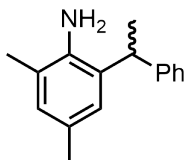
Scheme 4.5.2: Preliminary transfer hydrodeuteration of 1,1-disubstituted alkenes.

Beyond enantioselectivity, the underlying challenge of improving the hydroboration regioselectivity remains. This is difficult to address, likely requiring full catalyst redesign. Described in chapter 3, pre-catalyst **1a** was active in the transfer hydrogenation of alkenes. In this case, only one reduced product is observed (no isomerisation to the internal alkene). Transfer hydrogenation is suggested to proceed by the same hydride insertion as seen in hydroboration, thus this should be the enantiodetermining step. Preliminary results indicate that pre-catalyst (*R*)-**23** undergoes similar reactivity with α -ethylstyrene, shown in scheme 4.5.2. Unfortunately, with no access to chiral gas-chromatography, the product enantiomeric ratio could not be determined. Given access to such a method, transfer hydrogenation could be a more suitable transformation for investigating enantioselectivity, alleviating the regioselectivity challenges observed with alkene hydroboration.

4.6 Experimental

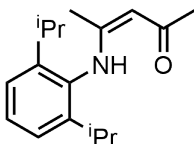
4.6.1 (*rac*)-Ligand and Complex Syntheses

Synthesis of (*rac*)-15



To a vigorously stirred solution of 2,4-dimethylaniline (15 mL, 121 mmol, 1.0 equiv.) and styrene (20 mL, 174 mmol, 1.4 equiv.) dissolved in xylenes (25 mL), trifluoromethanesulfonic acid (3 mL) was added dropwise. The vessel was sealed and stirred at 160 °C for 72 hours. The solution was concentrated under reduced pressure, washed with 1M NaOH solution (100 mL) and extracted with ethyl acetate (3 × 100 mL). Organic extracts were combined, washed with saturated brine solution, dried over MgSO₄, filtered and concentrated under reduced pressure. Remaining xylenes and 2,4-dimethylaniline were removed by vacuum distillation (60 °C, 5 × 10⁻² mbar). Remaining pink solid was dissolved in hot petroleum ether and cooled to -20 °C, yielding the title compound as off-white crystals (21.6 g, 95.9 mmol, 79 %). Spectroscopic data are consistent with literature precedent. ²¹³ **¹H NMR** (CDCl₃, 400 MHz) δ 7.30-7.17 (m, 5H, ArH), 6.99 (s, 1H, ArH) 6.84 (s, 1H, ArH), 4.07 (q, *J*=7.2 Hz, 1H, ArCH), 3.32 (s (br), 2H, NH₂), 2.29 (s, 3H, ArCH₃), 2.11 (s, 3H, ArCH₃), 1.62 (d, *J*=7.2 Hz, 3H, CHCH₃); ¹³**C{¹H}** NMR (CDCl₃, 100 MHz) δ 146.1 (ArCCH), 140.0 (ArC_{NH}), 129.4 (ArCH), 129.4 (ArC), 128.9 (2^{Ph}CH), 127.6 (2^{Ph}CH), 127.1 (ArC), 126.4 (ArCH), 125.9 (ArCH), 122.8 (ArC), 40.5 (HCCH₃), 22.3 (ArCCH₃), 20.9 (H₃CCH), 17.8 (ArCCH₃); **MS** (ESI): predicted: 226.1596, found: 226.1593 [M+H]⁺.

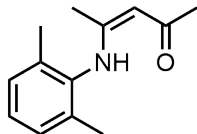
Synthesis of 16



A stirred solution of acetyl acetone (12 mL, 116 mmol, 1.1 equiv.), 2,6-diisopropylaniline (20 mL, 106 mmol, 1.0 equiv.) and p-toluenesulfonic acid (0.5 g) in toluene (100 mL) were heated to reflux for 16 hours with incorporation of a Dean-Stark trap. Solution was cooled and concentrated under reduced pressure. Yellow oil was dissolved in diethyl ether (100 mL) and washed with deionised water (100 mL). Organic phase was separated and the aqueous layer extracted three times with diethyl ether. Organic phases were combined and washed with 1M HCl solution (200 mL). Organic phase was separated, dried over MgSO₄, filtered and solvent was removed under reduced pressure. Yellow oil was dissolved in pentane and cooled to -78 °C yielding the title compound as colourless crystals (9.18 g, 44.9 mmol, 42%). Spectroscopic data are consistent with literature precedent. ²²⁶ **¹H NMR** (CDCl₃, 400 MHz) δ 12.05 (s (br), 1H, NH), 7.31-7.16 (m, 3H, ArH), 5.21 (s, 1H, OCCH), 3.03 (hept, *J*=6.9 Hz, 2H, (H₃C)₂CH), 2.12 (s, 3H, CH₃),

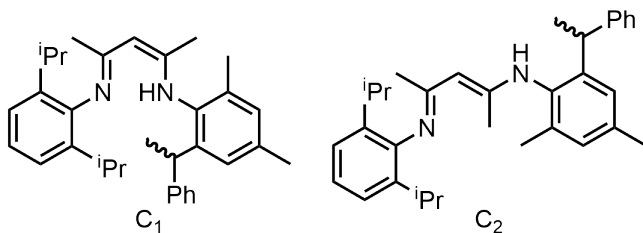
1.63 (s, 3H, CH₃), 1.21 (d, *J*=6.9 Hz, 6H, 2HCCH₃), 1.15 (d, *J*=6.8 Hz, 6H, 2HCCH₃); ¹³C{¹H} NMR (CDCl₃, 100 MHz) δ 196.0 (OC), 163.4 (HNCCH₃), 146.4 (2^{Ar}CCH), 133.7 (^{Ar}CNH), 128.4 (^{Ar}CH), 123.7 (2^{Ar}CH), 95.7 (CH), 29.2 (OCCH₃), 28.6 (^{iPr}C), 24.7 (^{iPr}C), 22.8 (^{iPr}C), 19.3 (HNCCH₃); MS (ESI): predicted: 260.2014, found 260.2014 [M+H]⁺.

Synthesis of 17



A stirred solution of acetyl acetone (2.57 mL, 25.0 mmol, 1.0 equiv.), 2,6-dimethylaniline (3.08 mL, 25.0 mmol, 1.0 equiv.) and p-toluenesulfonic acid (0.5 g) in toluene (500 mL) were heated to reflux for 16 hours with incorporation of a Dean-Stark trap. Solution was cooled and concentrated under reduced pressure. Yellow oil was dissolved in diethyl ether (100 mL) and washed with deionised water (3 × 100 mL). Organic phase was separated, dried over MgSO₄, filtered and solvent was removed under reduced pressure. Yellow oil was dissolved in hexane and cooled to -20 °C yielding the title compound as colourless crystals (1.54 g, 7.58 mmol, 30%). Spectroscopic data are consistent with literature precedent.²²⁶ ¹H NMR (CDCl₃, 400 MHz) δ 12.23 (s, 1H, NH), 7.05-6.94 (s (br), 1H, ArH), 6.99-6.94 (m, 2H, ArH), 5.18 (s, 1H, CH), 3.31 (s, 3H, CH₃), 2.23 (s, 3H, CH₃), 2.10 (s, 3H, CH₃), 1.84 (s, 3H, CH₃); ¹³C{¹H} NMR (CDCl₃, 100 MHz) δ 196.0 (CO), 161.8 (CN), 136.4 (ArC), 135.0 (ArC), 133.8 (ArC), 131.6 (ArCNH), 127.1 (ArCH), 126.4 (ArCH), 96.8 (CH), 29.2 (CH₃), 21.1 (CH₃), 19.7 (CH₃), 18.1 (CH₃); MS (ESI): predicted: 204.1388, found 204.1388 [M+H]⁺.

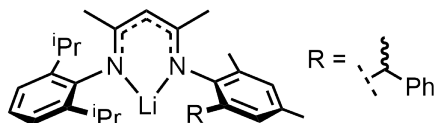
Synthesis of (*rac*)-18



In a two-neck round bottom flask under N₂, (*rac*)-**15** (1.00 g, 4.44 mmol, 1.0 equiv.) and p-toluenesulfonic acid (844 mg, 4.44 mmol, 1.0 equiv.) were dissolved in dry toluene (100 mL) and refluxed for 30 minutes with incorporation of a Dean-Stark trap, where a white precipitate forms. A solution of **16** (1.15 g, 4.44 mmol, 1.0 equiv.) in toluene (50 mL) was added and the mixture was heated to reflux for 72 hours. The solution was cooled and solvent was removed under reduced pressure. Oil was dissolved in diethyl ether (200 mL) and an aqueous Na₂CO₃ (941 mg, 8.88 mmol, 2.0 equiv.) solution (100 mL) was added and stirred until homogeneity was achieved. The aqueous phase was separated and extracted with diethyl ether (3 × 100 mL). Organic phases were combined, dried over MgSO₄, filtered and solvent was removed under reduced pressure. Resultant yellow oil was dried azeotropically with diethyl ether three times and dissolved in hot methanol. Solution was decanted from insoluble residue and cooled to -20 °C, yielding

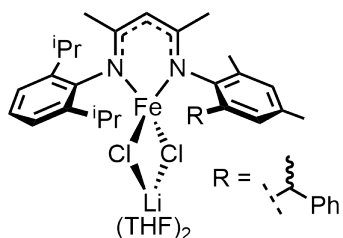
the title compound as colourless crystals (1.28 g, 3.06 mmol, 69%). $^1\text{H NMR}$ (CDCl_3 , 400 MHz) δ (0.8 : 0.2 mixture of conformers (*cis*-C₁ (major) and *trans*-C₂ (minor))), 12.33 (s (br), 1H, C₁, NH), 12.02 (s (br), 1H, C₂, NH), 7.27-7.08 (m, 8H, C₁ + C₂, ArH), 7.03 (s, 1H, C₁, ArH), 6.89 (s, 1H, C₁, ArH), 6.84 (s, 1H, C₂, ArH), 6.74 (s, 1H, C₂, ArH), 4.88 (s, 1H, C₂, CH), 4.72 (s, 1H, C₁, CH), 4.47 (q, $J=7.6$ Hz, 1H, C₂, H₃CCH), 4.35 (q, $J=7.3$ Hz, 1H, C₁, H₃CCH), 3.33 (hept, $J=7.0$ Hz, 1H, C₁, (H₃C)₂CH), 3.07 (m, 1H, C₁+ 2C₂, (H₃C)₂CH), 2.32 (s, 3H, C₁, ArCH₃), 2.21 (s, 3H, C₂, ArCH₃), 2.12 (s, 3H, C₂, ArCH₃), 2.05 (s, 3H, C₁, ArCH₃), 1.71 (s, 3H, C₁, HNCCH₃), 1.68 (s, 3H, C₂, HNCCH₃), 1.58 (d, $J=7.2$ Hz, 3H, C₂), 1.50 (d, $J=7.3$ Hz, 3H, C₁, HCCH₃), 1.30 (d, $J=6.9$ Hz, 3H, C₁, ⁱPrCH₃), 1.24 (d, $J=6.9$ Hz, 3H, C₁, ⁱPrCH₃), 1.22 (d, $J=6.9$ Hz, 3H, C₁, ⁱPrCH₃), 1.21 (d, $J=6.9$ Hz, 3H, C₂), 1.16 (d, $J=7.0$ Hz, 3H, C₂), 1.09 (d, $J=6.8$ Hz, 3H, C₁, ⁱPrCH₃), 1.06 (s, 3H, C₁, NCCH₃), 0.98 (d, $J=6.9$ Hz, 3H, C₂); $^{13}\text{C}\{^1\text{H}\}$ NMR (CDCl_3 , 100 MHz) δ (*cis*-C₁ (major)) 163.5 (NC), 160.0 (HNC), 146.8 (ArC), 143.3 (ArC), 143.3 (ArC), 141.7 (ArC), 140.0 (ArC), 139.3 (ArC), 133.4 (ArC), 131.3 (ArC), 129.0 (ArC), 128.3 (ArC), 128.2 (ArC), 128.2 (ArC), 127.8 (ArC), 126.6 (ArC), 125.7 (ArC), 125.6 (ArC), 125.6 (ArC), 125.1 (ArC), 123.2 (ArC), 123.1 (ArC), 93.5 (HNCCH), 40.3 (H₃CCH), 28.7 (ⁱPrCH), 28.5 (ⁱPrCH), 24.5 (ⁱPrCH₃), 24.5 (ⁱPrCH₃), 23.2 (ⁱPrCH₃), 22.8 (ⁱPrCH₃), 22.6 (HCCH₃), 21.3 (*p*-ArCCH₃), 20.6 (HNCCH₃), 20.0 (NCCH₃) 18.2 (*o*-ArCCH₃); MS (ESI): predicted: 467.3426, found: 467.3422 [M+H]⁺; IR: cm⁻¹ 3061, 3023, 2960, 2923, 2868, 1618, 1546, 1432, 1274; **sc-XRD** relevant crystallographic data are reported in the X-ray crystallography section.

Synthesis of (*rac*)-21



Aliquot taken during synthesis of (*rac*)-22. $^1\text{H NMR}$ ($\text{C}_6\text{D}_6/\text{THF}$ mix, 400 MHz) δ 7.47 (d, $J=7.6$ Hz, 2H, ArH), 7.24-7.05 (m, 8H, ArH), 4.92 (s, 1H, backboneCH), 4.64 (q, $J=7.3$ Hz, 1H, H₃CCH), 3.55 (hept, $J=6.9$ Hz, 1H, ⁱPrCH), 3.38 (hept, $J=7.0$ Hz, 1H, ⁱPrCH), 2.22 (s, 3H, ArCH₃), 2.21 (s, 3H, ArCH₃), 1.91 (s, 3H, CH₃), 1.60 (d, $J=7.3$ Hz, 3H, ⁱPrCH₃), 1.49 (s, 3H, CH₃), 1.37 (d, $J=7.0$ Hz, 3H, ⁱPrCH₃), 1.27 (d, $J=6.9$ Hz, 6H, 2ⁱPrCH₃), 1.15-1.13 (m, 3H, HCCH₃).

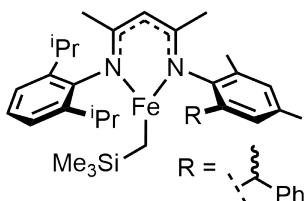
Synthesis of (*rac*)-22



To an ampoule containing a stirred solution of (*rac*)-18 (375 mg, 0.803 mmol, 1.0 equiv.) in THF (10 mL) at -78 °C, ⁿBuLi (2.5 M in hexanes, 321 μL , 0.803 mmol, 1.0 equiv.) was added dropwise. The solution was warmed to room temperature and stirred for 1 hour. The ampoule was transferred to the glovebox

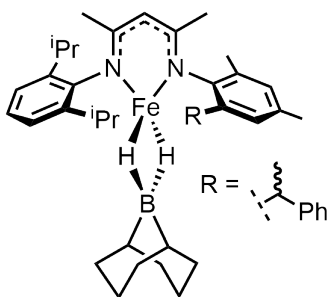
and $\text{FeCl}_2 \cdot (\text{THF})_{1.5}$ (187 mg, 0.803 mmol, 1.0 equiv.) was added. The solution was stirred for a further 1 hour. The solution was concentrated, extracted with toluene and isolated by cannula filtration. Filtrate was concentrated and cooled to $-20\text{ }^\circ\text{C}$, yielding the title compound as yellow single-crystals (113 mg, 0.152 mmol, 19%). **CHN** calculated for $\text{C}_{41}\text{H}_{57}\text{Cl}_2\text{FeLiN}_2\text{O}_2$: C, 66.22; H, 7.73, N, 3.77; found: C, 63.80; H, 7.29; N, 3.77; **MP** $146\text{--}147\text{ }^\circ\text{C}$ (decomposition); **UV/vis** 331.0 nm; **sc-XRD** relevant crystallographic data are reported in the X-ray crystallography section.

Synthesis of (*rac*)-23



To a flame-dried ampoule containing a stirred solution of (*rac*)-18 (449 mg, 0.962 mmol, 1.0 equiv.), dissolved in THF (20 mL) at $-78\text{ }^\circ\text{C}$, $^n\text{BuLi}$ (2.35 M in hexanes, 409 μL , 0.962 mmol, 1.0 equiv.) was added dropwise. The solution was warmed to room temperature and reaction proceeded for 1 hour. The ampoule was transferred to the glovebox and $\text{FeCl}_2 \cdot (\text{THF})_{1.5}$ (226 mg, 0.962 mmol, 1.0 equiv.) was added. The solution was stirred for a further 1 hour. LiCH_2TMS (90.6 mg, 0.962 mmol, 1.0 equiv.) was added and the solution was stirred for a further 1 hour. The solution was concentrated and residual THF removed by azeotropic drying in pentane ($3 \times 5\text{ mL}$). The mixture was raised in pentane (20 mL) and isolated by cannula filtration through a pad of celite. The filtrate was concentrated and cooled to $-20\text{ }^\circ\text{C}$, yielding the title compound as olive green crystals (250 mg, 0.411 mmol, 43%). **$^1\text{H NMR}$** (C_6D_6 , 500 MHz) δ 101.26, 81.55, 79.35, 44.15, 43.32, 12.17, 11.09, -4.45, -6.13, -6.22, -10.65, -14.95, -57.50, -59.77, -65.37, -87.60, -97.22; **CHN** calculated for $\text{C}_{37}\text{H}_{52}\text{FeN}_2\text{Si}$: C, 73.00; H, 8.61; N, 4.60; found: C, 72.87; H, 8.60; N, 4.64; **MP** $96\text{--}99\text{ }^\circ\text{C}$ (melt); **UV/vis** 328.6 nm; **sc-XRD** relevant crystallographic data are reported in the X-ray crystallography section.

Synthesis of (*rac*)-24

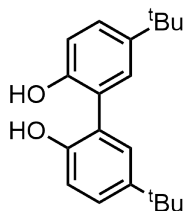


To an ampoule containing a solution of (*rac*)-23 (777 mg, 1.28 mmol, 1.0 equiv.) dissolved in toluene (5 mL), 9-borabicyclo(3.3.1)nonane dimer (311 mg, 1.28 mmol, 1.0 equiv.) was added. The mixture was heated to $60\text{ }^\circ\text{C}$ for 16 hours. The solution was concentrated, dissolved in pentane (5 mL) and cooled to $-20\text{ }^\circ\text{C}$, yielding the title compound as pink crystals (297 mg, 0.461 mmol, 36%). **$^1\text{H NMR}$** (C_6D_6 , 500 MHz)

δ 1382.0, 162.10, 160.37, 84.15, 82.52, 73.72, 70.39, 56.31, 53.77, 51.78, 43.03, 38.16, 33.41, 25.44, 22.39, 20.96, 20.16, 8.35, 3.70, 0.08, -0.84, -19.52, -25.24, -30.62, -48.55; **CHN** calculated for $C_{41}H_{57}FeBN_2$: C, 76.40; H, 8.91; N, 4.35; found: C, 75.91; H, 9.03; N, 4.12; **MP** 154-156 °C (melt); **UV/vis** 248.60 nm; **sc-XRD** relevant crystallographic data are reported in the X-ray crystallography section.

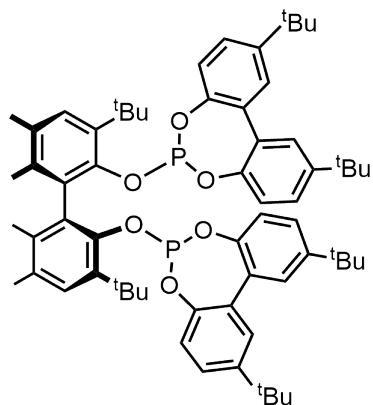
4.6.2 (*R*)-Ligand and Complex Syntheses

Synthesis of 28'



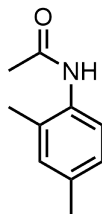
Title compound was synthesised following literature procedure.²¹⁴ To a stirred solution of 2,2'-biphenol (11.2 g, 60.2 mmol, 1.0 equiv.) and *t*BuCl (52.4 mL, 482 mmol, 8.0 equiv.) in dichloromethane (250 mL) at -78 °C, AlCl₃ (16.1 g, 120 mmol, 2.0 equiv.) was added in 2 g portions across 30 minutes. Solution was stirred at -78 °C for 6 hours, warmed to room temperature and stirred for a further 12 hours. The mixture was quenched by dropwise addition of deionised water (150 mL), followed by saturated NaHCO₃ solution (150 mL). The organic layer was separated and the aqueous phase extracted three times with dichloromethane. The organic layers were combined, washed with brine, dried over MgSO₄, filtered and solvent was removed under reduced pressure. Crude product was purified by FCC (SiO₂, hexane and ethyl acetate (80:20)) followed by recrystallisation from hot toluene, yielding the title compound as a colourless solid (9.07 g, 30.4 mmol, 51%). Spectroscopic data are consistent with literature precedent.²¹⁴ ¹H NMR (CDCl₃, 300 MHz) δ 7.35 (dd, $J=8.5, 2.5$ Hz, 2H, ArH), 7.26 (d, $J=2.5$ Hz, 1H, ArH), 6.97 (d, $J=8.5$ Hz, 2H, ArH), 5.29 (s (br), 2H, OH), 1.32 (s, 18H, ^tBuH); ¹³C{¹H} NMR (CDCl₃, 75 MHz) δ 150.8 (ArCOH), 144.5 (ArCCH), 128.1 (ArCH), 127.1 (ArCH), 123.2 (ArC), 116.2 (ArCH), 34.4 ((H₃C)₃C), 31.7 (C(CH₃)₃); **MS** (ESI): predicted: 321.1831, found: 321.1813 [M+Na]⁺.

Synthesis of 28



Title compound was synthesised following literature procedure.²¹⁴ To a flame dried J-Young schlenk flask under nitrogen atmosphere, 5,5'-di-*t*-butyl-[1,1'-biphenyl]-2,2'-diol (504 mg, 1.69 mmol, 3.0 equiv.) was added and cycled three times. PCl₃ (1.47 mL, 16.9 mmol, 30.0 equiv.) was added via subaseal and heated to 85 °C for 2 hours (turns homogeneous after 10 minutes). Solution was cooled to room temperature and excess PCl₃ was removed under reduced pressure in the presence of a secondary trap. Chlorophosphite was dried for 5 hours before (*S*)-(-)-3,3'-di-*t*-butyl-5,5',6,6',-tetramethylbiphenyl-2,2'-diol (200 mg, 0.564 mmol, 1.0 equiv.) and 4-dimethylaminopyridine (13.8 mg, 0.113 mmol, 0.2 equiv.) were added under nitrogen. Solids were cycled three times before being raised in dry THF (10 mL). Dry NEt₃ (330 μL, 2.37 mmol, 4.2 equiv.) was added dropwise over 2 minutes and the resulting white suspension was stirred at room temperature for 16 hours. Mixture was filtered through a pad of celite and washed with diethyl ether (100 mL). Filtrate was concentrated under reduced pressure and purified by FCC (neutral Al₂O₃, petroleum ether and ethyl acetate (95:5)), yielding the title compound as a white powder (445 mg, 0.442 mmol, 78%). Spectroscopic data are consistent with literature.²¹⁴ **¹H NMR** (CDCl₃, 400 MHz) δ 7.38 (dd, *J*=11.0, 2.4 Hz, 4H, ArH), 7.31 (s, 2H, ArH), 7.28 (dd, *J*=8.5, 2.4 Hz, 2H, ArH), 7.20 (dd, *J*=8.5, 2.4 Hz, 2H, ArH), 6.91 (dd, *J*=13.6, 8.5 Hz, 4H, ArH), 2.31 (s, 6H, ArCH₃), 1.91 (s, 6H, ArCH₃), 1.35 (s, 36H, *p*-C(CH₃)₃), 1.33 (s, 18H, *o*-C(CH₃)₃); **¹³C{¹H} NMR** (CDCl₃, 100 MHz) δ 150.1 (ArC), 147.6 (ArC), 147.5 (ArC), 147.4 (ArC), 137.9 (ArC), 136.1 (ArC), 131.5 (ArC), 131.1 (ArC), 130.9 (ArC), 129.7 (ArC), 129.2 (ArC), 126.4 (ArC), 125.7 (ArC), 125.7 (ArC), 122.5 (ArC), 122.0 (ArC), 35.0 (ArCH₃), 34.6 (ArCH₃), 31.7 (CH), 30.7 (CH), 20.7 (CH₃), 17.5 (CH₃); **³¹P{¹H} NMR** (CDCl₃, 162 MHz) δ 140.87; [α]²⁵_D +90.2 (*c* = 0.2, CH₂Cl₂).

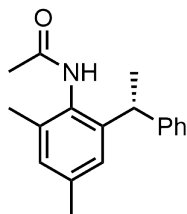
Synthesis of 29



Title compound synthesised by modified literature method.²¹⁴ To a stirred solution of 2,4-dimethylaniline (5.0 mL, 40.4 mmol, 1.0 equiv.) and pyridine (1.9 mL, 24.2 mmol, 0.6 equiv.) in dichloromethane (100 mL) at 0 °C, acetic anhydride (4.2 mL 44.5 mmol, 1.1 equiv.) was added dropwise and allowed to stir for 15 minutes. The solution was heated to reflux and stirred for a further 3 hours. The solution was cooled and washed with a saturated NaHCO₃ solution. The organic phase was separated and the aqueous phase extracted three times with dichloromethane. The organic phases were combined, washed with brine, dried over MgSO₄, filtered and solvent was removed under reduced pressure. The crude product was recrystallised from hot hexane yielding the title compound as off-white crystals (6.55 g, 40.1 mmol, 99%). Title compound was sublimed before use in hydroarylation experiments. Spectroscopic data are consistent with previous literature.²²⁷ **¹H NMR** (CDCl₃, 300 MHz) δ 7.52 (d, *J*=8.6 Hz, 1H, *o*-ArH), 7.00 (m, 2H, 2*m*-ArH), 2.28 (s, 3H, CH₃), 2.21 (s, 3H, CH₃), 2.17 (s, 3H, OCCH₃); **¹³C{¹H} NMR** (CDCl₃, 75 MHz) δ 168.53 (OC), 135.26 (*o*-ArCCH₃), 132.94 (ArCN) 131.17 (ArCH), 130.04 (*p*-ArCCH₃),

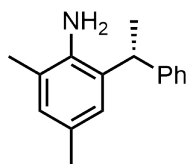
127.25 ($^{Ar}C\text{H}$) 124.00 ($^{Ar}C\text{H}$), 24.15 ($C\text{H}_3$), 20.91 ($C\text{H}_3$), 17.79 ($C\text{H}_3$); **MS** (ESI): predicted: 164.1075, found: 164.1072 $[M+H]^+$.

Synthesis of (*R*)-30



To a flame dried J-Young schlenk flask under argon atmosphere containing **29** (1.00 g, 6.13 mmol, 1.0 equiv.), $[\text{Ir}(\text{COD})_2]\text{BF}_4$ (152 mg, 0.306 mmol, 0.05 equiv.), (*S*)-(-)-bidentate phosphite (308 mg, 0.306 mmol, 0.05 equiv.), toluene (50 mL) was added. Styrene (3.52 mL, 30.6 mmol, 5.0 equiv.) was added and the vessel was sealed and heated to 110 °C for 72 hours (purple homogeneous solution forms and turns yellow after 3 hours). Solution was cooled and solvent was removed under reduced pressure. Product was isolated by FCC (SiO_2 , toluene and ethyl acetate (30:70)) yielding the title compound as an off-white solid (1.60 g, 5.98 mmol, 98%, 9:1 mixture of rotamers). **Rf** = 0.45 (Ethyl acetate/toluene, 70:30); **^1H NMR** (CDCl_3 , 400 MHz) δ 7.30-7.12 (m, 5H, PhH), 7.05 (s, 1H, ArH_3), 6.97 (s, 1H, ArH_3), 4.17 (q, $J=7.2$ Hz, 1H, H_3CCH), 2.33 (s, 3H, CH_3), 2.14 (s, 3H, CH_3), 2.05 (s, 3H, CH_3), 1.56 (d, $J=7.2$ Hz, 3H, HCCH_3); **$^{13}\text{C}\{^1\text{H}\}$ NMR** (CDCl_3 , 100 MHz) δ 168.8 (CO), 137.3 ($\text{HC}^{Ar}\text{CCNH}$), 136.5 ($^{Ar}\text{CCHCH}_3$), 131.1 (^{Ar}CNH), 129.8 (^{Ar}CH), 128.8 (2^{Ar}CH), 128.7 ($^{Ar}\text{CCH}_3$), 128.0 ($^{Ar}\text{CCH}_3$), 127.4 (2^{Ar}CH), 126.3 (^{Ar}CH), 126.0 (^{Ar}CH), 40.9 (H_3CCH), 23.2 (H_3CCO), 21.9 (H_3CCH), 21.4 ($^{Ar}\text{CCH}_3$), 18.5 ($^{Ar}\text{CCH}_3$); **MS** (ESI), predicted: 290.1521, found: 290.1521 $[M+\text{Na}]^+$; **IR**: cm^{-1} 3261, 3024, 2967, 2930, 1646, 1519, 1272, 857; $[\alpha]_D^{25}$ +5.0 ($c = 5.0$, CH_2Cl_2).

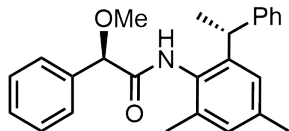
Synthesis of (*R*)-15



A sealed vessel containing (**R**)-30 (1.58 g, 5.91 mmol, 1.0 equiv.), 3M HCl (20 mL) and dioxane (20 mL) was heated to 110 °C for 16 hours. The solution was cooled and diluted with ethyl acetate (100 mL) and sodium hydroxide solution (15% w/w, 120 mL). The organic phase was separated and the aqueous phase was extracted three times with ethyl acetate. The organic phases were combined, washed with saturated brine solution, dried over MgSO_4 , filtered and dried under reduced pressure. Crude product was purified by FCC (SiO_2 , petroleum ether and ethyl acetate (95:5)) yielding the title compound as a colourless oil (982 mg, 4.36 mmol, 74%, e.r: 93:7). **Rf** = 0.15 (Petroleum ether/ethyl acetate, 95:5); **^1H NMR** (CDCl_3 , 400 MHz) δ 7.28 - 7.15 (m, 5H, PhH), 6.98 (s, 1H, ArH), 6.82 (s, 1H, ArH), 4.06 (q, $J=7.2$ Hz, 1H, H_3CCH), 3.29 (s (br), 2H, NH_2), 2.28 (s, 3H, CH_3), 2.08 (s, 3H, CH_3), 1.60 (d, $J=7.2$

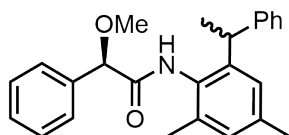
Hz, 3H, HCCH₃); ¹³C{¹H} NMR (CDCl₃, 100 MHz) δ 146.0 (ArC_{NH}), 139.9 (ArCCH), 129.3 (ArCH), 129.3 (ArC), 128.8 (2(ArCH)), 127.5 (2(ArCH)), 127.0 (ArC), 126.3 (ArCH), 125.8 (ArCH), 122.6 (ArC), 40.4 (H₃CCH), 22.2 (CH₃), 20.8 (CH₃), 17.7 (CH₃); MS (ESI): predicted: 226.1596, found: 226.1596 [M+H]⁺; IR: cm⁻¹ 3452, 3378, 2967, 2920, 2870, 1623, 1483, 1449, 857; [α]_D²⁵ -56.5 (c = 4.0, CH₂Cl₂).

Synthesis of (*R*)-31



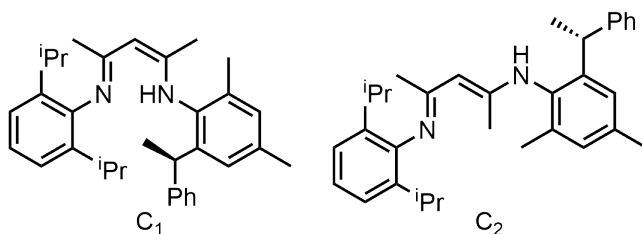
A solution of (*R*)-(-)- α -methoxyphenylacetic acid (62.2 mg, 0.374 mmol, 1.0 equiv.) and triethylamine (104 μ L, 0.746 mmol, 2.0 equiv.) dissolved in dichloromethane (5 mL) was purged with nitrogen for 20 minutes. The stirred solution was cooled to 0 °C and thionylchloride (57.9 μ L, 0.746 mmol, 2.0 equiv.) was added dropwise under a flow of nitrogen. The resulting pale yellow solution was stirred at 0 °C for 30 minutes. Meanwhile, a solution containing (*R*)-15 (84.0 mg, 0.374 mmol, 1.0 equiv.) in dichloromethane (5 mL) was purged with nitrogen for 20 minutes. This solution was then added dropwise, under a flow of nitrogen, into the acid chloride solution at 0 °C. The dark yellow solution was warmed to room temperature and stirred for a further 16 hours. Saturated NaHCO₃ (10 mL) was added, the organic phase was separated and washed three times with deionised water. The organic phase was separated, dried over MgSO₄, filtered and solvent was removed under reduced pressure. Crude mixture was purified by FCC (SiO₂, petroleum ether and ethyl acetate, 90:10) yielding the title compound as an off-white solid (52 mg, 0.139 mmol, 37%, 93:7 mixture of diastereoisomers (R,R/R,S)). **Rf** = 0.10 (Petroleum ether/ethyl acetate, 90:10); ¹H NMR (CDCl₃, 400 MHz) δ 7.69 (s (br), 1H, (R,R) & (R,S), HH), 7.49-7.11 (m, 10H, (R,R) & (R,S), ArH), 7.03 (s, 0.07H, (R,S), ArH), 6.99 (s, 0.93H, (R,R), ArH), 6.90 (s, 0.07H, (R,S), ArH), 6.87 (s, 0.93H, (R,R), ArH), 4.74 (s, 0.93H, (R,R), OCH₃), 4.69 (s, 0.07H, (R,S), OCH₃), 4.18 (q, *J*=7.2 Hz, 0.93H, (R,R), H₃CCH), 4.04 (q, *J*=7.2 Hz, 0.07H, (R,S), H₃CCH), 3.38 (s, 0.21H, (R,S), CH₃), 3.35 (s, 2.79H, (R,R), CH₃), 2.27 (s, 2.79H, (R,R), CH₃), 2.26 (s, 0.21H, (R,S), CH₃), 1.92 (s, 2.79H, (R,R), CH₃), 1.53 (d, *J*=7.2, 2.79H, (R,R), HCCH₃), 1.44 (d, *J*=7.2 Hz, 0.21H, (R,S), HCCH₃); ¹³C{¹H} NMR (CDCl₃, 100 MHz) δ 169.2 (CO (R,S)), 168.9 (CO (R,R)), 146.0 (ArC, (R,R)), 142.0 (ArC, (R,R)), 137.0 (ArC, (R,R)), 136.9 (ArC, (R,R)), 136.1 (ArC, (R,R)), 130.02 (ArC, (R,R)), 129.6 (ArC, (R,R)), 128.6 (ArC, (R,R)), 128.5 (ArC, (R,R)), 127.7 (ArC, (R,R)), 127.1 (ArC, (R,R)), 126.2 (ArC, (R,R)), 125.7 (ArC, (R,R)), 84.3 (HCOCH₃, (R,R)), 84.1 (HCOCH₃, (R,S)), 57.5 (OCH₃, (R,S)), 57.2 (OCH₃, (R,R)), 40.3 (HCCH₃, (R,R)), 40.1 (HCCH₃, (R,S)), 22.4 (H₃CCH, (R,S)), 22.1 (H₃CCH, (R,R)), 21.8 (ArCCH₃, (R,S)), 21.4 (ArCCH₃, (R,R)), 18.7 (ArCCH₃, (R,S)), 18.4 (ArCCH₃, (R,R)); MS (ESI): predicted: 374.2120, found: 374.2116 [M+H]⁺; IR: cm⁻¹ 3372, 3278, 2967, 2930, 1670, 1493, 1098.

Synthesis of (*rac*)-31



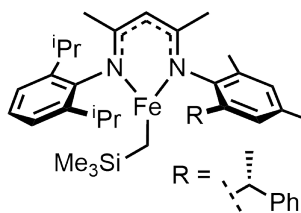
Synthesised as shown for (**R**)-**31** on 0.601 mmol scale. $^1\text{H NMR}$ (CDCl_3 , 400 MHz) δ 7.73 (s, 1H, (R,R) ArH), 7.71 (s, 1H, (R,S) ArH), 7.48-6.90 (m, 22H, (R,R) & (R,S), ArH), 4.78 (s, 1H, (R,R), OCH_3), 4.73 (s, 1H, (R,S), OCH_3), 4.18 (q, $J=7.2$ Hz, 1H, (R,R), H_3CCH), 4.04 (q, $J=7.2$ Hz, 1H, (R,S), H_3CCH), 3.40 (s, 3H, (R,S), CH_3), 3.38 (s, 3H, (R,R), CH_3), 2.31 (s, 3H, (R,R), CH_3), 2.29 (s, 3H, (R,S), CH_3), 2.08 (s, 3H, (R,S), CH_3), 1.95 (s, 3H, (R,R), CH_3), 1.53 (d, $J=7.2$, 3H, (R,R), HCCH_3), 1.44 (d, $J=7.2$ Hz, 3H, (R,S), HCCH_3).

Synthesis of (**R**)-**18**



In a two-neck round bottom flask under N_2 , (**R**)-**15** (982 mg, 4.36 mmol, 1.0 equiv.) and *p*-toluenesulfonic acid (829 mg, 4.36 mmol, 1.0 equiv.) were dissolved in dry toluene (50 mL) and refluxed for 30 minutes with incorporation of a Dean-Stark trap, where a white precipitate forms. A solution of **16** (1.13 g, 4.36 mmol, 1.0 equiv.) in toluene (20 mL) was added and the mixture was heated to reflux for 72 hours. The solution was cooled and solvent was removed under reduced pressure. Oil was dissolved in diethyl ether (100 mL) and an aqueous Na_2CO_3 (924 mg, 8.72 mmol, 2.0 equiv.) solution (100 mL) was added and stirred until homogeneity was achieved. The aqueous phase was separated and extracted three times with diethyl ether. Organic phases were combined, dried over MgSO_4 , filtered and solvent was removed under reduced pressure. Resultant yellow oil was dried azeotropically with diethyl ether three times, yielding the title compound as a off-white solid. Crude product was used without further purification. $^1\text{H NMR}$ (CDCl_3 , 400 MHz) δ (0.8 : 0.2 mixture of conformers (C_1 (major) and C_2 (minor)), 12.34 (s (br), 1H, C_1 , NH), 12.02 (s (br), 1H, C_2 , NH), 7.27 - 7.08 (m, 8H, $\text{C}_1 + \text{C}_2$, ArH), 7.04 (s, 1H, C_1 , ArH), 6.89 (s, 1H, C_1 , ArH), 6.84 (s, 1H, C_2 , ArH), 6.75 (s, 1H, C_2 , ArH), 4.89 (s, 1H, C_2 , CH), 4.72 (s, 1H, C_1 , CH), 4.47 (q, $J=7.2$ Hz, 1H, C_2 , H_3CCH), 4.36 (q, $J=7.2$ Hz, 1H, C_1 , H_3CCH), 3.33 (hept, $J=7.0$, 1H, C_1 , $(\text{H}_3\text{C})_2\text{CH}$), 3.17-2.98 (m, 1H, $\text{C}_1 + 2\text{C}_2$, $(\text{H}_3\text{C})_2\text{CH}$), 2.32 (s, 3H, C_1 , Ar CH_3), 2.21 (s, 3H, C_2 , Ar CH_3), 2.12 (s, 3H, C_2 , Ar CH_3), 2.06 (s, 3H, C_1 , Ar CH_3), 1.71 (s, 3H, C_1 , HNC CH_3), 1.68 (s, 3H, C_2 , HNC CH_3), 1.58 (d, $J=7.2$ Hz, 3H, C_2), 1.51 (d, $J=7.3$ Hz, 3H, C_1 , HC CH_3), 1.30 (d, $J=6.9$ Hz, 3H, C_1 , $^i\text{PrCH}_3$), 1.29 (d, $J=6.9$ Hz, 3H, C_1 , $^i\text{PrCH}_3$), 1.22 (d, $J=6.9$ Hz, 3H, C_1 , $^i\text{PrCH}_3$), 1.21 (d, 3H, C_2), 1.16 (d, $J=6.9$ Hz, 3H, C_2), 1.10 (d, $J=6.8$ Hz, 3H, C_1 , $^i\text{PrCH}_3$), 1.06 (s, 3H, C_1 , NC CH_3), 0.98 (d, $J=6.8$ Hz, 3H, C_2); $^{13}\text{C}\{^1\text{H}\}$ NMR (CDCl_3 , 100 MHz) δ (C_1 (major)) 163.5 (NC), 160.0 (HNC), 146.8 (ArC), 143.3 (ArC), 143.3 (ArC), 141.7 (ArC), 140.0 (ArC), 139.3 (ArC), 133.4 (ArC), 131.3 (ArC), 128.9 (ArC), 128.3 (ArC), 128.2 (ArC), 128.1 (ArC), 127.8 (ArC), 126.5 (ArC), 125.7 (ArC), 125.7 (ArC), 125.6 (ArC), 125.1 (ArC), 123.1 (ArC), 123.1 (ArC), 93.5 (HNCCH), 40.3 (H_3CCH), 28.7 ($^i\text{PrCH}$), 28.5 ($^i\text{PrCH}$), 24.5 ($^i\text{PrC}, \text{H}_3$), 24.5 ($^i\text{PrCH}_3$), 23.2 ($^i\text{PrCH}_3$), 22.8 ($^i\text{PrCH}_3$), 22.6 (HC CH_3), 21.3 (*p*-ArC CH_3), 20.6 (HNC CH_3), 20.0 (NC CH_3), 18.2 (*o*-ArC CH_3); MS (ESI): predicted: 467.3426, found: 467.3428 $[\text{M}+\text{H}]^+$; IR: cm^{-1} 3061, 3024, 2960, 2924, 2870, 1620, 1546, 1436, 1279; $[\alpha]_D^{25}$ +133.0 ($c = 4.0$, CH_2Cl_2).

Synthesis of (*R*)-**23**



To a flame-dried ampoule containing a stirred solution of (*R*)-**18** (442 mg, 0.948 mmol, 1.0 equiv.), dissolved in THF (10 mL) at -78 °C, ⁿBuLi (2.5 M in hexanes, 379 μL, 0.948 mmol, 1.0 equiv.) was added dropwise. The solution was warmed to room temperature and reaction proceeded for 1 hour. The ampoule was transferred to the glovebox and FeCl₂·(THF)_{1.5} (223 mg, 0.948 mmol, 1.0 equiv.) was added. The solution was stirred for a further 1 hour. 25% of the reaction mixture was removed for analysis of (*R*)-**22**. LiCH₂TMS (66.9 mg, 0.711 mmol, 0.75 equiv.) was added and the solution was stirred for a further 1 hour. The solution was concentrated and residual THF removed by azeotropic drying in pentane (3 × 5 mL). The mixture was raised in pentane (20 mL) and isolated by cannula filtration through a pad of celite. The filtrate was concentrated, yielding the title compound as olive green solid (282 mg, 0.463 mmol, 65% based on 0.75 equiv.). ¹H NMR (C₆D₆, 500 MHz) δ 101.67, 81.53, 79.33, 43.87, 43.48, 12.40, 11.34, -4.41, -6.12, -6.22, -10.50, -14.78, -57.18, -59.27, -65.47, -87.45, -97.12.

4.6.3 Enantioselective Hydroboration

(*R/S*)-**1/2-32**

To a J-Young NMR tube, containing *trans*-β-methylstyrene (32.4 μL, 0.25 mmol, 1.0 equiv.) and (*R*)-**23** (15.2 mg, 0.025 mmol, 10 mol%) dissolved in C₆D₆ (500 μL), HBpin (36.3 μL, 0.25 mmol, 1.0 equiv.) was added. The tube was sealed and heated to 60 °C for 48 hours. The tube was exposed to air, concentrated under a flow of N₂, filtered through a silica plug (CH₂Cl₂) and concentrated, yielding the title compound as a colourless oil (58.6 mg, 0.238 mmol, 95%). [α]_D²⁵ -9.92 (c = 1.2, CH₂Cl₂). Regioisomeric ratio was determined by ¹H NMR spectroscopy. Data in agreement with previous literature.^{213,228} ¹H NMR (CDCl₃, 400 MHz) δ **1-32**: 7.21-7.05 (m, 5H, ArH), 2.16 (t, *J*=7.9 Hz, 1H, BCH), 1.87-1.76 (m, 1H, CH_aH_b), 1.57-1.71 (m, 1H, CH_aH_b), 1.15 (s, 6H, 2CH₃), 1.13 (s, 6H, 2CH₃), 0.85 (t, *J*=7.3 Hz, 3H, CH₃); **2-32**: 7.21-7.05 (m), 2.77-2.72 (m, 0.22H, CH_aH_b), 2.51-2.45 (m, 0.23 H, CH_aH_b), 0.91 (d, *J*=7.4 Hz, 0.62H, CH₃); ¹³C{¹H} NMR (CDCl₃, 100 MHz) δ **1-32**: 143.5 (ArCC), 128.5 (ArCH), 128.3 (ArCH), 125.2 (ArCH), 83.4 (CO), 25.9 (CH₂), 24.8 (2CH₃), 24.7 (2CH₃), 14.1 (CH₃); **2-32**: 142.8, 129.0, 128.7, 125.7, 83.1, 38.7, 24.8, 15.3; ¹¹B NMR (CDCl₃, 128 MHz) δ 33.5.

Enantiomeric ratio was determined by chiral HPLC after oxidation to the corresponding alcohol: **1-32** and **2-32** were dissolved in diethyl ether (2 mL). Sodium hydroxide solution (1M, 2 mL) and hydrogen peroxide solution (10 wt.%, 2 mL) were added and the vessel was sealed and stirred for 16 hours at room temperature. The mixture was raised in diethyl ether (5 mL) and the organic layer was separated. Organic phase was concentrated yielding the title alcohol as a colourless oil. OD-Chiracel, 99:1/hexane:IPA, 1 mL min⁻¹, 27.4 bar, 220 nm. Values listed as an overall product ratio based on ¹H NMR spectrum integration,

HPLC trace and literature precedent.²²⁹ (*S*)-1-32 and (*S*)-2-32 would not completely separate on HPLC column. Therefore, relative ratios between (*R*)-2-32 and (*S*)-2-32 are assumed as 1:1 based on peak height, to allow enantiomeric ratio of major products (*R*)-1-32 and (*S*)-1-32 to be estimated.

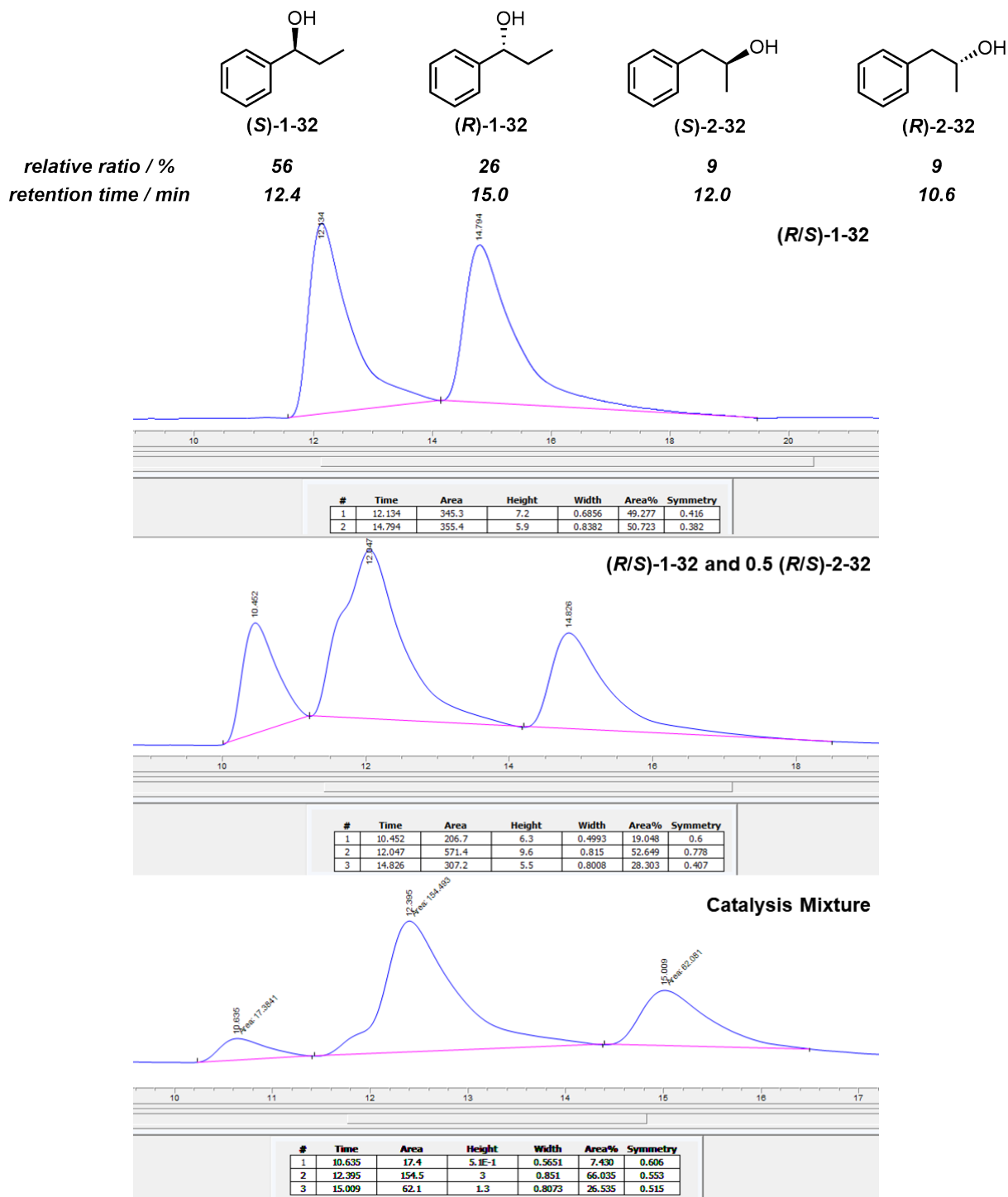
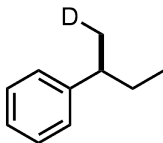


Figure 4.6.1: HPLC trace for (*S*)-1-32, (*R*)-1-32, (*S*)-2-32, (*R*)-2-32.

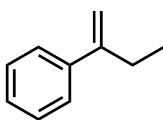
4.6.4 Transfer Hydrogenation

1-(Methyl-*d*₁)propylbenzene



To a J-Young NMR tube containing α -ethylstyrene (34.8 μL , 0.25 mmol, 1.0 equiv.), (**R**)-**23** (7.6 mg, 0.0125 mmol, 5 mol%) and aniline- N,N-d_2 (23.3 μL , 0.25 mmol, 1.0 equiv.) dissolved in C_6D_6 (500 μL), diphenylsilane (46.4 μL , 0.25 mmol, 1.0 equiv.) was added. The vessel was sealed and monitored by ^1H NMR spectroscopy until full conversion was achieved after 48 hours at room temperature. Spectroscopic data are in agreement with previous literature.²³⁰ ^1H NMR (C_6D_6 , 500 MHz) δ 7.19-7.05 (m, 5H), 2.42 (h, $J=6.9$ Hz, 1H), 1.49 (m, 2H), 1.12 (m, 2H), 0.76 (t, $J=7.4$ Hz, 3H).

α -Ethylstyrene



Title compound synthesised following modified literature procedure.²³¹ To a flame dried schlenk containing Ph_3PMeI (4.85 g, 12.0 mmol, 1.2 equiv.) suspended in THF (100 mL) at 0 $^\circ\text{C}$, $^n\text{BuLi}$ (2.5 M in hexanes, 4.8 mL, 12.0 mmol, 1.2 equiv.) was added dropwise. The vessel was sealed and stirred for 1 hour. 1-Phenylpropan-1-one (1.34 g, 10.0 mmol, 1.0 equiv.) was added and the solution was warmed to room temperature where the reaction proceeded for 16 hours. The solution was cooled to 0 $^\circ\text{C}$ and quenched with saturated ammonium chloride solution (100 mL). Petroleum ether (3 \times 50 mL) was added and the organic phase separated. Organic extracts were combined, dried over Na_2SO_4 , filtered and concentrated under reduced pressure. Crude product was purified by FCC (SiO_2 , pentane) yielding the title compound as a colourless oil (795 mg, 6.01 mmol, 60%). Spectroscopic data are in agreement with previous literature. ^1H NMR (CDCl_3 , 300 MHz) δ 7.41-7.38 (m, 2H), 7.32-7.17 (m, 3H), 5.25 (m, 1H), 5.03 (m, 1H), 2.48 (m, 2H), 1.08 (m, 3H); $^{13}\text{C}\{^1\text{H}\}$ NMR (CDCl_3 , 75 MHz) δ 150.1 ($^{\text{Ar}}\text{C}$), 141.6 ($^{\text{Ar}}\text{C}$), 128.4 ($^{\text{Ar}}\text{C}$), 127.4 ($^{\text{Ar}}\text{C}$), 126.1 (C), 111.1 ($\text{C}=\text{CH}_2$), 28.2 (CH_2), 13.1 (CH_3).

4.6.5 Computational Method

Density functional theory calculations were executed using Gaussian 16, A.03.¹⁰³ All geometry optimizations were computed with the BP86 functional, accompanied by the ultrafine integral grid option 'int=grid=ultrafine'. Iron atoms were defined using the Stuttgart-Dresden Effective Core Potentials and basis sets (SDDAll).¹⁰⁴ Other atoms were described with double- ζ plus polarization 6-31G** basis sets, defined as 'BS1'.^{105,106} Frequency calculations at the same level of theory were used to generate free energies, with energy minima (confirmed with no imaginary frequencies), corresponding to the relevant intermediate species along the reaction coordinate and saddle points (confirmed with one imaginary frequency), corresponding to the relevant TS. Single point energy corrections were calculated at the B3PW91-D3BJ/Def2-TZVP/IEF-PCM(C_6H_6) level, with Ahlrichs triple- ζ basis set deployed on all atoms.¹⁰⁷ This method follows that employed by Webster and co-workers, following successful benchmarking against

an experimental β -hydrogen transfer with an analogous iron-BDK system.⁶² Free-energy profiles are valued in kcalmol⁻¹ at the B3PW91-D3BJ/Def2-TZVP/IEF-PCM(C₆H₆)/BP86/**BS1** theory level described above.¹⁰⁸

Following Webster and co-workers study,⁶² empirical dispersion corrections were calculated with Grimme's D3¹⁰⁹ addition to KS-DFT, with the Becke-Johnson damping function.¹¹⁰ Benzene solvent corrections were deployed using the IEF-PCM implemented in Gaussian 16, using optimised geometries at the BP86/**BS1** level.¹¹¹ All corrections and scaling factors were applied using the GoodVibes programme, frequency cut-off 100.0 cm⁻¹ (T = 298.15 K, C = 1.0 mol L⁻¹, vibrational scale factor = 1.0).¹¹²

All iron containing structures for catalyst activation were optimised in both the quintet (denoted **⁵X**) and triplet (denoted **³X**) spin states to identify whether any spin-crossover mechanism is operable, again following preceding work by Webster and co-workers.⁶²

Chapter 5

Synthesis of Cage-Dense, PN-Containing Polymers of Varying Electron Density

5.1 Introduction

The continued dependence on polymeric materials, and requirement for enhanced chemical and mechanical properties, has led to their systematic modification. Therefore, countless examples of polymers containing one- (for example, poly(lactide)) and two-dimensional (for example, Kevlar) fragments within the repeat unit backbone, along with combinations of the two (for example, poly(ethylene terephthalate)), have emerged. Scarcely explored are ‘cage-dense’ polymers derived from three-dimensional, cage-like fragments within the backbone (shown in scheme 5.1.1). Polymer properties reflect those of the (co-)monomers used in their synthesis.²³² Cage-like molecules are inherently conformationally constrained.²³³ Therefore, it is surprising they are under-exploited in polymeric materials. Their conformational rigidity is mirrored in the corresponding polymer, leading to desirable properties (for example, high glass transition temperature (T_g) and melting temperature (T_m)).

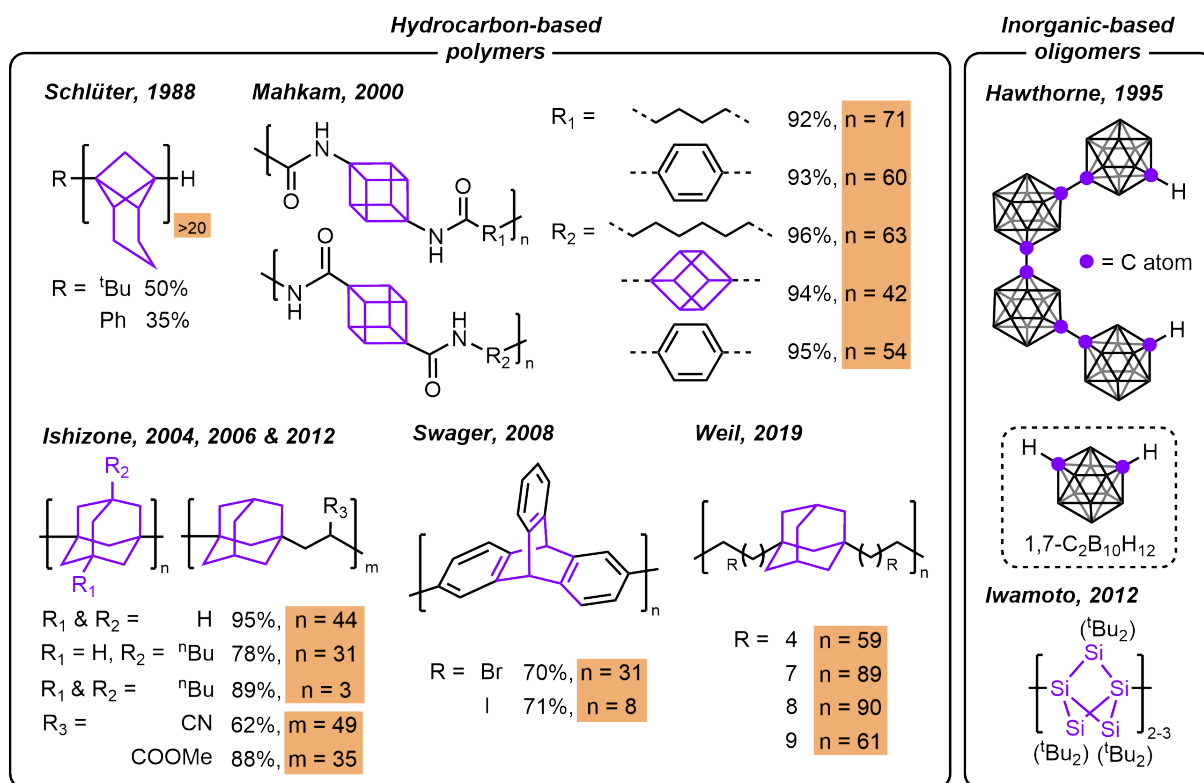
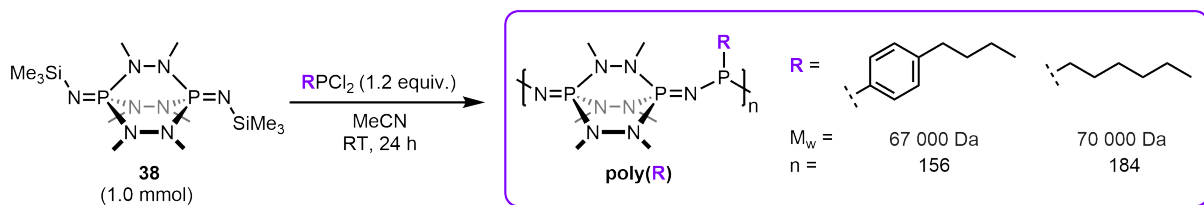


Figure 5.1.1: Literature precedent for cage-dense, hydrocarbon-based polymers and inorganic-based oligomers.^{234–242}

The first example of a cage-dense polymer was reported by Schlüter.²³⁴ Poly([1.1.1]propellanes) were synthesised by initiation of [1.1.1]propellane with organolithium reagents in an approximate degree of polymerisation (DP) greater than 20. Low molecular weights (M_W) were attributed to poor polymer solubility. Furthermore, [1.1.1]propellane monomers are challenging to synthesise because of the tendency to readily undergo ring-opening polymerisation. Mahkam and Sanjani described the synthesis of cubane-containing polyamides in M_W s greater than 10 kDa.²³⁵ Polymers demonstrated high thermal stability (temperature of maximum decomposition rate ($T_{d, max}$) = 300-390 °C) and no observed T_g . Thermal properties were attributed to a combination of amide bonds and rigid cage-dense polymer backbone. However, use of

cubane-based monomers carry the synthetic challenge of a five- or eight-step synthesis. Ishizone and co-workers synthesised poly(1,3-adamantanes) by ring-opening polymerisation.^{236–238} High M_W (up to 23 kDa) polymers were generated with excellent thermal properties ($T_g = 123\text{--}231\text{ }^\circ\text{C}$, $T_{d, 10\%} = 398\text{--}486\text{ }^\circ\text{C}$). Dehydroadamantanes were synthesised in up to five-steps. Swager and Chen synthesised poly(2,6-triptycene) with M_W up to 8.9 kDa. The cage-dense polymer showed good thermal properties with no T_g (between $20\text{--}340\text{ }^\circ\text{C}$) and high $T_{d, 5\%}$ ($440\text{ }^\circ\text{C}$). 2,6-Dihalotriptycene monomers were synthesised by a three-step method. In a recent study, Weil and co-workers synthesised poly(1,3-adamantylene alkylenes) by diene-metathesis polycondensation.²⁴⁰ High M_W cage-dense polymers (16.5–35.2 kDa) were generated with improved stability compared to their two-dimensional analogues. Adamantyl-derived polymers demonstrated a $T_{d, 5\%}$ 30 and 64 $^\circ\text{C}$ higher than two-dimensional 1,4-cyclohexyl- and 1,4-phenyl-derived polymers, respectively. Literature precedent suggests that cage-dense polymers have promising thermal properties. However, monomer instability and challenging syntheses limit their exploration in chemical research.



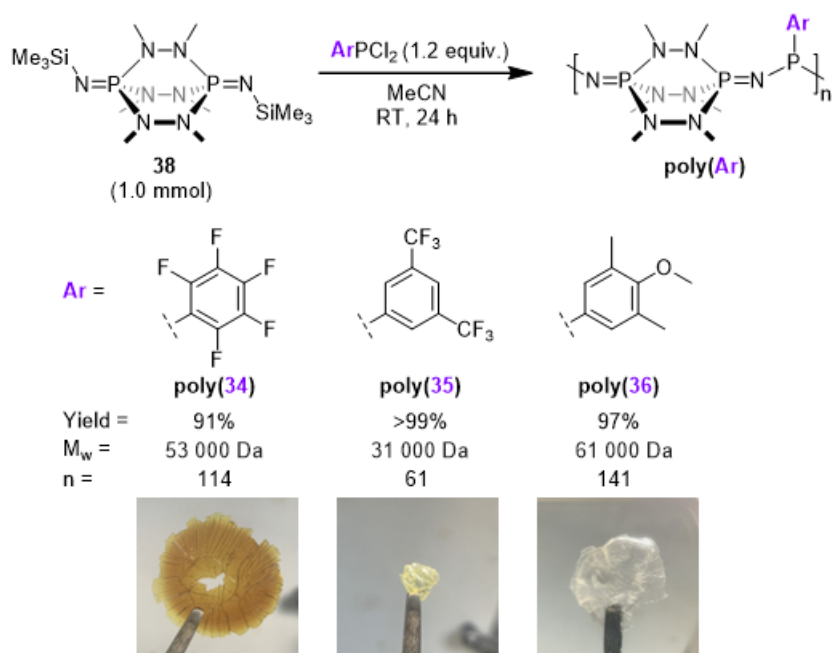
Scheme 5.1.1: Synthesis of cage-dense, PN-containing polymers (ongoing work by Chitnis and co-workers).²⁴³

Ongoing work by Chitnis and co-workers detailed the scalable synthesis of PN-containing inorganic cage **38**.²⁴³ P^{III} -cage precursor (**37**) is synthesised by reaction of commercially available 1,2-dimethylhydrazine dihydrochloride and tris(dimethylamino)phosphine on $>10\text{ g}$ scale.²⁴⁴ Cage **38** is generated by oxidation of **37** with trimethylsilyl azide on the $>2\text{ g}$ scale.²⁴⁵ Cage **38** shows high thermal ($80\text{ }^\circ\text{C}$, 7 days) and chemical stability (no reaction with potassium metal, sodium hydride, radical initiators and caesium fluoride). The facile synthesis and stability of **38** circumvents the previous challenges associated with generating cage-containing monomers- a versatile synthon for exploring cage-dense polymer chemical-space. Co-polymerisation with (n hexyl)dichlorophosphine or (4- n butyl)dichlorophosphine, yields PN-containing polymers in high molecular weight (67 and 70 kDa, respectively, see scheme **5.1.1**). Inorganic cage-dense oligomers (with non-carbon atoms in the polymer backbone) derived from carboranes and perisilastaffanes have been synthesised (see scheme **5.1.1**).^{241,242} However, high M_W polymers are, thus far, elusive. Alternatively functionalised phosphine linkers could lead to enhanced properties in the corresponding co-polymer (for example, solubility, DP, air- and moisture-stability and mechanical properties). This chapter details the synthesis and characterisation of an array of PN-containing polymers derived from (aryl)dichlorophosphine co-monomers. *In situ* reaction monitoring experiments provide insight into the polymerisation mechanism, along with the impact of electron-density on reaction rate.

5.2 Synthesis and Characterisation of Cage-Dense Polymers

5.2.1 Polymer Synthesis and Characterisation

Consideration was given to investigate if the cage-dense PN-polymer properties could be tuned with choice of phosphorus linker. Inspired by the success of (4-ⁿbutylphenyl)dichlorophosphine as a co-monomer, aryldichlorophosphines **34-36** were synthesised for further investigation. Incorporation of fluorinated functionality often leads to enhanced solubility.²⁴⁶ Therefore, higher M_w s may be accessible before polymer precipitation occurs. Furthermore, resolubilising the polymers after precipitation has not yet been achieved. Improving polymer solubility will assist with their manipulation and characterisation. Despite high air- and moisture-stability, (4-ⁿbutylphenyl)dichlorophosphine-derived polymers are brittle. Improved air-stability is suspected to arise from electron-deficiency at phosphorus making oxidation more challenging. Alternatively functionalised aryl phosphines could lead to enhanced mechanical properties, whilst retaining chemical stability.



Scheme 5.2.1: Synthesis, properties and thin-films of polymers **poly(34)**, **poly(35)** and **poly(36)**.

PN-cage **38** was reacted with aryldichlorophosphines **34-36**, shown in scheme **5.2.1**. In all cases, polymerisation occurs generating co-polymers **poly(34)-poly(36)** in excellent yield (91% - >99%). Drop-casting of crude polymer mixtures into a Teflon mould leads to thin-films of **poly(34)-poly(36)**. These films are brittle (as seen for (4-ⁿbutylphenyl)dichlorophosphine), indicating that substitution at the aryl-phosphine is insufficient to significantly impact the mechanical properties. For **poly(35)** and **poly(36)**, these films display poor air- and moisture-stability, with discolouration observed after 24 hours. In contrast, **poly(34)** shows excellent air- and moisture-stability, with no discolouration after >4 weeks. Stability of **poly(34)** is attributed to the difficult oxidation at the electron deficient phosphorus.

Resolubilising **poly(34)-poly(36)** was challenging. Therefore, solution-state NMR characterisation was undertaken on crude reaction mixtures. A representative example (**poly(35)**) is shown in figure

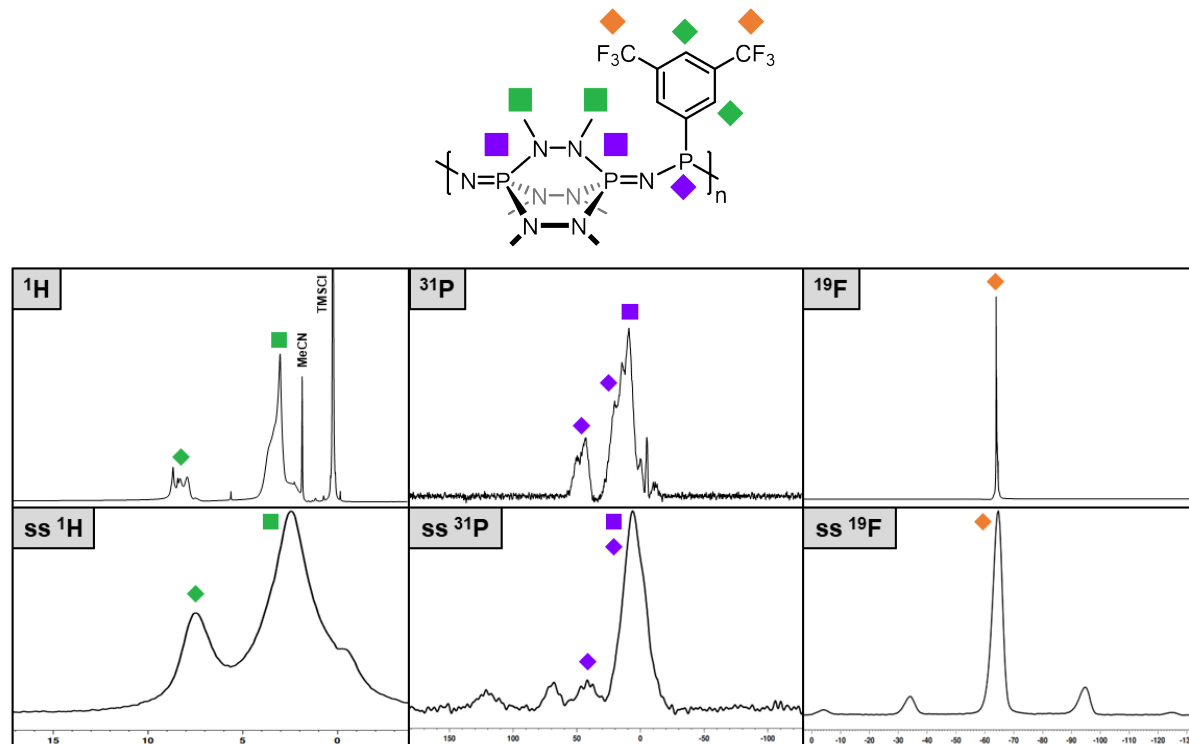


Figure 5.2.1: Solution- (top, 500 MHz, CD₃CN, 298 K) and solid-state (bottom) NMR spectra of **poly(35)**.

5.2.1. Significant peak broadening is observed in the solution-state ¹H NMR spectrum for the Ar-H and N-Me protons, with chemical shifts of 8.58-7.37 and 4.18-2.03 ppm, respectively. Two major environments are observed in the ³¹P NMR spectrum at 51.9-32.9 and 26.3-2.9 ppm in 1:5 integral ratio, respectively. The former is suspected to be the Ar-P nuclei. The latter is suggested to be a combination of cage N-P-N, and second Ar-P nuclei. Multiple ³¹P environments are proposed to arise from atacticity. The ¹⁹F NMR spectrum reveals a single broad peak at -62.0- -63.1 ppm. In all cases, solid-state NMR (ssNMR) spectroscopy of purified polymers revealed ¹H, ³¹P and ¹⁹F chemical shifts analogous to the solution-state. M_W determination by size exclusion chromatography (SEC) could not be performed, because of poor polymer solubility in THF. Instead, an estimate of polymer M_W was determined by diffusion-ordered NMR spectroscopy (DOSY) on crude samples.²⁴⁷ High M_Ws were observed for polymers **poly(34)**, **poly(35)** and **poly(36)** at 53, 31 and 61 kDa, with DPs of 114, 61 and 141, respectively. Polymer M_Ws and DPs were comparable to 4-ⁿbutylphenyl- and ⁿhexyl-derived polymers at 67 and 70 kDa, and 156 and 184 respectively. No trend between phosphine electron-density and polymer M_W was discovered. This contradicts the hypothesis that fluorinated aryldichlorophosphines will lead to increased M_W. To achieve high M_W polymers from condensation co-polymerisation, precise quantities of co-monomers are required. Therefore, differences in polymer M_W and DP are likely to arise from weighing error. From differential scanning calorimetry (DSC) no glass transition, melting or crystallisation temperature were observed between 0-120 °C. The same was seen for organic cage-dense polymers (described in section 5.1), a consequence of conformationally robust cage molecules in the polymer backbone. Polymers display good thermal stability with T_{d, max} of 348, 302 and 398 °C, respectively.

5.2.2 Repeat-Unit and End-Group Determination

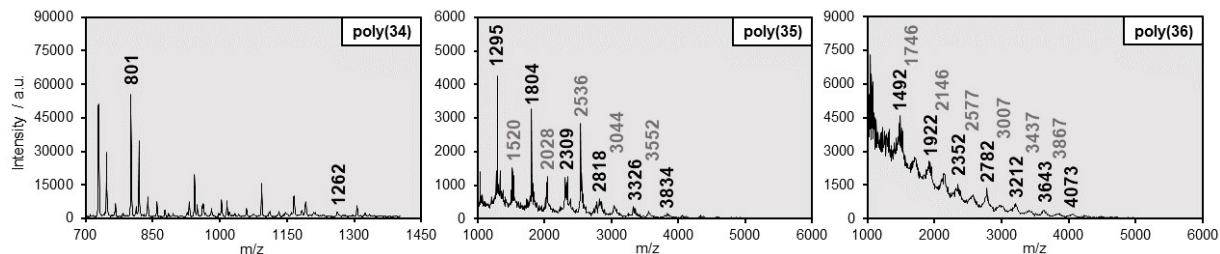


Figure 5.2.2: MALDI-TOF spectra for **poly(34)**-**poly(36)**. Repeat unit exact mass: 462.1, 508.1 and 430.2 Da, respectively.

The repeat unit and end-group of **poly(34)**-**poly(36)** were determined by matrix-assisted laser desorption/ionisation-time of flight spectrometry (MALDI-TOF) (shown in figure 5.2.2). Polymer **poly(34)** showed fragment peaks at 801 and 1262 m/z. A difference of 461 m/z is in agreement with the expected mass for the cage-phosphine-linker repeat unit (462 Da). End-group analysis revealed a mass-to-charge ratio of 338 m/z. This is in agreement with the expected mass for a protonated cage-SiMe₃-terminated polymer ($[M+H]^+$, 338 Da). Polymer **poly(35)** displays a fragment peak series containing 1295 and 1804 m/z. A difference of 509 m/z is in agreement with the expected mass for the cage-phosphine-linker repeat unit (508 Da). End-group analysis revealed a mass-to-charge ratio of 279 m/z. This is in agreement with the expected mass for a arylchlorophosphine-terminated polymer (279 Da). Finally, **poly(36)** displays a fragment peak series containing 1492 and 1922 m/z. A difference of 431 m/z is in agreement with the expected mass for the cage-phosphine-linker repeat unit (430 Da). End-group analysis revealed a mass-to-charge ratio of 201 m/z. This is in agreement with the expected mass for a arylchlorophosphine-terminated polymer (201 Da). In all cases, MALDI reveals the expected repeat unit and end-group for cage-dense polymers.

5.3 Mechanism for Polymerisation

From polymer characterisation, there is no clear trend between phosphine linker electronics and polymer M_w or DP. Consequently, consideration shifted to the rate of polymerisation and the influence of phosphine electrophilicity. NMR spectroscopy-scale polymerisations were undertaken for *in situ* reaction monitoring experiments, shown in figure 5.3.1. Mechanical agitation is required to solubilise **38** in MeCN, so this is not a suitable solvent for reaction monitoring. Instead, DCM was selected. Ongoing work by Chitnis and co-workers demonstrated that polymerisation occurs in DCM.²⁴³ However, poor polymer solubility led to a low DP. Nevertheless, DCM should provide a sensible description for the rate of polymerisation during the early stages of reaction when M_w is low. In all cases, rapid formation of TMSCl is observed for **poly(34)**, **poly(35)** and **poly(36)**, reaching concentrations of 0.11 M, 0.09 M and 0.09 M respectively, within 5 minutes of reaction. The maximum [TMSCl] that can be produced under these conditions is 0.17 M, indicating over 50% conversion occurs within the first 5 minutes of reaction. Rate of TMSCl formation then slows. For **poly(34)**, the reaction ends after 2 hours, with a [TMSCl] of 0.13 M. Polymer **poly(35)**

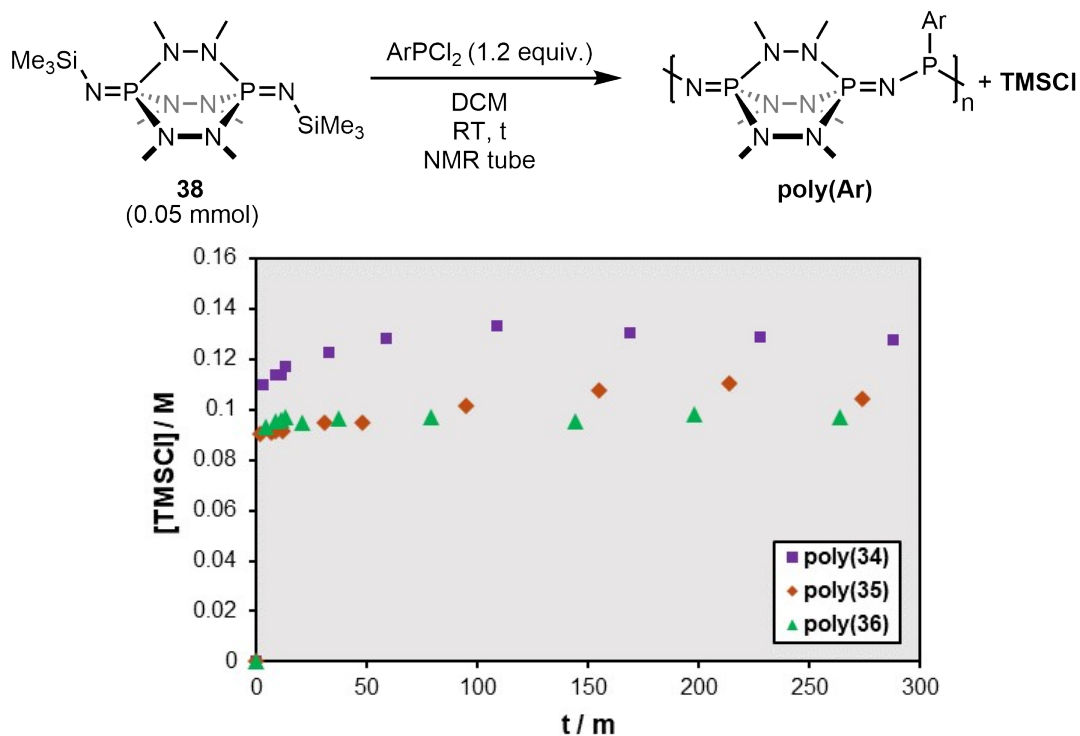


Figure 5.3.1: Reaction monitoring trace for the co-polymerisation of **38** and ArPCl₂.

proceeds at a slower rate, reaching 0.11 M [TMSCl] after 3 hours of reaction. In both cases, the termination of the reaction is accompanied by polymer precipitation. Polymer **poly(36)** remains in solution. However, conversion is slow- reaching a maximum [TMSCl] of 0.10 M after 5 hours. Monitoring experiments suggest the rate of polymerisation increases with phosphine electron deficiency, likely caused by increased electrophilicity at phosphorus (phosphine linker electrophilicity follows the trend **34**>**35**>**36**).

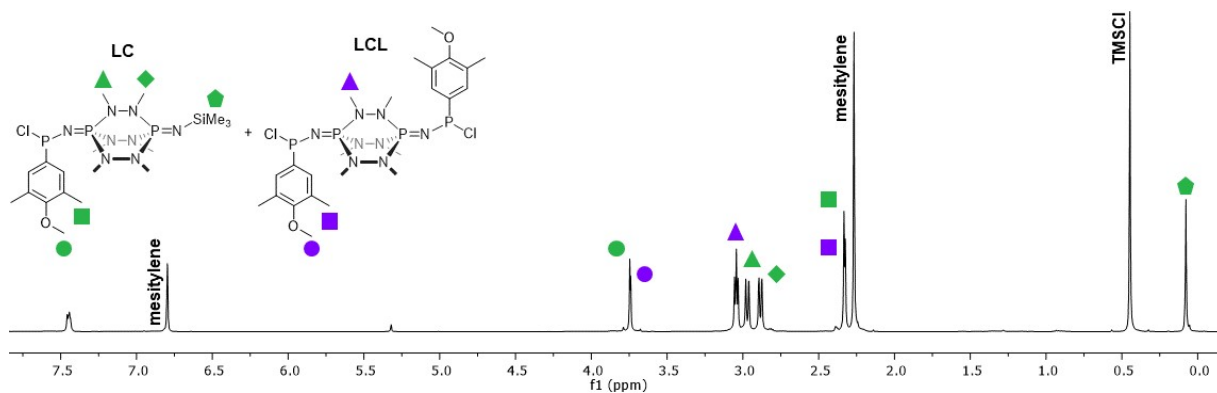


Figure 5.3.2: ¹H NMR spectra of **36** and **38** polymerisation, measured after 5 minutes (400 MHz, CD₂Cl₂, 298 K).

Intrigued by the rapid formation of TMSCl, the initial stages of the polymerisation were inspected in more detail. The ¹H NMR spectra recorded for **poly(36)** after 5 minutes is shown in figure 5.3.2 as a representative example. Two species are identified in 0.6:0.4 ratio, proposed to be cage-phosphine-linker telomer (**LC**, shown in green) and phosphine-linker-cage-phosphine-linker oligomer (**LCL**, shown in purple), respectively. Notably, **36** and **38** are completely consumed within 5 minutes, leading to

the formation of **LC** and **LCL**. The rate of TMSCl production then slows dramatically, suggesting the reaction between **LC** and **LCL** to give longer-chain polymers is less facile. This is accompanied by slow peak broadening in the ^1H NMR spectra. This behaviour is indicative of a step-growth polymerisation mechanism. These findings are corroborated by Chitnis and co-workers in ongoing work, as polymer M_w increases exponentially with time.²⁴³ The significant drop in rate of TMSCl production suggests that formation of **LC** and **LCL** occurs during polymer initiation. The propagation between **LC** and **LCL** is slow, potentially caused by a combination of factors: 1) **LC** is larger than **38**. Thus, it is a weaker nucleophile. 2) Nitrogen-to-phosphorus π -donation occurs in **LCL**. Therefore, the electrophilicity of **LCL** is reduced.

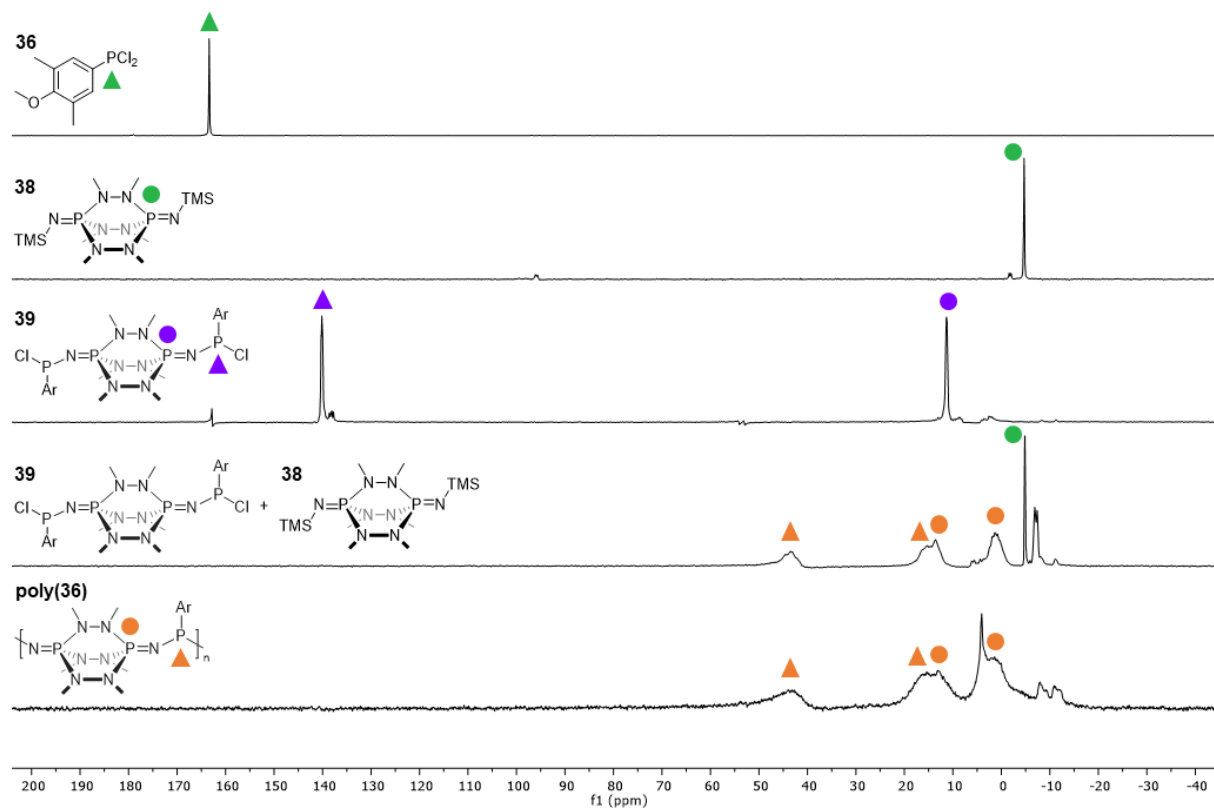


Figure 5.3.3: ^{31}P NMR spectra for step-wise polymerisation experiment (202 MHz, CD_3CN , 298 K).

The controlled initiation allowed step-wise polymerisation to be explored, shown in figure 5.3.3. When combining 2.0 equivalents of **36** with 1.0 equivalent of **38**, a defined species is observed in the ^{31}P NMR spectrum with chemical shifts at 140.2 and 11.4 ppm. These shifts are indicative of a $\text{AA}'\text{XX}'$ spin system. Resonances in the ^1H NMR spectra overlap with previously hypothesised **LCL** (shown in figure 5.3.2). Single-crystals were grown from pentane vapour diffusion into a saturated DCM solution. The solid-state structure is shown in figure 5.3.4, revealing **LCL** species **39**. 1.0 equivalent of **39** was reacted with 1.2 equivalent of **38**. Compound **39** is consumed forming a polymeric species, with chemical shifts comparable to **poly(36)**. These results provide evidence for a living polymerisation and chain-end control. This is corroborated in ongoing work, where chain-end control leads to the construction of block copolymers.²⁴³

Experimental investigation indicates that the condensation-polymerisation of **38** with dichlorophosphines proceeds by a step-growth mechanism. Rapid formation of TMSCl occurs during the early stages

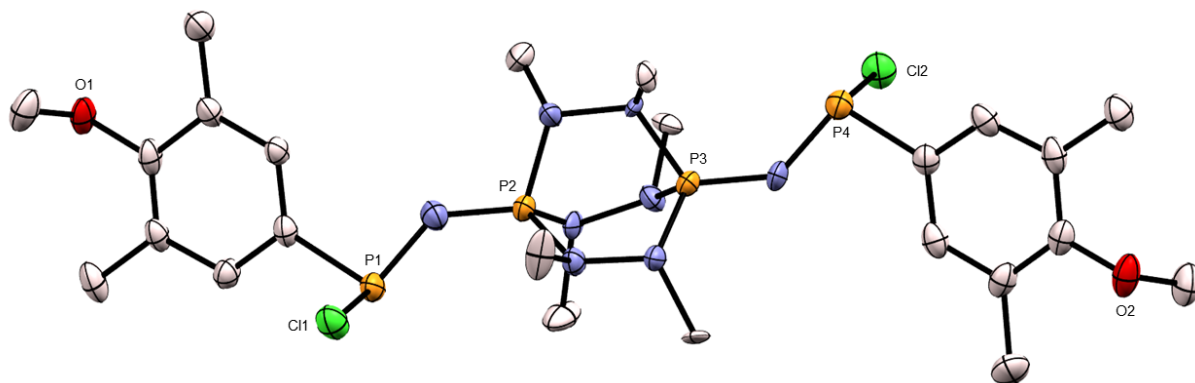
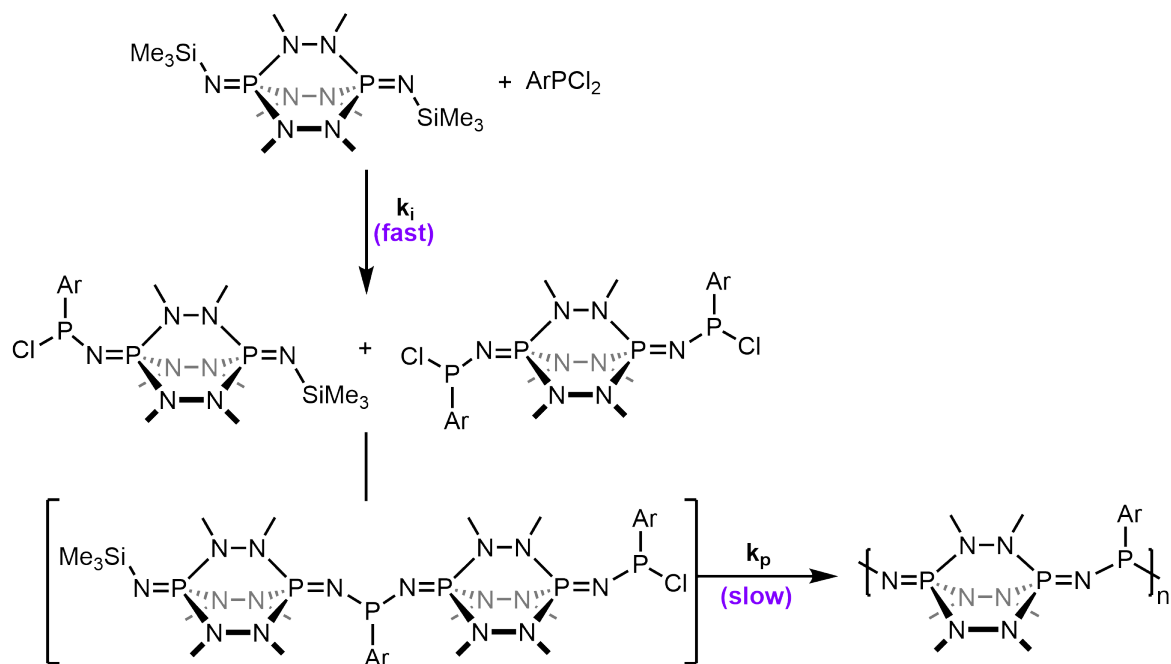


Figure 5.3.4: Single-crystal XRD structure of **39**. Ellipsoids are represented at 50% probability and hydrogen atoms omitted for clarity.

of the reaction leading to low M_W species **LC** and **39**, evidenced by *in situ* reaction monitoring experiments. TMSCl formation dramatically slows, indicating formation of **LC** and **39** is an initiation event. Furthermore, the isolation of **39** suggests the rate of initiation is greater than the rate of polymerisation ($k_i \gg k_p$). Compounds **LC** and **39** combine to give high M_W polymers. k_p is larger for electron-deficient phosphines, evidenced by TMSCl production following the trend **34**>**35**>**36**.

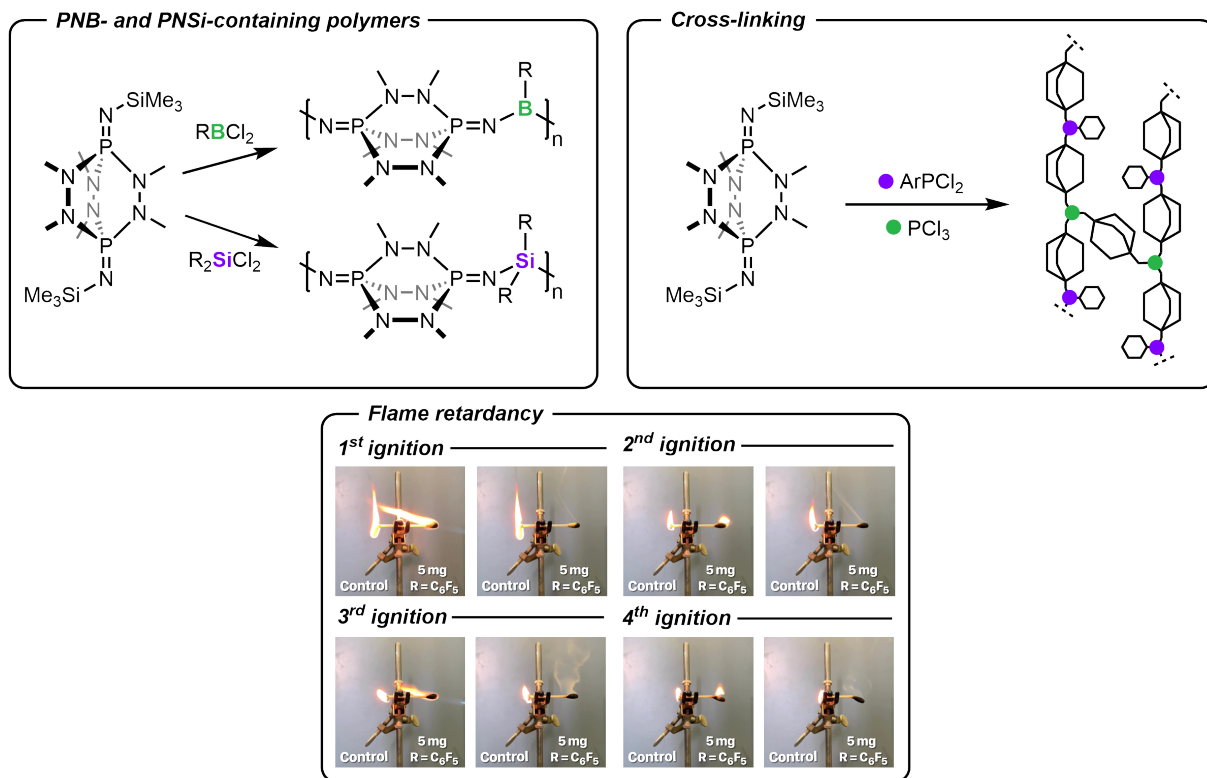


Scheme 5.3.1: Mechanism for step-growth polymerisation of **38** and dichlorophosphines.

5.4 Conclusions and Future Work

A selection of PN-containing, cage-dense polymers (**poly(34)**-**poly(36)**) were synthesised by reaction of aryldichlorophosphines (**34**-**36**) with **38**. In all cases high M_W polymers were generated with estimated DP of 114, 61 and 141, respectively. No T_g was observed, consistent with literature precedent for cage-dense

polymers. MALDI-TOF reveals the expected repeat unit and end-group mass for **poly(34)**-**poly(36)**. *In situ* reaction monitoring indicated polymerisation proceeds by a step-growth mechanism. Rapid formation of short-chain **LC** and **LCL** occurs in an initiation event. Propagation between **LC** and **LCL** is slow allowing for the isolation of intermediate **39**. Intermediate **39** undergoes polymerisation with **38**, indicative of a living polymerisation.



Scheme 5.4.1: Proposed synthesis of PNB/PNSi-containing- and cross-linked polymers, and flame retardancy test.

The versatility of the cage synthon for construction of alternative heteroatom-rich polymers remains to be explored. Metathesis of the nitrogen-silicon bond with boron- or silicon-chlorides, may yield heteroatom rich poly(borylphosphazenes) or poly(silylphosphazenes) (shown in figure 5.4.1). Literature search revealed no examples of PNB- or PNSi-containing polymers.²⁴⁸ Out of scientific curiosity, and applications of BN- (ceramics) and PN-containing (flame retardants) polymers, these materials warrant further investigation.^{249,250} Leading flame retardant poly(phosphazenes) display $T_{5\%}$ temperatures up to 309 °C.²⁵⁰ Cross-linking has been shown to improve thermal stability.²⁵¹ By doping trichlorophosphine into standard polymerisation conditions, cross-linking can be induced and controlled (shown in figure 5.4.1). Cross-linked **poly(34)**-**poly(36)** may lead to enhanced thermal stability. Initial tests suggest **poly(34)** share the flame-retardant properties observed for poly(phosphazenes) (shown in figure 5.4.1). Because of the unique properties of cage-dense polymers, along with the scalability of cage synthon **38**, the influence of dimensionality in polymer science can endure.

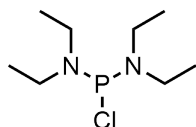
5.5 Experimental

5.5.1 General Considerations

Reagents were purchased from Fisher Scientific or Merck and dried and distilled prior to use. THF, C₆H₆ and C₆D₆ were dried over Na/benzophenone and distilled prior to use. DCM, CD₂Cl₂, CH₃CN and CD₃CN were dried over CaH₂ and distilled prior to use. NMR spectra were collected at 300 or 500 MHz on Agilent or Bruker instruments in DCM, CD₂Cl₂, CH₃CN or CD₃CN at 298 K and referenced to the residual solvent peak. Reactions were undertaken using standard glovebox (Ar, 0.1 ppm H₂O and 0.1 ppm O₂) and Schlenk line (N₂) techniques unless otherwise stated.

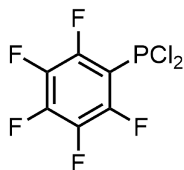
5.5.2 Chlorophosphine Synthesis

Synthesis of bis(diethylamino)chlorophosphine, **33**



Title compound synthesised following modified literature procedure.²⁵² To a flame-dried schlenk containing a vigorously stirred solution of PCl₃ (8.8 mL, 101 mmol, 1.0 equiv.) in diethyl ether (200 mL) at -78 °C, a HNEt₂ (43.0 mL, 416 mmol, 4.0 equiv.) solution in diethyl ether (50 mL) was added dropwise over 10 minutes, where a white precipitate forms. The mixture was warmed to room temperature and stirred for 72 hours. The mixture was filtered through a pad of celite, and the filtrate concentrated under reduced pressure. Oil was purified by vacuum distillation (85 °C, 4 × 10⁻² mbar) yielding the title compound as a colourless oil (18.6 g, 88.3 mmol, 87%). Spectroscopic data in agreement with literature.²⁵² ¹H NMR (CH₃CN, 500 MHz) δ 4.01 (dq, *J*=11.6, 7.1 Hz, 4H, CH₂), 1.97 (t, *J*=7.1 Hz, 6H, CH₃); ³¹P NMR (CH₃CN, 202 MHz) δ 161.1 (s).

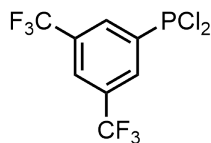
Synthesis of pentafluorophenyldichlorophosphine, **34**



Title compound synthesised following modified literature procedure.²⁵³ To a flame-dried schlenk containing activated magnesium turnings (1.09 g, 45.0 mmol, 1.5 equiv.) in diethyl ether (100 mL), pentafluorobromobenzene (4.11 mL, 33.0 mmol, 1.1 equiv.) was added dropwise over 10 minutes. The mixture was refluxed for 2 hours. The Grignard solution was added dropwise by canula filtration to a stirring solution of bis(diethylamino)chlorophosphine (6.32 g, 30.0 mmol, 1.0 equiv.) at -78 °C in diethyl ether (200 mL). The solution was warmed to room temperature and stirred for 16 hours where a precipitate forms. The mixture was cooled to -78 °C and HCl solution (2M in diethyl ether, 75.0 mL, 150 mmol, 5.0 equiv.) was

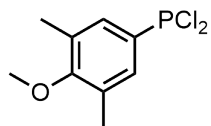
added dropwise. The mixture was warmed to room temperature and stirred for 5 hours. The mixture was concentrated under reduced pressure, raised in pentanes (100 mL) and filtered through a pad of celite. Crude mixture was concentrated and purified by vacuum distillation (50 °C, 2.5×10^{-2} mbar), yielding the title compound as a colourless oil (5.64 g, 21.0 mmol, 70%). ^{31}P NMR (CH₃CN, 202 MHz) δ 136.0 (t, $J=57.0$ Hz); ^{19}F NMR (CH₃CN, 471 MHz) δ -132.6 (d, $J=62.4$ Hz, 2F, $^{\circ}\text{CF}$), -147.2 (ddd, $J=19.9$, 16.2, 6.3 Hz, 1F, $^{\text{p}}\text{CF}$), -161.9 (tt, $J=19.3$, 6.3 Hz, 2F, $^{\text{m}}\text{CF}$).

Synthesis of (3,5-trifluoromethylphenyl)dichlorophosphine, 35



To a flame-dried schlenk containing a stirred solution of bis(3,5-trifluoromethyl)bromobenzene (3.78 g, 12.9 mmol, 1.0 equiv.) in diethyl ether (200 mL) at -78 °C, ⁿBuLi (2.5 M in hexanes, 6.0 mL, 15.0 mmol, 1.16 equiv.) was added dropwise over 10 minutes. The mixture was warmed to room temperature and stirred 6 hours. The solution was cooled to -78 °C and a solution of bis(diethylamino)chlorophosphine (3.0 g, 13.2 mmol, 1.1 equiv.) in diethyl ether (50 mL) was added dropwise over 10 minutes. The solution was warmed to room temperature and stirred for 16 hours where a white precipitate forms. The mixture was cooled to 0 °C and HCl solution (2M in diethyl ether, 64.7 mmol, 5.0 equivs.) was added dropwise. The mixture was warmed to room temperature and stirred for 3 hours. The mixture was filtered through a pad of celite and washed with pentanes (3 \times 50 mL). The solution was concentrated and purified by vacuum distillation (70 °C, 5×10^{-2} mbar), yielding the title compound as a colourless oil (2.16 g, 6.86 mmol, 53%). Spectroscopic data in agreement with literature.²⁵³ ^1H NMR (CH₃CN, 500 MHz) δ 8.36 (d, $J=7.0$ Hz, 2H, $^{\circ}\text{CH}$), 8.08 (s, 1H, $^{\text{p}}\text{CH}$); ^{31}P NMR (CH₃CN, 202 MHz) δ 152.0 (s); ^{19}F NMR (CH₃CN, 471 MHz) δ -63.4 (s).

Synthesis of (3,5-dimethyl-4-methoxyphenyl)dichlorophosphine, 36

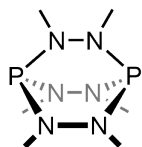


To a flame-dried schlenk containing a stirred solution of 4-methoxy-3,5-dimethylbromobenzene (1.48 mL, 9.30 mmol, 1.0 equiv.) in diethylether (50 mL) at -78 °C, ⁿBuLi (2.5 M in hexanes, 4.30 mL, 10.7 mmol, 1.16 equiv.) was added dropwise over 10 minutes. The solution was warmed to room temperature and stirred for 3 hours where a white precipitate forms. The mixture was cooled to -78 °C and a solution of bis(diethylamino)chlorophosphine (2.15 g, 10.2 mmol, 1.1 equiv.) in diethylether (25 mL) was added dropwise over 5 minutes. The suspension was warmed to room temperature and stirred for 16 hours. The mixture was cooled to 0 °C and HCl (2.0 M in diethylether, 23.5 mL, 46.5 mmol, 5.0 equiv.) was added dropwise over 5 minutes. The mixture was warmed to room temperature and stirred for 3 hours. The precipitates were removed by filtration through a pad of celite and washed with hexane. The filtrate was

concentrated and purified by vacuum distillation (140 °C, 5×10^{-2} mbar) yielding the title compound as a colourless oil (1.63 g, 6.88 mmol, 74%). $^1\text{H NMR}$ (CD_3CN , 500 MHz) δ 7.62 (d, $J=9.6$ Hz, 2H, ArH), 3.75 (s, 3H, OMe), 2.32 (s, 6H, ArMe); $^{13}\text{C}\{^1\text{H}\}$ NMR (CD_3CN , 125 MHz) δ 162.4 (ArCOMe), 135.6 (d, $J=51.3$ Hz, ArCP), 133.4 (d, $J=9.8$ Hz, ArCMe), 131.9 (d, $J=33.4$ Hz, ArCH), 60.4 (MeO), 16.3 (ArMe); $^{31}\text{P NMR}$ (CD_3CN , 202 MHz) δ 163.4 (t, $J=9.6$ Hz); **IR** (cm^{-1}) 2938.9, 1584.7, 1479.2, 1276.8, 1222.7, 1010.5, 888.1.

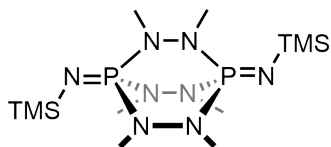
5.5.3 Syntheses of PN-Cages

Synthesis of **37**



To a flame-dried schlenk containing 1,2-dimethyl-hydrazine dihydrochloride (24.2 g, 182 mmol, 1.5 equiv.) suspended in toluene (500 mL), tris(dimethylamino)phosphine (22.0 mL, 121 mmol, 1.0 equiv.) was added. The reaction was heated to reflux for 72 hours under N_2 , where a white precipitate forms. The mixture was concentrated, extracted with pentane (4×100 mL), and the solution isolated by cannula filtration. The filtrate was concentrated yielding the title compound as a colourless solid (12.3 g, 52.1 mmol, 43%). Compound **37** was used without further purification. $^1\text{H NMR}$ (CH_3CN , 500 MHz) δ 2.79-2.74 (m, 18H, CH_3); $^{31}\text{P NMR}$ (CD_3CN , 202 MHz) δ 106.9 (s).

Synthesis of **38**



To a high-pressure tube containing **37** (2.0 g, 8.47 mmol, 1.0 equiv.) dissolved in toluene (10 mL) under an N_2 atmosphere, trimethylsilyl azide (5.6 mL, 42.4 mmol, 5.0 equiv.) was added. The tube was sealed and heated to 140 °C behind a blast shield. The tube was cooled, opened and the solution transferred to a flame-dried schlenk-flask. *Note: care must be taken when opening the tube to vent the high-pressure of N_2 .* Volatiles were removed under reduced pressure. Crude solid was purified by sublimation, yielding the title compound as colourless crystals (1.10 g, 2.68 mmol, 32%). $^1\text{H NMR}$ (CH_2Cl_2 , 500 MHz) δ 2.78 (t, $J=5.7$ Hz, 18H, NCH_3), 0.02 (s, 18H, SiCH_3); $^{31}\text{P NMR}$ (CH_2Cl_2 , 202 MHz) δ -3.6 (s).

5.5.4 Polymer Synthesis

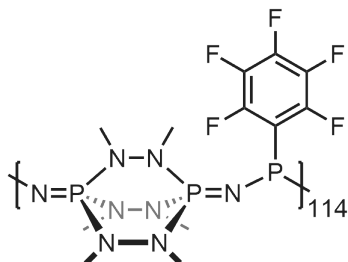
General Method for Polymerisation

To a screw-cap vial containing a stirred suspension of **38** (410 mg, 1.00 mmol, 1.0 equiv.) in acetonitrile (10 mL), dichlorophosphine (1.20 mmol, 1.2 equiv.) was added. The vessel was sealed and stirred at

room temperature for 24 hours, where the mixture becomes homogeneous after 2-5 minutes. The solution was concentrated (2 mL) and precipitated into a vortex of cold diethylether (10 mL). The precipitate was isolated by centrifuge, washed with pentane (3×5 mL) and dried, yielding the title compound.

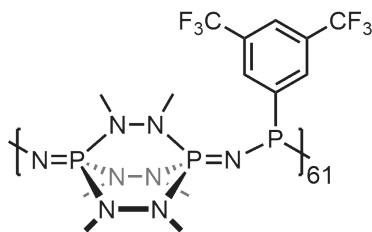
Polymer Spectroscopic Data

Synthesis of poly(34)



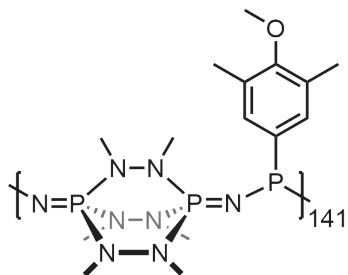
Title compound isolated as a glassy yellow solid (461 mg, 0.907 mmol, 91%). **¹H NMR** (CD₃CN, 500 MHz) δ 3.80–2.25 (br m, 558H, NMe), 0.10-0.06 (br m, 18H, NSiMe₃); **¹³C{¹H} NMR** (CD₃CN, 125 MHz) δ 149.0, 146.9, 139.5, 137.5, 37.4; **³¹P NMR** (CD₃CN, 202 MHz) δ 26.8-20.7 (br m), 12.0-7.6 (br m), 6.8- -4.12 (br m), -6.7- -8.8 (br m); **¹⁹F{¹H} NMR** (CD₃CN, 471 MHz) δ -128.7- -163.5 (br); **¹H ssNMR** (400 MHz) δ 3.0, 1.0 ; **³¹P ssNMR** (162 MHz) δ 20.0, 4.0; **¹⁹F ssNMR** (659 MHz) δ 159.0; **IR** (cm⁻¹) 2842, 1641, 1462, 1343, 1207, 978, 619; **TGA** T_d , 2% 130 °C, T_d , max 348 °C, T_d , max 430 °C; **DSC** no glass transition, melting or crystallisation temperature were observed. **MALDI-TOF** is discussed in section 5.2.

Synthesis of poly(35)



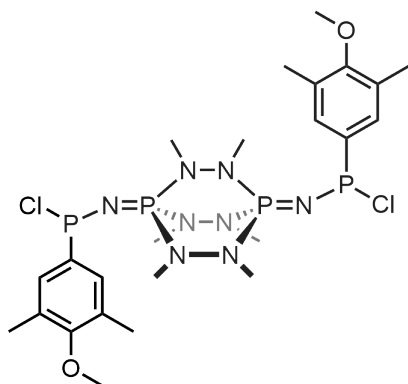
Title compound isolated as an off-white powder (533 mg, 1.05 mmol, >99%). **¹H NMR** (CD₃CN, 500 MHz) δ 8.58-7.37 (br m, 1100H, ArH), 4.18-2.03 (br m, 4400H, NMe₃), 0.06 (br s, 18H, NSiMe₃); **¹³C{¹H} NMR** (CD₃CN, 125 MHz) δ 136.3-124.6 (br m, ArC), 121.1-120.4 (br m, ArCH), 119.7-117.3 (br m, ArCH); **³¹P NMR** (CD₃CN, 202 MHz) δ 51.9-32.9 (br m, ArP) 26.3- -2.9 (br m, NPN), -5.5- -10.4 (br m, PNSiMe₃); **¹⁹F NMR** (CD₃CN, 471 MHz) δ -62.0- -63.1 (br m); **¹H ssNMR** (400 MHz) δ 7.0, 2.0 ; **³¹P ssNMR** (162 MHz) δ 42.0, 6.0; **¹⁹F ssNMR** (659 MHz) δ -65.0; **IR** (cm⁻¹) 2944, 2902, 2803, 1281, 1189, 1134, 1058, 977, 782, 678; **TGA** T_d , 2% 155 °C, T_d , max 302 °C; **DSC** no glass transition, melting or crystallisation temperature were observed. **MALDI-TOF** is discussed in section 5.2.

Synthesis of poly(36)



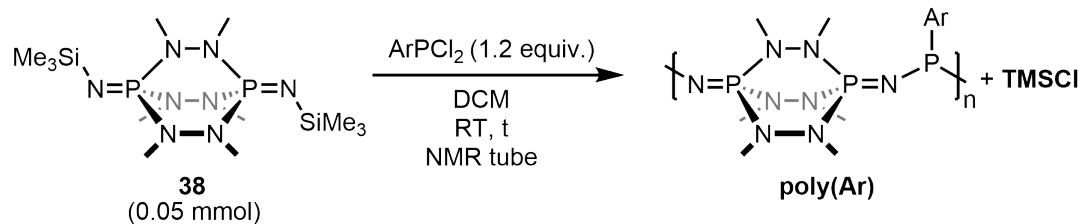
Title compound isolated as a white powder (417 mg, 0.969 mmol, 97%). $^1\text{H NMR}$ (CD_3CN , 500 MHz) δ 7.64-6.21 (br m, 14H, ArH), 3.97-3.49 (br m, OMe), 3.38-2.58 (br m, 126H, NMe), 2.35-2.07 (br m, 42H, ArMe), 0.06 (br m, 18H, SiMe_3); $^{13}\text{C}\{^1\text{H}\}$ NMR (CD_3CN , 125 MHz) δ 162.7-161.9 (br m, ArC=OMe), 133.9-129.6 (br m, 1,2,3-ArC), 60.6 (br s, OMe), 37.7 (br s, NMe), 16.5 (br s, ArMe); $^{31}\text{P NMR}$ (CD_3CN , 202 MHz) δ 51.0-38.2 (br m, ArP), 20.9-9.1 (br m), 6.1- -2.0 (br m), -6.3- -13.1 (br m); $^1\text{H ssNMR}$ (400 MHz) δ 7.0, 2.0; $^{31}\text{P ssNMR}$ (162 MHz) δ 45.0, 12.0, 0.0; IR (cm^{-1}) 2938, 1438, 1319, 1281, 1222, 1115, 983, 681; TGA T_d , 2% 91 °C, T_d , max 398 °C; DSC no glass transition, melting or crystallisation temperature were observed; MS expected for $\text{C}_{15}\text{H}_{30}\text{N}_8\text{OP}_3$: 431.1755, found: 431.1749 ([H-repeat unit-Cl] $^+$). MALDI-TOF is discussed in section 5.2.

Synthesis of 39



To a stirred solution of (3,5-dimethyl-4-methoxyphenyl)dichlorophosphine (94.8 μL , 0.5 mmol, 2.5 equiv.) in DCM (1 mL), a solution of **38** (82.1 mg, 0.2 mmol, 1.0 equiv.) dissolved in DCM (1 mL) was added dropwise. The solution was stirred for 1 hour at room temperature. The solution was concentrated and washed with pentane (3×5 mL). Crude white solid was dried and crystallised by vapour diffusion of pentane into a saturated DCM solution, yielding the title compound as colourless single crystals (115 mg, 0.172 mmol, 86%). $^1\text{H NMR}$ (CD_3CN , 500 MHz) δ 7.43 (d, $J=7.3$ Hz, 4H, ArH), 3.73 (s, 6H, OMe), 3.03 (t, $J=5.9$ Hz, 18H, NMe), 2.31 (s, 12H, ArMe); $^{13}\text{C}\{^1\text{H}\}$ NMR (CD_3CN , 125 MHz) δ 159.6 (C=OMe), 141.5 (dt, $J=35.7, 9.7$ Hz, CP), 131.5 (d, $J=7.3$ Hz, CMe), 130.2 (d, $J=27.2$ Hz, HCCP), 60.1 (OMe), 37.4 (NMe), 16.6 (CMe); $^{31}\text{P NMR}$ (CD_3CN , 202 MHz) δ 140.2 (m, ArP(Cl)), 11.4 (s, NPN); IR (cm^{-1}) 2939.2, 2361.8, 1591.6, 1460.9, 1285.3, 1225.9, 1119.5, 1057.8, 982.7, 838.6, 681.2, 610.6; MP 175-177 °C; sc-XRD relevant crystallographic data are reported in the X-ray crystallography section.

5.5.5 General Method for Reaction Monitoring Experiments



To a NMR tube containing **38** (0.05 mmol, 1.0 equiv.) and mesitylene (0.05 mmol) dissolved in DCM-*d*₂ (600 μL), ArPCl₂ (0.06 mmol, 1.2 equiv.) was added. The vessel was sealed and TMSCl production was monitored by ¹H NMR spectroscopy.

Chapter 6

Crystal Data and References

Table 6.0.1: sc-XRD data and structure refinement for **1b**, **1c**, **1c'**, **3a** and **3b**.

Compound	1b	1c	1c'	3a	3b
Empirical formula	C ₅₀ H ₇₂ Fe ₂ N ₄ Si ₂	C ₄₆ H ₆₄ Fe ₂ N ₄ Si ₂	C ₃₈ H ₄₂ FeN ₄	C ₃₇ H ₅₇ BFeN ₂	C ₂₉ H ₄₁ BFeN ₂
Formula Weight	448.50	840.89	610.60	596.50	484.30
Temperature / K	150.00(10)	150.01(10)	149.9(5)	150.00(10)	150.00(10)
Crystal system	orthorhombic	monoclinic	monoclinic	orthorhombic	monoclinic
Space Group	Cmce	P2 ₁ /c	P2 ₁ /n	Pnma	C2/c
a / Å	18.7305(7)	19.3467(3)	10.7368(5)	19.2143(4)	18.1664(2)
b / Å	14.4274(7)	17.5923(3)	17.6817(8)	20.1989(4)	12.4604(2)
c / Å	17.8945(7)	13.5223(2)	17.6420(9)	9.3011(2)	23.9387(3)
α / °	90	90	90	90	90
β / °	90	91.7570(10)	95.170(4)	90	94.823(1)
γ / °	90	90	90	90	90
Volume / Å ³	4835.7(4)	4600.19(13)	3335.6(3)	3609.83(13)	5399.59(13)
Z	4	4	4	4	8
ρ _{calc} / g cm ⁻³	1.232	1.214	1.216	1.098	1.191
μ / mm ⁻¹	5.557	5.809	0.483	3.518	4.596
F(000)	1920.0	1792.0	1296.0	1296.0	2080.0
Crystal size / mm ³	0.231 × 0.174 × 0.063	0.395 × 0.289 × 0.212	0.292 × 0.2 × 0.191	0.170 × 0.134 × 0.089	0.289 × 0.214 × 0.166
Radiation	Cu Kα (λ = 1.54184)	Cu Kα (λ = 1.54184)	Mo Kα (λ = 0.71073)	Cu Kα (λ = 1.54184)	Cu Kα (λ = 1.54184)
2θ range / °	9.18 to 179.056	6.792 to 146.724	5.98 to 56.564	8.756 to 147.32	7.412 to 146.078
Index ranges	-20 ≤ h ≤ 22, -17 ≤ k ≤ 17, -23 ≤ l ≤ 22	-23 ≤ h ≤ 18, -21 ≤ k ≤ 21, -13 ≤ l ≤ 16	-14 ≤ h ≤ 14, -22 ≤ k ≤ 23, -23 ≤ l ≤ 23	-23 ≤ h ≤ 23, -25 ≤ k ≤ 19, -11 ≤ l ≤ 11	-22 ≤ h ≤ 17, -15 ≤ k ≤ 15, -29 ≤ l ≤ 28
Reflections collected	24539	38393	29321	26996	26805
Independent reflections	2517 [R _{int} = 0.0368, R _{sigma} = 0.0170]	9154 [R _{int} = 0.0454, R _{sigma} = 0.0386]	8207 [R _{int} = 0.0710, R _{sigma} = 0.0959]	3739 [R _{int} = 0.0594, R _{sigma} = 0.0315]	5384 [R _{int} = 0.0360, R _{sigma} = 0.0237]
Data/restraints/parameters	2517/5/163	9154/464/621	8207/0/396	3739/0/204	5384/0/312
Goodness-of-fit on F ²	1.107	1.027	1.024	1.042	1.035
Final R indexes [I > 2σ (I)]	R ₁ = 0.0419, wR ₂ = 0.1149	R ₁ = 0.0409, wR ₂ = 0.0849	R ₁ = 0.0647, wR ₂ = 0.0997	R ₁ = 0.0425, wR ₂ = 0.1052	R ₁ = 0.0329, wR ₂ = 0.0842
Final indexes [all data]	R ₁ = 0.0433, wR ₂ = 0.1161	R ₁ = 0.0587, wR ₂ = 0.0923	R ₁ = 0.1149, wR ₂ = 0.1157	R ₁ = 0.0491, wR ₂ = 0.1091	R ₁ = 0.0363, wR ₂ = 0.0865
Largest diff. peak/hole / e Å ⁻³	0.60/-1.00	0.44/-0.32	0.32/-0.34	0.25/-0.25	0.24/-0.33

Table 6.0.2: sc-XRD data and structure refinement for **4b**, **4b'**, **6a**, **6b** and **8b**.

Compound	4b	4b'	6a	6b	8b
Empirical formula	C ₄₂ H ₅₂ Fe ₂ N ₄	C ₄₂ H ₅₀ FeN ₄	C ₄₀ H ₅₀ FeN ₂ O	C ₆₄ H ₆₈ Fe ₂ N ₄ O ₂	C ₂₂ H ₂₈ FeI ₂ N ₂
Formula Weight	724.57	666.71	630.67	1036.92	630.11
Temperature / K	150.00(10)	150.00(10)	150.00(10)	150.00(10)	150.00(10)
Crystal system	orthorhombic	monoclinic	monoclinic	triclinic	triclinic
Space Group	Pnma	P2 ₁ /n	P2 ₁ /n	P-1	P-1
a / Å	21.9805(5)	10.9682(1)	11.3855(2)	11.1689(6)	9.8669(2)
b / Å	16.4818(4)	17.6194(2)	14.3388(2)	12.1591(5)	13.6941(3)
c / Å	10.6196(2)	18.8246(2)	21.2289(3)	12.3186(8)	18.9575(4)
α / °	90	90	90	110.273(5)	104.807(2)
β / °	90	95.320(1)	93.592(2)	114.828(6)	92.5462(19)
γ / °	90	90	90	98.512(4)	102.712(2)
Volume / Å ³	3847.25(15)	3622.24(7)	3458.90(9)	1336.91(15)	2401.93(10)
Z	4	4	4	1	4
ρ _{calc} / g cm ⁻³	1.251	1.223	1.211	1.288	1.742
μ / mm ⁻¹	6.290	3.589	3.733	4.720	25.270
F(000)	1536.0	1424.0	1352.0	548.0	1224.0
Crystal size / mm ³	0.162 × 0.119 × 0.085	0.286 × 0.21 × 0.123	0.149 × 0.065 × 0.058	0.128 × 0.063 × 0.018	0.204 × 0.189 × 0.139
Radiation	Cu Kα (λ = 1.54184)	Cu Kα (λ = 1.54184)	Cu Kα (λ = 1.54184)	Cu Kα (λ = 1.54184)	Cu Kα (λ = 1.54184)
2θ range / °	9.248 to 145.172	6.886 to 145.168	7.444 to 145.77	8.258 to 144.95	6.876 to 145.32
Index ranges	-27 ≤ h ≤ 27, -18 ≤ k ≤ 20, -13 ≤ l ≤ 12	-9 ≤ h ≤ 13, -21 ≤ k ≤ 20, -23 ≤ l ≤ 23	-14 ≤ h ≤ 14, -17 ≤ k ≤ 17, -18 ≤ l ≤ 26	-13 ≤ h ≤ 13, -12 ≤ k ≤ 15, -15 ≤ l ≤ 15	-8 ≤ h ≤ 12, -16 ≤ k ≤ 16, -23 ≤ l ≤ 22
Reflections collected	43158	38573	29567	12742	23870
Independent reflections	3952 [R _{int} = 0.0642, R _{sigma} = 0.0277]	7182 [R _{int} = 0.0414, R _{sigma} = 0.0290]	6875 [R _{int} = 0.0486, R _{sigma} = 0.0371]	5232 [R _{int} = 0.0507, R _{sigma} = 0.0719]	9432 [R _{int} = 0.0413, R _{sigma} = 0.0416]
Data/restraints/parameters	3952/6/283	7182/0/436	6875/0/407	5232/445/421	9432/0/501
Goodness-of-fit on F ²	1.027	1.025	1.027	1.010	0.975
Final R indexes [I > 2σ (I)]	R ₁ = 0.0390, wR ₂ = 0.0969	R ₁ = 0.0336, wR ₂ = 0.0834	R ₁ = 0.0361, wR ₂ = 0.0827	R ₁ = 0.0487, wR ₂ = 0.1137	R ₁ = 0.0336, wR ₂ = 0.0797
Final indexes [all data]	R ₁ = 0.0453, wR ₂ = 0.1002	R ₁ = 0.0383, wR ₂ = 0.0864	R ₁ = 0.0442, wR ₂ = 0.0868	R ₁ = 0.0604, wR ₂ = 0.1209	R ₁ = 0.0388, wR ₂ = 0.0811
Largest diff. peak/hole / e Å ⁻³	1.06/-0.32	0.23/-0.31	0.25/-0.28	0.77/-0.35	2.43/-0.91

Table 6.0.3: sc-XRD data and structure refinement for **12b**, (*rac*)-**18**, (*rac*)-**22**, (*rac*)-**23**, (*rac*)-**24** and **39**.

Compound	12b	(<i>rac</i>)- 18	(<i>rac</i>)- 22	(<i>rac</i>)- 23	(<i>rac</i>)- 24	39
Empirical formula	C ₃₇ H ₄₇ FeN ₂ PSi	C ₃₃ H ₄₂ N ₂	C ₄₁ H ₅₇ Cl ₂ FeLiN ₂ O ₂	C ₃₇ H ₅₂ FeN ₂ Si	C ₄₁ H ₅₇ BFeN ₂	C ₂₄ H ₄₀ Cl ₂ N ₈ O ₂ P ₄
Formula Weight	634.67	466.68	743.57	608.74	644.54	667.42
Temperature / K	150.01(10)	150.00(10)	150.00(10)	150.00(10)	150.00(10)	150.00(10)
Crystal system	monoclinic	orthorhombic	triclinic	triclinic	triclinic	monoclinic
Space Group	P2 ₁ /n	Pbca	P-1	P-1	P-1	P2 ₁ /c
a / Å	18.2018(2)	13.03294(13)	10.6445(6)	9.5609(4)	11.7884(6)	7.3182(4)
b / Å	10.8333(1)	16.43634(18)	17.7030(9)	11.8549(4)	12.5317(5)	15.6706(9)
c / Å	18.6244(2)	26.4239(3)	22.8754(13)	15.9987(5)	12.6678(4)	13.8456(8)
α / °	90	90	82.191(5)	86.031(3)	82.815(3)	90
β / °	103.083(1)	90	80.960(5)	77.959(3)	87.579(3)	92.622(2)
γ / °	90	90	74.441(4)	87.380(3)	89.981(4)	90
Volume / Å ³	3577.14(7)	5660.36(10)	4081.1(4)	1768.29(11)	1855.02(13)	1586.16(16)
Z	4	8	4	2	2	2
ρ _{calc} / g cm ⁻³	1.178	1.095	1.210	1.143	1.154	1.397
μ / mm ⁻¹	4.311	0.472	4.427	0.486	3.462	0.444
F(000)	1352.0	2032.0	1584.0	656.0	696.0	700.0
Crystal size / mm ³	0.27 × 0.128 × 0.109	0.389 × 0.298 × 0.114	0.167 × 0.128 × 0.074	0.827 × 0.432 × 0.183	0.147 × 0.109 × 0.069	0.3 × 0.21 × 0.16
Radiation	Cu Kα (λ = 1.54184)	Cu Kα (λ = 1.54184)	Cu Kα (λ = 1.54184)	Mo Kα (λ = 0.71073)	Cu Kα (λ = 1.54184)	Mo Kα (λ = 0.71073)
2θ range / °	7.722 to 146.588	9.284 to 146.072	5.208 to 146.502	6.07 to 59.42	7.04 to 146.74	3.928 to 60.352
Index ranges	-22 ≤ h ≤ 21, -11 ≤ k ≤ 13, -23 ≤ l ≤ 23	-16 ≤ h ≤ 13, -19 ≤ k ≤ 20, -32 ≤ l ≤ 32	-13 ≤ h ≤ 13, -21 ≤ k ≤ 21, -28 ≤ l ≤ 28	-13 ≤ h ≤ 11, -14 ≤ k ≤ 16, -21 ≤ l ≤ 20	-14 ≤ h ≤ 14, -15 ≤ k ≤ 14, -14 ≤ l ≤ 15	-10 ≤ h ≤ 9, -22 ≤ k ≤ 21, -19 ≤ l ≤ 19
Reflections collected	49222	60396	17667	15269	19569	38819
Independent reflections	7188 [R _{int} = 0.0420, R _{sigma} = 0.0271]	5658 [R _{int} = 0.0644, R _{sigma} = 0.0241]	17667 [R _{sigma} = 0.1015]	8142 [R _{int} = 0.0279, R _{sigma} = 0.0613]	7409 [R _{int} = 0.0323, R _{sigma} = 0.0415]	4673 [R _{int} = 0.0316, R _{sigma} = 0.0184]
Data/restraints/parameters	7188/0/392	5658/14/349	17667/23/910	8142/0/382	7409/78/450	4673/8/244
Goodness-of-fit on F ²	1.044	1.075	0.839	1.030	1.029	1.122
Final R indexes [I >= 2σ]	R ₁ = 0.0311, wR ₂ = 0.0786	R ₁ = 0.0558, wR ₂ = 0.1499	R ₁ = 0.0562, wR ₂ = 0.1233	R ₁ = 0.0480, wR ₂ = 0.1131	R ₁ = 0.0397, wR ₂ = 0.1002	R ₁ = 0.0424, wR ₂ = 0.1033
Final indexes [all data]	R ₁ = 0.0346, wR ₂ = 0.0806	R ₁ = 0.0626, wR ₂ = 0.1554	R ₁ = 0.1148, wR ₂ = 0.1381	R ₁ = 0.0663, wR ₂ = 0.1273	R ₁ = 0.0448, wR ₂ = 0.1043	R ₁ = 0.0469, wR ₂ = 0.1070
Largest diff. peak/hole / e Å ⁻³	0.36/-0.29	0.29/-0.18	0.65/-0.47	0.99/-0.70	0.43/-0.23	0.83/-0.34

References

- [1] S. G. McGeachin, *Can. J. Chem.*, 1968, **46**, 1903–1912.
- [2] R. Bonnett, D. C. Bradley and K. J. Fisher, *Chem. Commun.*, 1968, **15**, 886–887.
- [3] J. E. Parks and R. H. Holm, *Inorg. Chem.*, 1968, **7**, 1408–1416.
- [4] W. E. Piers and D. J. Emslie, *Coord. Chem. Rev.*, 2002, **233-234**, 131–155.
- [5] A. A. Mohamed, *Coord. Chem. Rev.*, 2010, **254**, 1918–1947.
- [6] D. Zhu and P. H. Budzelaar, *Dalton Trans.*, 2013, **42**, 11343–11354.
- [7] S. P. Sarish, S. Nembenna, S. Nagendran and H. W. Roesky, *Acc. Chem. Res.*, 2011, **44**, 157–170.
- [8] Y. C. Tsai, *Coord. Chem. Rev.*, 2012, **256**, 722–758.
- [9] L. Bourget-Merle, M. F. Lappert and J. R. Severn, *Chem. Rev.*, 2002, **102**, 3031–3065.
- [10] C. Chen, S. M. Bellows and P. L. Holland, *Dalton Trans.*, 2015, **44**, 16654–16670.
- [11] S. P. Green, C. Jones and A. Stasch, *Science*, 2007, **318**, 1754–1757.
- [12] A. F. Pécharman, A. L. Colebatch, M. S. Hill, C. L. McMullin, M. F. Mahon and C. Weetman, *Nat. Commun.*, 2017, **8**, 15022–15029.
- [13] B. Rösch, T. X. Gentner, J. Langer, C. Färber, J. Eysel, L. Zhao, C. Ding, G. Frenking and S. Harder, *Science*, 2021, **371**, 1125–1128.
- [14] S. F. McWilliams, D. L. Broere, C. J. Halliday, S. M. Bhutto, B. Q. Mercado and P. L. Holland, *Nature*, 2020, **584**, 221–226.
- [15] A. Fürstner, *ACS Cent. Sci.*, 2016, **2**, 778–789.
- [16] S. M. Jowitt, G. M. Mudd and J. F. Thompson, *Commun. Earth Environ.*, 2020, **13**, 1–8.
- [17] *Risk List 2015 - An update to the supply risk index for elements or element groups that are of economic value*, British geological survey technical report, 2015.
- [18] P. A. Frey and G. H. Reed, *ACS Chem. Biol.*, 2012, **7**, 1477–1481.
- [19] C. Bolm, J. Legros, J. Le Pailh and L. Zani, *Chem. Rev.*, 2004, **104**, 6217–6254.

- [20] *ICH harmonised guideline, guideline for elemental impurities Q3D (R1)*, European Medicines Agency Technical Report March, 2019.
- [21] J. V. Obligacion and P. J. Chirik, *Nat. Rev. Chem.*, 2018, **2**, 15–34.
- [22] W. Sun and Q. Sun, *Acc. Chem. Res.*, 2019, **52**, 2370–2381.
- [23] M. Guo, T. Corona, K. Ray and W. Nam, *ACS Cent. Sci.*, 2019, **5**, 13–28.
- [24] D. Wei and C. Darcel, *Chem. Rev.*, 2019, **119**, 2550–2610.
- [25] J. M. Smith, R. J. Lachicotte and P. L. Holland, *Chem. Commun.*, 2001, 1542–1543.
- [26] V. C. Gibson, E. L. Marshall, D. Navarro-Llobet, A. J. White and D. J. Williams, *J. Chem. Soc., Dalton Trans.*, 2002, 4321–4322.
- [27] J. Vela, J. M. Smith, R. J. Lachicotte and P. L. Holland, *Chem. Commun.*, 2002, **2**, 2886–2887.
- [28] J. Vela, J. M. Smith, Y. Yu, N. A. Ketterer, C. J. Flaschenriem, R. J. Lachicotte and P. L. Holland, *J. Am. Chem. Soc.*, 2005, **127**, 7857–7870.
- [29] T. Braun and R. P. Hughes, *Organometallic Fluorine Chemistry*, Springer, 2015, pp. 143–197.
- [30] T. J. Sciarone, A. Meetsma and B. Hessen, *Inorganica Chim. Acta*, 2006, **359**, 1815–1825.
- [31] M. M. Rodriguez, E. Bill, W. W. Brennessel and P. L. Holland, *Science*, 2011, **334**, 780–784.
- [32] M. J. Rose and P. K. Mascharak, *J. Am. Chem. Soc.*, 2006, **218**, 756–769.
- [33] E. Bernoud, P. Oulié, R. Guillot, M. Mellah and J. Hannedouche, *Angew. Chem. Int. Ed.*, 2014, **53**, 4930–4934.
- [34] T. E. Müller, K. C. Hultsch, M. Yus, F. Foubelo and M. Tada, *Chem. Rev.*, 2008, **108**, 3795–3892.
- [35] R. L. Webster, *Dalton Trans.*, 2017, **46**, 4483–4498.
- [36] T. R. Dugan, E. Bill, K. C. Macleod, W. W. Brennessel and P. L. Holland, *Inorg. Chem.*, 2014, **53**, 2370–2380.
- [37] T. R. Dugan and P. L. Holland, *J. Organomet. Chem.*, 2009, **694**, 2825–2830.
- [38] M. P. Crockett, A. S. Wong, B. Li and J. A. Byers, *Angew. Chem. Int. Ed.*, 2020, **59**, 5392–5397.
- [39] M. D. Curtis, L. G. Bell and W. M. Butler, *Organometallics*, 1985, **4**, 701–707.
- [40] D. H. Berry and L. J. Procopio, *J. Am. Chem. Soc.*, 1989, **111**, 4100–4101.
- [41] P. I. Djurovich, P. J. Carroll and D. H. Berry, *Organometallics*, 1994, **13**, 2551–2553.
- [42] B. Coutant, F. Quignard and A. Choplin, *J. Chem. Soc., Chem. Commun.*, 1995, 137–138.
- [43] A. Kempter, C. Gemel and R. A. Fischer, *Chem. Eur. J.*, 2007, **13**, 2990–3000.

- [44] M. Gómez-Gallego and M. A. Sierra, *Chem. Rev.*, 2011, **111**, 4857–4963.
- [45] T. Pirali, M. Serafini, S. Cargnin and A. A. Genazzani, *J. Med. Chem.*, 2019, **62**, 5276–5297.
- [46] F. Alonso, I. P. Beletskaya and M. Yus, *Chem. Rev.*, 2002, **102**, 4009–4091.
- [47] J. Y. Corey, *Chem. Rev.*, 2016, **116**, 11291–11435.
- [48] J. Campos, A. C. Esqueda, J. López-Serrano, L. Sánchez, F. P. Cossio, A. De Cozar, E. Álvarez, C. Maya and E. Carmona, *J. Am. Chem. Soc.*, 2010, **132**, 16765–16767.
- [49] G. C. Fortman, H. Jacobsen, L. Cavallo and S. P. Nolan, *Chem. Commun.*, 2011, **47**, 9723–9725.
- [50] J. Campos, M. Rubio, A. C. Esqueda and E. Carmona, *J. Label Compd. Radiopharm.*, 2012, **55**, 29–38.
- [51] V. M. Iluc, A. Fedorov and R. H. Grubbs, *Organometallics*, 2012, **31**, 39–41.
- [52] K. A. Smart, E. Mothes-Martin, T. Annaka, M. Grellier and S. Sabo-Etienne, *Adv. Synth. Catal.*, 2014, **356**, 759–764.
- [53] T. Ayed, J. C. Barthelat, B. Tangour, C. Pradère, B. Donnadieu, M. Grellier and S. Sabo-Etienne, *Organometallics*, 2005, **24**, 3824–3826.
- [54] D. Schmidt, T. Zell, T. Schaub and U. Radius, *Dalton Trans.*, 2014, **43**, 10816–10827.
- [55] Y. Kratish, D. Bravo-Zhivotovskii and Y. Apeloig, *ACS Omega*, 2017, **2**, 372–376.
- [56] T. Komuro, T. Osawa, R. Suzuki, D. Mochizuki, H. Higashi and H. Tobita, *Chem. Commun.*, 2019, **55**, 957–960.
- [57] R. Zhou, J. Li, H. W. Cheo, R. Chua, G. Zhan, Z. Hou and J. Wu, *Chem. Sci.*, 2019, **10**, 7340–7344.
- [58] M. A. Esteruelas, A. Martínez, M. Oliván and A. Vélez, *J. Org. Chem.*, 2020, **85**, 15693–15698.
- [59] M. Horn, L. H. Schappele, G. Lang-Wittkowski, H. Mayr and A. R. Ofial, *Chem. Eur. J.*, 2013, **19**, 249–263.
- [60] Z. Lin, *Chem. Soc. Rev.*, 2002, **31**, 239–245.
- [61] D. Gasperini, A. K. King, N. T. Coles, M. F. Mahon and R. L. Webster, *ACS Catal.*, 2020, **10**, 6102–6112.
- [62] M. Espinal-Viguri, S. E. Neale, N. T. Coles, S. A. MacGregor and R. L. Webster, *J. Am. Chem. Soc.*, 2019, **141**, 572–582.
- [63] H. Braunschweig, F. Guethlein, L. Mailänder and T. B. Marder, *Chem. Eur. J.*, 2013, **19**, 14831–14835.
- [64] D. J. Nelson, J. D. Egbert and S. P. Nolan, *Dalton Trans.*, 2013, **42**, 4105–4109.

- [65] A. L. Colebatch, B. W. Hawkey Gilder, G. R. Whittell, N. L. Oldroyd, I. Manners and A. S. Weller, *Chem. Eur. J.*, 2018, **24**, 5450–5455.
- [66] M. A. Esteruelas, A. Martínez, M. Oliván and A. Vélez, *J. Org. Chem.*, 2020, **85**, 15693–15698.
- [67] P. L. Callaghan, R. Fernández-Pacheco, N. Jasim, S. Lachaize, T. B. Marder, R. N. Perutz, E. Rivalta and S. Sabo-Etienne, *Chem. Commun.*, 2004, **4**, 242–243.
- [68] L. Qiao, L. Zhang, G. Liu and Z. Huang, *Tetrahedron*, 2019, **75**, 4138–4142.
- [69] A. W. Cummins, S. Li, D. R. Willcox, T. Muilu, J. H. Docherty and S. P. Thomas, *Tetrahedron*, 2020, **76**, 131084–131089.
- [70] T. G. Linford-Wood, N. T. Coles and R. L. Webster, *Green Chem.*, 2021, **23**, 2703–2709.
- [71] A. K. King, A. Buchard, M. F. Mahon and R. L. Webster, *Chem. Eur. J.*, 2015, **21**, 15960–15963.
- [72] P. L. Holland, *Acc. Chem. Res.*, 2008, **41**, 905–914.
- [73] B. R. Elvidge, S. Arndt, T. P. Spaniol and J. Okuda, *Dalton Trans.*, 2006, **60**, 890–901.
- [74] G. Zhang, J. Wu, S. Zheng, M. C. Neary, J. Mao, M. Flores, R. J. Trovitch and P. A. Dub, *J. Am. Chem. Soc.*, 2019, **141**, 15230–15239.
- [75] D. F. Evans, *J. Chem. Soc.*, 1959, 2003–2005.
- [76] G. A. Bain and J. F. Berry, *J. Chem. Educ.*, 2008, **85**, 532–536.
- [77] J. C. Ott, H. Wadepohl, M. Enders and L. H. Gade, *J. Am. Chem. Soc.*, 2018, **140**, 17413–17417.
- [78] J. Burés, *Angew. Chem. Int. Ed.*, 2016, **55**, 16084–16087.
- [79] J. Burés, *Angew. Chem. Int. Ed.*, 2016, **55**, 2028–2031.
- [80] M. P. Crockett, A. S. Wong, B. Li and J. A. Byers, *Angew. Chem. Int. Ed.*, 2020, **59**, 5392–5397.
- [81] D. Wu, R. Wang, Y. Li, R. Ganguly, H. Hirao and R. Kinjo, *Chem*, 2017, **3**, 134–151.
- [82] T. L. Cottrell, *The Strength of Chemical Bonds*, Butterworths, London, 2nd edn., 1958.
- [83] J. Knizek and H. Nöth, *Eur. J. Inorg. Chem.*, 2011, 1888–1900.
- [84] J. Cid, H. Gulyâs, J. J. Carbó and E. Fernández, *Chem. Soc. Rev.*, 2012, **41**, 3558–3570.
- [85] C. R. Woof, T. G. Linford-Wood, M. F. Mahon and R. L. Webster, *Synthesis*, 2022, **54**, 10.1055/a-1902–5592.
- [86] K. Takaki, G. Koshoji, K. Komeyama, M. Takeda, T. Shishido, A. Kitani and K. Takehira, *J. Org. Chem.*, 2003, **68**, 6554–6565.
- [87] C. A. Busacca, E. Farber, J. Deyoung, S. Campbell, N. C. Gonnella, N. Grinberg, N. Haddad, H. Lee, S. Ma, D. Reeves, S. Shen and C. H. Senanayake, *Org. Lett.*, 2009, **11**, 5594–5597.

- [88] Y. Huang, S. A. Pullarkat, M. Yuan, Y. Ding, Y. Li and P. H. Leung, *Organometallics*, 2010, **29**, 536–542.
- [89] M. Espinal-Viguri, A. K. King, J. P. Lowe, M. F. Mahon and R. L. Webster, *ACS Catal.*, 2016, **6**, 7892–7897.
- [90] A. K. King, K. J. Gallagher, M. F. Mahon and R. L. Webster, *Chem. Eur. J.*, 2017, **23**, 9039–9043.
- [91] A. K. King, A. Buchard, M. F. Mahon and R. L. Webster, *Chem. Eur. J.*, 2015, **21**, 15960–15963.
- [92] S. S. Al-Juaid, C. Eaborn, P. B. Hitchcock, M. S. Hill and J. S. Smith, *Organometallics*, 2000, **19**, 3224–3231.
- [93] C. Eaborn, M. S. Hill, P. B. Hitchcock and D. J. Smith, *Chem. Commun.*, 2000, **2**, 691–692.
- [94] M. P. Coles, S. E. Sözerli, J. D. Smith and P. B. Hitchcock, *Organometallics*, 2007, **26**, 6691–6693.
- [95] D. H. Lee, J. Y. Jung and M. J. Jin, *Chem. Commun.*, 2010, **46**, 9046–9048.
- [96] R. Jiao, M. Xue, X. Shen, Y. Zhang, Y. Yao and Q. Shen, *Eur. J. Inorg. Chem.*, 2010, 2523–2529.
- [97] D. T. Carey, E. K. Cope-Eatough, E. Vilaplana-Mafé, F. S. Mair, R. G. Pritchard, J. E. Warren and R. J. Woods, *Dalton Trans.*, 2003, 1083–1093.
- [98] T. G. Linford-Wood, M. F. Mahon, M. N. Grayson and R. L. Webster, *ACS Catal.*, 2022, **12**, 2979–2985.
- [99] S. B. Kan, R. D. Lewis, K. Chen and F. H. Arnold, *Science*, 2016, **354**, 1048–1051.
- [100] G. P. Marsh, P. J. Parsons, C. McCarthy and X. G. Corniquet, *Org. Lett.*, 2007, **9**, 2005–2008.
- [101] Z. Zhao, L. Racicot and G. K. Murphy, *Angew. Chem. Int. Ed.*, 2017, **56**, 11620–11623.
- [102] H. Clavier, K. L. Jeune, I. D. Riggi, A. Tenaglia and G. Buono, *Org. Lett.*, 2011, **13**, 308–311.
- [103] G. Frisch, M. J.; Trucks, G. W.; Schlegel, H. B.; Scuseria, G. E.; Robb, M. A.; Cheeseman, J. R.; Scalmani, B. G. Barone, V.; Petersson, G. A.; Nakatsuji, H.; Li, X.; Caricato, M.; Marenich, A. V.; Bloino, J.; Janesko, J. L. W.-Y. Gomperts, R.; Mennucci, B.; Hratchian, H. P.; Ortiz, J. V.; Izmaylov, A. F.; Sonnenberg, D. Z. D.; Ding, F.; Lipparini, F.; Egidi, F.; Goings, J.; Peng, B.; Petrone, A.; Henderson, T.; Ranasinghe, J. I. V. G.; Gao, J.; Rega, N.; Zheng, G.; Liang, W.; Hada, M.; Ehara, M.; Toyota, K.; Fukuda, R.; Hasegawa, J. E. M.; Nakajima, T.; Honda, Y.; Kitao, O.; Nakai, H.; Vreven, T.; Throssell, K.; Montgomery, J. A. J.; Peralta, T. A. K. Ogliaro, F.; Bearpark, M. J.; Heyd, J. J.; Brothers, E. N.; Kudin, K. N.; Staroverov, V. N.; Keith, J. R.; Normand, J.; Raghavachari, K.; Rendell, A. P.; Burant, J. C.; Iyengar, S. S.; Tomasi, J.; Cossi, M.; Millam, J. M.; Klene, M.; Adamo, C.; Cammi, R.; Ochterski, J. W.; Martin, R. L.; Morokuma, K.; Farkas, O.; Foresman and D. J. B.; Fox, *Gaussian 16, Revision A.03*, 2016.
- [104] M. J. Frisch, J. A. Pople and J. S. Binkley, *J. Chem. Phys.*, 1984, **80**, 3265–3269.

- [105] R. Ditchfield, W. J. Hehre and J. A. Pople, *J. Chem. Phys.*, 1971, **54**, 724–728.
- [106] P. C. Hariharan and J. A. Pople, *Theoret. Chim. Acta*, 1973, **28**, 213–222.
- [107] F. Weigend and R. Ahlrichs, *Phys. Chem. Chem. Phys.*, 2005, **7**, 3297–3305.
- [108] A. D. Becke, *J. Chem. Phys.*, 1993, **98**, 5648–5652.
- [109] S. Grimme, J. Antony, S. Ehrlich and H. Krieg, *J. Chem. Phys.*, 2010, **132**, 154104–154119.
- [110] S. Grimme, S. Ehrlich and L. Goerigk, *J. Comput. Chem.*, 2011, **32**, 1456–1465.
- [111] J. Tomasi, B. Mennucci and R. Cammi, *Chem. Rev.*, 2005, **105**, 2999–3093.
- [112] G. Luchini, J. Alegre-Raquena, Y. Guan, I. Funes-Ardoiz and R. Paton, *GoodVibes: version 3.0.1*.
- [113] J. G. D. Vries and C. J. Elsevier, *The Handbook of Homogeneous Hydrogenation*, Wiley-VCH, Weinheim, 2007.
- [114] J. A. Osborn, F. H. Jardine, J. F. Young and G. Wilkinson, *J. Am. Chem. Soc. A*, 1966, 1711–1732.
- [115] M. Weller, T. Overton, J. Rourke and F. Armstrong, *Inorganic Chemistry*, Oxford University Press, Oxford, 6th edn., 2014, pp. 728–762.
- [116] C. Bianchini, A. Meli, M. Peruzzini, F. Vlzza and F. Zanolini, *Organometallics*, 1989, **8**, 2080–2082.
- [117] C. Bianchini, A. Meli, M. Peruzzini, P. Frediani, C. Bohanna, M. A. Esteruelas and L. A. Oro, *Organometallics*, 1992, **11**, 138–145.
- [118] S. C. Bart, E. Lobkovsky and P. J. Chirik, *J. Am. Chem. Soc.*, 2004, **126**, 13794–13807.
- [119] R. J. Trovitch, E. Lobkovsky, E. Bill and P. J. Chirik, *Organometallics*, 2008, **27**, 1470–1478.
- [120] R. P. Yu, J. M. Darmon, J. M. Hoyt, G. W. Margulieux, Z. R. Turner and P. J. Chirik, *ACS Catal.*, 2012, **2**, 1760–1764.
- [121] M. D. Bhor, A. G. Panda, S. R. Jagtap and B. M. Bhanage, *Catal. Lett.*, 2008, **124**, 157–164.
- [122] D. Srimani, Y. Diskin-Posner, Y. Ben-David and D. Milstein, *Angew. Chem. Int. Ed.*, 2013, **52**, 14131–14134.
- [123] T. N. Gieshoff, M. Villa, A. Welther, M. Plois, U. Chakraborty, R. Wolf and A. Jacobi Von Wangelin, *Green Chem.*, 2015, **17**, 1408–1413.
- [124] P. Lu, X. Ren, H. Xu, D. Lu, Y. Sun and Z. Lu, *J. Am. Chem. Soc.*, 2021, **143**, 12433–12438.
- [125] B. A. Le Bailly and S. P. Thomas, *RSC Adv.*, 2011, **1**, 1435–1445.
- [126] E. N. Frankel, E. A. Emken, H. M. Peters, V. L. Davison and R. O. Butterfield, *J. Org. Chem.*, 1965, **29**, 3292–3297.
- [127] D. Wang and D. Astruc, *Chem. Rev.*, 2015, **115**, 6621–6686.

- [128] H. Meerwein and R. Schmidt, *Justus Liebigs Ann. Chem.*, 1925, **444**, 221–238.
- [129] A. Verley, *Bull. Soc. Chim. Fr.*, 1925, **37**, 537–542.
- [130] W. Ponndorf, *Angew. Chem.*, 1926, **39**, 138–143.
- [131] R. Cohen, C. R. Graves, S. B. T. Nguyen, J. M. Martin and M. A. Ratner, *J. Am. Chem. Soc.*, 2004, **126**, 14796–14803.
- [132] W. E. Doering and R. W. Young, *J. Am. Chem. Soc.*, 1950, **72**, 631.
- [133] A. Fujii, S. Hashiguchi, N. Uematsu, T. Ikariya and R. Noyori, *J. Am. Chem. Soc.*, 1996, **118**, 2521–2522.
- [134] S. Horn and M. Albrecht, *Chem. Commun.*, 2011, **47**, 8802–8804.
- [135] V. H. Mai and G. I. Nikonov, *Organometallics*, 2016, **35**, 943–949.
- [136] G. K. Zieliński, J. Majtczak, M. Gutowski and K. Grela, *J. Org. Chem.*, 2018, **83**, 2542–2553.
- [137] Y. Y. Li, S. L. Yu, W. Y. Shen and J. X. Gao, *Acc. Chem. Res.*, 2015, **48**, 2587–2598.
- [138] T. Nishiguchi and K. Fukuzumi, *Chem. Commun.*, 1971, 139–140.
- [139] T. Nishiguchi and K. Fukuzumi, *Bull. Chem. Soc. Jpn.*, 1972, **45**, 1656–1660.
- [140] C. Bianchini, E. Farnetti, M. Graziani, M. Peruzzini and A. Polo, *Organometallics*, 1993, **12**, 3753–3761.
- [141] G. Wienhöfer, F. A. Westerhaus, R. V. Jagadeesh, K. Junge, H. Junge and M. Beller, *Chem. Commun.*, 2012, **48**, 4827–4829.
- [142] M. Kamitani, Y. Nishiguchi, R. Tada, M. Itazaki and H. Nakazawa, *Organometallics*, 2014, **33**, 1532–1535.
- [143] C. Johnson and M. Albrecht, *Catal. Sci. Technol.*, 2018, **8**, 2779–2783.
- [144] P. V. Kattamuri and J. G. West, *J. Am. Chem. Soc.*, 2020, **142**, 19316–19326.
- [145] N. M. Hein, Y. Seo, S. J. Lee and M. R. Gagné, *Green Chem.*, 2019, **21**, 2662–2669.
- [146] B. Ndaba, I. Chiyanzu and S. Marx, *Biotechnol. Rep.*, 2015, **8**, 1–9.
- [147] R. O. Sauer, W. J. Scheiber and S. D. Brewer, *J. Am. Chem. Soc.*, 1946, **68**, 962–963.
- [148] N. S. Shaikh, K. Junge and M. Beller, *Org. Lett.*, 2007, **9**, 5429–5432.
- [149] K. Muller, A. Schubert, T. Jozak, A. Ahrens-Botzong, V. Schünemann and W. R. Thiel, *ChemCatChem*, 2011, **3**, 887–892.
- [150] A. P. Dieskau, J. M. Begouin and B. Plietker, *Eur. J. Org. Chem.*, 2011, 5291–5296.

- [151] J. Zheng, L. C. Misal Castro, T. Roisnel, C. Darcel and J. B. Sortais, *Inorganica Chim. Acta*, 2012, **380**, 301–307.
- [152] Q. Liang, N. J. Liu and D. Song, *Dalton Trans.*, 2018, **47**, 9889–9896.
- [153] L. C. Castro, D. Bézier, J. B. Sortais and C. Darcel, *Adv. Synth. Catal.*, 2011, **353**, 1279–1284.
- [154] C. D. Zotto, D. Virieux and J. M. Campagne, *Synlett*, 2009, **2**, 276–278.
- [155] N. S. Shaikh, S. Enthaler, K. Junge and M. Beller, *Angew. Chem. Int. Ed.*, 2008, **47**, 2497–2501.
- [156] S. Enthaler, *ChemCatChem*, 2010, **2**, 1411–1415.
- [157] H. Jaafar, H. Li, L. C. Misal Castro, J. Zheng, T. Roisnel, V. Dorcet, J. B. Sortais and C. Darcel, *Eur. J. Inorg. Chem.*, 2012, 3546–3550.
- [158] H. Li, M. Achard, C. Bruneau, J. B. Sortais and C. Darcel, *RSC Adv.*, 2014, **4**, 25892–25897.
- [159] Y. Sunada, H. Kawakami, T. Imaoka, Y. Motoyama and H. Nagashima, *Angew. Chem. Int. Ed.*, 2009, **48**, 9511–9514.
- [160] S. Zhou, K. Junge, D. Addis, S. Das and M. Beller, *Angew. Chem. Int. Ed.*, 2009, **48**, 9507–9510.
- [161] A. Volkov, E. Buitrago and H. Adolfsson, *Eur. J. Org. Chem.*, 2013, 2066–2070.
- [162] K. Junge, B. Wendt, S. Zhou and M. Beller, *Eur. J. Org. Chem.*, 2013, 2061–2065.
- [163] S. Enthaler, *ChemCatChem*, 2011, **3**, 666–670.
- [164] D. Decker, H. J. Drexler, D. Heller and T. Beweries, *Cat. Sci. Technol.*, 2020, **10**, 6449–6463.
- [165] N. Cox, H. Dang, A. M. Whittaker and G. Lalic, *Tetrahedron*, 2014, **70**, 4219–4231.
- [166] K. Semba, T. Fujihara, T. Xu, J. Terao and Y. Tsuji, *Adv. Synth. Catal.*, 2012, **354**, 1542–1550.
- [167] A. M. Whittaker and G. Lalic, *Org. Lett.*, 2013, **15**, 1112–1115.
- [168] L. Longwitz and T. Werner, *Angew. Chem. Int. Ed.*, 2020, **59**, 2760–2763.
- [169] B. Lamberson, T. N. Nguyen, H. Wehr and T. Thananattthanachon, *Energy Technol.*, 2020, **8**, 2000716–2000721.
- [170] Y. Kamei, Y. Seino, Y. Yamaguchi, T. Yoshino, S. Maeda, M. Kojima and S. Matsunaga, *Nat. Commun.*, 2021, **12**, 966–975.
- [171] C. R. Woof, D. J. Durand, N. Fey, E. Richards and R. L. Webster, *Chem. Eur. J.*, 2021, **27**, 5972–5977.
- [172] M. A. Farcaş-Johnson, S. H. Kyne and R. L. Webster, *Chem. Eur. J.*, 2022, **28**, 1–6.
- [173] C. A. Jaska and I. Manners, *J. Am. Chem. Soc.*, 2004, **126**, 2698–2699.
- [174] M. E. Sloan, A. Staubitz, K. Lee and I. Manners, *Eur. J. Org. Chem.*, 2011, 672–675.

- [175] Y. Zhang, P. Wang, Y. Gao, Y. Zhang, Z. H. Qi, W. Liu and Y. Wang, *Int. J. Hydrog. Energy*, 2018, **43**, 2043–2049.
- [176] N. T. Coles, *Ph.D. thesis*, University of Bath, 2019.
- [177] N. T. Coles, M. F. Mahon and R. L. Webster, *Organometallics*, 2017, **36**, 2262–2268.
- [178] K. Müller, K. Stark, B. Müller and W. Arlt, *Energy Fuels*, 2012, **26**, 3691–3696.
- [179] A. Rossin and M. Peruzzini, *Chem. Rev.*, 2016, **116**, 8848–8872.
- [180] R. Moury and U. B. Demirci, *Energies*, 2015, **8**, 3118–3141.
- [181] N. E. Stubbs, A. P. Robertson, E. M. Leitao and I. Manners, *J. Organomet. Chem.*, 2013, **730**, 84–89.
- [182] P. Ballinger and F. A. Long, *J. Am. Chem. Soc.*, 1960, **82**, 795–798.
- [183] Z. P. Vang, S. J. Hintzsche and J. R. Clark, *Chem. Eur. J.*, 2021, **27**, 9988–10000.
- [184] J. C. Walker and M. Oestreich, *Org. Lett.*, 2018, **20**, 6411–6414.
- [185] Z. P. Vang, A. Reyes, R. E. Sonstrom, M. S. Holdren, S. E. Sloane, I. Y. Alansari, J. L. Neill, B. H. Pate and J. R. Clark, *J. Am. Chem. Soc.*, 2021, **143**, 7707–7718.
- [186] A. Reyes, E. R. Torres, Z. P. Vang and J. R. Clark, *Chem. Eur. J.*, 2022, **28**, e202104340.
- [187] S. P. Cummings, T. N. Le, G. E. Fernandez, L. G. Quiambao and B. J. Stokes, *J. Am. Chem. Soc.*, 2016, **138**, 6107–6110.
- [188] C. Qin and H. M. Davies, *J. Am. Chem. Soc.*, 2014, **136**, 9792–9796.
- [189] T. N. Gieshoff, M. Villa, A. Welther, M. Plois, U. Chakraborty, R. Wolf and A. Jacobi Von Wangelin, *Green Chem.*, 2015, **17**, 1408–1413.
- [190] T. Fukuyama, T. Nishikawa and I. Ryu, *Eur. J. Org. Chem.*, 2020, 1424–1428.
- [191] S. M. Leckie, G. J. Harkness and M. L. Clarke, *Chem. Commun.*, 2014, **50**, 11511–11513.
- [192] S. Xu, J. S. Boschen, A. Biswas, T. Kobayashi, M. Pruski, T. L. Windus and A. D. Sadow, *Dalton Trans.*, 2015, **44**, 15897–15904.
- [193] P. J. Rushworth, D. G. Hulcoop and D. J. Fox, *J. Org. Chem.*, 2013, **78**, 9517–9521.
- [194] G. Dilauro, A. F. Quivelli, P. Vitale, V. Capriati and F. M. Perna, *Angew. Chem. Int. Ed.*, 2019, **58**, 1799–1802.
- [195] A. Volkov, K. P. J. Gustafson, C.-W. Tai, O. Verho, J.-E. Bäckvall and H. Adolfsson, *Angew. Chem. Int. Ed.*, 2015, **54**, 5122–5126.
- [196] R. C. Betori, C. M. May and K. A. Scheidt, *Angew. Chem. Int. Ed.*, 2019, **58**, 16490–16494.

- [197] H. Duan, L. Meng, D. Bao, H. Zhang, Y. Li and A. Lei, *Angew. Chem. Int. Ed.*, 2010, **49**, 6387–6390.
- [198] P. O. Oguadinma and F. Schaper, *Organometallics*, 2009, **28**, 4089–4097.
- [199] I. El-Zoghbi, S. Latreche and F. Schaper, *Organometallics*, 2010, **29**, 1551–1559.
- [200] F. Drouin, P. O. Oguadinma, T. J. Whitehorne, R. E. Prudhomme and F. Schaper, *Organometallics*, 2010, **29**, 2139–2147.
- [201] S. Latreche and F. Schaper, *Inorganica Chim. Acta*, 2011, **365**, 49–53.
- [202] D. Kong, Y. Peng, D. Li, Y. Li, P. Chen and J. Qu, *Inorg. Chem. Commun.*, 2012, **22**, 158–161.
- [203] M. Cheng, A. B. Attygalle, E. B. Lobkovsky and G. W. Coates, *J. Am. Chem. Soc.*, 1999, **121**, 11583–11584.
- [204] I. El-Zoghbi, M. Kebdani, T. J. Whitehorne and F. Schaper, *Organometallics*, 2013, **32**, 6986–6995.
- [205] W. C. Ellis, Y. Jung, M. Mulzer, R. Di Girolamo, E. B. Lobkovsky and G. W. Coates, *Chem. Sci.*, 2014, **5**, 4004–4011.
- [206] E. A. Weerawardhana, A. Pena, M. Zeller and W. T. Lee, *Inorganica Chim. Acta*, 2017, **460**, 29–34.
- [207] C. N. D. Bruin-Dickason, C. A. Rosengarten, G. B. Deacon and C. Jones, *Chem. Commun.*, 2021, **57**, 1599–1602.
- [208] Y. Yu, J. M. Smith, C. J. Flaschenriem and P. L. Holland, *Inorg. Chem.*, 2006, **45**, 5742–5751.
- [209] T. R. Dugan, X. Sun, E. V. Rybak-Akimova, O. Olatunji-Ojo, T. R. Cundari and P. L. Holland, *J. Am. Chem. Soc.*, 2011, **133**, 12418–12421.
- [210] F. Spitzer, C. Graßl, G. Balázs, E. M. Zolnhofer, K. Meyer and M. Scheer, *Angew. Chem. Int. Ed.*, 2016, **55**, 4340–4344.
- [211] S. P. Green, C. Jones and A. Stasch, *Angew. Chem. Int. Ed.*, 2008, **47**, 9079–9083.
- [212] B. Rösch, T. X. Gentner, J. Eyselien, A. Friedrich, J. Langer and S. Harder, *Chem. Commun.*, 2020, **56**, 11402–11405.
- [213] M. Espinal-Viguri, C. R. Woof and R. L. Webster, *Chem. Eur. J.*, 2016, **22**, 11605–11608.
- [214] S. Grélaud, P. Cooper, L. J. Feron and J. F. Bower, *J. Am. Chem. Soc.*, 2018, **140**, 9351–9356.
- [215] A. E. Cherian, E. B. Lobkovsky and G. W. Coates, *Chem. Commun.*, 2003, **3**, 2566–2567.
- [216] A. E. Cherian, G. J. Domski, J. M. Rose, E. B. Lobkovsky and G. W. Coates, *Org. Lett.*, 2005, **7**, 5135–5137.
- [217] E. Braconi and N. Cramer, *Angew. Chem. Int. Ed.*, 2020, **59**, 16425–16429.
- [218] J. Chen, T. Xi and Z. Lu, *Org. Lett.*, 2014, **16**, 6452–6455.

- [219] A. Suzuki, *Angew. Chem. Int. Ed.*, 2011, **50**, 6722–6737.
- [220] C. Sandford and V. K. Aggarwal, *Chem. Commun.*, 2017, **53**, 5481–5494.
- [221] L. Zhang, D. Peng, X. Leng and Z. Huang, *Angew. Chem. Int. Ed.*, 2013, **52**, 3676–3680.
- [222] A. D. McNaught and A. Wilkinson, *IUPAC. Compendium of Chemical Technology , (the Gold Book)*, Blackwell Scientific Publications, Oxford, 2nd edn., 1997.
- [223] C. N. Ayala, M. H. Chisholm, J. C. Gallucci and C. Krempner, *Dalton Trans.*, 2009, 9237–9245.
- [224] A. E. Cherian, J. M. Rose, E. B. Lobkovsky and G. W. Coates, *J. Am. Chem. Soc.*, 2005, **127**, 13770–13771.
- [225] K. M. Brands and A. J. Davies, *Chem. Rev.*, 2006, **106**, 2711–2733.
- [226] A. P. Prakasham, M. K. Gangwar and P. Ghosh, *Eur. J. Inorg. Chem.*, 2019, **2019**, 295–313.
- [227] R. M. N. Kalla, J. Lim, J. Bae and I. Kim, *Tetrahedron Lett.*, 2017, **58**, 1595–1599.
- [228] R. Newar, W. Begum, N. Akhtar, N. Antil, M. Chauhan, A. Kumar, P. Gupta, J. Malik, Balendra and K. Manna, *Eur. J. Inorg. Chem.*, 2022, **2022**, 1–7.
- [229] D. Liu, K. Ouyang and N. Yang, *Tetrahedron*, 2016, **72**, 1018–1023.
- [230] J. J. Dunsford, E. R. Clark and M. J. Ingleson, *Angew. Chem. Int. Ed.*, 2015, **54**, 5688–5692.
- [231] S. Zhang, D. Bedi, L. Cheng, D. K. Unruh, G. Li and M. Findlater, *J. Am. Chem. Soc.*, 2020, **142**, 8910–8917.
- [232] H. T. H. Nguyen, P. Qi, M. Rostagno, A. Feteha and S. A. Miller, *J. Mater. Chem. A*, 2018, **6**, 9298–9331.
- [233] M. D. Levin, P. Kaszynski and J. Michl, *Chem. Rev.*, 2000, **100**, 169–234.
- [234] A. D. Schlüter, *Angew. Chem. Int. Ed.*, 1988, **27**, 296–298.
- [235] M. Mahkam and N. S. Sanjani, *Polym. Int.*, 2000, **49**, 260–264.
- [236] T. Ishizone, S. I. Matsuoka, S. Sakai, W. Harada and H. Tajima, *Macromolecules*, 2004, **37**, 7069–7071.
- [237] S. I. Matsuoka, N. Ogiwara and T. Ishizone, *J. Am. Chem. Soc.*, 2006, **128**, 8708–8709.
- [238] S. Inomata, S. I. Matsuoka, S. Sakai, H. Tajima and T. Ishizone, *Macromolecules*, 2012, **45**, 4184–4195.
- [239] Z. Chen and T. M. Swager, *Macromolecules*, 2008, **41**, 6880–6885.
- [240] J. Friebel, C. P. Ender, M. Mezger, J. Michels, M. Wagner, K. B. Wagener and T. Weil, *Macromolecules*, 2019, **52**, 4483–4491.

- [241] X. Yang, W. Jiang, C. B. Knobler, M. D. Mortimer and M. F. Hawthorne, *Inorganica Chim. Acta*, 1995, **240**, 371–378.
- [242] T. Iwamoto, D. Tsushima, E. Kwon, S. Ishida and H. Isobe, *Angew. Chem. Int. Ed.*, 2012, **51**, 2340–2344.
- [243] J. Bedard, T. G. Linford-Wood, B. C. Thompson, U. Werner-Zwanziger, K. M. Marczenko, R. A. Musgrave and S. S. Chitnis, *J. Am. Chem. Soc.*, 2023, **145**, 7569–7579.
- [244] D. S. Payne, H. Noth and G. Henniger, *Chem. Commun.*, 1965, **14**, 327–329.
- [245] M. Bermann and J. R. Van Wazer, *Inorg. Chem.*, 1973, **13**, 737–738.
- [246] S. Tian, J. Sun, K. Jin, J. Wang, F. He, S. Zheng and Q. Fang, *ACS Appl. Mater. Interfaces*, 2014, **6**, 20437–20443.
- [247] W. Li, H. Chung, C. Daeffler, J. A. Johnson and R. H. Grubbs, *Macromolecules*, 2012, **45**, 9595–9603.
- [248] A. M. Priegert, B. W. Rawe, S. C. Serin and D. P. Gates, *Chem. Soc. Rev.*, 2016, **45**, 922–953.
- [249] N. P. Chauhan, N. S. Hosmane and M. Mozafari, *Mater. Today Chem.*, 2019, **14**, 100184–100204.
- [250] X. Zhou, S. Qiu, X. Mu, M. Zhou, W. Cai, L. Song, W. Xing and Y. Hu, *Compos. B Eng.*, 2020, **202**, 108397–108414.
- [251] S. Rothmund and I. Teasdale, *Chem. Soc. Rev.*, 2016, **45**, 5200–5215.
- [252] A. N. Barrett, C. R. Woof, C. A. Gault, D. Gasperini, M. F. Mahon and R. L. Webster, *Inorg. Chem.*, 2021, **60**, 16826–16833.
- [253] E. E. Coyle, B. J. Doonan, A. J. Holohan, K. A. Walsh, F. Lavigne, E. H. Krenske and C. J. O'Brien, *Angew. Chem. Int. Ed.*, 2014, **53**, 12907–12911.